Understanding the *trans*-cleavage Activity of CRISPR-Cas Systems for RNA Detection Applications

by

Wei Feng

A thesis submitted in partial fulfillment of the requirements for the degree of Doctor of Philosophy

in

Analytical and Environmental Toxicology

Department of Laboratory Medicine and Pathology

University of Alberta

Abstract

The discovery and characterization of Clustered Regularly Interspaced Short Palindromic Repeats (CRISPR) systems with *trans*-cleavage activity led to the rise of CRISPR-based diagnostics. A ribonucleoprotein (RNP), consisting of a CRISPR-associated protein (Cas) and a CRISPR RNA (crRNA) or single guide RNA (sgRNA), recognizes a target nucleic acid sequence. The binding of RNP to the specific nucleic acid activates CRISPR-Cas systems, e.g., CRISPR-Cas12a and CRISPR-Cas13a, which can *trans*-cleave reporter nucleic acids to generate measurable signals. The performance of such CRISPR-based assays depends on the kinetics of the *trans*-cleavage activity. The first objective of my thesis is to study and maximize the *trans*-cleavage activity of CRISPR-Cas13a systems. CRISPR-Cas systems have also been combined with nucleic acid amplification techniques to meet the high sensitivity requirement for molecular detection of pathogens. However, the incompatibility of multiple techniques and reaction conditions poses challenges to the development of highly sensitive and accurate assays with simple operations. The second objective of my thesis is to integrate CRISPR-Cas systems with other nucleic acid amplification techniques for broader applications to RNA detection.

I systematically studied how the length of the RNA target, reagent composition, and reaction conditions affected the *trans*-cleavage activity of Cas13a. The improved understanding contributed to the development of a sensitive assay for the detection of microRNA at ambient temperature using Cas13a. This broadened the application of Cas13a-based assays to short, small RNA molecules; previous assays were only applicable to longer RNA sequences. My characterization of the effect of short RNA or crRNA on the two most

common Cas13a enzymes provided guidance for choosing Cas13a enzymes for different applications.

I observed unusual effects of the reaction temperature on the *trans*-cleavage activity, and performed an in-depth study on the thermal behavior of two Cas enzymes: LwaCas13a and LbuCas13a. I differentiated the effect of temperature on several reaction steps during the operation of Cas13a. By testing a set of rationally designed target RNA, I was able to precisely assess the temperature preference of *trans*-cleavage activity upon Cas13a activation. I discovered that upon activation, the preferred temperature for high *trans*-cleavage activity of Cas13a was around ambient temperature, lower than the temperatures commonly used by others for detection. This feature is useful for simplifying Cas13a-based assays.

Detection of RNA using CRISPR-Cas alone is limited by the slow kinetics of the *trans*-cleavage process. Integrating CRISPR technology with nucleic acid amplification techniques overcomes the limitation in sensitivity. A strategy to integrate reverse transcription (RT), recombinase polymerase amplification (RPA), and CRISPR-Cas12a nuclease reactions into a single tube was developed, resulting in the sensitive detection of SARS-CoV-2. All reactions were integrated into a single, closed tube, and the assay was achieved under an isothermal condition (40 °C).

The understanding gained from this thesis helps guide the development of CRISPR-based assays. The strategies of integrating CRISPR technology with isothermal amplification techniques can be applied to the detection of various types of RNA molecules.

Preface

1. Part of the contents in sections 1, 1.1, 1.2, 1.4, 1.5, and 6.2 has been published in Feng, W.[Δ], Newbigging, A. M.[Δ], Tao, J.[Δ], Cao, Y.[Δ], Peng, H.[Δ], Le, C.[Δ], Wu, J., Pang, B., Li, J., Tyrrell, D. L., Zhang, H. and Le, X. C., CRISPR technology incorporating amplification strategies: molecular assays for nucleic acids, proteins, and small molecules. *Chem. Sci.* **2021,** *12* (13), 4683-4698.

Feng, Newbigging, Tao, Cao, Peng, and Le, contributed to data curation, formal analysis, visualization, validation, writing – original draft, and writing – review & editing. I wrote half of the first draft for sections "Fundamental features of CRIPSR-Cas systems" and "Incorporating CRISPR-Cas after nucleic acid amplification to improve the specificity of assays", and substantially revised the entire manuscript. Wu, and Pang, contributed to data curation, formal analysis, and writing a component of the original draft, review & editing. Juan Li, and D. Lorne Tyrrell, contributed to funding acquisition, resources, supervision, and writing – review & editing. Hongquan Zhang, and X. Chris Le contributed to conceptualization, data curation, formal analysis, funding acquisition, project administration, resources, supervision, writing – original draft, and writing – review & editing. This feature review is a product of the collaboration of four research groups led by Professors X. Chris Le, Juan Li, D. Lorne Tyrrell, and Hongquan Zhang. These four professors mentored their students and postdoctoral fellows who contributed jointly to this review paper.

2. Part of the content in section 1.5 has been published in Feng, W.[Δ], Newbigging, A. M.[Δ], Le, C.[Δ], Pang, B.[Δ], Peng, H.[Δ], Cao, Y., Wu, J., Abbas, G., Song, J., Wang, D.-B., Cui,

M., Tao, J., Tyrrell, D. L., Zhang, X.-E., Zhang, H. and Le, X. C., Molecular Diagnosis of COVID-19: Challenges and Research Needs. *Anal. Chem.* **2020,** *92* (15), 10196-10209.

Feng, Newbigging, and C. Le, contributed to data curation, formal analysis, visualization, Validation, writing – original draft, and writing – review & editing. I contributed to the first draft for the section "Isothermal Amplification Incorporated with CRISPR Technology", substantially rewrote around half of the manuscript and supporting information, and revised the entire manuscript and supporting information. Pang, Peng, Cao, Wu, Abbas, Song, Wang, Cui, and Tao were delegated to write the first draft of individual sections, and contributed to data curation, formal analysis, visualization, and manuscript review. Tyrrell contributed to resources, supervision, and writing – review & editing. X-E Zhang contributed to supervision, formal analysis, writing a component of the original draft, and review & editing. H Zhang, and XC Le contributed to conceptualization, data curation, formal analysis, funding acquisition, project administration, resources, supervision, writing – original draft, and writing – review & editing. Further permission related to the material excerpted should be directed to the ACS.

3. Chapter 5 has been published: Feng, W.[Δ], Peng, H.[Δ], Xu, J., Liu, Y., Pabbaraju, K., Tipples, G., Joyce, M. A., Saffran, H. A., Tyrrell, D. L., Babiuk, S., Zhang, H. and Le, X. C., Integrating Reverse Transcription Recombinase Polymerase Amplification with CRISPR Technology for the One-Tube Assay of RNA. *Anal. Chem.* **2021,** *93* (37), 12808-12816.

I completed the experiments together with Dr. Hanyong Peng, a postdoctoral fellow. Dr. Peng developed the assay for sensitive DNA detection, then identified the importance of RNase H for RT-RPA. We characterized the effect of RNase H. I further optimized and

characterized the performance of the RNA assay and applied this assay to the analysis of clinical samples, and collected relevant data for the manuscript. Xu and Liu contributed to RT-qPCR analysis of different genes. Pabbaraju, and Tipples contributed to RT-qPCR analysis of clinical samples. Joyce and Saffran helped with the preparation of viral RNA. I wrote the first draft of the manuscript and supplementary information and contributed to multiple rounds of editing. Co-authors helped with review and editing. Tyrrell, Babiuk, Zhang and Le are collaborating principal investigators (PIs), who contributed to funding acquisition, project administration, manuscript editing, and supervision.

4. Research on the detection of SARS-CoV-2 (Chapter 5) received ethics approval from the University of Alberta Health Research Ethics Board, project name “Development of rapid point-of-care tests”, protocol #00099788.

Acknowledgements

I would like to express my greatest gratitude to my supervisor, Dr. Chris Le, for all his guidance and support. I always enjoy discussing and writing with Dr. Le. His research and teaching abilities are admirable. His insights and questions motivate me to think deeply and comprehensively, and I always look forward to our next discussion. There is also a lot of teaching and mentoring that is imperceptible, in writing, communication, and mentoring younger scientists. My skills improved over time in the process of working with him. During the past five years, I have been excited to experience different parts of research work together with Dr. Le. I cherish all the opportunities I have had, and the sense of accomplishment has built up and made me enjoy doing research and become confident. There is still a lot to learn from Dr. Le.

I would also like to thank Dr. Hongquan Zhang and Dr. Michael Weinfeld for serving on my supervisory committee. I am glad to see that you are always curious about science and supporting me. I am also grateful for all the detailed guidance, training, and help from Dr. Hongquan Zhang and Dr. Hanyong Peng. It means a lot to me to continually have the opportunity to discuss with people who are knowledgeable and experienced.

My thanks to all the supportive people I have worked with in the Division of Analytical and Environmental Toxicology. Thank you to Dr. Xing-Fang Li for caring and continued support, Dr. Andrei Drabovich for helpful scientific questions and suggestions for my presentation and writing, Katerina Carastathis for helping with all sorts of paperwork and Xiufen Lu for helping with lots of orders and caring. Thank everyone who has taught me experiential, writing, exam, and presentation skills, Aleks, Michael, Yanming, Ashley,

Lindsay and many other scientists. Thank those who joined the group at a similar time to me and continued to help me in classes and life.

I thank Dr. Monika Keelan, and Dr. Jelena Holovati for their support as Graduate Coordinators, as well as Cheryl Titus, Lennora Crilov, and Barbara Thomson for their assistance.

I would also like to thank everyone who has reminded me to take breaks and enjoy nature. Thank you to family and friends who have continued to be understanding, encouraging and supportive during this time.

I would like to thank all of our collaborators for the research discussed in Chapter 5, from Alberta Precision Laboratories, Dr. Lorne Tyrrell's group, and Dr. Shawan Babiuk.

Thank you to all the funding agencies mentioned in my publications.

Table of Contents

Chapter 1. Introduction 1

1.1 Fundamental features of CRISPR-Cas systems that have been used for RNA detection . 3

1.2 Using CRISPR-Cas systems with *trans*-cleavage activity to recognize target nucleic acids and generate amplified detection signals 9

1.3 Enzyme kinetics of CRISPR-Cas12 and Cas13 systems and the limit of detection of CRISPR-based diagnostics 11

1.4 CRISPR technology incorporating isothermal amplification strategies for sensitive and specific nucleic acid detection 15

1.5 SARS-CoV-2 RNA detection and quickly advanced CRISPR techniques for this purpose 19

1.5.1 Molecular diagnosis of COVID-19 19

1.5.2 Advances in CRISPR technology for the detection of SARS-CoV-2 RNA 21

1.6 Rationale and the scope of this thesis 25

1.7 References 28

Chapter 2. microRNA detection at ambient temperature using CRISPR-LwaCas13a 44

2.1 Introduction 44

2.2 Experimental Section 45

2.2.1 Cas13a expression and purification 45

2.2.2 *In vitro* transcription of RNA 47

2.2.3 Optimization of the reaction composition for the best target recognition and signal generation 48

2.2.4 The performance of Cas13a-mediated RNA detection at different temperatures 49

2.2.5 Detection of microRNA-10b at ambient temperature 49

2.3 Results and Discussion 50

2.3.1 Expression, purification, and characterization of LwaCas13a and LbuCas13a .. 50

2.3.2 Detection of microRNA using CRISPR-Cas13a 53

2.3.3 The reaction composition for efficient microRNA recognition and high LwaCas13a *trans*-cleavage activity 54

2.3.4 Performance of microRNA detection within a wide range of temperatures 61

2.3.5 Sensitivity and specificity of the microRNA detection assay 64

2.4 Conclusion 69

2.5 References 70

Chapter 3. Effects of short target and spacer length on the activity of LwaCas13a and LbuCas13a 73

3.1 Introduction 73

3.2 Experimental Section 75

3.2.1 Production of protein and RNA 75

3.2.2 Characterizing the effect of the target RNA length on the *trans*-cleavage activity of Cas13a 77

3.2.3 Characterizing the effect of spacer length on the *trans*-cleavage activity of Cas13a 78

3.3 Results and Discussion 80

3.3.1 The effect of short target RNA length on the *trans*-cleavage activity of LwaCas13a 80

3.3.2 The effect of short spacer length on the *trans*-cleavage activity of LwaCas13a 85

3.3.3 LwaCas13a requires longer spacers and target RNA than LbuCas13a..... 87

3.3.4 Potential mechanism for the insufficient activation of LwaCas13a when using short RNA 88

3.4 Conclusion 91

3.5 References..... 93

Chapter 4. LwaCas13a and LbuCas13a have high *trans*-cleavage activity at ambient temperature upon activation 95

4.1 Introduction..... 95

4.2 Experimental Section..... 98

4.2.1 Cas13a expression and purification 98

4.2.2 Production of crRNA and target RNA 99

4.2.3 Comparing *trans*-cleavage activities using different activators at different temperatures 101

4.2.4 Comparing *trans*-cleavage activities with and without pre-annealing of crRNAs and targets 103

4.3 Results and Discussion 104

4.3.1 Design of experiments to study the *trans*-cleavage activity at different temperatures 104

4.3.2 *Trans*-cleavage activity of activated LwaCas13a has an optimal temperature around 27–32 °C regardless of the protospacer sequence composition 108

4.3.3 The optimal temperature of the *trans*-cleavage activity of activated Cas13a is independent of the structure of RNA activators 112

4.3.4 The optimal temperature of *trans*-cleavage activity is independent of the spacer length 117

4.3.5 The thermal behavior of the *trans*-cleavage activity of a second Cas13a, LbuCas13a 121

4.4 Conclusion 123

4.5 References 125

Chapter 5. Integrating Reverse Transcription Recombinase Polymerase Amplification with CRISPR Technology for One-Tube Assay of RNA 128

5.1 Introduction 128

5.2 Experimental Section 130

5.2.1 SARS-CoV-2 viral RNA 130

5.2.2 RT-RPA and Cas12a reactions in a single tube 133

5.2.3 Analysis of clinical samples for the S gene of SARS-CoV-2 RNA 133

5.3 Results and Discussion 134

5.3.1 Integration of reverse transcription (RT), recombinase polymerase amplification (RPA), and CRISPR-Cas12a detection in a single tube 134

5.3.2 Optimization of RPA-CRISPR-Cas12a in a single tube 136

5.3.3 Challenges and necessity for rapid initiation of the RPA reaction 140

5.3.4 Removal of the RNA template after reverse transcription significantly improves the performance of the single-tube RT-RPA-Cas12a assay 146

5.3.5 Single-tube RT-RPA-CRISPR-Cas12a assay for detection of SARS-CoV-2 RNA 153

5.3.6 Analysis of RNA extracted from respiratory swab clinical samples 160

5.4 Conclusion 163

5.5 References 164

Chapter 6. Summarizing Discussion and Future Directions for Research 170

6.1 Summarizing Discussion 170

6.2 Future Directions for Research 174

6.2.1 Further understanding of the activation and operation mechanism of CRISPR-Cas systems for better performance of CRISPR-based diagnostics 174

6.2.2 Utilizing the *trans*-cleavage activity for biosensing signal amplification in live cells 176

6.3 References 178

Bibliography 182

Appendix A. Additional information on techniques combining isothermal amplification and CRISPR-Cas systems for the detection of SARS-CoV-2 203

List of Tables

Table 1-1. Key features of each CRISPR-Cas system 8

Table 1-2. The Michaelis-Menten kinetics of Cas13a and Cas12a 13

Table 2-1. Target RNA and crRNA sequences 48

Table 2-2. Fluorescence signal amplification rate 66

Table 3-1. The sequence of target RNA and crRNA used in Chapter 3 76

Table 3-2. A comparison of the RNA length requirement of LwaCas13a and LbuCas13a .. 88

Table 3-3. The target-crRNA duplex melting temperatures (T_m) with different numbers of paired bases. 89

Table 4-1. crRNA and target sequences 100

Table 4-2. Activator RNA sequences and secondary structures 107

Table 5-1. Primers and probes for RT-PCR assay of the S gene and for *in vitro* RNA transcription. 131

Table 5-2. Primers and probes for RT-PCR assays of the RdRP gene and for *in vitro* RNA transcription 132

Table 5-3. Thermal cycling program for RT-qPCR. 132

Table A1. Techniques combining isothermal amplification and CRISPR-Cas systems with *trans*-cleavage activities for the detection of SARS-CoV-2 RNA 203

List of Figures

Figure 1-1. Fundamental components of CRISPR-Cas9, -Cas12a, -Cas12f, and -Cas13a systems. 6

Figure 1-2. Three representative nucleic acid detection platforms using the *trans*-cleavage activity of CRISPR-Cas12a and -Cas13a. 10

Figure 1-3. Techniques that use CRISPR-Cas systems to generate amplified signals from amplicons produced by nucleic acid amplification techniques. 18

Figure 1-4. Genome organization of SARS-CoV-2 and the relative positions of gene targets detected using seven reverse transcription polymerase chain reaction (RT-PCR) methods shared by the World Health Organization (WHO) as its in-house assays. 21

Figure 2-1. Representative SDS-PAGE gels of purified LwaCas13a (A) and LbuCas13a (B). 51

Figure 2-2. Characterization of the *trans*-cleavage activity of Cas13a (LwaCas13a). 53

Figure 2-3. Schematics of microRNA detection using CRISPR-Cas13a. 54

Figure 2-4. Significant reduction of sensitivity when switching target from long target ssRNA1 (161 nt) to short target microRNA-10b (23 nt) before optimization of reaction conditions. 55

Figure 2-5. Optimization of Cas13a concentration, crRNA concentration, and crRNA annealing. 56

Figure 2-6. Effect of the concentration of reporter on the signal generation facilitated by the *trans*-cleavage activity of the crRNA-Cas13a ribonucleoprotein. 58

Figure 2-7. Effect of Mg^{2+} on the *trans*-cleavage kinetics of Cas13a in the detection of microRNA-10b. 59
Figure 2-8. Effect of buffer pH and detergent concentration on the *trans*-cleavage activity and kinetics. 60
Figure 2-9. *Trans*-cleavage kinetics of LwaCas13a and LbuCas13a and fluorescence increase from the detection of miR-10b at different temperatures. 63
Figure 2-10. The sensitivity of microRNA-10b detection at ambient temperature. 65
Figure 2-11. A calibration curve of the fluorescence intensity in response to the concentration of fully cleaved RNA reporter (RNaseAlert). 66
Figure 2-12. Specificity of this miR-10b assay by comparing the detection of microRNA-10b to the detection of synthetic RNA sequences with single-nucleotide mismatches. 68

Figure 3-1. A comparison of the *trans*-cleavage activity of LwaCas13a in response to 23-nt microRNA-10b and an extended target. 81
Figure 3-2. Insufficient activation of LwaCas13a by targets shorter than 23 nt. 83
Figure 3-3. LwaCas13a activities in response to 23-nt target RNAs that form 19, 21, and 23-bp duplexes with crRNA. 84
Figure 3-4. Effect of the spacer length on the *trans*-cleavage activity of LwaCas13a. 86
Figure 3-5. Insufficient activation of LwaCas13a by targets shorter than 23 nt, even if the temperature was reduced for better crRNA-target binding. 90
Figure 3-6. Effect of the spacer length on the *trans*-cleavage activity of LbuCas13a. 91

Figure 4-1. A calibration curve of the fluorescence generation in response to the cleavage of RNA reporter (RNaseAlert) measured by StepOnePlus™ RT-PCR instrument (Applied Biosystems)..... 102

Figure 4-2. The *trans*-cleavage activity of Cas13a and the schematics of my study of its thermal behavior. 106

Figure 4-3. Delay in the initiation of *trans*-cleavage activity at low temperature suggests that low temperature (<23 °C) is not favorable for the formation of ribonucleoprotein. 108

Figure 4-4. LwaCas13a shows higher *trans*-cleavage activity at 27 °C than 37 °C in response to 2 activators with different nucleotide composition. 111

Figure 4-5. The effect of temperature on the *trans*-cleavage kinetics by LwaCas13a when using activator ssRNA1-161nt, and the reduction of the required temperature after the pre-annealing of crRNA and the target. 115

Figure 4-6. The effect of temperature on the *trans*-cleavage kinetics of LwaCas13a when using activator ssRNA1-33nt, with and without pre-annealing of crRNA and the target.. 117

Figure 4-7. The consistent effect of temperature on the *trans*-cleavage kinetics of LwaCas13a when using activator ssRNA3 together with spacers of different lengths. 119

Figure 4-8. The consistent effect of temperature on the *trans*-cleavage kinetics of LwaCas13a when using activator ssRNA2 together with spacers of different lengths. 121

Figure 4-9. The *trans*-cleavage kinetics of LbuCas13a at 17–42 °C..... 122

Figure 5-1. Schematics showing integration of reverse transcription (RT), recombinase polymerase amplification (RPA), and CRISPR-Cas12a-mediated fluorescence generation for isothermal (40 °C) single-tube detection of specific RNA. 135

Figure 5-2. RPA primers, CRISPR RNA (crRNA), and their target region in the Spike gene (S gene) of the SARS-CoV-2 genome. 137
Figure 5-3. Optimization of the concentrations of MgOAc and crRNA-Cas12a ribonucleoprotein (RNP) for the single-tube RPA-Cas12a assay. 138
Figure 5-4. Fluorescence intensity, measured over time, from the single-tube RPA-Cas12a assay for the detection of DNA sequence of the SARS-CoV-2 S gene, ranging from 5 copies to 10^6 copies. 139
Figure 5-5. Detection of fluorescence intensity and visualization of fluorescence color captured on a smartphone camera. 140
Figure 5-6. Detection of a specific S gene sequence of SARS-CoV-2 RNA using the one-tube RT-PRA-Cas12 assay. 141
Figure 5-7. SYBR Green detection of the RPA reaction mixtures containing either 100 copies of the target DNA or no target DNA. 142
Figure 5-8. The stability of crRNA-Cas12a ribonucleoprotein (RNP) activity in RPA reaction solution, measured by fluorescence intensity of the reporter (A) and initial cleavage rate of the *trans*-cleavage activity of crRNA-Cas12a RNP (B). 144
Figure 5-9. Activity of crRNA-Cas12a RNP in the RPA reaction solution supplemented with 100 copies of DNA target. 145
Figure 5-10. Comparison of reverse transcriptases and supplementation of RNase H in the detection of the S gene of SARS-CoV-2 RNA using the integrated RT-RPA-Cas12a assay. 148
Figure 5-11. Fluorescence produced from the *trans*-cleavage of ssDNA reporter by Cas12a RNP in the presence or absence of RNase H. 149

Figure 5-12. RNase H shortens the time for positive detection of the RNA targets in both the S gene and RdRp gene. 151
Figure 5-13. RPA primers, CRISPR RNA (crRNA) sets, and their target regions in the RdRP gene of SARS-CoV-2. 153
Figure 5-14. Comparison of a two-step (A) with a one-step (B) RT-RPA-Cas12a assay for the S gene of SARS-CoV-2 RNA. 155
Figure 5-15. Detection of the S gene of SARS-CoV-2 RNA using the single-tube RT-RPA-Cas12a assay. 156
Figure 5-16. Reproducibility of the single-tube RT-RPA-Cas12a assay for low levels of viral RNA. 157
Figure 5-17. Specificity of the single-tube RT-RPA-Cas12a assay for SARS-CoV-2 over SARS-CoV and MERS-CoV. 159
Figure 5-18. Results from the analysis of varying concentrations of SARS-CoV-2 S gene using RT-qPCR and the single-tube RT-RPA-Cas12a assay. 160
Figure 5-19. Results from the RT-RPA-Cas12a analysis of 46 clinical upper respiratory swab samples using real-time fluorescence detection (A and B) and end-point (90 min) visualization (C). 161
Figure 5-20. Fluorescence measurements from the analyses of 46 clinical samples (upper respiratory swabs samples) using the single-tube RT-RPA-Cas12a assay. 162

List of Abbreviations

bp	base pair
Cas	CRISPR-associated
cDNA	complementary DNA
COVID-19	coronavirus disease of 2019
CRISPR	clustered regularly interspaced short palindromic repeats
crRNA	CRISPR RNA
DETECTR	DNA Endonuclease-Targeted CRISPR Trans Reporter
dsDNA	double-stranded deoxyribonucleic acid
DR	direct repeat
E gene	envelope protein gene
EUA	emergency use authorization
FAM	fluorescein amidite
HEPN	"higher eukaryotes and prokaryotes nucleotide" binding domains of Cas13a that mediate the cleavage of ssRNA
miRNA	microRNA
HUDSON	Heat Unextracted Diagnostic Samples to Obliterate Nucleases
IPTG	isopropyl β-D-1-thiogalactopyranoside
IVT	*in vitro* transcription
LAMP	loop-mediated isothermal amplification
LOD	limit of detection
LbuCas13a	CRISPR-associated protein 13a from *Leptotrichia buccalis*

LwaCas13a	CRISPR-associated protein 13a from *Leptotrichia wadei*
N gene	nucleocapsid protein gene
nt	nucleotide
NTC	non-target controls
PAM	protospacer adjacent motif
PAMmer	PAM-presenting oligonucleotides
RT-qPCR	quantitative reverse transcription-polymerase chain reaction or real-time reverse transcription-polymerase chain reaction
PFS	protospacer flanking site
PMSF	phenylmethylsulfonyl fluoride
POC	Point-of-care
RdRp	RNA-dependent RNA polymerase
RPA	recombinase polymerase amplification
RNP	ribonucleoprotein
RT	reverse transcription/transcriptase
S gene	Spike protein gene
SARS-CoV-2	severe acute respiratory syndrome coronavirus 2
sgRNA	single-guide RNA
SHERLOCK	Specific High-Sensitivity Enzymatic Reporter UnLOCKing
SNP	single-nucleotide polymorphism
ssDNA	single-stranded deoxyribonucleic acid
ssRNA	single-stranded ribonucleic acid
TCEP	Tris (2-carboxyethyl) phosphine

T_m	melting temperature
tracrRNA	*trans*-activating CRISPR RNA
VOC	variant of concern

Chapter 1. Introduction*

Clustered Regularly Interspaced Short Palindromic Repeats (CRISPR) systems are naturally existing systems in bacteria and archaea that function as the acquired (adaptive) immunity against phages.[1] Procaryotes integrate a partial phage gene as a spacer into the CRISPR array in the genome[1] and prevent the proliferation of phages by producing CRISPR RNA-Cas ribonuclease effectors to cleave phage DNA or RNA. The spacer within CRISPR RNA guides Cas proteins to the complementary phage nucleic acid for cleavage.[1] Discovered CRISPR-Cas systems have diverse functions and have been classified into two classes and six types.[1] Each of the Class 2 systems uses a single Cas protein for nucleic acid targeting and cleavage, specifically, Cas9 (type II), Cas12 (type V), or Cas13 (type VI).[1]

The RNA-guided nucleic acid targeting and cleavage function of CRISPR-associate (Cas) proteins make them advantageous for genome and transcriptome editing.[2-6] Targeting a particular gene sequence can be achieved by using a corresponding crRNA or a single-guide RNA (sgRNA) designed to recognize the gene site.[2-6] Upon target binding, Cas9 and Cas12 ribonucleoproteins cleave the target DNA and generate a double-strand break.[2-6] Cas13 recognizes and cleaves target RNA. Previous genome editing technologies require nucleic acid binding proteins, and each target site requires one fusion protein engineered according to

* Part of the contents in this chapter has been published in:
1. Feng, W. Δ, Newbigging, A. M. Δ, Tao, J. Δ, Cao, Y. Δ, Peng, H. Δ, Le, C. Δ, Wu, J., Pang, B., Li, J., Tyrrell, D. L., Zhang, H. and Le, X. C., CRISPR technology incorporating amplification strategies: molecular assays for nucleic acids, proteins, and small molecules. *Chem. Sci.* **2021,** *12* (13), 4683−4698.
2. Feng, W. Δ, Newbigging, A. M. Δ, Le, C. Δ, Pang, B. Δ, Peng, H. Δ, Cao, Y., Wu, J., Abbas, G., Song, J., Wang, D.-B., Cui, M., Tao, J., Tyrrell, D. L., Zhang, X.-E., Zhang, H. and Le, X. C., Molecular diagnosis of COVID-19: Challenges and research needs. *Anal. Chem.* **2020,** *92* (15), 10196−10209.

the sequence, so the applicability is limited. Since the elucidation of the function and mechanism of the CRISPR-Cas9 system, it has been extensively used for gene editing in different organisms and has transformed the field of genome editing.[2-6]

CRISPR technology has also been used for molecular detection of diverse targets, ranging from nucleic acids to viruses.[7-11] Detection and quantification of disease-related nucleic acids, such as human biomarkers and pathogens genes, are essential for biological studies and molecular diagnostics. Accurate nucleic acid quantification relies on real-time quantitative polymerase chain reaction (qPCR). Isothermal nucleic acid amplification techniques have also been developed for simple, rapid nucleic acid detection. Nucleic acid sequencing is required for the identification of new pathogens and mutations within nucleic acids. Incorporating CRISPR-Cas systems with various detection platforms and nucleic acid amplification strategies enables the generation of amplified detection signals, enrichment of low-abundance molecular targets, improvements in analytical specificity and sensitivity, and development of point-of-care (POC) diagnostic techniques. These systems take advantage of various Cas proteins for their particular features, including RNA-guided endonuclease activity, sequence-specific recognition and cleavage, and multiple turnover *trans*-cleavage activity of Cas12 and Cas13. Successful integrations of CRISPR technology with nucleic acid amplification techniques have resulted in highly sensitive and rapid detection of SARS-CoV-2, the causative agent of COVID-19.

CRISPR-Cas technologies continue to revolutionize analytical applications, and their full potential has yet to be reached. The discovery and modification of CRISPR-Cas systems are ongoing to meet the need in performance. Meanwhile, the application of CRISPR-based detection is expanding to nucleic acids with distinct features in length, modification, and

origin, as well as to small molecules and proteins.[12] Further advances require a better understanding of the operation mechanism and preference of various CRISPR-Cas systems.

1.1 Fundamental features of CRISPR-Cas systems that have been used for RNA detection

CRISPR-Cas systems generally function as RNA-guided endonucleases. crRNA guides Cas proteins to specific nucleic acid sequences, where hybridization initiates the nuclease activity of Cas proteins, resulting in nucleic acid cleavage.[2] Some systems, such as those that use Cas9, require a *trans*-activating CRISPR RNA (tracrRNA), which binds to crRNA, forming an RNA hybrid.[2, 9, 13] The crRNA and tracrRNA can be linked into a single guide RNA (sgRNA).[2] Many CRISPR-Cas systems have been discovered and characterized with each exhibiting distinct cleavage functions and activities, thus making CRISPR technology stand out for diverse applications. **Figure 1-1** shows the components of the four CRISPR-Cas systems, and **Table 1-1** summarizes their unique features that have been used for developing analytical techniques.

Cas9 is well studied for its programmable endonuclease activity.[2, 5, 14-16] The sgRNA of CRISPR-Cas9 systems contains a hairpin-rich region that binds to Cas9 and a 20-nucleotide "spacer" region that binds with the complementary "protospacer" region in the target strand of a dsDNA duplex. Binding between the sgRNA and the DNA target brings Cas9 into close proximity to the target (**Figure 1-1A**). The His-Asn-His (HNH) domain of Cas9 cleaves the strand that is complementary to sgRNA (target strand), and the RuvC domain of Cas9 cleaves the other strand of the dsDNA (non-target strand).[17] The combined endonuclease activities of the HNH and RuvC domains achieve the cleavage of both strands of the dsDNA of interest,

leaving behind two blunt ends or a "protospacer adjacent motif" (PAM)-distal 5' overhang.[18] Cas9 can target innumerable DNA sequences; the only requirement is the presence of a "protospacer adjacent motif" (PAM) located 3-4 nucleotides (nt) downstream from the protospacer.[3, 19] Unlike restriction endonucleases, CRISPR-Cas9 systems cleave the specific sites that are pre-determined by specific sgRNA sequences. CRISPR-Cas9 systems can also be programmed to target single-stranded DNA (ssDNA) or single-stranded RNA (ssRNA) by introducing a PAM-presenting oligonucleotides (PAMmer) sequence. A PAMmer is typically designed to hybridize with the target strand and form a pseudo-PAM region to activate Cas9.[20-21]

When a single amino acid in either the RuvC (Cas9D10A) or HNH (Cas9H840A) domain is mutated, Cas9 behaves as a nickase (nCas9); in the first case, it nicks only the target strand of a dsDNA duplex, and in the second case, it nicks only the non-target strand.[2, 22-23] Mutating both RuvC and HNH domains produces deactivated Cas9 (dCas9), which is still guided by sgRNA to bind to nucleic acid targets, but does not cleave them.[24]

Cas12, including the well-known subtypes Cas12a and Cas12f (previously referred to as Cas14),[1, 25] lacks the HNH domain, but is still able to achieve PAM-dependent cleavage of dsDNA with its RuvC domain alone (**Figure 1-1B**).[9, 26-27] Cleavage of both the target strand and its complementary non-target strand by Cas12a produces 5–7 nt overhangs because the cleavage sites on the two strands are staggered. Cas12 also targets and cleaves ssDNA, but does not require a PAM recognition.[26] (**Figure 1-1C**) Distinctly, Cas12 cleaves not only the target DNA strand (*cis*-cleavage), Cas12 also exhibits *trans*-cleavage activity (also referred to as collateral cleavage), which cleaves ssDNA indiscriminately.[9, 28-30] Another important feature of Cas12 is its multiple-turnover nuclease activity, which can be harnessed for the

amplified detection of nucleic acid targets, including products of other nucleic acid amplification techniques. Although less is known about Cas12f, existing evidence has shown two promising features: Cas12f has a smaller size compared to Cas9 and other Cas12 subtypes (**Table 1-1**), making Cas12f useful for imaging applications within cells. Cas12f also has better specificity toward ssDNA activation than Cas12a; thus, Cas12f has been used to distinguish single nucleotide differences at certain protospacer sites.[30] In addition, RNA can also activate the *trans*-cleavage of Cas14a1 to cleave ssDNA reporter, which broadened the application of Cas14 for RNA analyses.[31]

Compared to recombinases and nucleases (e.g., nicking and restriction endonucleases) that have been used in nucleic acid amplification techniques, CRISPR-Cas systems have distinct advantages for improving nucleic acid detection and molecular diagnostics. Both Cas9 and Cas12 enable the unwinding of specific dsDNA without the need for single-stranded binding proteins (SSB) that are otherwise required for unwinding dsDNA when recombinases are used. This unwinding ability of Cas12 facilitates the imaging of specific dsDNA sequences in living cells[32-33] and the development of new fluorescence in-situ hybridization (FISH) techniques for localized detection of nucleic acids.[34] The CRISPR-Cas9 and -Cas12 systems allow cleavage of both strands or a single strand of different dsDNA sequences by simply altering crRNA, whereas nicking and restriction endonucleases only work on dsDNA sequences containing or adjacent to specific recognition sites. Consequently, the CRISPR-Cas9 and -Cas12 systems can potentially replace nicking or restriction endonucleases for nucleic acid amplification with improved performance.

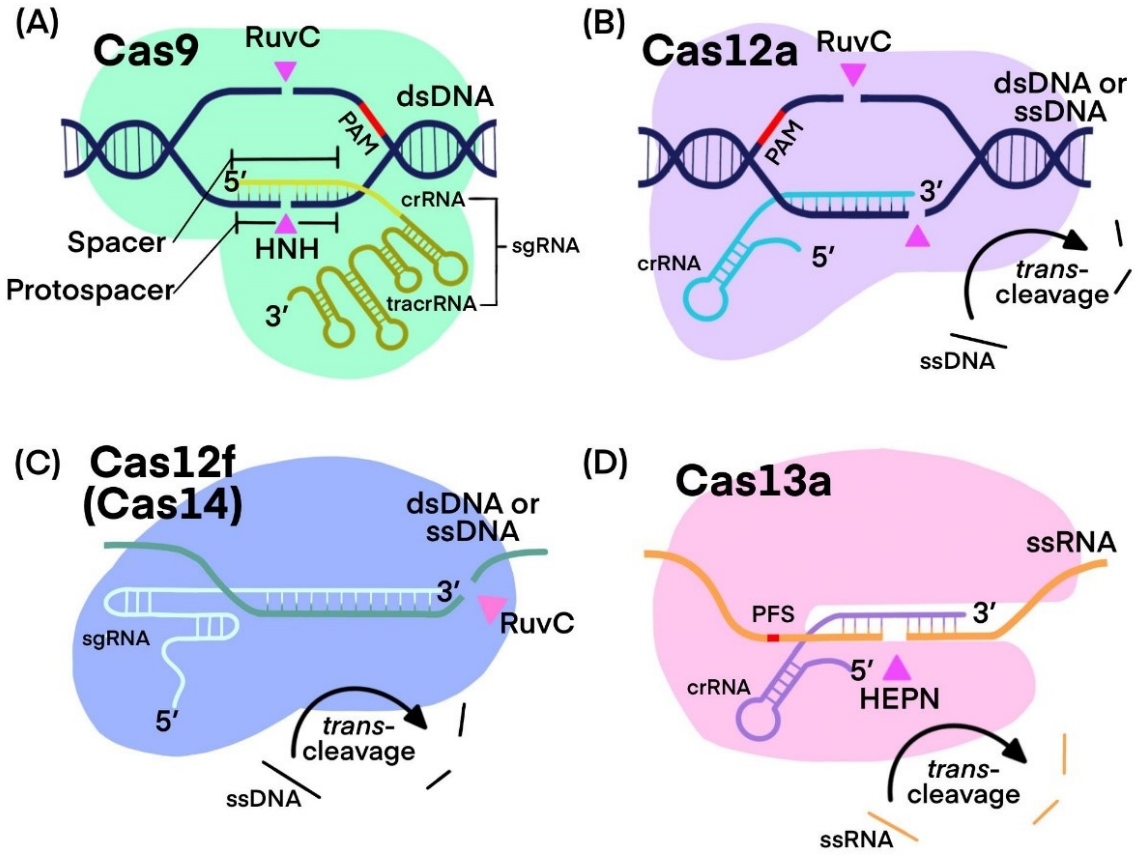

Figure 1-1. Fundamental components of CRISPR-Cas9, -Cas12a, -Cas12f, and -Cas13a systems. Pink triangles indicate *cis*-cleavage sites. Reproduced from Ref. [12] with permission from the Royal Society of Chemistry.

CRISPR-Cas13 systems target and cleave ssRNA. After Cas13 binds to a target ssRNA, its two domains, called HEPN (higher eukaryotes and prokaryotes nucleotide-binding) domains, are brought together through a conformational change to initiate *cis*- and *trans*-cleavage activities.[35-37] (**Figure 1-1D**) Whereas Cas9 requires PAM, Cas13a and Cas13b proteins prefer a specific nucleotide next to the 3' end of the protospacer, called the

protospacer flanking site (PFS).[13, 36] Cas13 cannot be used as a nicking enzyme because the cleavage site of Cas13 on its target is not fixed, and multiple sites on one target can be cleaved.[38] CRISPR-Cas13 systems exhibit *trans*-cleavage activity that is activated by a specific target, and thus have been widely used as molecular switches.

Although most Cas12 and Cas13 systems can tolerate mismatches between spacer and target strands, crRNA or gRNA can be modified to improve the specificity of CRISPR-based detection. For example, single-nucleotide specificity has been achieved for nucleic acid detection by introducing a synthetic mismatch between crRNA and target.[28, 39] However, the activity and specificity of Cas systems vary among different originating species and target sites. Systematic optimization of crRNA may be required when an existing technique is applied to different targets.

Table 1-1. Key features of each CRISPR-Cas system

	Cas9	Cas12	Cas 12f (Cas14)	Cas13
Representative subtypes, homologs, and /or variants	Deactivated Cas 9 (dCas9) Cas 9 nickase, (nCas9)**:** Cas9D10A, and Cas9H840A	Cas12a (Cpf 1): *Lachnospiraceae bacterium* Cas12a, LbCas12a Cas12b: *Alicyclobacillus acidiphilus* Cas12b, AapCas12b, *Alicyclobacillus acidoterrestris* Cas12b, AacCas12b	Cas14a	Cas13a (C2c2): *Leptotrichia buccalis* Cas13a, LbuCas13a, *Leptotrichia wadei* Cas13a, LwaCas13a Cas13b
Size (according to Uniprot)	~1400 amino acids (aa) (*Streptococcus pyogenes* Cas 9, SpCas9)	~1300 aa (LbCas12a)	400-700 aa	~1160 aa (LbuCas13a)
Target (activator)	dsDNA [2] ssDNA and ssRNA if PAMmer is provided [20-21] ssRNA [40]	ssDNA dsDNA[9]	ssDNA dsDNA [25] ssRNA (Cas14a1) [31]	ssRNA[7, 41]
Commonly used spacer length	20 nucleotide (nt) [42]	20 nt [9]	20 nt [30]	20 nt [43] or 28 nt [7]
***Cis*-cleavage products of dsDNA**	Blunt ends or PAM-distal 5' overhang [2, 18]	For dsDNA, the sticky end contains a 5–7 nt overhang [9]	Sticky end[34]	Not applicable
Specificity	The 6–8 nt near PAM are more specific than other locations; [42] Mismatch in PAM region significantly impairs the activity of SpCas9. [2]	For dsDNA, 4–6 nt at the 3′ end of crRNA is less specific than other locations;[44] Cannot achieve single nucleotide specificity for ssDNA target [30]	Seed region is more specific than other locations in sgRNA [30]	The use of a synthetic mismatch in crRNA results in a single-nucleotide specificity [7]
***Trans*-cleavage substrates**	Not applicable	ssDNA [9]	ssDNA [30]	ssRNA[13, 41]

1.2 Using CRISPR-Cas systems with *trans*-cleavage activity to recognize target nucleic acids and generate amplified detection signals

The *trans*-cleavage activity of Cas12 and Cas13 is turned on upon the recognition of a specific nucleic acid. This feature makes Cas12 and Cas13 useful for the detection of nucleic acids. Cas12 targets DNA, while Cas13 recognizes RNA and has been used for the detection of different types of RNA, including pathogen RNA[43], microRNA[45], and N^1-methyladenosine.[46] When detecting different targets, a crRNA can be designed to have its spacer region complementary to part of the target DNA or RNA, so that the crRNA-Cas ribonucleoprotein (RNP) complexes specifically recognize targets of interest.

The *trans*-cleavage activity has been used to generate amplified signals. Functionalized single-stranded DNA (ssDNA) is often used as a reporter for Cas12, and ssRNA is often used for Cas13. As the *trans*-cleavage is non-specific, once activated by the target, Cas proteins cleave the reporter and generate signals. Each activated Cas protein cleaves multiple reporters and thus produces amplified signals. For fluorescence detection, the reporters are labeled with a fluorophore and a quencher, and the Cas cleavage of reporters removes the quencher from the fluorophore and restores the fluorescence (**Figure 1-2A**).[9, 38, 47] For electrochemical detection, one end of the reporters is labeled with redox-reactive molecules, and the other end is attached to an electrode surface.[48-49] Cas proteins cleave reporters and release the redox-reactive molecules, which disrupt electron transfer near the electrode and thus provide a measurable electrochemical signal change (**Figure 1-2B**). For hydrogel-based detection, ssDNA serve as linkers of hydrogel polymers. The cleavage of ssDNA by Cas12 changes the properties of hydrogel and results in permeability change. Such changes can produce

measurable signals using dyes together with the hydrogel (**Figure 1-2C**).[50] The ssDNA linker can also be used to link nanoparticles and control the movement of nanoparticles.[51]

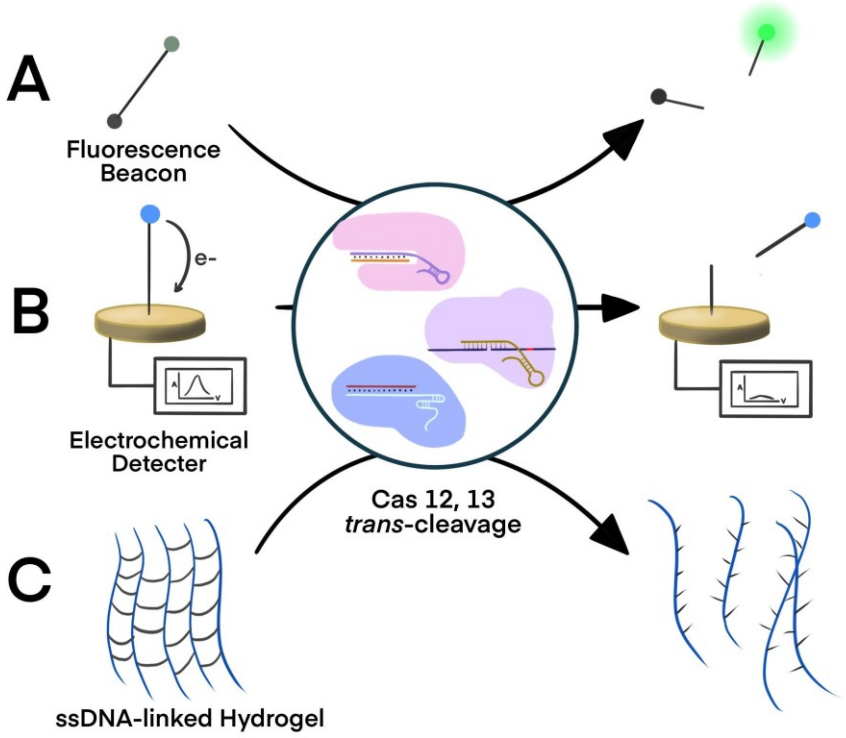

Figure 1-2. Three representative nucleic acid detection platforms using the *trans*-cleavage activity of CRISPR-Cas12a and -Cas13a. *Trans*-cleavage of ssDNA or ssRNA linker built into (A): a fluorophore and quencher pair,[45-46] (B): a redox-reactive molecule and electrode,[48-49] or (C): hydrogel.[50] Reproduced from Ref.[12] with permission from the Royal Society of Chemistry.

1.3 Enzyme kinetics of CRISPR-Cas12 and Cas13 systems and the limit of detection of CRISPR-based diagnostics

The kinetics of *trans*-cleavage determines the signal amplification rate and thus the analytical sensitivity of CRISPR-based assays, especially when the CRISPR-Cas system is not coupled with other amplification techniques. However, as Ramachandran and Santiago[52] reported, early characterizations of the kinetics of *trans*-cleavage activity have overestimated it because of calculation errors.[9, 53-55] Some authors have corrected their kinetics data.[9, 53-55] I have summarized the updated data and the later reported kinetics of the commonly used LbuCas13a and LbCas12a in **Table 1-2**, including the data from Ramachandran and Santiago's experiments[52]. LbCas12a is the Cas12a homolog most used for DNA detection. LbuCas13a and LwaCas13a enzymes are the ones most used for RNA detection. LbuCas13a has the highest *trans*-cleavage activity among several tested Cas13a homologs[56]. LbuCas13a generated measurable *trans*-cleavage activity in response to fM levels of ssRNA activator, followed by LwaCas13a which can generate measurable signals in response to pM levels of activators.[56]

These analyses are based on Michaelis-Menten kinetics which considers the enzyme-substrate binding and the cleavage of substrates as two individual reactions and provides the equilibrium constant of the binding reaction (K_M) and the rate constant of the cleavage reaction (k_{cat}) (**Equation 1-1** and **Equation 1-2**). The turnover number (k_{cat}) is the maximum number of substrates cleaved by one activated Cas enzyme in one second if the substrates are present in an unlimited amount. The turnover number is calculated using **Equation 1-1** and **Equation 1-2**. **Equation 1-1** is used to calculate the maximum cleavage velocity (V_{max}) by measuring the initial cleavage velocity (V_{int}) of reactions with a fixed concentration of enzyme

([E]) and gradient concentrations of substrates ([S]) (in excess amount). Then the k_{cat} is calculated by dividing the maximum velocity (V_{max}) by the fixed concentration of enzyme ([E]) (**Equation 1-2).** K_M represents the concentration of substrate when the initial velocity (V_{int}) is half of the maximum velocity (V_{max}), and also the disassociation constant of the RNP-reporter complex. k_{cat}/K_M is the catalytic efficiency that considers the rate of both the enzyme-substrate binding and the cleavage process.

$$V_{int} = \frac{V_{max}[S]}{K_M + [S]} \qquad \text{Equation 1-1}$$

$$k_{cat} = \frac{V_{max}}{[E]} \qquad \text{Equation 1-2}$$

Several groups have measured the kinetics of LbCas12a, and the reported k_{cat} ranges from 0.07 s^{-1} to 17 s^{-1}.[9, 52-53, 57] Although initially reporting a turnover number as high as 1250/s,[8] Chen et al.[55] corrected the turnover number of LbCas12a to be 17/s. The turnover number 1250/s was incorrect because the fluorescence generation rate (arbitrary unit/s) was directly used as the initial cleavage rate. The correct process is to convert the fluorescence generation rate to the reporter cleavage rate (M/s) by using a calibration curve showing the amount of fluorescence generated in response to the complete cleavage of reporters in different concentrations. The variation in rate constants of the same enzyme could be caused by the accuracy or the various conditions of measurement. In addition to subtypes/homologs of Cas[56], the sequence of crRNA, the choice of the target site, reporter type[57], reaction temperature, and co-factor concentration also contribute to the difference in kinetics.

The turnover number of LbuCas13a measured by Nalefski et al.[57] using Michaelis-Menten kinetics is around 12–320/s, higher than the turnover number (k_{cat}) of LbCas12a (1–

3 s^{-1}) measured by the same group (**Table 1-2**). The binding between the ssRNA substrate and activated Cas13a is moderate, with a K_M of hundreds to one thousand nM. It is not as strong as that of LbCas12a, according to multiple reports on LbCas12a. The catalytic efficiency (k_{cat}/K_M) of Cas13a is at a similar level to that of Cas12a, around 10^7 M^{-1} s^{-1}.

Table 1-2. The Michaelis-Menten kinetics of Cas13a and Cas12a

Ref.	Cas	Target	Reporter	k_{cat} (s^{-1})	K_M (nM)	k_{cat}/K_M (M^{-1} s^{-1})
Chen et al. [9, 53]	LbCas12a	ssDNA dsDNA	DNaseAlert	3 17	6.2×10^2 1.01×10^3	5.0×10^6 1.7×10^7
Ramach-andran et al. [52]	LbCas12a	ssDNA dsDNA	TTATTATT	0.07–0.09	96–274	10^5–10^6
Nalefski et al. [57]	LbCas12a	dsDNA 1	C_{10} C_{20} DNaseAlert	2.77 2.26 1.30	28 28 26	9.8×10^7 8.0×10^7 5.1×10^7
		dsDNA 2	C_{10} C_{20} DNaseAlert	3.83 2.28 1.02	35 18 23	1.1×10^8 1.3×10^8 4.4×10^7
Nalefski et al. [57]	LbuCas13a	ssRNA1	U_{10} U_{20} RNaseAlert	>12 16.7 27.1	>1000 760 294	1.03×10^7 2.2×10^7 9.2×10^7
		ssRNA3	U_{10} U_{20} RNaseAlert	320 273 17.1	2230 1500 101	1.43×10^8 1.82×10^8 1.7×10^8

The turnover number (k_{cat}) indicates the maximum signal amplification rate. The lower theoretical limit of detection can be estimated by dividing the concentration of signal molecule required for the detector to give a positive signal by the maximum signal amplification fold in a certain time period. Of course, this theoretical lower limit cannot be reached.

The difference in the *trans*-cleavage activity and the limit of detection caused by the choice of target site has been constantly observed, yet the underlying mechanism is not clear. Fozouni et al.[43] tested different crRNA for the detection of the N gene of SARS-CoV-2. At a target concentration of 2.89×10^5 copies/μL, 12 crRNA of LbuCas13a with different spacers showed distinct performance: some generated very high signals, yet some of the crRNA could not facilitate Cas13a activation. I suppose this is because of the effect of the target site on either the RNP-target binding process or the *trans*-cleavage activity.

Although the mechanism is not clear, there are some strategies that aid in the choice of the target site for high *trans*-cleavage activity. For example, "ADAPT" (Activity-informed Design of All-inclusive Patrolling of Targets) is a model-based, automatic integrated tool for the design of crRNA to achieve good performance of CRISPR-based diagnostics.[58] It predicts crRNA that has a high diagnostic signal, which is achieved by screening over 19,000 crRNA-target pairs and training a deep neural network. ADAPT also analyzes related viral genomes to ensure the sensitivity and specificity of assays.

The limit of detection has been directly characterized by testing serially diluted targets. When using only Cas13a for signal amplification, 10–1000 fM RNA molecules (10^5–10^7 copies/reaction) in each reaction have been successfully detected, and the sensitivity relies highly on the choice of target site/sequence.[7, 43] Recently, Fozouni et al.[43] reported successful detection of 270 copies of SARS-CoV-2 RNA genome per μL and 100 copies of *in vitro* prepared partial genome per μL, by targeting two well-chosen sites in the RNA at the same time and using a sensitive fluorescence detector. Unfortunately, to achieve a sensitivity down to a few dozen copies of pathogen RNA per specimen, an initial nucleic acid amplification of target RNA is required. [59-60]

1.4 CRISPR technology incorporating isothermal amplification strategies for sensitive and specific nucleic acid detection

The *trans*-cleavage activity of Cas12 and Cas13 has been used to detect amplification products (amplicons) of various nucleic acid amplification techniques. Integrating a CRISPR-Cas system after nucleic acid amplification improves the nucleic acid detection and achieves three main benefits. First, CRISPR-Cas systems recognize specific sequences of amplicons and differentiate the specific amplicons from byproducts of amplification reactions, thereby improving the specificity. Second, the multiple turnover *trans*-cleavage activity of Cas12 and Cas13 leads to repeated cleavage of nucleic acid signaling reporters, generating amplified readout signals for detection, thus improving sensitivity. Third, CRISPR-Cas systems facilitate the generation of diverse readout signals, broadening applicability.

The recognition of specific sequences by CRISPR-Cas acts as a confirmation that the intended sequences were amplified and detected. In one example, Nucleic Acid Sequence-Based Amplification (NASBA)[61] was combined with CRISPR-Cas9, resulting in a NASBA-CRISPR Cleavage assay. The requirement of Cas9 for its target sequence to contain a PAM region was used to distinguish between American and African strains of Zika virus (ZIKV) (**Figure 1-3A**).[62] After amplification using NASBA, the amplicons of American ZIKV contained a PAM region and permitted Cas9-mediated cleavage, while the amplicons of the African ZIKV without PAM remained uncut. The intact amplicon of the African ZIKV interacted with a subsequent sensing system to induce an observable color change. Thus, two strains differing by one nucleotide in the PAM region were differentiated.

Cas proteins with switchable *trans*-cleavage activity can be used to generate amplified signals after isothermal amplification of a specific target molecule. This strategy is exemplified in SHERLOCK (Specific High-Sensitivity Enzymatic Reporter UnLOCKing), facilitated by CRISPR-Cas13. Target DNA or RNA was amplified by recombinase polymerase amplification (RPA) or reverse transcription (RT) RPA[63], respectively. RPA was chosen because it is highly sensitive, rapid, and has an operation temperature (37–42 °C) compatible with that of Cas13 (~37 °C). After RPA, amplicons were transcribed into ssRNA by T7 polymerase. The amplified ssRNA product initiated CRISPR-Cas13a *trans*-cleavage activity and generated an amplified fluorescence signal for detection (**Figure 1-3B**).[7] A sample preparation technique, known as Heat Unextracted Diagnostic Samples to Obliterate Nucleases (HUDSON), has been developed to be paired with SHERLOCK.[64] The HUDSON-SHERLOCK assay was able to detect Zika and Dengue viruses in patients' urine and saliva samples at an equivalent nucleic acid concentration as low as 1 copy/μL. Multiple nucleic acids have also been analyzed simultaneously using the SHERLOCK platform by taking advantage of the preferential cleavage activity of Cas13a and Cas13b orthologs for various dinucleotide motifs at their respective cleavage sites.[39] The different CRISPR-Cas13 orthologs could then be paired with pre-designed reporters. The reporters consisted of each of the orthologs' preferred dinucleotide motifs and different fluorophore-quencher pairs. For example, in the same reaction solution, LwaCas13a cleaved reporters for detecting Zika virus, which consisted of an adenine-uracil site and TEX red fluorescence dye, and CcaCas13b cleaved reporters containing a uracil-adenine site and Cy5 far-red fluorescence dye for the detection of Dengue virus.

A similar strategy to SHERLOCK was developed, except using CRISPR-Cas12 instead of CRISPR-Cas13. Because Cas12 targets DNA, the DNA amplicons can be directly detected without the need for additional transcription (**Figure 1-3C**). An RPA-Cas12a detection platform, termed DNA Endonuclease-Targeted CRISPR Trans Reporter (DETECTR), was able to identify viral strains from DNA extracted from patient samples. [9]

A DETECTR technique using the Cas14a (Cas12f) protein was able to discriminate single nucleotide polymorphisms (SNPs) in HERC2, a gene involved in eye color.[30] (**Figure 1-3E**) The CRISPR-Cas14a (Cas12f) system requires full complementarity in the seed region of sgRNA, a feature considered for achieving single nucleotide specificity. The SNPs of the HERC2 gene residing in the seed region in the middle of the protospacer, as well as SNPs within the PAM region, completely deactivated Cas14a.[30] Due to the single nucleotide specificity in the seed region, the Cas14a-DETECTR technique successfully distinguished the SNP corresponding to blue eyes from that of brown eyes.

Other nucleic acid amplification techniques have also been paired with CRISPR-Cas systems. For example, a technique called one-HOur Low-cost Multipurpose highly Efficient System (HOLMES) used PCR to amplify target nucleic acids and detected the amplified products using a CRISPR-Cas12a system (**Figure 1-3D**).[65] HOLMES version 2 detected amplicons from PCR and loop-mediated isothermal amplification (LAMP). However, because the nucleic acid target did not have a suitable PAM region nearby, HOLMES version 2 used two strategies. First, because ssDNA activation of Cas12 is PAM independent, asymmetric PCR was used to generate ssDNA amplicons to avoid the requirement of PAM. Second, since amplicons from LAMP were dsDNA, PAM sequences were introduced through careful design of primers. Both ssDNA and dsDNA amplicons initiated the *trans*-cleavage activity of Cas12a

for detection. The PCR amplification and CRISPR-Cas12a detection steps must be conducted separately because the CRISPR-Cas12a system is inactive at the denaturation temperature (95 °C) used during PCR. Typical reaction temperatures for LAMP and RT-LAMP (60-65 °C) [66] could be tolerated by Cas12b (>40 °C). Therefore, incorporating LAMP or RT-LAMP with CRISPR-Cas12b has enabled isothermal amplification and signal generation to occur in one procedural step.[67]

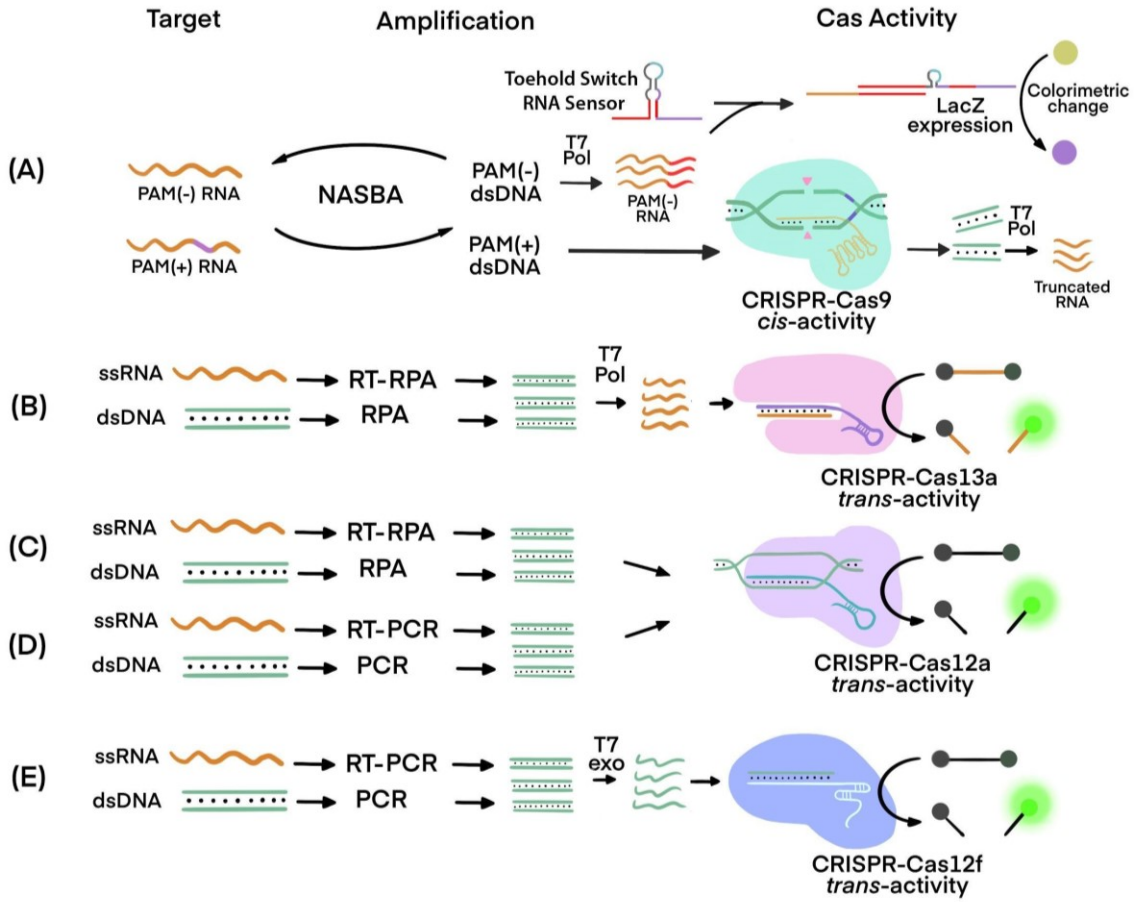

Figure 1-3. Techniques that use CRISPR-Cas systems to generate amplified signals from amplicons produced by nucleic acid amplification techniques. (A): Nucleic Acid Sequence-Based Amplification CRISPR Cleavage (NASBA-CC) followed by CRISPR-Cas9.

A difference in the presence or absence of a PAM sequence in the viral RNA was used to differentiate the viral strains.[62] (B): Specific High-sensitivity Enzymatic Reporter unLOCKing (SHERLOCK) assay incorporating recombinase polymerase amplification (RPA) with Cas13a.[7] T7 RNA polymerase was necessary before the CRISPR-Cas13a reaction. (C): DNA Endonuclease-Targeted CRISPR Trans Reporter (DETECTR) assay incorporating RPA with CRISPR-Cas12a.[9] (D): one HOur Low-cost Multipurpose highly Efficient System (HOLMES) incorporating PCR amplification with CRISPR-Cas12a *trans*-cleavage activity.[65] (E): RT-PCR or PCR incorporated with CRISPR-Cas12f (Cas14a).[30] Pol: polymerase. RT: Reverse transcription. T7 Pol: T7 polymerase. T7 exo: T7 exonuclease. Reproduced from Ref.[12] with permission from the Royal Society of Chemistry.

1.5 SARS-CoV-2 RNA detection and quickly advanced CRISPR techniques for this purpose

1.5.1 Molecular diagnosis of COVID-19

The coronavirus disease of 2019 (COVID-19) has caused more than 5,899,000 deaths worldwide as of February 2022. The causative infectious agent of this pandemic is the severe acute respiratory syndrome coronavirus-2 (SARS-CoV-2).[68-74] Molecular diagnosis of COVID-19 primarily relies on the detection of RNA of the SARS-CoV-2 virus.[75-77]

The early identification and sequencing of SARS-CoV-2 by Wu *et al.*[68] and Zhou *et al.*[69] enabled the rapid development of reverse transcription (RT) PCR techniques for detecting specific sequences of the SARS-CoV-2 genome[78] (**Figure 1-4**). SARS-CoV-2 is a positive sense RNA virus, which means that the viral genome of SARS-CoV-2 encodes proteins. The

SARS-CoV-2 genome is 29,903 nucleotides (nt) in length and encodes non-structural proteins and four structural proteins, the spike (S), envelope (E), membrane (M), and nucleocapsid (N) proteins(**Figure 1-4**).[68]

Targets for the detection of SARS-CoV-2 include the genes encoding for the N, E, and S proteins, the open reading frame 1ab (Orf1ab), and the RNA-dependent RNA polymerase (RdRp) gene, which is located within Orf1ab (**Figure 1-4**).[79-80] The choice of targets affects the analytical specificity of RT-PCR assays. The E gene is highly conserved among all beta coronaviruses, and the N gene may cross-react with other coronaviruses.[81] The RdRP gene can be used to differentiate SARS-CoV-2 from the SARS-CoV virus.[69] The S gene is also useful for differentiating SARS-CoV-2 because it is highly divergent from other coronaviruses.[69] At the time of the outbreak, the WHO quickly made available seven RT-PCR assays for diagnosis of COVID-19 developed by scientists from around the world (**Figure 1-4**).[82] These protocols provide access to standard technical guidelines for viral RNA detection. The Germany protocols of the first real-time RT-PCR assays targeting the RdRP, E, and N genes of SARS-CoV-2 were published on January 23, 2020.[78] Their RT-PCR assay targeting the RdRP gene resulted in the highest analytical sensitivity (3.6 RNA copies/reaction at 95% detection probability).[78] In assays developed later, the use of the N gene as the RT-PCR target resulted in SARS-CoV-2 detection that was 10 times more sensitive than when the Orf1b gene was used.[79] Since then, the Foundation for the Innovation of Research Diagnostics (FIND), a WHO collaborating center, has collated commercially available tests to detect SARS-CoV-2.[83] Researchers can choose different targets or multiple targets of RT-PCR assays according to their needs. Diagnostic challenges include time-consuming pre-analytical and analytical

processes and the requirement for well-equipped laboratories with trained personnel to conduct RT-qPCR.[77]

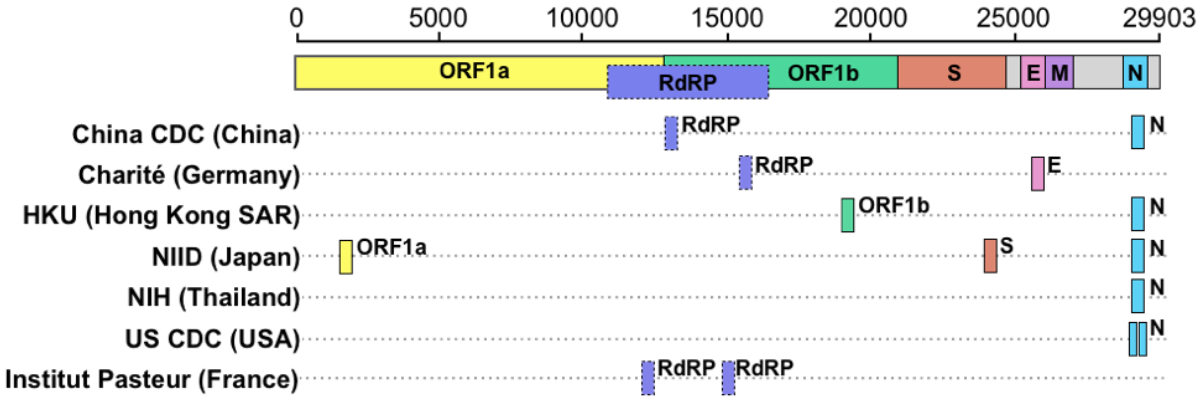

Figure 1-4. Genome organization of SARS-CoV-2 and the relative positions of gene targets detected using seven reverse transcription polymerase chain reaction (RT-PCR) methods shared by the World Health Organization (WHO) as its in-house assays. ORF: open reading frame; RdRP: RNA-dependent RNA polymerase; S: spike protein; E: envelope protein; and N: nucleocapsid protein. Reproduced from Ref.[84] with permission from the American Chemical Society.

1.5.2 Advances in CRISPR technology for the detection of SARS-CoV-2 RNA

SHERLOCK and DETECTR are being used to develop potential POC tests to address the diagnostic needs of the COVID-19 pandemic **(Table A1)**.[10, 85] Using RT-RPA and Cas13, Zhang et al.[85] developed a SHERLOCK lateral flow technique, which was able to detect 10–

100 copies of SARS-CoV-2 genes per μL in under one hour. Broughton et al.[10] developed SARS-CoV-2 DETECTR, using RT-LAMP and CRISPR-Cas12, to detect the viral genes encoding the envelope (E) and nucleocapsid (N) proteins. The authors reported a 100% clinical specificity from the analysis of RNA of clinical samples. Both DETECTR and SHERLOCK techniques require only heating blocks or water baths, lateral flow dipsticks, a microcentrifuge (for SHERLOCK), pipettes, and pipette tips, which are all portable and amenable to POC testing. Three assays using RT-LAMP and CRISPR technology have been approved by the US FDA emergency use authorization (EUA) for the diagnosis of COVID-19.[86]

CRISPR-based diagnostics has been advanced to be integrated, single-tube analyses.[87] This enabled simple operation and reduced the chance of amplicon contamination of the working environment due to the process of opening tubes. To overcome the problem of incompatibility of RT-LAMP or RT-RPA with CRISPR-Cas12a or Cas13a, one approach was to place reagents separately in the same reaction tube, after amplification, the tube was inverted and flicked to mix the amplicon with the CRISPR-based detection reagents **(Table A1)**.[88] Further integration of the amplification reaction and CRISPR-Cas reaction into a homogeneous reaction required solving the incompatibility of the two reactions. An improved version of SHERLOCK screening test for COVID-19, SHERLOCK Testing in One Pot (STOP), integrated sample processing, nucleic acid amplification, and detection in one pot.[8] Joung et al.[8] released viral RNA from nasopharyngeal swabs by incubating the swabs with QuickExtract reagents for 10 min at room temperature or 60 °C. The released RNA was captured on magnetic beads and amplified using RT-LAMP, and the amplicon was detected using CRISPR-Cas12b. This one-pot assay achieved the detection of 100 copies of SARS-

CoV-2 RNA within 1 h. Analysis of 202 SARS-CoV-2 positive samples and 200 SARS-CoV-2 negative samples demonstrated a clinical sensitivity of 93.1% and a clinical specificity of 98.5%. Key to the success of this "one-pot" assay was the use of a new Cas ortholog, AapCas12b, because this enzyme (from *Alicyclobacillus acidiphilus*) remained active at the temperature of RT-LAMP reactions (60 °C). The previously used, commercially available Cas12a operates at a lower temperature (e.g., 25–40 °C), which is incompatible with temperature conditions of RT-LAMP **(Table A1)**.

RT-RPA has also been combined with CRISPR for the detection of SARS-CoV-2.[85, 89] The operation temperature of RT-RPA (37–42 °C) is similar to that of Cas12a (~37 °C). Thus, RT-RPA isothermal amplification and CRISPR-Cas12a detection are considered compatible in principle. In practice, however, it is challenging to achieve reproducible detection of SARS-CoV-2 in a single tube. Zhang and colleagues pointed out that "while we have focused on recombinase polymerase amplification in the past,[7, 39, 64] LAMP reagents are readily available from multiple commercial suppliers, are easily multiplexed,[63] and rely on defined buffers that are amenable to optimization with Cas enzymes".[8] My **Chapter 5** focused on this issue and provided a solution. Ding et al. [90] have also solved such issue with a different strategy **(Table A1)**.

There are more than 100 pathogens causing community-acquired pneumonia, and 30% of these are viruses.[91] The ability to test multiple pathogens in a multiplex manner enables accurate diagnoses and identifies cross-infection by multiple viruses. Such molecular assays also reduce the need for microbiological methods or sequencing which require more time or cost. Ackerman et al.[60] developed a microwell array platform, CARMEN, and demonstrate the potential of CRISPR technology in high-throughput and comprehensive diagnostics of

multiple viral infections. PCR or RPA amplicons of different target molecules were dispersed into droplets, as were the CRISPR mixes containing reporters and different crRNA for different pathogens. The identity of samples (amplicons) and crRNA were color-coded by controlling the ratio of four fluorophores that were added into the amplicon mix and the CRISPR mix. For each analysis on a chip that holds thousands of reactions, the droplets of the amplicon mixes were paired with the droplets of the CRISPR mixes; each microwell held a random pair of droplets with one droplet from each mix. The positive-or-negative signal generated from each microwell can be interpreted by using color-coding to identify the specific sample and pathogen within that microwell.

Another advance of CRISPR technology during the fight against the COVID-19 pandemic is the development of compatible pre-analytical techniques for quick and efficient RNA extraction from different types of samples. Upper respiratory swabs are still the most accepted sample type for the molecular diagnoses of COVID-19. Direct lysis techniques including the advanced version of HUDSON, and magnetic beads-based RNA extraction techniques that are compatible with the CRISPR assays have been used, to avoid the traditional RNA extraction process using column or magnetic beads, to simplify the overall analyses.[8, 59] Saliva samples are also of great interest due to the easy collection and high viral concentration. Pre-analytical techniques that remove the effect of the saliva matrix and allow good performance of CRISPR-based analysis are also advancing.[92]

The ability to differentiate mutations within the target region of CRISPR-Cas systems is useful for the detection and differentiation of variants of concern. High throughput sequencing has been used to monitor mutations in the SARS-CoV-2 genome, which is important for understanding the evolution of the virus and its transmission between animal hosts. [93-94] The

WHO has announced five variants of concern (VOCs), Alpha, Beta, Gamma, Delta, and Omicron.[95] Each variant has multiple mutations within the Spike protein gene, with mostly single nucleotide nutation and some delectation of several continued nucleotides. CRISPR-Cas systems are able to differentiate sequences with multiple nucleotide differences. For the differentiation of VOCs, crRNA can be designed to detect only the mutated strain by having it target the representative mutation site of a specific VOC.[92, 96] The signal difference between two assays using crRNA that only differ by one nucleotide may not be as significant. Careful optimization is required to ensure specificity. One applicable strategy is to design two crRNAs: one matching perfectly with the original strain, and the other matching with a typical mutated sequence of a specific VOC. The detection of mutation or differentiation of VOCs was achieved by comparing the reaction signals using the two different crRNA when testing the same sample.[96]

1.6 Rationale and the scope of this thesis

The CRISPR technology has revolutionized the field of gene editing by significantly improving the simplicity and efficiency of gene editing.[2, 4, 97] With a better understanding of the activity of Cas proteins, the application of CRISPR technology has also been successfully extended to molecular diagnostics.[9, 11-12, 39, 64] The applications to the detection of pathogens and genetic mutations have demonstrated the feasibility of sensitive, specific and portable diagnostic assays using the CRISPR technology.[64] During the pandemic, the simplicity and performance of CRISPR-based diagnostics have been continually advanced.[93-94]

As Cas13a systems can be directly activated by RNA, the detection of RNA using CRISPR technology can be conducted simply in a single-step homogenous reaction. Cas13a

serves the function of target recognition as well as signal generation. The analytical specificity and sensitivity depend highly on the kinetics of the target recognition and *trans*-cleavage activity, yet detailed mechanisms and kinetics of this process remain vague. Human functional RNA and pathogen RNA are diverse in length, nucleotide composition, and secondary structure. It is unclear yet how such factors affect the behavior of Cas13a. This poses challenges to broadening the application of the CRISPR-Cas13a system without affecting the sensitivity and specificity. In addition to the effect of RNA, understanding the performance of Cas13a under different experimental conditions also helps with developing strategies to improve the sensitivity, stability, and specificity of analytical techniques. Such understanding would also help with the development of novel analytical techniques.

Though the direct RNA detection using only Cas13a is simple to design and operate, the sensitivity of such assays is usually not sufficient for ultra-sensitive detection of pathogen RNA. This calls for the need to integrate CRISPR technology with nucleic acid amplification techniques. Some isothermal amplification techniques have been used together with CRISPR technology. Challenges remain to move from a proof-of-concept to clinical application. The improvement of current CRISPR-based diagnostics became more necessary during the pandemic. In the case of SARS-CoV-2 RNA detection for COVID-19 diagnoses, the accuracy, operation simplicity, degree of automation, turnover time, reagent accessibility, and sample type compatibility of assays are all important. Meeting such needs requires understanding the CRISPR systems and improvements in assay chemistry.

The goal of my thesis is to study the *trans*-cleavage activity of CRISPR-Cas systems and its compatibility with other nucleic acid amplification techniques, for broadening the

application of CRISPR-Cas systems to RNA detection and improving assay performance. Specific projects are outlined below.

In **Chapter 2**, I developed an assay using LwaCas13a for the detection of microRNA. I systematically optimized the reaction conditions of LwaCas13a for short RNA detection. Although other relevant techniques all operate at 37 °C, I discovered that both LwaCas13a and LbuCas13a performed the best at around 23 °C when detecting microRNA. Thus, I achieved microRNA detection at ambient temperature. In **Chapter 3**, I studied the effect of short RNA length on the operation of LwaCas13a and LbuCas13a. I showed that there is insufficient LwaCas13a activation when using spacers or activator RNA shorter than 23 nt. This observation from my studies of LwaCas13a is distinct from the understanding of commonly used LbuCas13a. **In Chapter 4**, I systematically studied the thermal behavior of LwaCas13a and LbuCas13a and investigated whether their thermal behaviors depend on the target RNA sequence. By discriminating the kinetics of each operation step, I revealed the high *trans*-cleavage of Cas13a enzymes at ambient temperature upon activation. Although the formation of crRNA-Cas13a-target complexes may require a higher temperature when using complicated target RNA, the high *trans*-cleavage activity at ambient temperature is useful for potential point-of-care testing applications. In **Chapter 5**, I studied issues and solutions for the successful integration of reverse transcription (RT), recombinase polymerase amplification (RPA), and CRISPR-Cas12a nuclease reactions into a single tube under an isothermal conditions (40 °C), and developed an integrated assay for the detection of SARS-CoV-2 RNA.

1.7 References

1. Karvelis, T., Bigelyte, G., Young, J. K., Hou, Z., Zedaveinyte, R., Budre, K., Paulraj, S., Djukanovic, V., Gasior, S., Silanskas, A., Venclovas, C. and Siksnys, V., PAM recognition by miniature CRISPR-Cas12f nucleases triggers programmable double-stranded DNA target cleavage. *Nucleic Acids Res.* **2020,** *48* (9), 5016-5023.
2. Jinek, M., Chylinski, K., Fonfara, I., Hauer, M., Doudna, J. A. and Charpentier, E., A Programmable Dual-RNA-Guided DNA Endonuclease in Adaptive Bacterial Immunity. *Science* **2012,** *337* (6096), 816-821.
3. Knott, G. J. and Doudna, J. A., CRISPR-Cas guides the future of genetic engineering. *Science* **2018,** *361* (6405), 866-869.
4. Cong, L., Ran, F. A., Cox, D., Lin, S. L., Barretto, R., Habib, N., Hsu, P. D., Wu, X. B., Jiang, W. Y., Marraffini, L. A. and Zhang, F., Multiplex Genome Engineering Using CRISPR/Cas Systems. *Science* **2013,** *339* (6121), 819-823.
5. Mali, P., Yang, L. H., Esvelt, K. M., Aach, J., Guell, M., DiCarlo, J. E., Norville, J. E. and Church, G. M., RNA-Guided Human Genome Engineering via Cas9. *Science* **2013,** *339* (6121), 823-826.
6. Adli, M., The CRISPR tool kit for genome editing and beyond. *Nat. Commun.* **2018,** *9*, 1911.
7. Gootenberg, J. S., Abudayyeh, O. O., Lee, J. W., Essletzbichler, P., Dy, A. J., Joung, J., Verdine, V., Donghia, N., Daringer, N. M., Freije, C. A., Myhrvold, C., Bhattacharyya, R. P., Livny, J., Regev, A., Koonin, E. V., Hung, D. T., Sabeti, P. C., Collins, J. J. and Zhang, F., Nucleic acid detection with CRISPR-Cas13a/C2c2. *Science* **2017,** *356* (6336), 438-442.

8. Joung, J., Ladha, A., Saito, M., Kim, N.-G., Woolley, A. E., Segel, M., Barretto, R. P. J., Ranu, A., Macrae, R. K., Faure, G., Ioannidi, E. I., Krajeski, R. N., Bruneau, R., Huang, M.-L. W., Yu, X. G., Li, J. Z., Walker, B. D., Hung, D. T., Greninger, A. L., Jerome, K. R., Gootenberg, J. S., Abudayyeh, O. O. and Zhang, F., Detection of SARS-CoV-2 with SHERLOCK One-Pot Testing. *New Engl. J. Med.* **2020,** *383* (15), 1492-1494.
9. Chen, J. S., Ma, E. B., Harrington, L. B., Da Costa, M., Tian, X. R., Palefsky, J. M. and Doudna, J. A., CRISPR-Cas12a target binding unleashes indiscriminate single-stranded DNase activity. *Science* **2018,** *360* (6387), 436-439.
10. Broughton, J. P., Deng, X., Yu, G., Fasching, C. L., Servellita, V., Singh, J., Miao, X., Streithorst, J. A., Granados, A., Sotomayor-Gonzalez, A., Zorn, K., Gopez, A., Hsu, E., Gu, W., Miller, S., Pan, C.-Y., Guevara, H., Wadford, D. A., Chen, J. S. and Chiu, C. Y., CRISPR–Cas12-based detection of SARS-CoV-2. *Nat. Biotechnol.* **2020,** *38*, 870-874.
11. Tang, Y., Gao, L., Feng, W., Guo, C., Yang, Q., Li, F. and Le, X. C., The CRISPR–Cas toolbox for analytical and diagnostic assay development. *Chem. Soc. Rev.* **2021,** *50* (21), 11844-11869.
12. Feng, W., Newbigging, A. M., Tao, J., Cao, Y., Peng, H., Le, C., Wu, J., Pang, B., Li, J., Tyrrell, D. L., Zhang, H. and Le, X. C., CRISPR technology incorporating amplification strategies: molecular assays for nucleic acids, proteins, and small molecules. *Chem. Sci.* **2021,** *12* (13), 4683-4698.
13. Abudayyeh, O. O., Gootenberg, J. S., Konermann, S., Joung, J., Slaymaker, I. M., Cox, D. B. T., Shmakov, S., Makarova, K. S., Semenova, E., Minakhin, L., Severinov, K., Regev, A., Lander, E. S., Koonin, E. V. and Zhang, F., C2c2 is a single-component programmable RNA-guided RNA-targeting CRISPR effector. *Science* **2016,** *353* (6299), aaf5573.

14. Chang, N. N., Sun, C. H., Gao, L., Zhu, D., Xu, X. F., Zhu, X. J., Xiong, J. W. and Xi, J. J., Genome editing with RNA-guided Cas9 nuclease in Zebrafish embryos. *Cell Res.* **2013,** *23* (4), 465-472.

15. Hsu, P. D., Lander, E. S. and Zhang, F., Development and applications of CRISPR-Cas9 for genome engineering. *Cell* **2014,** *157* (6), 1262-1278.

16. Jinek, M., East, A., Cheng, A., Lin, S., Ma, E. B. and Doudna, J., RNA-programmed genome editing in human cells. *Elife* **2013,** *2*, e00471.

17. Nishimasu, H., Ran, F. A., Hsu, P. D., Konermann, S., Shehata, S. I., Dohmae, N., Ishitani, R., Zhang, F. and Nureki, O., Crystal structure of Cas9 in complex with guide RNA and target DNA. *Cell* **2014,** *156* (5), 935-949.

18. Stephenson, A. A., Raper, A. T. and Suo, Z., Bidirectional degradation of DNA cleavage products catalyzed by CRISPR/Cas9. *J. Am. Chem. Soc.* **2018,** *140* (10), 3743-3750.

19. Hsu, P. D., Scott, D. A., Weinstein, J. A., Ran, F. A., Konermann, S., Agarwala, V., Li, Y. Q., Fine, E. J., Wu, X. B., Shalem, O., Cradick, T. J., Marraffini, L. A., Bao, G. and Zhang, F., DNA targeting specificity of RNA-guided Cas9 nucleases. *Nat. Biotechnol.* **2013,** *31* (9), 827-832.

20. O'Connell, M. R., Oakes, B. L., Sternberg, S. H., East-Seletsky, A., Kaplan, M. and Doudna, J. A., Programmable RNA recognition and cleavage by CRISPR/Cas9. *Nature* **2014,** *516*, 263-266.

21. Ma, E., Harrington, L. B., O'Connell, M. R., Zhou, K. and Doudna, J. A., Single-stranded DNA cleavage by divergent CRISPR-Cas9 enzymes. *Mol Cell* **2015,** *60* (3), 398-407.

22. Gasiunas, G., Barrangou, R., Horvath, P. and Siksnys, V., Cas9–crRNA ribonucleoprotein complex mediates specific DNA cleavage for adaptive immunity in bacteria. *Proc. Natl. Acad. Sci.* **2012,** *109* (39), E2579-E2586.

23. Ran, F. A., Hsu, P. D., Lin, C.-Y., Gootenberg, J. S., Konermann, S., Trevino, A. E., Scott, D. A., Inoue, A., Matoba, S., Zhang, Y. and Zhang, F., Double nicking by RNA-guided CRISPR Cas9 for enhanced genome editing specificity. *Cell* **2013,** *154* (6), 1380-1389.

24. Qi, L. S., Larson, M. H., Gilbert, L. A., Doudna, J. A., Weissman, J. S., Arkin, A. P. and Lim, W. A., Repurposing CRISPR as an RNA-guided platform for sequence-specific control of gene expression. *Cell* **2013,** *152* (5), 1173-1183.

25. Makarova, K. S., Wolf, Y. I., Iranzo, J., Shmakov, S. A., Alkhnbashi, O. S., Brouns, S. J. J., Charpentier, E., Cheng, D., Haft, D. H., Horvath, P., Moineau, S., Mojica, F. J. M., Scott, D., Shah, S. A., Siksnys, V., Terns, M. P., Venclovas, Č., White, M. F., Yakunin, A. F., Yan, W., Zhang, F., Garrett, R. A., Backofen, R., van der Oost, J., Barrangou, R. and Koonin, E. V., Evolutionary classification of CRISPR–Cas systems: a burst of class 2 and derived variants. *Nat. Rev. Microbiol.* **2020,** *18*, 67-83.

26. Zetsche, B., Gootenberg, J. S., Abudayyeh, O. O., Slaymaker, I. M., Makarova, K. S., Essletzbichler, P., Volz, S. E., Joung, J., van der Oost, J., Regev, A., Koonin, E. V. and Zhang, F., Cpf1 Is a Single RNA-Guided Endonuclease of a Class 2 CRISPR-Cas System. *Cell* **2015,** *163* (3), 759-771.

27. Shmakov, S., Abudayyeh, O. O., Makarova, K. S., Wolf, Y. I., Gootenberg, J. S., Semenova, E., Minakhin, L., Joung, J., Konermann, S., Severinov, K., Zhang, F. and Koonin, E. V., Discovery and Functional Characterization of Diverse Class 2 CRISPR-Cas Systems. *Mol. Cell* **2015,** *60* (3), 385-397.

28. Li, S.-Y., Cheng, Q.-X., Liu, J.-K., Nie, X.-Q., Zhao, G.-P. and Wang, J., CRISPR-Cas12a has both *cis*- and *trans*-cleavage activities on single-stranded DNA. *Cell Res.* **2018,** *28*, 491-493.

29. Swarts, D. C. and Jinek, M., Mechanistic Insights into the *cis*- and *trans*-Acting DNase Activities of Cas12a. *Mol. Cell* **2019,** *73* (3), 589-600.e4.

30. Harrington, L. B., Burstein, D., Chen, J. S., Paez-Espino, D., Ma, E., Witte, I. P., Cofsky, J. C., Kyrpides, N. C., Banfield, J. F. and Doudna, J. A., Programmed DNA destruction by miniature CRISPR-Cas14 enzymes. *Science* **2018,** *362* (6416), 839-842.

31. Wei, Y., Yang, Z., Zong, C., Wang, B., Ge, X., Tan, X., Liu, X., Tao, Z., Wang, P., Ma, C., Wan, Y. and Li, J., *trans* Single-Stranded DNA Cleavage *via* CRISPR/Cas14a1 Activated by Target RNA without Destruction. *Angew. Chem. Int. Ed.* **2021,** *60* (45), 24241-24247.

32. Chen, B., Gilbert, L. A., Cimini, B. A., Schnitzbauer, J., Zhang, W., Li, G.-W., Park, J., Blackburn, E. H., Weissman, J. S., Qi, L. S. and Huang, B., Dynamic imaging of genomic loci in living human cells by an optimized CRISPR/Cas system. *Cell* **2013,** *155* (7), 1479-1491.

33. Wu, X., Mao, S., Ying, Y., Krueger, C. J. and Chen, A. K., Progress and challenges for live-cell imaging of genomic loci using CRISPR-based platforms. *Genomics Proteomics Bioinformatics* **2019**, *17* (2), 119-128.

34. Zhang, K., Deng, R., Teng, X., Li, Y., Sun, Y., Ren, X. and Li, J., Direct visualization of single-nucleotide variation in mtDNA using a CRISPR/Cas9-mediated proximity ligation assay. *J. Am. Chem. Soc.* **2018,** *140* (36), 11293-11301.

35. Konermann, S., Lotfy, P., Brideau, N. J., Oki, J., Shokhirev, M. N. and Hsu, P. D., Transcriptome Engineering with RNA-Targeting Type VI-D CRISPR Effectors. *Cell* **2018,** *173* (3), 665-676.e14.

36. Smargon, A. A., Cox, D. B., Pyzocha, N. K., Zheng, K., Slaymaker, I. M., Gootenberg, J. S., Abudayyeh, O. A., Essletzbichler, P., Shmakov, S., Makarova, K. S., Koonin, E. V. and Zhang, F., Cas13b is a type VI-B CRISPR-associated RNA-guided RNase differentially regulated by accessory proteins Csx27 and Csx28. *Mol. Cell* **2017,** *65* (4), 618-630.e7.

37. Zhang, C., Konermann, S., Brideau, N. J., Lotfy, P., Wu, X., Novick, S. J., Strutzenberg, T., Griffin, P. R., Hsu, P. D. and Lyumkis, D., Structural basis for the RNA-guided ribonuclease activity of CRISPR-Cas13d. *Cell* **2018,** *175* (1), 212-223. e17.

38. Kellner, M. J., Koob, J. G., Gootenberg, J. S., Abudayyeh, O. O. and Zhang, F., SHERLOCK: nucleic acid detection with CRISPR nucleases. *Nat. Protoc.* **2019,** *14*, 2986-3012.

39. Gootenberg, J. S., Abudayyeh, O. O., Kellner, M. J., Joung, J., Collins, J. J. and Zhang, F., Multiplexed and portable nucleic acid detection platform with Cas13, Cas12a, and Csm6. *Science* **2018,** *360* (6387), 439-444.

40. Strutt, S. C., Torrez, R. M., Kaya, E., Negrete, O. A. and Doudna, J. A., RNA-dependent RNA targeting by CRISPR-Cas9. *elife* **2018,** *7*, e32724.

41. East-Seletsky, A., O'Connell, M. R., Knight, S. C., Burstein, D., Cate, J. H. D., Tjian, R. and Doudna, J. A., Two distinct RNase activities of CRISPR-C2c2 enable guide-RNA processing and RNA detection. *Nature* **2016,** *538*, 270-273.

42. Pattanayak, V., Lin, S., Guilinger, J. P., Ma, E., Doudna, J. A. and Liu, D. R., High-throughput profiling of off-target DNA cleavage reveals RNA-programmed Cas9 nuclease specificity. *Nat. Biotechnol.* **2013,** *31*, 839-843.

43. Fozouni, P., Son, S., Díaz de León Derby, M., Knott, G. J., Gray, C. N., D'Ambrosio, M. V., Zhao, C., Switz, N. A., Kumar, G. R., Stephens, S. I., Boehm, D., Tsou, C.-L., Shu, J., Bhuiya, A., Armstrong, M., Harris, A. R., Chen, P.-Y., Osterloh, J. M., Meyer-Franke, A., Joehnk, B., Walcott, K., Sil, A., Langelier, C., Pollard, K. S., Crawford, E. D., Puschnik, A. S., Phelps, M., Kistler, A., DeRisi, J. L., Doudna, J. A., Fletcher, D. A. and Ott, M., Amplification-free detection of SARS-CoV-2 with CRISPR-Cas13a and mobile phone microscopy. *Cell* **2021,** *184* (2), 323-333.e9.

44. Kleinstiver, B. P., Tsai, S. Q., Prew, M. S., Nguyen, N. T., Welch, M. M., Lopez, J. M., McCaw, Z. R., Aryee, M. J. and Joung, J. K., Genome-wide specificities of CRISPR-Cas Cpf1 nucleases in human cells. *Nat. Biotechnol.* **2016,** *34* (8), 869-874.

45. Shan, Y., Zhou, X., Huang, R. and Xing, D., High-Fidelity and Rapid Quantification of miRNA Combining crRNA Programmability and CRISPR/Cas13a trans-Cleavage Activity. *Anal. Chem.* **2019,** *91* (8), 5278-5285.

46. Chen, Y., Yang, S., Peng, S., Li, W., Wu, F., Yao, Q., Wang, F., Weng, X. and Zhou, X., N1-Methyladenosine detection with CRISPR-Cas13a/C2c2. *Chem. Sci.* **2019,** *10* (10), 2975-2979.

47. Qin, P., Park, M., Alfson, K. J., Tamhankar, M., Carrion, R., Patterson, J. L., Griffiths, A., He, Q., Yildiz, A., Mathies, R. and Du, K., Rapid and Fully Microfluidic Ebola Virus Detection with CRISPR-Cas13a. *ACS Sens.* **2019,** *4* (4), 1048-1054.

48. Bruch, R., Baaske, J., Chatelle, C., Meirich, M., Madlener, S., Weber, W., Dincer, C. and Urban, G. A., CRISPR/Cas13a-Powered Electrochemical Microfluidic Biosensor for Nucleic Acid Amplification-Free miRNA Diagnostics. *Adv. Mater.* **2019,** *31* (51), 1905311.

49. Dai, Y., Somoza, R. A., Wang, L., Welter, J. F., Li, Y., Caplan, A. I. and Liu, C. C., Exploring the Trans-Cleavage Activity of CRISPR-Cas12a (cpf1) for the Development of a Universal Electrochemical Biosensor. *Angew. Chem. Int. Ed.* **2019,** *58* (48), 17399-17405.

50. English, M. A., Soenksen, L. R., Gayet, R. V., de Puig, H., Angenent-Mari, N. M., Mao, A. S., Nguyen, P. Q. and Collins, J. J., Programmable CRISPR-responsive smart materials. *Science* **2019,** *365* (6455), 780-785.

51. Shao, N., Han, X., Song, Y., Zhang, P. and Qin, L., CRISPR-Cas12a Coupled with Platinum Nanoreporter for Visual Quantification of SNVs on a Volumetric Bar-Chart Chip. *Anal. Chem.* **2019,** *91* (19), 12384-12391.

52. Ramachandran, A. and Santiago, J. G., CRISPR Enzyme Kinetics for Molecular Diagnostics. *Anal. Chem.* **2021,** *93* (20), 7456-7464.

53. Erratum for the Report "CRISPR-Cas12a target binding unleashes indiscriminate single-stranded DNase activity" by J. S. Chen, E. Ma, L. B. Harrington, M. Da Costa, X. Tian, J. M. Palefsky, J. A. Doudna. *Science* **2021,** *371* (6531), eabh0317.

54. Slaymaker, I. M., Mesa, P., Kellner, M. J., Kannan, S., Brignole, E., Koob, J., Feliciano, P. R., Stella, S., Abudayyeh, O. O., Gootenberg, J. S., Strecker, J., Montoya, G. and Zhang, F., High-Resolution Structure of Cas13b and Biochemical Characterization of RNA Targeting and Cleavage. *Cell Rep.* **2019,** *26* (13), 3741-3751.e5.

55. Slaymaker, I. M., Mesa, P., Kellner, M. J., Kannan, S., Brignole, E., Koob, J., Feliciano, P. R., Stella, S., Abudayyeh, O. O., Gootenberg, J. S., Strecker, J., Montoya, G. and Zhang, F., High-resolution structure of cas13b and biochemical characterization of RNA targeting and cleavage. *Cell Rep.* **2021,** *34* (10), 108865.

56. East-Seletsky, A., O'Connell, M. R., Burstein, D., Knott, G. J. and Doudna, J. A., RNA Targeting by Functionally Orthogonal Type VI-A CRISPR-Cas Enzymes. *Mol. Cell* **2017,** *66* (3), 373-383.

57. Nalefski, E. A., Patel, N., Leung, P. J. Y., Islam, Z., Kooistra, R. M., Parikh, I., Marion, E., Knott, G. J., Doudna, J. A., Le Ny, A.-L. M. and Madan, D., Kinetic analysis of Cas12a and Cas13a RNA-Guided nucleases for development of improved CRISPR-Based diagnostics. *iScience* **2021,** *24*, 102996.

58. Metsky, H. C., Welch, N. L., Pillai, P. P., Haradhvala, N. J., Rumker, L., Mantena, S., Zhang, Y. B., Yang, D. K., Ackerman, C. M., Weller, J., Blainey, P. C., Myhrvold, C., Mitzenmacher, M. and Sabeti, P. C., Designing sensitive viral diagnostics with machine learning. *Nat. Biotechol.* **2022**, https://doi.org/10.1038/s41587-022-01213-5

59. Arizti-Sanz, J., Freije, C. A., Stanton, A. C., Petros, B. A., Boehm, C. K., Siddiqui, S., Shaw, B. M., Adams, G., Kosoko-Thoroddsen, T.-S. F., Kemball, M. E., Uwanibe, J. N., Ajogbasile, F. V., Eromon, P. E., Gross, R., Wronka, L., Caviness, K., Hensley, L. E., Bergman, N. H., MacInnis, B. L., Happi, C. T., Lemieux, J. E., Sabeti, P. C. and Myhrvold, C., Streamlined inactivation, amplification, and Cas13-based detection of SARS-CoV-2. *Nat. Commun.* **2020,** *11*, 5921.

60. Ackerman, C. M., Myhrvold, C., Thakku, S. G., Freije, C. A., Metsky, H. C., Yang, D. K., Ye, S. H., Boehm, C. K., Kosoko-Thoroddsen, T.-S. F., Kehe, J., Nguyen, T. G., Carter,

A., Kulesa, A., Barnes, J. R., Dugan, V. G., Hung, D. T., Blainey, P. C. and Sabeti, P. C., Massively multiplexed nucleic acid detection using Cas13. *Nature* **2020,** *582*, 277-282.

61. Compton, J., Nucleic acid sequence-based amplification. *Nature* **1991,** *350*, 91-92.
62. Pardee, K., Green, A. A., Takahashi, M. K., Braff, D., Lambert, G., Lee, J. W., Ferrante, T., Ma, D., Donghia, N., Fan, M., Daringer, N. M., Bosch, I., Dudley, D. M., O'Connor, D. H., Gehrke, L. and Collins. J. J., Rapid, low-cost detection of Zika virus using programmable biomolecular components. *Cell* **2016,** *165* (5), 1255-1266.
63. Piepenburg, O., Williams, C. H., Stemple, D. L. and Armes, N. A., DNA Detection Using Recombination Proteins. *PLOS Biol.* **2006,** *4* (7), e204.
64. Myhrvold, C., Freije, C. A., Gootenberg, J. S., Abudayyeh, O. O., Metsky, H. C., Durbin, A. F., Kellner, M. J., Tan, A. L., Paul, L. M., Parham, L. A., Garcia, K. F., Barnes, K. G., Chak, B., Mondini, A., Nogueira, M. L., Isern, S., Michael, S. F., Lorenzana, I., Yozwiak, N. L., MacInnis, B. L., Bosch, I., Gehrke, L., Zhang, F. and Sabeti, P. C., Field-deployable viral diagnostics using CRISPR-Cas13. *Science* **2018,** *360* (6387), 444-448.
65. Li, S.-Y., Cheng, Q.-X., Wang, J.-M., Li, X.-Y., Zhang, Z.-L., Gao, S., Cao, R.-B., Zhao, G.-P. and Wang, J., CRISPR-Cas12a-assisted nucleic acid detection. *Cell Discovery* **2018,** *4*, 20.
66. Notomi, T., Mori, Y., Tomita, N. and Kanda, H., Loop-mediated isothermal amplification (LAMP): principle, features, and future prospects. *J Microbiol.* **2015,** *53* (1), 1-5.
67. Li, L. X., Li, S. Y., Wu, N., Wu, J. C., Wang, G., Zhao, G. P. and Wang, J., HOLMESv2: A CRISPR-Cas12b-Assisted Platform for Nucleic Acid Detection and DNA Methylation Quantitation. *ACS synth. biol.* **2019,** *8* (10), 2228-2237.

68. Wu, F., Zhao, S., Yu, B., Chen, Y.-M., Wang, W., Song, Z.-G., Hu, Y., Tao, Z.-W., Tian, J.-H., Pei, Y.-Y., Yuan, M.-L., Zhang, Y.-L., Dai, F.-H., Liu, Y., Wang, Q.-M., Zheng, J.-J., Xu, L., Holmes, E. C. and Zhang, Y.-Z., A new coronavirus associated with human respiratory disease in China. *Nature* **2020,** *579*, 265-269.

69. Zhou, P., Yang, X.-L., Wang, X.-G., Hu, B., Zhang, L., Zhang, W., Si, H.-R., Zhu, Y., Li, B., Huang, C.-L., Chen, H.-D., Chen, J., Luo, Y., Guo, H., Jiang, R.-D., Liu, M.-Q., Chen, Y., Shen, X.-R., Wang, X., Zheng, X.-S., Zhao, K., Chen, Q.-J., Deng, F., Liu, L.-L., Yan, B., Zhan, F.-X., Wang, Y.-Y., Xiao, G.-F. and Shi, Z.-L., A pneumonia outbreak associated with a new coronavirus of probable bat origin. *Nature* **2020,** *579*, 270-273.

70. Zhu, N., Zhang, D., Wang, W., Li, X., Yang, B., Song, J., Zhao, X., Huang, B., Shi, W., Lu, R., Niu, P., Zhan, F., Ma, X., Wang, D., Xu, W., Wu, G., Gao, G. F. and Tan, W., A Novel Coronavirus from Patients with Pneumonia in China, 2019. *New Engl. J. Med.* **2020,** *382* (8), 727-733.

71. Wu, Z. and McGoogan, J. M., Characteristics of and important lessons from the coronavirus disease 2019 (COVID-19) outbreak in China: summary of a report of 72 314 cases from the Chinese Center for Disease Control and Prevention. *JAMA* **2020,** *323* (13), 1239-1242.

72. Wang, D., Hu, B., Hu, C., Zhu, F., Liu, X., Zhang, J., Wang, B., Xiang, H., Cheng, Z., Xiong, Y., Zhao, Y., Li, Y., Wang, X. and Peng, Z., Clinical characteristics of 138 hospitalized patients with 2019 novel coronavirus–infected pneumonia in Wuhan, China. *JAMA* **2020,** *323* (11), 1061-1069.

73. Huang, C., Wang, Y., Li, X., Ren, L., Zhao, J., Hu, Y., Zhang, L., Fan, G., Xu, J., Gu, X., Cheng, Z., Yu, T., Xia, J., Wei, Y., Wu, W., Xie, X., Yin, W., Li, H., Liu, M., Xiao, Y.,

Gao, H., Guo, L., Xie, J., Wang, G., Jiang, R., Gao, Z., Jin, Q., Wang, J. and Cao, B., Clinical features of patients infected with 2019 novel coronavirus in Wuhan, China. *Lancet* **2020,** *395* (10223), 497-506.

74. Zhou, F., Yu, T., Du, R., Fan, G., Liu, Y., Liu, Z., Xiang, J., Wang, Y., Song, B., Gu, X., Guan, L., Wei, Y., Li, H., Wu, X., Xu, J., Tu, S., Zhang, Y., Chen, H. and Cao, B., Clinical course and risk factors for mortality of adult inpatients with COVID-19 in Wuhan, China: a retrospective cohort study. *Lancet* **2020,** *395* (10229), 1054-1062.
75. World Health Organization (WHO), Coronavirus disease (COVID-19) technical guidance: Laboratory testing for 2019-nCoV in humans. https://www.who.int/emergencies/diseases/novel-coronavirus-2019/technical-guidance/laboratory-guidance (accessed May 12, 2020).
76. Carter, L. J., Garner, L. V., Smoot, J. W., Li, Y., Zhou, Q., Saveson, C. J., Sasso, J. M., Gregg, A. C., Soares, D. J., Beskid, T. R., Jervey, S. R. and Liu, C., Assay Techniques and Test Development for COVID-19 Diagnosis. *ACS Cent. Sci.* **2020,** *6* (5), 591-605.
77. Udugama, B., Kadhiresan, P., Kozlowski, H. N., Malekjahani, A., Osborne, M., Li, V. Y. C., Chen, H., Mubareka, S., Gubbay, J. B. and Chan, W. C. W., Diagnosing COVID-19: The Disease and Tools for Detection. *ACS Nano* **2020,** *14* (4), 3822-3835.
78. Corman, V. M., Landt, O., Kaiser, M., Molenkamp, R., Meijer, A., Chu, D. K. W., Bleicker, T., Brünink, S., Schneider, J., Schmidt, M. L., Mulders, D. G., Haagmans, B. L., van der Veer, B., van den Brink, S., Wijsman, L., Goderski, G., Romette, J.-L., Ellis, J., Zambon, M., Peiris, M., Goossens, H., Reusken, C., Koopmans, M. P. and Drosten, C., Detection of 2019 novel coronavirus (2019-nCoV) by real-time RT-PCR. *Euro Surveill.* **2020,** *25* (3), 2000045.

79. Chu, D. K. W., Pan, Y., Cheng, S. M. S., Hui, K. P. Y., Krishnan, P., Liu, Y., Ng, D. Y. M., Wan, C. K. C., Yang, P., Wang, Q., Peiris, M. and Poon, L. L. M., Molecular diagnosis of a novel coronavirus (2019-nCoV) causing an outbreak of pneumonia. *Clin. Chem.* **2020,** *66* (4), 549-555.

80. Chan, J. F.-W., Yip, C. C.-Y., To, K. K.-W., Tang, T. H.-C., Wong, S. C.-Y., Leung, K.-H., Fung, A. Y.-F., Ng, A. C.-K., Zou, Z. and Tsoi, H.-W., Choi, G. K.-Y., Tam, A. R. Cheng, V. C.-C., Chan, K.-H., Tsang, O. T.-Y. and Yuen, K.-Y., Improved molecular diagnosis of COVID-19 by the novel, highly sensitive and specific COVID-19-RdRp/Hel real-time reverse transcription-PCR assay validated *in vitro* and with clinical specimens. *J. Clin. Microbiol.* **2020,** *58* (5), e00310-20.

81. Lu, R., Zhao, X., Li, J., Niu, P., Yang, B., Wu, H., Wang, W., Song, H., Huang, B., Zhu, N., Bi, Y., Ma, X., Zhan, F., Wang, L., Hu, T., Zhou, H., Hu, Z., Zhou, W., Zhao, L., Chen, J., Meng, Y., Wang, J., Lin, Y., Yuan, J., Xie, Z., Ma, J., Liu, W. J., Wang, D., Xu, W., Holmes, E. C., Gao, G. F., Wu, G., Chen, W., Shi, W. and Tan, W., Genomic characterisation and epidemiology of 2019 novel coronavirus: implications for virus origins and receptor binding. *Lancet* **2020,** *395* (10224), 565-574.

82. WHO, Molecular assays to diagnose COVID-19. https://www.who.int/who-documents-detail/molecular-assays-to-diagnose-covid-19-summary-table-of-available-protocols (accessed May 12, 2020).

83. Fundation for Innovative New Diagnostics (FIND), SARS-CoV-2 Diagnostic Pipeline. https://www.finddx.org/covid-19/pipeline/?section=show-all#diag_tab (accessed May 6, 2020).

84. Feng, W., Newbigging, A. M., Le, C., Pang, B., Peng, H., Cao, Y., Wu, J., Abbas, G., Song, J., Wang, D.-B., Cui, M., Tao, J., Tyrrell, D. L., Zhang, X.-E., Zhang, H. and Le, X. C., Molecular Diagnosis of COVID-19: Challenges and Research Needs. *Anal. Chem.* **2020,** *92* (15), 10196-10209.

85. Zhang, F., Abudayyeh, O. O. and Gootenberg, J. S. A protocol for detection of COVID-19 using CRISPR diagnostics 2020. https://www.broadinstitute.org/files/publications/special/COVID-19%20detection%20(updated).pdf. (accessed May 11, 2020)

86. The United States Food and Drug Administration (FDA), In Vitro Diagnostics EUAs - Molecular Diagnostic Tests for SARS-CoV-2. https://www.fda.gov/medical-devices/coronavirus-disease-2019-covid-19-emergency-use-authorizations-medical-devices/in-vitro-diagnostics-euas-molecular-diagnostic-tests-sars-cov-2 (accessed Febuary 24, 2022).

87. Feng, W., Peng, H., Xu, J., Liu, Y., Pabbaraju, K., Tipples, G., Joyce, M. A., Saffran, H. A., Tyrrell, D. L., Babiuk, S., Zhang, H. and Le, X. C., Integrating Reverse Transcription Recombinase Polymerase Amplification with CRISPR Technology for the One-Tube Assay of RNA. Anal. Chem. 2021, 93 (37), 12808-12816.

88. Pang, B., Xu, J., Liu, Y., Peng, H., Feng, W., Cao, Y., Wu, J., Xiao, H., Pabbaraju, K., Tipples, G., Joyce, M. A., Saffran, H. A., Tyrrell, D. L., Zhang, H. and Le, X. C., Isothermal Amplification and Ambient Visualization in a Single Tube for the Detection of SARS-CoV-2 Using Loop-Mediated Amplification and CRISPR Technology. *Anal. Chem.* **2020,** *92* (24), 16204-16212.

89. Ding, X., Yin, K., Li, Z., Lalla, R. V., Ballesteros, E., Sfeir, M. M. and Liu, C., Ultrasensitive and visual detection of SARS-CoV-2 using all-in-one dual CRISPR-Cas12a assay. *Nat. commun.* **2020,** *11* (1), 4711.

90. Ding, X., Yin, K., Li, Z. and Liu, C., All-in-One Dual CRISPR-Cas12a (AIOD-CRISPR) Assay: A Case for Rapid, Ultrasensitive and Visual Detection of Novel Coronavirus SARS-CoV-2 and HIV virus. *bioRxiv* **2020**, 2020.03.19.998724. https://doi.org/10.1101/2020.03.19.998724

91. Chen, N., Zhou, M., Dong, X., Qu, J., Gong, F., Han, Y., Qiu, Y., Wang, J., Liu, Y., Wei, Y., Xia, J. a., Yu, T., Zhang, X. and Zhang, L., Epidemiological and clinical characteristics of 99 cases of 2019 novel coronavirus pneumonia in Wuhan, China: a descriptive study. *Lancet* **2020,** *395* (10223), 507-513.

92. de Puig, H., Lee, R. A., Najjar, D., Tan, X., Soenksen, L. R., Angenent-Mari, N. M., Donghia, N. M., Weckman, N. E., Ory, A., Ng, C. F., Nguyen, P. Q., Mao, A. S., Ferrante, T. C., Lansberry, G., Sallum, H., Niemi, J. and Collins, J. J., Minimally instrumented SHERLOCK (miSHERLOCK) for CRISPR-based point-of-care diagnosis of SARS-CoV-2 and emerging variants. *Sci. Adv.* **2021,** *7* (32), eabh2944.

93. Forster, P., Forster, L., Renfrew, C. and Forster, M., Phylogenetic network analysis of SARS-CoV-2 genomes. *Proc. Natl. Acad. Sci.* **2020,** *117* (17), 9241-9243.

94. Uhler, C. and Shivashankar, G. V., Mechano-genomic regulation of coronaviruses and its interplay with ageing. *Nat. Rev. Mol. Cell Biol.* **2020,** *21*, 247-248.

95. WHO, Tracking SARS-CoV-2 variants https://www.who.int/en/activities/tracking-SARS-CoV-2-variants/ (accessed Febuary 24, 2022).

96. Arizti-Sanz, J., Bradley, A. D., Zhang, Y. B., Boehm, C. K., Freije, C. A., Grunberg, M. E., Kosoko-Thoroddsen, T.-S. F., Welch, N. L., Pillai, P. P., Mantena, S., Kim, G., Uwanibe, J. N., John, O. G., Eromon, P. E., Kocher, G., Gross, R., Lee, J. S., Hensley, L. E., Happi, C. T., Johnson, J., Sabeti, P. C. and Myhrvold, C., Equipment-free detection of SARS-CoV-2 and Variants of Concern using Cas13. *medRxiv* **2021**, 2021.11.01.21265764. https://doi.org/10.1101/2021.11.01.21265764

97. DiCarlo, J. E., Norville, J. E., Mali, P., Rios, X., Aach, J. and Church, G. M., Genome engineering in *Saccharomyces cerevisiae* using CRISPR-Cas systems. *Nucleic Acids Res.* **2013,** *41* (7), 4336-4343.

Chapter 2. microRNA detection at ambient temperature using CRISPR-LwaCas13a

2.1 Introduction

Functional RNAs have different lengths. At the short end of the length spectrum, non-coding RNA such as microRNA (miRNA) can be as short as 22 nt. microRNA plays an important role in cells regulating the expression of messenger RNA.[1-3] Some microRNAs are related to the development of cancers and are considered potential biomarkers for cancer diagnostics.[1-3] Current studies use RT-PCR[4] to quantify the concentration of microRNA in cell lysates. There are also techniques that do not require thermal cycling and nucleic acid amplification and thus hold promises for microRNA analysis not only in test tubes but also in physiological conditions such as in cells.[5] Given the low abundance and the short length of microRNAs, efficient signal amplification is required.[5]

CRISPR-Cas13a systems are very useful for RNA detection because they can be directly activated by RNA targets.[6-10] Although most targets detected by CRISPR-Cas13a are long RNA, microRNA may also be able to serve as an activator for Cas13a. However, the short length of microRNA presents challenges to assay development. The short length may not be sufficient for the activation of some Cas13a homologs. Without structural data on LwaCas13a, the essential interaction between crRNA-target duplex and LwaCas13a is unknown. Gootenberg et al.[10] have reported that LwaCas13a naturally requires 29–30 nt spacers and that shorter spacers impaired the detection sensitivity. Another challenge of the short length is that one cannot use multiple crRNA-Cas13a to bind the same molecule simultaneously to improve sensitivity. In

addition, the sequences of microRNA may not be ideal for high Cas13a activity because it is known that activator sequences affect the activity of Cas13a.

The aim of this chapter is to explore the potential of LwaCas13a for the detection of short microRNA. I used miR-10b (23 nt) as an example target, which is relevant to metastasis across multiple cancer types, including breast cancer.[11-13] I first optimized the reaction conditions and discussed key parameters for the high *trans*-cleavage activity of LwaCas13a for the detection of microRNA. Using LwaCas13a, I successfully developed a homogeneous assay for the detection of miR-10b. This assay, conducted in a single tube, achieved the detection of miR-10b at the low pM level.

While I was working on this chapter, another group published a similar study that demonstrated the feasibility of direct recognition of microRNA using another Cas13a enzyme, LbuCas13a.[14] Since then, LbuCas13a has been used together with multiple signal detection platforms, including fluorescence, electrochemistry, and microfluidic devices,[15] for the detection of microRNA. Granados-Riveron et al.[15] reviewed related literature on the use of Cas13a for the detection of microRNA. Little work is available on the use of LwaCas13a. Only two electrochemical detection techniques used LwaCas13a.[16-17]

2.2 Experimental Section

2.2.1 Cas13a expression and purification

LwaCas13a (Addgene, plasmid#90097) and LbuCas13a (Addgene, plasmid#83482) were expressed in Rosetta DE3 pLysS cells. Plasmids containing the LbuCas13a gene were replicated in DH5α cells and extracted with QIAprep Spin Miniprep Kit (Qiagen, #27104). Plasmids were then transformed into Rosetta DE3 pLysS competent cells (Novagen, #70956-

3). Rosetta cells were grown at 37 °C in 2xYT broth (Invitrogen, #22712-020) to reach an OD600 of 0.6. Protein expression was induced by supplementation with IPTG (Invitrogen, 15529-019) with a final concentration of 500 μM. Upon induction, cells were cooled to 18°C and grown for 16 h.

Cas13a was purified using immobilized Ni-affinity chromatography. Cell pellets were lysed by sonication, in lysis buffer [50 mM Tris-HCl pH 7.5, 500 mM NaCl, 0.5 mM PMSF, 5% glycerol, supplemented with EDTA-free protease inhibitor (Roche, #05892791001)]. Then cell debris was removed by centrifugation at 10,000g for 20 min, at 4 ˚C. I optimized the imidazole concentration for Ni column loading and gradient elution. Lysis buffer was switched to a buffer containing 50 mM Tris-HCl pH 7.5, 500 mM NaCl, and 30 mM imidazole by 100K ultrafiltration (Millipore, #UFC810024/#UFC510096) and incubated with Ni-NTA agarose (Invitrogen, #R901-01) for 1 h at 4 ˚C. The column was washed twice with a buffer containing 50 mM of Tris-HCl pH 7.5 and 500 mM of NaCl. Proteins were eluted with gradient imidazole. One mL of buffer containing 50 mM Tris-HCl pH 7.5, 500 mM NaCl, and imidazole in different concentrations were added consecutively, and eluates were collected. The gradient was 40 mM, 40 mM, 50 mM, 50 mM, 100 mM, 160 mM, and 250 mM. Cas13a-containing eluates were concentrated by 100K ultrafiltration and proteins were stored in storage buffer (30 mM Tris-HCl pH 7.5, 300 mM NaCl, 1 mM TCEP, 0.3 mM PMSF, 35% of glycerol, supplemented with 0.33× EDTA-free protease inhibitor).

The total protein concentration was measured by Bradford assay (Bio-Rad, #500-0006). The Cas13a purity was calculated by analyzing the photo intensity of each band in one eluate shown on the SDS-PAGE gel with Image J software. Purity = the photo intensity of the Cas13a

band / the total photo intensity of all bands in the same eluate. Unless otherwise specified, Cas13a concentration refers to the total protein concentration.

2.2.2 *In vitro* transcription of RNA

crRNAs were produced by *in vitro* T7 transcription. The 5' end of the crRNA is the direct repeat (DR). The spacer at the 3' end of the crRNA was designed to be a complementary region for miRNA. The DNA templates for T7 transcription were produced by fill-in PCR. Two long primers with 20-nt overlaps at the 3' end served as both primers and as the template for fill-in PCR. The forward primer contained a T7 promoter region and part of the DR. The reverse primer contained the spacer and part of the DR. PCR reactions were performed using Q5® Hi-Fidelity DNA Polymerase (NEB, #M0491L). The PCR program was 95 °C for 30 s, then 35 cycles consisting of 95 °C for 10s, 57 °C for 10 s, and 72 °C for 20 s, followed by 72 °C for 20 s. PCR products were purified with a MinElute PCR Purification Kit (Qiagen, #28006) and used as the template for T7 transcription (HiScribe™ T7 High Yield RNA Synthesis Kit, NEB, #E2040S). crRNA was purified with TRIzol Reagent (ThermoFisher Scientific, #15596026) and quantified using a NanoVue Plus Spectrophotometer (GE Healthcare). crRNA was subsequently aliquoted and stored at -80 °C. I also produced long target RNA following the same procedure. The crRNA and RNA targets tested are summarized in **Table 2-1**.

Table 2-1. Target RNA and crRNA sequences

Name of Sequence	Sequence
miR-10b (IDT)	UAC CCU GUA GAA CCG AAU UUG UG
miR-10b (T7 transcription)	GGUACCCUGUAGAACCGAAUUUGUG
miR-10b-Mismatch-1	GGUACACUGUAGAACCGAAUUUGUG
miR-10b-Mismatch-2	GGUACCAUGUAGAACCGAAUUUGUG
miR-10b-Mismatch-3	GGUACCCUGUAGAAGCGAAUUUGUG
miR-10b-Mismatch-4	GGUACCCUGUAGAACCUAAUUUGUG
miR-10b-Mismatch-5	GGUACCCUGUAGAACCGAAUUUUUG
extended miR-10b	AUCCUUGUAGUUAUGCU UACCCUGUAGAACCGAAUUUGUG AUGCUCUUG
crRNA with Lwa Cas13a for miR10b	GGG GAU UUA GAC UAC CCC AAA AAC GAA GGG GAC UAA AAC CAC AAA UUC GGU UCU ACA GGG UA
crRNA with LbuCas13a for miR10b	GGC CAC CCC AAA AAU GAA GGG GAC UAA AAC A CAC AAA UUC GGU UCU ACA GGG UA
ssRNA1 (161 nt)	G GGG GCC AGU GAA UUC GAG CUC GGU ACC CGG GGA UCC UCU AGA AAU AUG GAU UAC UUG GTA GAA CAG CAA UCU A CUC GAC CUG CAG GCA UGC AAG CUU GGC GUA AUC AUG GUC AUA GCU GUU UCC UGU GUU UAU CCG CUC ACA AUU CCA CAC AAC AUA CGA
crRNA with Lwa for ssRNA1	GGG GAU UUA GAC UAC CCC AAA AAC GAA GGG GAC UAA AAC UAG AUU GCU GUU CUA CCA AGU AAU CCA U

2.2.3 Optimization of the reaction composition for the best target recognition and signal generation

Unless otherwise noted, all fluorescence generated over time was measured by a microplate reader (Molecular Devices, FilterMax F5), with the excitation wavelength at 485

nm and emission wavelength at 535 nm. For the majority of the experiments, fluorescence was detected every 3 min for at least 1 h. The specific experimental conditions are listed in the figure caption of each figure.

2.2.4 The performance of Cas13a-mediated RNA detection at different temperatures

Cas13a and annealed crRNA were first incubated at 25 °C for 10–30 min. Then, chilled targets and reporters were added to chilled reactions on ice. The cleavage reaction contained 5 nM Cas13a, 0.5 nM crRNA, 40 mM Tris-HCl pH 7.5, 60 mM NaCl, 6 mM $MgCl_2$, 0.005% Tween-20, 30 nM RNaseAlert reporter, plus 200 pM targets for positive tests or 0 pM target for non-target controls. Then fluorescence at 535 nm (excitation at 485 nm) was measured for 1 h at multiple temperatures using a StepOnePlus™ RT-PCR instrument (Applied Biosystems). For accurate comparisons, reactions were conducted by preparing a master mix containing all reagents except targets and reporters. The two components were added to the reaction, and the mixture was immediately aliquoted to each reaction well (20 μL) and tested with minimal delay. The StepOnePlus™ RT-PCR instrument allows users to set 6 temperatures for 6 individual heating blocks.

2.2.5 Detection of microRNA-10b at ambient temperature

The reagents were mixed on a black 96-well plate at 25 °C. crRNA and TCEP-treated Cas13a were first incubated in reaction buffer at 25 °C for 0.5 h. Then miRNA (IDT) and reporter (RNaseAlert, IDT) were added. The final concentrations of the reagents were: 5 nM Cas13a, 0.5 nM crRNA, 40 mM Tris-HCl pH 7.5, 60 mM NaCl, 6 mM $MgCl_2$, 0.005% Tween-20, 30 nM RNaseAlert, and 0–500 pM miRNA. Fluorescence at 535 nm (excitation at 485 nm) was measured for 1 h at 25 °C using a fluorescence microplate reader (Molecular Devices,

FilterMax F5). The signal amplification fold was calculated by converting the raw fluorescence intensity to the concentration of reporters cleaved with a calibration constructed using the fluorescence generated by fully cleaved reporters of different concentrations.

2.3 Results and Discussion

2.3.1 Expression, purification, and characterization of LwaCas13a and LbuCas13a

I produced LwaCas13a and LbuCas13a in *E. coli* using a plasmid containing His-tagged Cas13a DNA sequences. I simplified the purification procedure by improving the performance of immobilized Ni affinity chromatography. I introduced imidazole during the incubation of protein with Ni-NTA agarose (Invitrogen, #R901-01) to improve the specificity of metal-protein binding and used gradient elution to maximize the purity of protein in one elution. The SDS-PAGE gel analysis results of eluates are shown in **Figure 2-1**.

The produced enzymes showed the desired *trans*-cleavage activity and minimal non-specific signal (**Figure 2-2**). The fluorescence response depended on the concentration of the target. There was minimal fluorescence increase in all negative groups which did not contain crRNA, Cas13a, or target molecules. The negative control without crRNA showed minimal fluorescence increase, indicating that there is almost no contaminating *E. coli* RNase activity in the Cas13a I prepared (**Figure 2-2**).

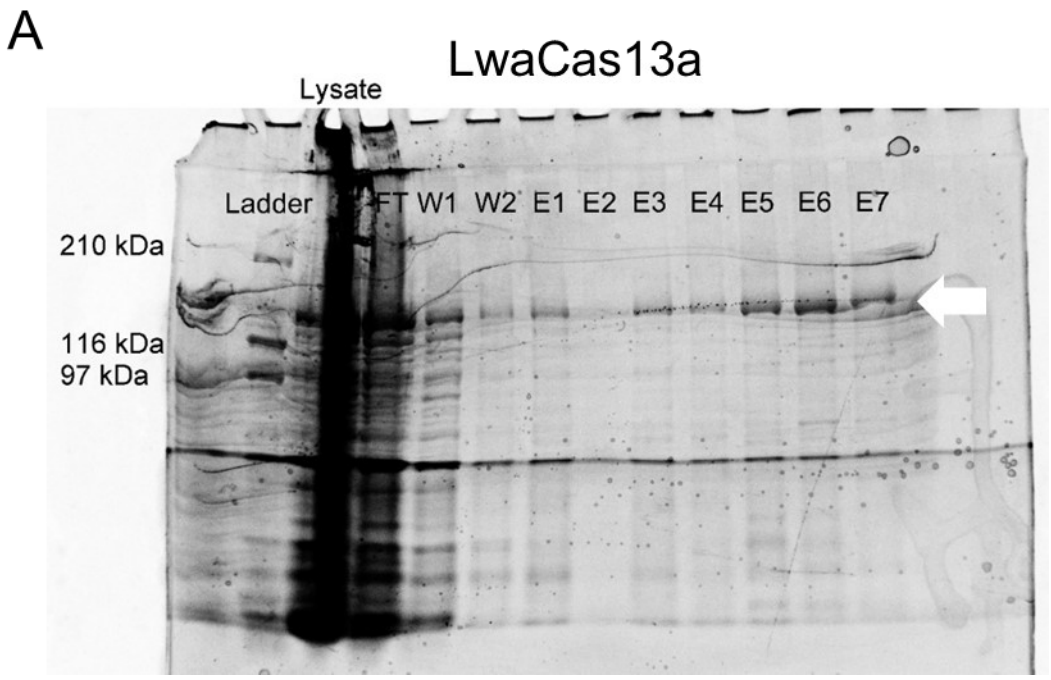

Figure 2-1. Representative SDS-PAGE gels of purified LwaCas13a (A) and LbuCas13a (B). A. The SDS-PAGE gel showing proteins in the lysate before purification, two consecutive washing solutions, and subsequent elution solutions from LwaCas13a purification. LwaCas13a has a molecular weight of around 150 kDa, and corresponding bands (indicated by the white arrow) were found in eluates with the highest concentration observed in eluate 5 (E5) and eluate 6 (E6). The yield of Cas13a was 28 μg/100 mL cell culture, and the purity was 79%. Lysate: cell lysate before protein purification; FT: protein flow through the Ni-NTA column; W1: first washing with imidazole-free buffer; W2: second washing with imidazole-free buffer; E1–7: eluate 1–7 eluted from the column with 1 mL of buffer containing 40 mM, 40 mM, 50 mM, 50 mM, 100 mM, 160 mM, 250 mM imidazole; Ladder: protein standards, Bio-Rad, #1610303. Proteins were stained using InstantBlue (C.B.S. Scientific, #95045-070).

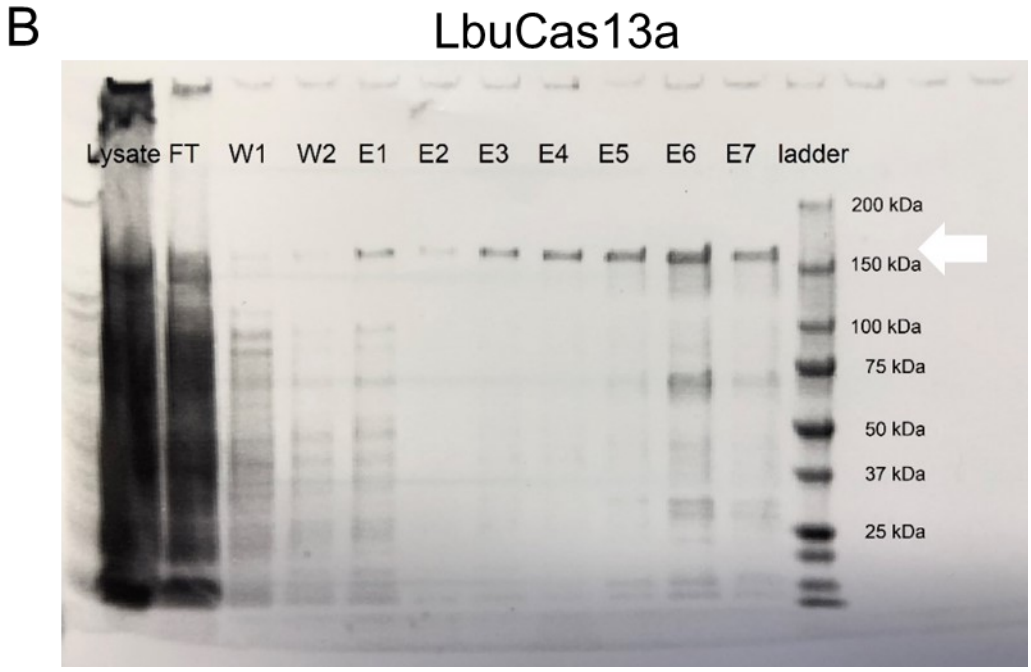

Figure 2-1. (B) The SDS-PAGE gel showing proteins in the cell lysate before purification, two consecutive washing solutions, and subsequent elution solutions from LbuCas13a purification. Eluted proteins have a molecular weight of slightly over 150 kDa and are indicated by the white arrow. Lysate: cell lysate before protein purification; FT: protein flow through the Ni-NTA column, W1: first washing with imidazole-free buffer; W2: second washing with imidazole-free buffer; E1–7: eluate 1–7 eluted from the column with 1 mL of buffer containing 40 mM, 40 mM, 50 mM, 50 mM, 100 mM, 160 mM, 250 mM imidazole; Ladder: protein standards, Bio-Rad, #161-0373. Proteins were stained using InstantBlue (C.B.S. Scientific, #95045-070)

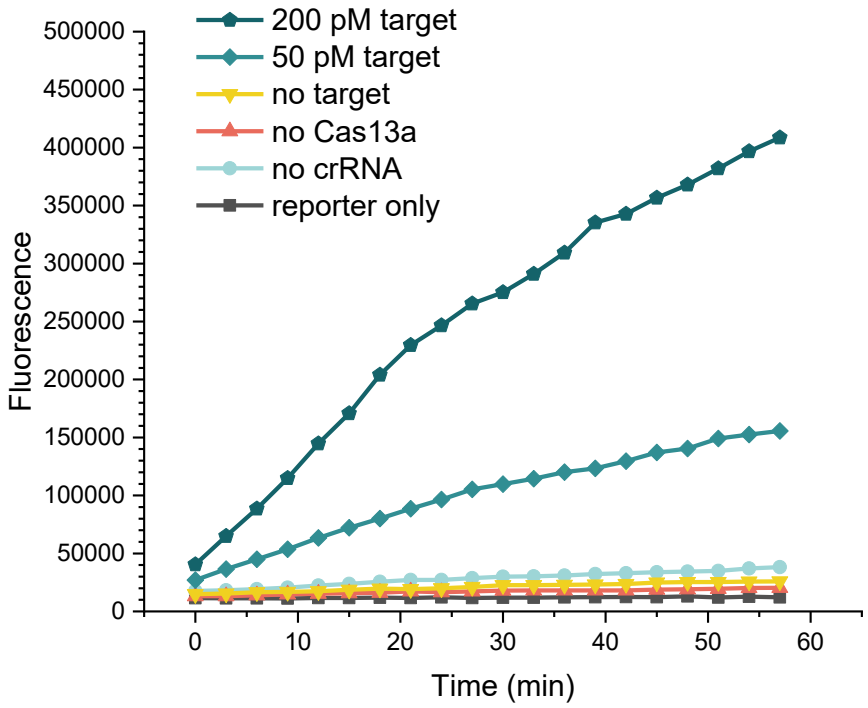

Figure 2-2. Characterization of the *trans*-cleavage activity of Cas13a (LwaCas13a).

2.3.2 Detection of microRNA using CRISPR-Cas13a

The microRNA detection using CRISPR-Cas13a requires only a single-step, homogeneous reaction (**Figure 2-3**). The 3' single-stranded spacer region of the crRNA is complementary to the whole sequence of microRNA, and thus microRNA activates the crRNA-Cas13a ribonucleoprotein (RNP). Consequently, the activated crRNA-Cas13a RNP cleaves multiple single-stranded RNA reporters that are dually labeled with a pair of fluorophore (F) and quencher (Q). The intensity of fluorescence of each reaction indicates the presence and the concentration of microRNA and can be measured, for example, using a microplate reader.

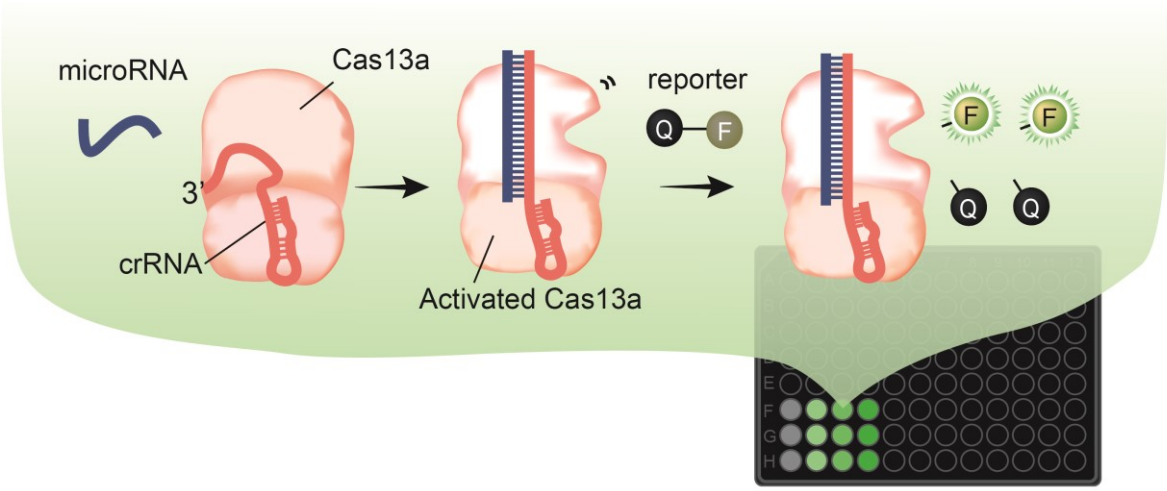

Figure 2-3. Schematics of microRNA detection using CRISPR-Cas13a. In the presence of a specific microRNA target, hybridization of the microRNA with crRNA initiates the RNase activity of Cas13a. The activated crRNA-Cas13a ribonucleoprotein cleaves multiple RNA reporters, generating amplified fluorescence signals.

2.3.3 The reaction composition for efficient microRNA recognition and high LwaCas13a *trans*-cleavage activity

I first detected a 161-nt target RNA (ssRNA1 in **Table 2-1**) using the established reaction conditions. The fluorescence intensities (**Figure 2-4A**) corresponded to the concentrations (10 pM, 100 pM, 1 nM) of the target ssRNA1. There was minimal background fluorescence when the reaction mixture did not contain crRNA or Cas13a. These results indicate that the system is able to detect ssRNA. However, when the target length was substantially shortened to microRNA-10b (23 nt), I observed a significant decrease in sensitivity **(Figure 2-4B).** Therefore, I further optimized the reaction conditions to detect microRNA-10b. I reasoned that sufficient microRNA recognition, signal generation and amplification are important to improve the signal-to-background ratio of the microRNA assay.

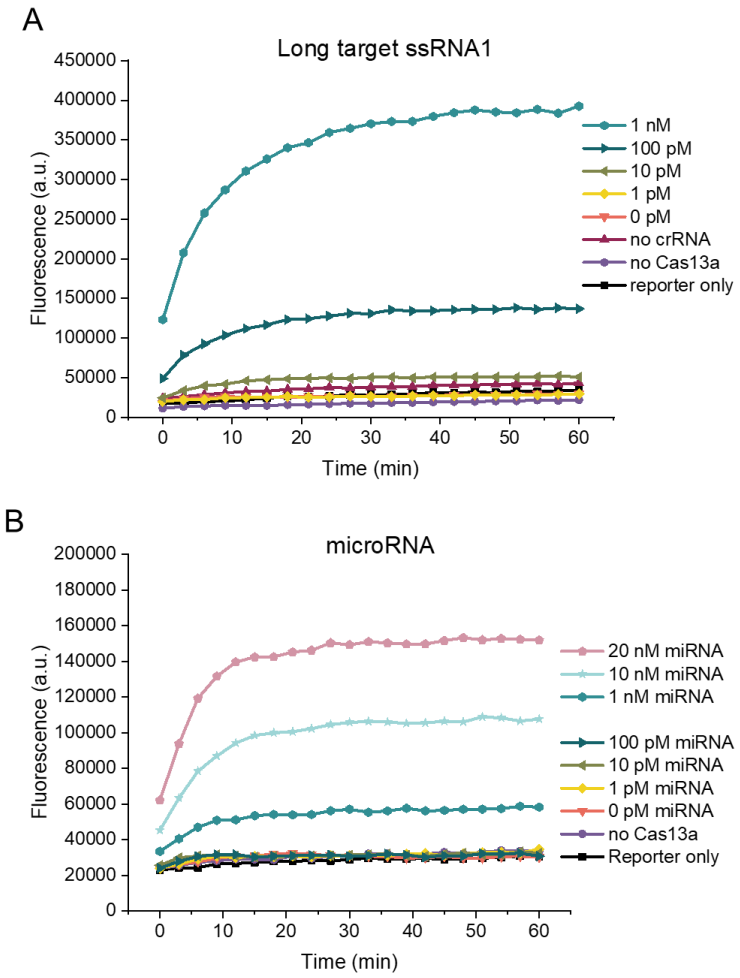

Figure 2-4. Significant reduction of sensitivity when switching target from long target ssRNA1 (161 nt) to short target microRNA-10b (23 nt) before optimization of reaction conditions. **A.** The detection of the 161-nt ssRNA1 target. The reagents 5 nM Cas13a, 20 nM crRNA, 40 mM Tris-HCl pH 7.5, 60 mM NaCl, 6 mM $MgCl_2$, and 0–1 nM ssRNA1 were first mixed and incubated at room temperature for 30 min, then 30 nM reporter RNA was added and the fluorescence generation within 1 h at 37 °C was measured with a microplate reader (Molecular Devices, FilterMax F5). **B.** The detection of the 23-nt microRNA-10b. The reaction proceeded under the same condition except that crRNA for microRNA-10b was annealed before mixing with other reagents.

One consideration is to ensure the proper formation of crRNA-Cas13a ribonucleoprotein and its recognition of microRNA. The ratio of crRNA to Cas13a and the annealing of the crRNA to form the appropriate secondary structure are important for high sensitivity (**Figure 2-5**). I optimized the concentration of crRNA and Cas13a. The high signal-to-background ratio when using lower crRNA (0.5 nM) compared to Cas13a (5 nM) is likely because of two reasons: (1) the extra crRNA could hybridize with the microRNA target, but Cas13a was not activated; (2) the extra crRNA in the test was also cleaved by Cas13a as a non-specific substrate, resulting in delayed cleavage of fluorescence reporters. crRNA interacts with Cas13a through a bulge-containing stem-loop structure, the annealing of crRNA may help with the formation of crRNA-Cas13a ribonucleoprotein. Thus, I optimized the assay by introducing a crRNA pre-annealing treatment, and this improved the signal-to-background ratio (**Figure 2-5C**).

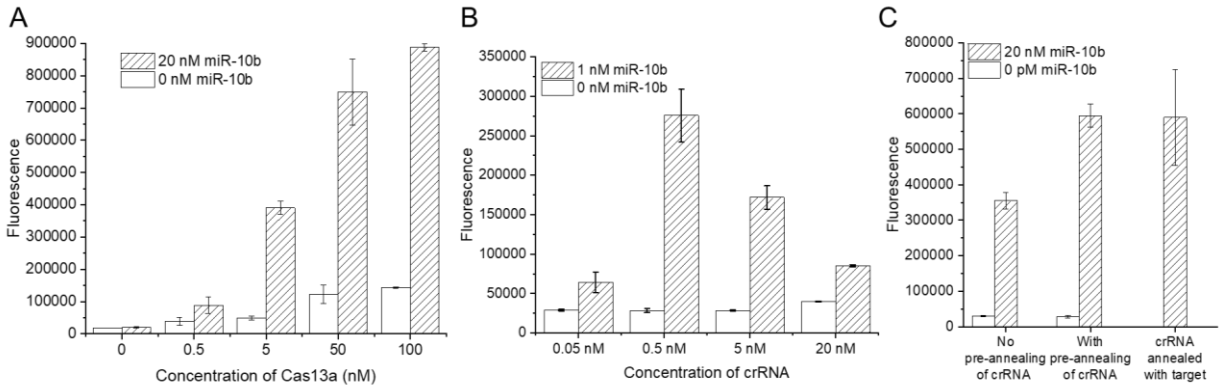

Figure 2-5. Optimization of Cas13a concentration, crRNA concentration, and crRNA annealing. **A.** Effect of the concentration of Cas13a on the microRNA-10b (miR-10b) detection. All reagents were mixed at 25 °C in a 96-well plate, including 0–100 nM Cas13a, 20 nM crRNA, 20 nM miR-10b, 30 nM reporter (RNaseAlert), and buffer containing 40 mM Tris-HCl pH 7.5, 60 mM NaCl, 6 mM $MgCl_2$, and 0.005% Tween-20. Fluorescence was measured at 25 ˚C for 1 h. Fluorescence at 18 min was shown in the graph. **B.** Effects of the concentration

of crRNA on the miR-10b detection. All reagents were mixed at 25 °C, including 5 nM Cas13a, 0.05–20 nM crRNA, 1 nM miR-10b, 30 nM RNaseAlert, and buffer containing 40 mM Tris-HCl pH 7.5, 60 mM NaCl, and 6 mM $MgCl_2$. Fluorescence was continuously measured at 37 °C for 1 h. Fluorescence at 18 min was plotted. **C.** Effects of pre-annealing of crRNA on the miR-10b detection. The pre-annealing was done by heating 1 μM crRNA in Tris-HCl buffer (40 mM, pH = 7.5) to 85 °C for 5 min and cooling down to 20 °C gradually in 20 min. The pre-annealed crRNA (20 nM) was mixed with other reagents at 25 °C, including 5 nM Cas13a, 20 nM miR-10b, 40 mM Tris-HCl pH 7.5, 60 mM NaCl, and 6 mM $MgCl_2$. crRNA annealed with equal moles of microRNA and crRNA that was not pre-annealed were also tested for comparison. After incubation at 37 °C for 30 min, 30 nM reporters were added. Fluorescence was monitored at 37 °C, and the fluorescence intensity at 18 min was plotted.

Another consideration is to ensure a high *trans*-cleavage rate upon the activation of crRNA-Cas13a ribonucleoprotein. I used a higher concentration of the reporter (30 nM) than crRNA-Cas13a RNP (0.5 nM) (**Figure 2-6**). The composition of the reaction buffer is also important for the performance of the microRNA assay because conditions such as the cofactor and buffer pH determine the *trans*-cleavage activity of Cas13a. Mg^{2+} is a common cofactor for nuclease and facilitates nucleic acid folding or inter-molecular interaction. For Cas13, Mg^{2+} serves as a cofactor, stabilizes crRNA folding[18], and enhances crRNA-target hybridization. I tested the effect of Mg^{2+} concentration, ranging from 0.12 mM to 15 mM, on the *trans*-cleavage activity (**Figure 2-7**). A lower concentration of Mg^{2+} resulted in reduced *trans*-cleavage activity. At physiological conditions, 0.5–1 mM of Mg^{2+}, the reaction rate was around half of that at the preferred Mg^{2+} concentration, 6 mM (**Figure 2-7A**). This suggests that Cas13a-based detection

of RNA in live cells (0.5–1 mM Mg^{2+}) could suffer from a reduced *trans*-cleavage activity . Further increasing Mg^{2+} concentration from 6 mM to 15 mM impaired the Cas13a activity. This may be due to RNA over-folding caused by high concentrations of Mg^{2+}.

Cas13a operates well within pH 7–7.5 (**Figure 2-8A**). Detergent Tween-20 (0.005% to 0.05%) enabled continual cleavage, likely because of reducing adsorption of reagents on the surface of wells (**Figure 2-8B and 2-8C).** All the experiments were prepared in an RNase-free cabinet, and RNase inhibitor is also needed otherwise.

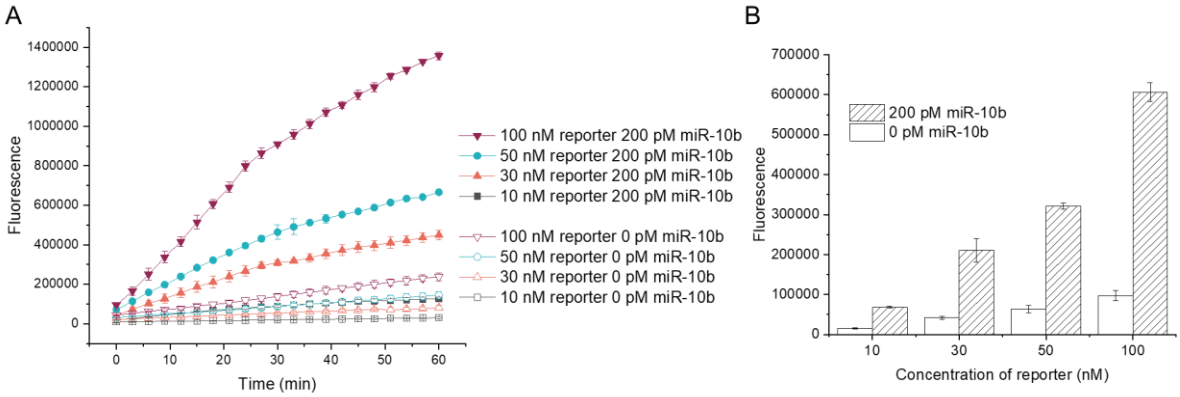

Figure 2-6. Effect of the concentration of reporter on the signal generation facilitated by the *trans*-cleavage activity of the crRNA-Cas13a ribonucleoprotein. Reactions contain 10 nM Cas13a, 0.5 nM crRNA, 0 or 200 pM miR-10b, 10–100 nM reporters, and the buffer (40 mM Tris-HCl pH 7.5, 60 mM NaCl, 6 mM $MgCl_2$, 0.005% Tween-20). **A.** Realtime fluorescence monitoring for 1 h at 27 °C. **B.** Comparison of fluorescence intensity measured at 18 min (data from **Figure 2-6A**).

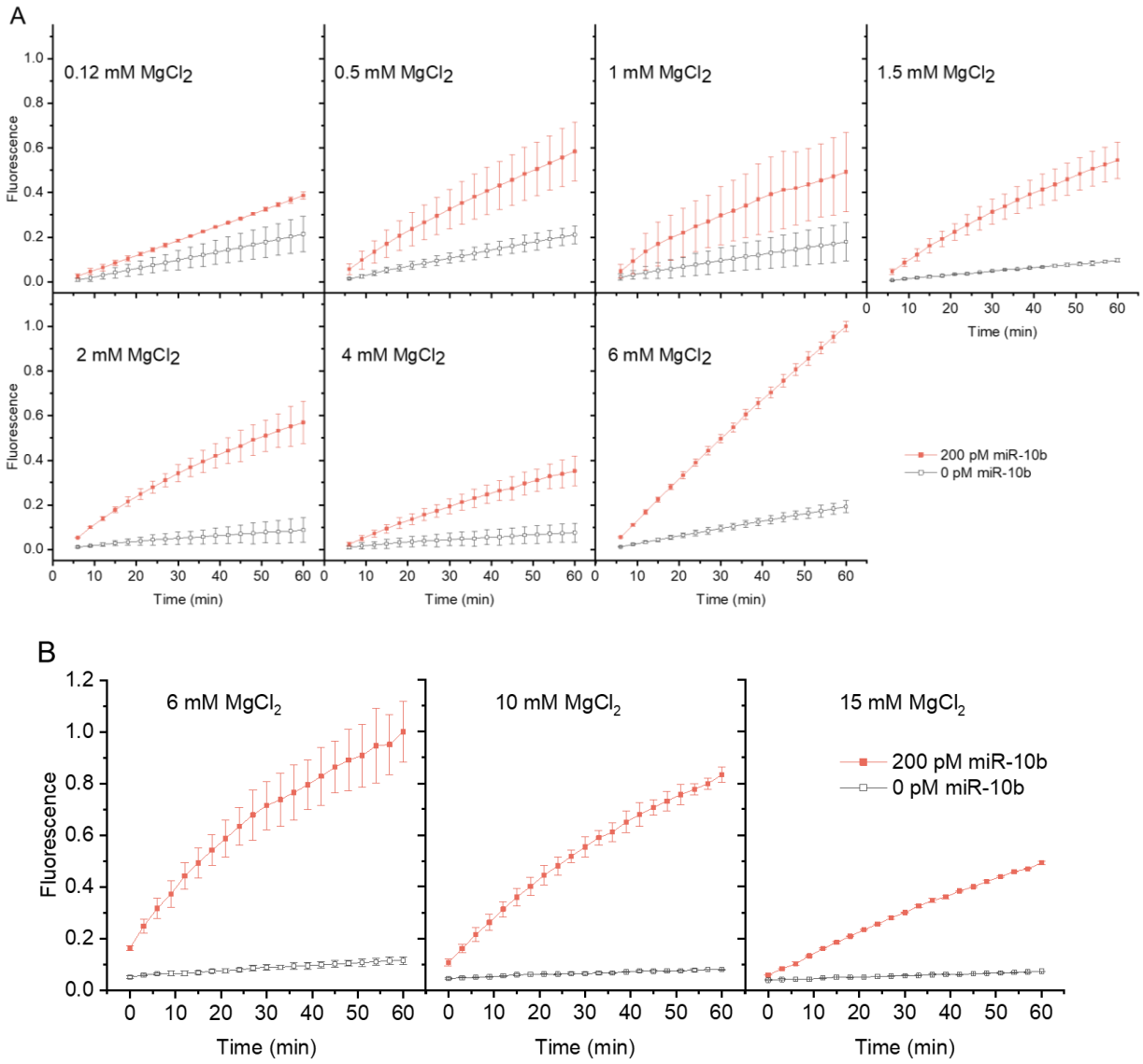

Figure 2-7. Effect of Mg^{2+} on the *trans*-cleavage kinetics of Cas13a in the detection of microRNA-10b. **A.** Effect of Mg^{2+} on the apparent *trans*-cleavage kinetics. Mg^{2+} concentrations lower than 6 mM resulted in reduced Cas13a activity. The crRNA and Cas13a were pre-incubated at high concentrations (25 nM crRNA and 250 nM Cas13a). The complexes were then added into reactions at a volume of 20 µL. The reaction only contained 0.12 mM $MgCl_2$ if no additional $MgCl_2$ was added. Reactions contained: 5 nM Cas13a, 0.5 nM crRNA, 0 or 200 pM miR-10b, 30 nM reporters, 40 mM Tris-HCl pH 7.5, 60 mM NaCl, 0.12–6 mM $MgCl_2$, and 0.005% Tween-20. Fluorescence was measured by StepOnePlus Applied

Biosystems. To focus on the increase of fluorescence and avoid the effect of well-to-well variation of fluorescence, fluorescence intensity from the first measurement was subtracted from the following measurement points. The fluorescence was normalized by taking the increase of fluorescence within 60 min of reaction with 6 mM Mg^{2+} as 1. **B.** Effect of Mg^{2+} on the overall reaction. Mg^{2+} concentrations much higher than 6 mM impaired the operation of Cas13a. crRNA and Cas13a were not pre-incubated. The reagents 5 nM Cas13a, 0.5 nM crRNA, 0 or 200 pM miR-10b, 30 nM reporters, 40 mM Tris-HCl pH 7.5, 60 mM NaCl, 6–15 mM $MgCl_2$, and 0.005% Tween-20 were mixed at the same time in the volume of 100 µL and the reaction proceeded at 27 °C. The fluorescence measured by a microplate reader (Molecular Devices, FilterMax F5) was normalized by setting the final fluorescence intensity of the test containing 6 mM Mg^{2+} as 1.

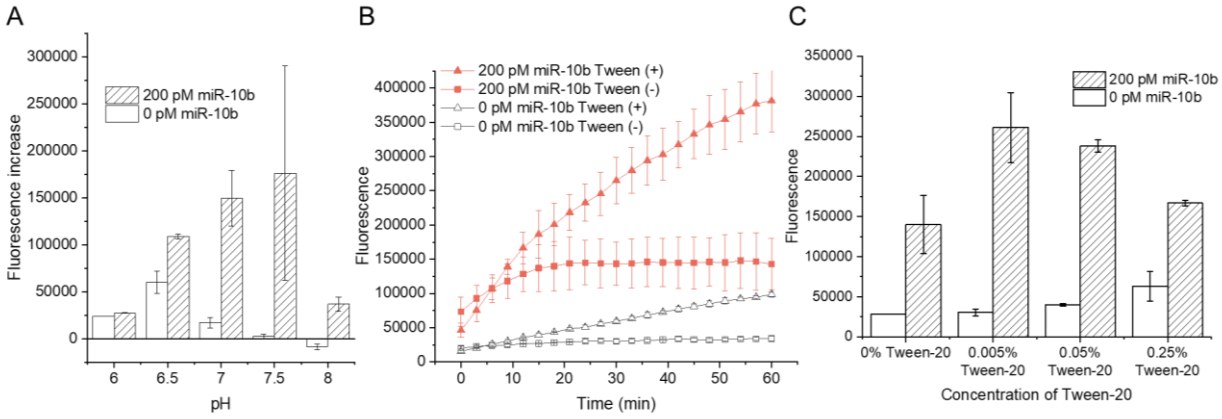

Figure 2-8. Effect of buffer pH and detergent concentration on the *trans*-cleavage activity and kinetics. A. The effect of reaction buffer pH on the detection of miR-10b. The pH of Tris-HCl buffer ranged from 6 to 8. Reactions contain 5 nM Cas13a, 0.5 nM crRNA, 0 or 200 pM miR-10b, 40 mM Tris-HCl, 60 mM NaCl, 6 mM $MgCl_2$, and 0.05% Tween-20. Fluorescence was monitored at 25 °C. **B.** The effect of Tween-20 in reaction buffer on the reaction kinetics.

Reactions contained 5 nM Cas13a, 0.5 nM crRNA, 0 or 200 pM miR-10b, 40 mM Tris-HCl, 60 mM NaCl, 6 mM $MgCl_2$, 30 nM reporter, supplemented with or without 0.05% Tween-20, and were monitored at 25 °C. **C.** Effect of the concentration of Tween-20 on the miR-10b detection. Reactions proceeded at 25 °C in a 96-well plate, and fluorescence at 18 min was plotted. Each reaction contained 5 nM Cas13a, 0.5 nM crRNA, 0 or 200 pM miR-10b, 40 mM Tris-HCl pH 7.5, 60 mM NaCl, 6 mM $MgCl_2$, Tween-20 in different v/v percentages, and 30 nM reporter.

2.3.4 Performance of microRNA detection within a wide range of temperatures

To characterize the activity of Cas13a and the performance of the microRNA detection techniques at different temperatures, I tested two Cas13a homologs that have shown high *trans*-cleavage kinetics. LwaCas13a worked in a very broad temperature range, from 7 to 42 °C **(Figure 2-9A and 2-9B)**. To eliminate the cleavage of substrates during preparation, I added chilled target and reporters to each chilled reaction on ice. Surprisingly, LwaCas13a ribonucleoprotein (RNP) works efficiently at even 7 °C, showing almost 1/3 of the maximum activity **(Figure 2-9A)**. Both the initial cleavage rate and the fluorescence generation within one hour suggested that the optimum temperature is 23–27 °C. When increasing the reaction from 27 to 42 °C, the activity decreased significantly. The cleavage rate also decreased over time at the higher temperatures (32–42 °C) (**Figure 2-9A**). A recent report showed that the thermal behavior of Cas13a varied among homologs and that free LwaCas13a denatured at 42 °C.[19] The unexpectedly lower activity at 32–37 °C than that at ambient temperature led me to systematically study the thermal behavior of Cas13a (**Chapter 4**). Similarly, when detecting

the same microRNA-10b target, LbuCas13a also worked within a broad temperature range, from 11 to 37 °C, and high signals were obtained within 19–32 °C (**Figure 2-9C and 2-9D**).

The detection of microRNA using both LwaCas13a and LbuCas13a can be carried out at ambient temperatures. The performance of the microRNA-10b assays is better at ambient temperatures (23 °C) than at the 37 °C temperature commonly used by reported CRISPR-based microRNA detection techniques. Using ambient temperature for detection reduces the need for power and temperature-control apparatuses.

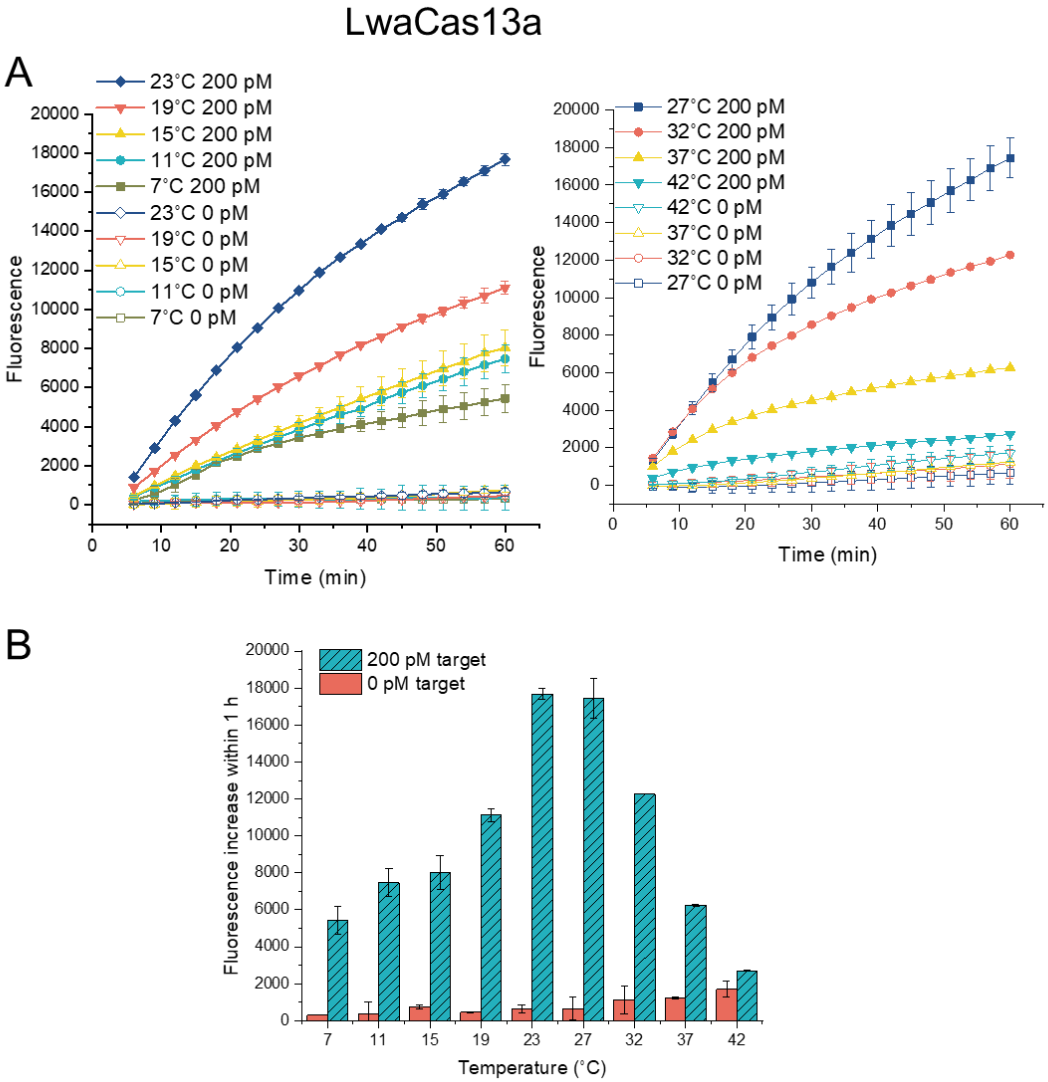

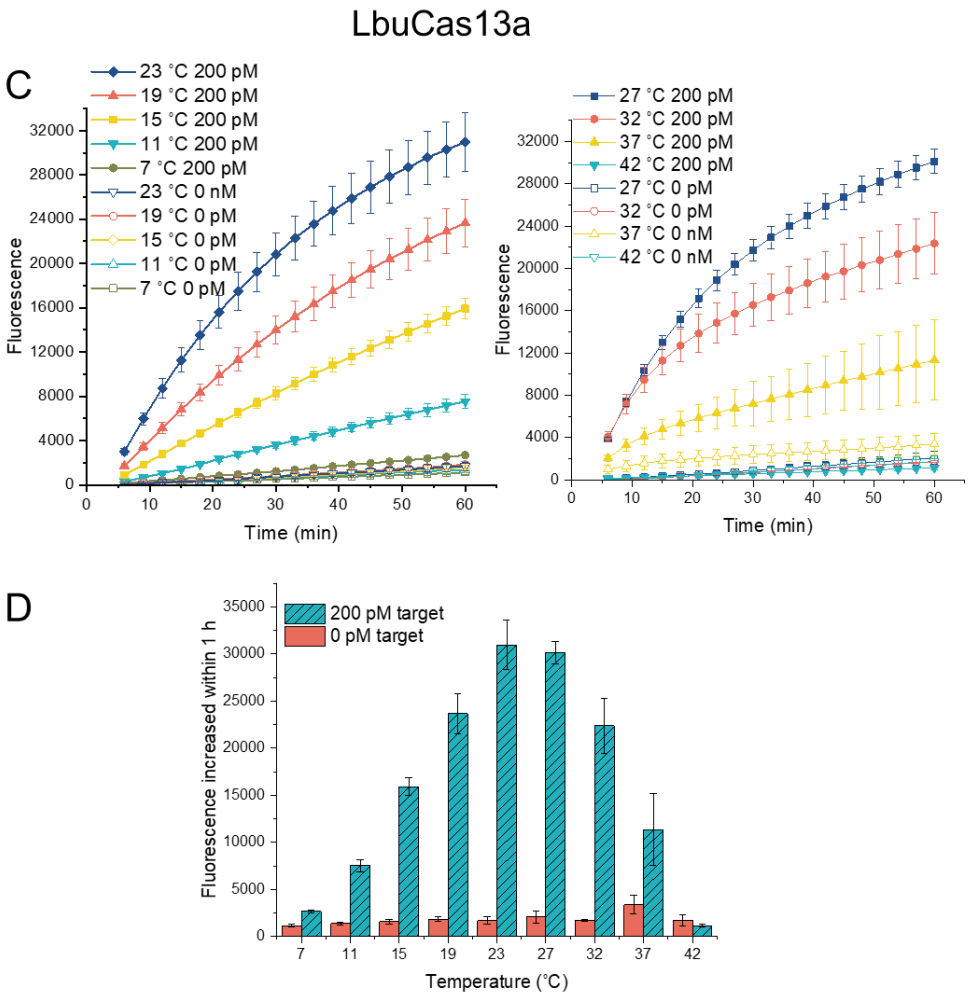

Figure 2-9. *Trans*-cleavage kinetics of LwaCas13a and LbuCas13a and fluorescence increase from the detection of miR-10b at different temperatures. **A**. LwaCas13a *trans*-cleavage kinetics at 7–42 °C. **B**. Fluorescence generated within 1 h by the *trans*-cleavage activity of LwaCas13a. **C**. LbuCas13a *trans*-cleavage kinetics at 7–42 °C. **D**. Fluorescence generated within 1 h by the *trans*-cleavage activity of LbuCas13a at temperatures ranging from 7 to 42 °C.

2.3.5 Sensitivity and specificity of the microRNA detection assay

To test the analytical sensitivity and the quantification potential of the microRNA detection technique, I tested 0.1–500 pM microRNA-10b and blank samples that contained no microRNA-10b. The assay, conducted at ambient temperature (~25 °C), shows a clear concentration-dependent fluorescence intensity (**Figure 2-10A and 2-10B**). Additional analysis of the initial cleavage rate also shows an expected concentration dependence (**Figure 2-10C**). Fluorescence generated from 5 pM microRNA-10b or higher was clearly differentiated from the background, as shown in both fluorescence vs time plots (**Figure 2-10A and 2-10B**) and in the initial rate vs concentration plot (**Figure 2-10C**). Lower microRNA, 0.1–2 pM, also resulted in small fluorescence increases above the background. The initial cleavage rate has a clear correlation with the concentration of microRNA-10b, with a dynamic range from 5 pM to 500 pM. (**Figure 2-10C**) Within the dynamic range, the signal amplification rate is approximately 1–7 fold/min (**Table 2-2**). The signal amplification fold is the amount of reporter cleaved over the amount of the target added. The amount of reporter cleaved was calculated using the measured fluorescence intensity and a calibration curve of fluorescence vs the concentration of the fully cleaved reporter (**Figure 2-11**).

The limit of detection of my microRNA assay, 5 pM in 100 µL, suggests that as few as 0.5 fmol or 8×10^6 microRNA molecules can be detected. Previous quantification of different microRNA in a variety of tissues has shown that there are dozens to over 10 thousand microRNA per cell.[4] Normally, RNA extracted from 10^5–10^6 cells were used as a sample for analysis. If there are 10 copies of a specific RNA in each cell, 10^6 cells would contain 10^7 microRNA molecules. Considering that there would always be some loss during microRNA extraction, assuming 80% of all microRNA were sufficiently extracted, microRNA in the cell

at a concentration higher than 10 copies/cell would be sufficient for our assay to generate detectable signals. These calculations show the potential of using this microRNA detection technique for the analysis of microRNA in cell lysates.

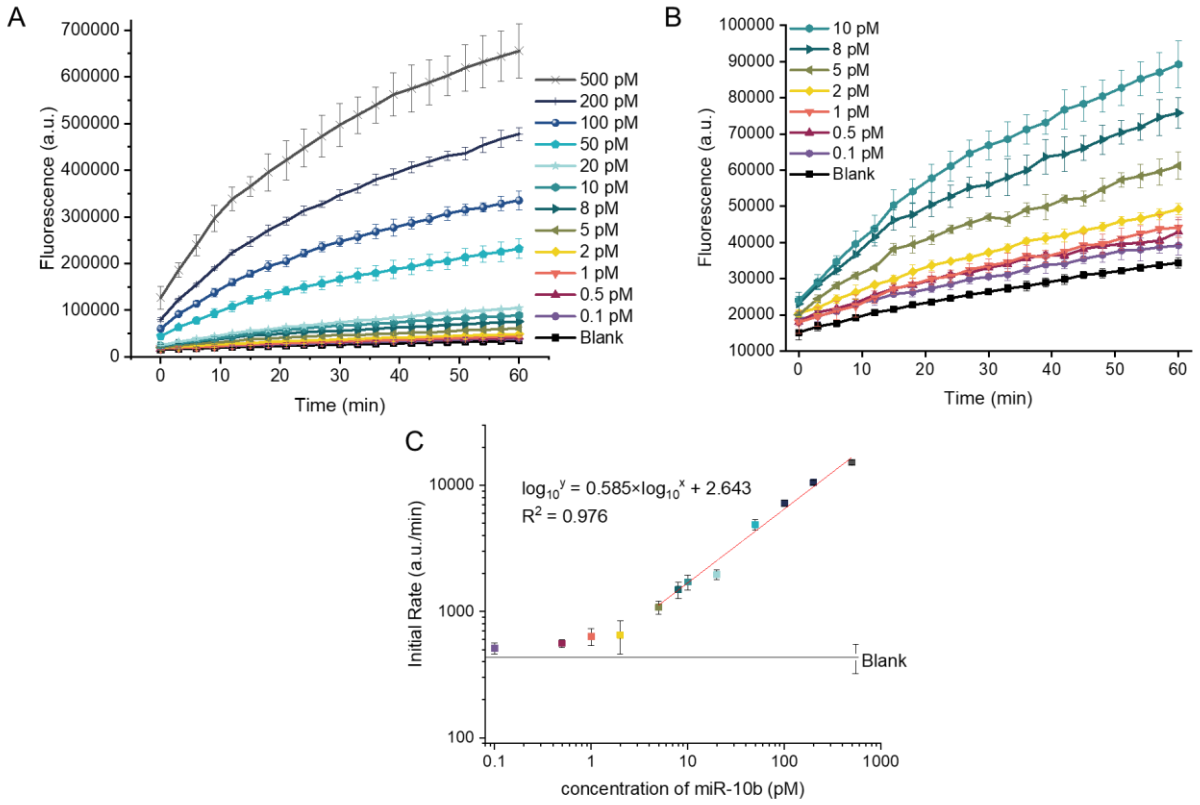

Figure 2-10. The sensitivity of microRNA-10b detection at ambient temperature.

A. Concentration-dependent fluorescence response detected over 60 min (n = 3 for positive tests and n = 6 for blank). **B.** Zoomed-in fluorescence curves of reaction with 0–10 pM microRNA -10b. **C.** Calibration curve of initial fluorescence-generation rate vs concentration of microRNA-10b. To minimize the errors from one measurement of fluorescence, I calculated the initial rate based on the increase of fluorescence within 3–15 min. The horizontal line in black indicates the average initial rate of blanks, and the error bar across it indicates the standard deviation of blank samples that did not contain microRNA-10b.

Table 2-2. Fluorescence signal amplification rate

Concentration of miRNA (pM)	Background Subtracted fluorescence increase in 18 min	Reporter cleaved (pM)*	Amplification fold/min
5	16717	438	5
8	24948	647	4
10	31371	814	5
50	109945	2853	3
100	171584	4453	2
200	248366	6448	2
500	372630	9671	1

*Concentrations of reporter cleaved were calculated based on a calibration curve of fluorescence vs reporter concentration in **Figure 2-11**.

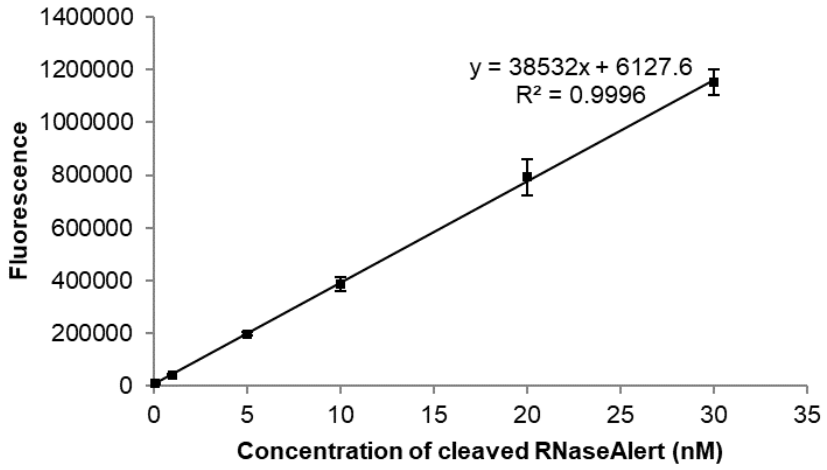

Figure 2-11. A calibration curve of the fluorescence intensity in response to the concentration of fully cleaved RNA reporter (RNaseAlert). The fluorescence was measured using a microplate reader (Molecular Devices, FilterMax F5). RNaseAlert at the concentrations of 0.1, 1, 5, 10, 20, and 30 nM was completely cleaved by RNase A for 1 h. The volume of each reaction was 100 μL. (n = 3)

The CRISPR-Cas13a system is able to distinguish sequences with more than one nucleotide mismatch. The RNA sequence composition of microRNA-10b is distinct from other discovered microRNAs. Thus, non-specific signals generated by other microRNAs would be minimal. I tested the sequence specificity of my microRNA assay under the most challenging scenario in which the synthetic RNA differs from the microRNA-10b sequence by only one nucleotide. Using T7 transcription, I produced miR-10b and five variants of single-base mismatch (**Figure 2-12A**). The results show that mismatches 1 and 2 (at positions 20 and 19) significantly impaired the *trans*-cleavage activity of Cas13a, and the selection factors were over 4. Mismatch 3 and 5 (at positions 11 and 3) impaired the *trans*-ssRNA cleavage slightly. Mismatch 4 (at position 9) shows no effect on the *trans*-ssRNA cleavage (**Figure 2-12**).

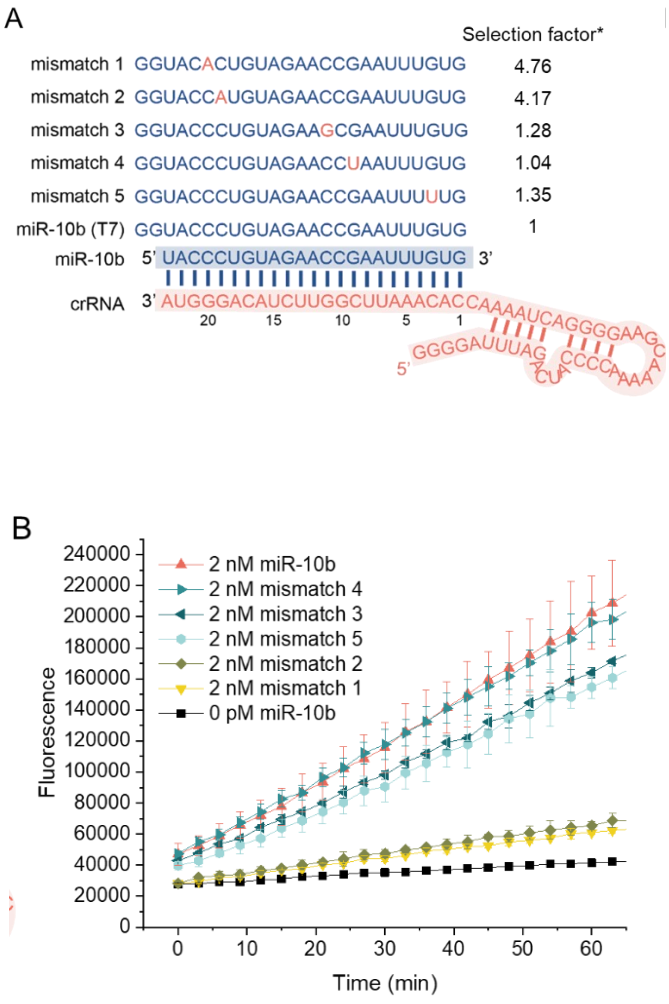

Figure 2-12. Specificity of this miR-10b assay by comparing the detection of microRNA-10b to the detection of synthetic RNA sequences with single-nucleotide mismatches. A. Illustration of mismatch positions of the sequences tested and discrimination factors between the mismatched target and the perfect target microRNA-10b (miR-10b). Two extra Guanine were introduced at the 5' end of all the sequences for efficient T7 transcription. Selection factors were calculated based on the fluorescence shown in **Figure 2-12B** with the equation: $Selection\ factor = \frac{Fluorescence\ increase\ in\ 60\ min_{[target]}}{Fluorescence\ increase\ in\ 60\ min_{[mismatch]}}$. **B.** Effect of mismatches at different positions on the *trans*-cleavage activity of Cas13a. *In vitro* transcribed miR-10b and 5 sequences with single-nucleotide mismatch were first mixed with other reagents and

incubated for 20 min at 25 °C, then the fluorescence were measured every 3 min for 1 h at 25 °C using a microplate reader (Molecular Devices, FilterMax F5). The reagents were 5 nM Cas13a, 0.5 nM crRNA, 30 nM reporter, 40 mM Tris-HCl pH 7.5, 60 mM NaCl, 6 mM $MgCl_2$, and 0.005% Tween-20.

2.4 Conclusion

CRISPR-Cas13a systems naturally operate as an RNA-activated RNase, and this feature is extremely useful for the development of RNA detection techniques. Here, I explored the potential of LwaCas13a from *Leptotrichia wadei* for the detection of short, single-stranded microRNA. The natural spacer length of LwaCas13a discovered in its original organism is mostly 29–30 nt.[10] microRNA are as short as 22 nt. A challenge is that the activation of Cas13a by the short microRNA is less efficient. I used a fluorescence detection system, carefully optimized the reaction condition, and achieved sensitive microRNA detection using LwaCas13a. The crRNA-Cas13a ribonucleoprotein sequence specifically recognizes microRNA. Binding to microRNA activates the crRNA-Cas13a ribonucleoprotein and its *trans*-cleavage activity to cleave single-stranded RNA reporters indiscriminately. Reporters were dually labeled with a fluorophore and a quencher at either end of the RNA. The cleavage of the RNA reporter separates the fluorophore from the quencher and restores the fluorescence. As few as 5 pM microRNA-10b can be detected, meaning that each reaction requires only 8×10^6 microRNA molecules to generate positive fluorescence signals. Such sensitivity suggests the potential of using this LwaCas13a technique to detect microRNA in cell lysate.

In contrast to the default temperature of 37 °C used in the literature, I have clearly demonstrated that the detection of microRNA was achieved at ambient temperature when using

LwaCas13a or LbuCas13a. The ambient temperature condition significantly simplified the assay requirements. The detection of microRNA-10b was more sensitive at 23 °C than at 37 °C using either of the two Cas13a homologs. In addition, my assay for microRNA was conducted in a homogeneous solution in which Cas13a, crRNA, and reporter were prepared and mixed in a single tube. The operation and instrumentation requirements are simple.

2.5 References

1. He, L. and Hannon, G. J., MicroRNAs: Small RNAs with a big role in gene regulation. *Nat. Rev. Genet.* **2004,** *5*, 522-531.
2. Calin, G. A. and Croce, C. M., MicroRNA signatures in human cancers. *Nat. Rev. Cancer* **2006,** *6* (11), 857-866.
3. Lu, J., Getz, G., Miska, E. A., Alvarez-Saavedra, E., Lamb, J., Peck, D., Sweet-Cordero, A., Ebet, B. L., Mak, R. H., Ferrando, A. A., Downing, J. R., Jacks, T., Horvitz, H. R. and Golub, T. R., MicroRNA expression profiles classify human cancers. *Nature* **2005,** *435*, 834-838.
4. Chen, C. F., Ridzon, D. A., Broomer, A. J., Zhou, Z. H., Lee, D. H., Nguyen, J. T., Barbisin, M., Xu, N. L., Mahuvakar, V. R., Andersen, M. R., Lao, K. Q., Livak, K. J. and Guegler, K. J., Real-time quantification of microRNAs by stem-loop RT-PCR. *Nucleic Acids Res.* **2005,** *33* (20), e179.
5. Peng, H. Y., Newbigging, A. M., Reid, M. S., Uppal, J. S., Xu, J. Y., Zhang, H. Q. and Le, X. C., Signal Amplification in Living Cells: A Review of microRNA Detection and Imaging. *Anal. Chem.* **2020,** *92* (1), 292-308.

6. East-Seletsky, A., O'Connell, M. R., Knight, S. C., Burstein, D., Cate, J. H. D., Tjian, R. and Doudna, J. A., Two distinct RNase activities of CRISPR-C2c2 enable guide-RNA processing and RNA detection. *Nature* **2016,** *538*, 270-273.
7. Knott, G. J., East-Seletsky, A., Cofsky, J. C., Holton, J. M., Charles, E., O'Connell, M. R. and Doudna, J. A., Guide-bound structures of an RNA-targeting A-cleaving CRISPR-Cas13a enzyme. *Nat. Struct. and Mol. Biol.* **2017,** (10), 825-833.
8. Liu, L., Li, X., Ma, J., Li, Z., You, L., Wang, J., Wang, M., Zhang, X. and Wang, Y., The Molecular Architecture for RNA-Guided RNA Cleavage by Cas13a. *Cell* **2017,** *170*, 714-726.
9. Liu, L., Li, X., Wang, J., Wang, M., Chen, P., Yin, M., Li, J., Sheng, G. and Wang, Y., Two Distant Catalytic Sites Are Responsible for C2c2 RNase Activities. *Cell* **2017,** *168* (1-2), 121-134.
10. Gootenberg, J. S., Abudayyeh, O. O., Lee, J. W., Essletzbichler, P., Dy, A. J., Joung, J., Verdine, V., Donghia, N., Daringer, N. M., Freije, C. A., Myhrvold, C., Bhattacharyya, R. P., Livny, J., Regev, A., Koonin, E. V., Hung, D. T., Sabeti, P. C., Collins, J. J. and Zhang, F., Nucleic acid detection with CRISPR-Cas13a/C2c2. *Science* **2017,** *356* (6336), 438-442.
11. Sheedy, P. and Medarova, Z., The fundamental role of miR-10b in metastatic cancer. *Am. J. Cancer Res.* **2018,** *8* (9), 1674-1688.
12. Ma, L., Teruya-Feldstein, J. and Weinberg, R. A., Tumour invasion and metastasis initiated by microRNA-10b in breast cancer. *Nature* **2007,** *449* (7163), 682-688.
13. Fozouni, P., Son, S., Díaz de León Derby, M., Knott, G. J., Gray, C. N., D'Ambrosio, M. V., Zhao, C., Switz, N. A., Kumar, G. R., Stephens, S. I., Boehm, D., Tsou, C.-L., Shu, J., Bhuiya, A., Armstrong, M., Harris, A. R., Chen, P.-Y., Osterloh, J. M., Meyer-Franke, A.,

Joehnk, B., Walcott, K., Sil, A., Langelier, C., Pollard, K. S., Crawford, E. D., Puschnik, A. S., Phelps, M., Kistler, A., DeRisi, J. L., Doudna, J. A., Fletcher, D. A. and Ott, M., Amplification-free detection of SARS-CoV-2 with CRISPR-Cas13a and mobile phone microscopy. *Cell* **2021,** *184* (2), 323-333.e9.

14. Shan, Y., Zhou, X., Huang, R. and Xing, D., High-Fidelity and Rapid Quantification of miRNA Combining crRNA Programmability and CRISPR/Cas13a trans-Cleavage Activity. *Anal. Chem.* **2019,** *91* (8), 5278-5285.
15. Granados-Riveron, J. T. and Aquino-Jarquin, G., CRISPR/Cas13-Based Approaches for Ultrasensitive and Specific Detection of microRNAs. *Cells* **2021,** *10* (7), 1655.
16. Bruch, R., Baaske, J., Chatelle, C., Meirich, M., Madlener, S., Weber, W., Dincer, C. and Urban, G. A., CRISPR/Cas13a-Powered Electrochemical Microfluidic Biosensor for Nucleic Acid Amplification-Free miRNA Diagnostics. *Adv. Mater.* **2019,** *31* (51), 1905311.
17. Bruch, R., Johnston, M., Kling, A., Mattmüller, T., Baaske, J., Partel, S., Madlener, S., Weber, W., Urban, G. A. and Dincer, C., CRISPR-powered electrochemical microfluidic multiplexed biosensor for target amplification-free miRNA diagnostics. *Biosens. Bioelectron.* **2021,** *177*, 112887.
18. Zhang, B., Ye, Y., Ye, W., Perčulija, V., Jiang, H., Chen, Y., Li, Y., Chen, J., Lin, J., Wang, S., Chen, Q., Han, Y.-S. and Ouyang, S., Two HEPN domains dictate CRISPR RNA maturation and target cleavage in Cas13d. *Nat. Commun.* **2019**, 10, 2544.
19. Mahas, A., Marsic, T., Lopez-Portillo Masson, M., Wang, Q., Aman, R., Zheng, C., Ali, Z., Alsanea, M., Al-Qahtani, A., Ghanem, B., Alhamlan, F. and Mahfouz, M., Characterization of a thermostable Cas13 enzyme for one-pot detection of SARS-CoV-2. *Proc. Natl. Acad. Sci. U.S.A.* **2022,** *119* (28), e2118260119.

Chapter 3. Effects of short target and spacer length on the activity of LwaCas13a and LbuCas13a

3.1 Introduction

crRNA-Cas13a ribonucleoproteins interact with their target RNA through the base pairing between the spacer of crRNA and the protospacer in the target.[1] Spacers interact with both Cas13a and the target RNA, thus affecting Cas13a activity. In bacteria, spacers are around 20–30 nt partial viral RNA sequence kept in the genome of bacteria,[1] and the spacer length varies among Cas13a homologs. For example, the spacers for LwaCas13a (*Leptotrichia wadei*) are usually 29–30 nt,[2] yet the spacers are 20 nt for LbuCas13a (*Leptotrichia buccalis*), LshCas13a (*Leptotrichia shahii*), and LseCas13a (*Listeria seeligeri*).[3] Among these Cas13a homologs, LbuCas13a and LwaCas13a have been widely used for RNA detection because of their high *trans*-cleavage activity and thus high analytical sensitivity.[4] In a crRNA-Cas13a ribonucleoprotein, the spacer of crRNA is located in the center of the nuclease (NUC) lobe of Cas13a.[1] Within the spacer region, some bases of some nucleotides have extensive interaction with Cas13a and are exposed to solvent. These nucleotides may serve as a central seed region for target binding, e.g., nucleotides 9 to 15 of crRNA for LbuCas13a.[5-6] The hybridization between crRNA and target RNA induces a significant conformational change of Cas13a, thus activating Cas13a. Upon target binding, the phosphate-sugar backbone of the spacer and the target have strong interactions with Cas13a.[5]

Engineering of the guide RNA has been an important and successful strategy to improve the specificity of CRISPR technology. Although the target recognition is sequence-specific, Cas systems may also be activated by nucleic acids that differ by a few nucleotides from the

perfect target. Specificity has been improved by the truncation of guide RNA for the Cas9 system[7] or the introduction of artificial mismatches in the spacer of the LwaCas13a enzyme.[8] These modifications weakened the spacer-target interaction, and thus reduced the off-target effect. The strategy depends on the type and ortholog of Cas enzymes because it is also important to avoid interrupting key interactions between RNA and Cas proteins, and to maintain Cas activity. Modifications of natural crRNA require structural and functional understanding. Biochemical characterization on the effect of target and spacer length on LbuCas13a has been conducted, while only one equivalent study using LwaCas13a is available.

For LbuCas13a, Liu et al.[5] have revealed that the 3' end of the target RNA is required to be paired with the spacer and cannot be truncated at all. A minimum length of 18 nt is required for measurable LbuCas13a activity if the target is truncated from its 5' end. Higher activity requires a 20-nt target. Shan et al.[9] have reported high *trans*-cleavage activity when using spacers longer than 20 nt, to detect a 23-nt target RNA, yet the activity is still observable when using spacers as short as 14 nt. Overall, a 20-nt spacer-target duplex is required for the effective operation of LbuCas13a, which is also supported by the structural study of the interaction within one crRNA-LbuCas13a-target ternary complex.[5] Meanwhile, Tambe et al.[6] have reported that the binding affinity toward the same target is the same when using 20- or 24-nt spacers.

The commonly used spacer length for LwaCas13a in RNA detection applications is 28 nt. Gootenberg et al.[8] used spacers of 20, 23, and 28 nt to recognize a 170-nt target. Shortening the spacer length reduced the fluorescence signal by 4–6 times. My successful development

of microRNA detection techniques (**Chapter 2**) suggests that a 23-nt target can activate LwaCas13a.

The aim of this chapter is to study the effect of short targets (activators) and crRNA on *trans*-cleavage activity. I have previously optimized the reaction conditions to allow LwaCas13a to operate efficiently with a 23-nt activator (**Chapter 2**). Using the same conditions, I studied the *trans*-cleavage activity of LwaCas13a in response to shorter targets and spacers. I found that 23-nt RNA targets and spacers are required for efficient activation of LwaCas13a. Shorter targets (<23 nt) may not be able to active LwaCas13a efficiently. Such a length requirement is distinct from other Cas13a homologs that require only a 20-nt target-spacer duplex. The mechanism of insufficient LwaCas13a activation by short RNA is not fully understood but may be related to RNA-protein interaction rather than RNA-RNA hybridization. The reaction conditions are favorable for the hybridization of short RNA, yet 20–22-nt spacers that work well with LbuCas13a failed to activate LwaCas13a.

3.2 Experimental Section

3.2.1 Production of protein and RNA

LwaCas13a and LbuCas13a were produced as described in section 2.1 of Chapter 2. crRNA and long RNA targets were produced as described in section 2.2 of Chapter 2. The sequences of RNA used or analyzed are listed in **Table 3-1**.

Table 3-1. The sequence of target RNA and crRNA used in Chapter 3

Name of Sequence	Sequence
miR-10b (IDT)	UAC CCU GUA GAA CCG AAU UUG UG
miR-10b (T7 transcription)	GGUACCCUGUAGAACCGAAUUUGUG
extended miR-10b	AUCCUUGUAGUUAUGCU UACCCUGUAGAACCGAAUUUGUG AUGCUCUUG
LwaCas13a crRNA for miR-10b	GGGGAUUUAGACUACCCCAAAAACGAAGGGGACUAAA AC CACAAAUUCGGUUCUACAGGGUA
LbuCas13a crRNA for miR-10b	GGCCACCCCAAAAAUGAAGGGGACUAAAACA CACAAAUUCGGUUCUACAGGGUA
ssRNA1 (161 nt)	GGGGGCCAGUGAAUUCGAGCUCGGUACCCGGGGAUCC UCUAGAAAU AUGGAUUACUUGGTAGAACAGCAAUCUA CUCGACCUGCAGGCAUGCAAGCUUGGCGUAAUCAUGG UCAUAGCUGUUUCCUGUGUUUAUCCGCUCACAAUUCC ACACAACAUACGA
LwaCas13a crRNA for ssRNA1 (28nt spacer)	GGGGAUUUAGACUACCCCAAAAACGAAGGGGACUAA AAC UAGAUUGCUGUUCUACCAAGUAAUCCAU
LwaCas13a crRNA for ssRNA1 (26nt spacer)	GGGGAUUUAGACUACCCCAAAAACGAAGGGGACUAA AAC UAGAUUGCUGUUCUACCAAGUAAUCC
LwaCas13a crRNA for ssRNA1 (24nt spacer)	GGGGAUUUAGACUACCCCAAAAACGAAGGGGACUAAA AC UAGAUUGCUGUUCUACCAAGUAAU
LwaCas13a crRNA for ssRNA1 (22nt spacer)	GGGGAUUUAGACUACCCCAAAAACGAAGGGGACUAAA AC UAGAUUGCUGUUCUACCAAGUA
ssRNA2	CAGUAGUAGUCGUCAGUCAGUUCAGUCAGGUAAGUAU
LwaCas13a crRNA for ssRNA2 (32 nt spacer)	GGGGAUUUAGACUACCCCAAAAACGAAGGGGACUAAA AC UACUUACCUGACUGAACUGACUGACGACUACU
LwaCas13a crRNA for ssRNA2 (28 nt spacer)	GGGGAUUUAGACUACCCCAAAAACGAAGGGGACUAAA AC UACUUACCUGACUGAACUGACUGACGAC
LwaCas13a crRNA for ssRNA2 (26 nt spacer)	GGGGAUUUAGACUACCCCAAAAACGAAGGGGACUAAA AC UACUUACCUGACUGAACUGACUGACG
LwaCas13a crRNA for ssRNA2 (24 nt spacer)	GGGGAUUUAGACUACCCCAAAAACGAAGGGGACUAAA AC UACUUACCUGACUGAACUGACUGA
LwaCas13a crRNA for ssRNA2 (22 nt spacer)	GGGGAUUUAGACUACCCCAAAAACGAAGGGGACUAAA AC UACUUACCUGACUGAACUGACU

Name of Sequence	Sequence
LwaCas13a crRNA for ssRNA2 (20 nt spacer)	GGGGAUUUAGACUACCCCAAAAACGAAGGGGACUAAA AC UACUUACCUGACUGAACUGA
LbuCas13a crRNA for ssRNA2 (32 nt spacer)	GGCCACCCCAAAAAUGAAGGGGACUAAAACA UACUUACCUGACUGAACUGACUGACGACTACT
LbuCas13a crRNA for ssRNA2 (28 nt spacer)	GGCCACCCCAAAAAUGAAGGGGACUAAAACA UACUUACCUGACUGAACUGACUGACGAC
LbuCas13a crRNA for ssRNA2 (26 nt spacer)	GGCCACCCCAAAAAUGAAGGGGACUAAAACA UACUUACCUGACUGAACUGACUGACG
LbuCas13a crRNA for ssRNA2 (24 nt spacer)	GGCCACCCCAAAAAUGAAGGGGACUAAAACA UACUUACCUGACUGAACUGACUGA
LbuCas13a crRNA for ssRNA2 (22 nt spacer)	GGCCACCCCAAAAAUGAAGGGGACUAAAACA UACUUACCUGACUGAACUGACU
LbuCas13a crRNA for ssRNA2 (20 nt spacer)	GGCCACCCCAAAAAUGAAGGGGACUAAAACA UACUUACCUGACUGAACUGA
ssRNA3	AAUAGGAUGGAGUGAGAGAGGAGAAGAGU
LwaCas13a crRNA for ssRNA3 (28 nt spacer)	GGGGAUUUAGACUACCCCAAAAACGAAGGGGACUAAA AC ACUCUUCUCCUCUCUCACUCCAUCCUAUU
LwaCas13a crRNA for ssRNA3 (26 nt spacer)	GGGGAUUUAGACUACCCCAAAAACGAAGGGGACUAAA AC ACUCUUCUCCUCUCUCACUCCAUCCUA
LwaCas13a crRNA for ssRNA3 (24 nt spacer)	GGGGAUUUAGACUACCCCAAAAACGAAGGGGACUAAA AC ACUCUUCUCCUCUCUCACUCCAUCC
LwaCas13a crRNA for ssRNA3 (22 nt spacer)	GGGGAUUUAGACUACCCCAAAAACGAAGGGGACUAAA AC ACUCUUCUCCUCUCUCACUCCAU

3.2.2 Characterizing the effect of the target RNA length on the *trans*-cleavage activity of Cas13a

To study the effect of short target (activator) length on LwaCas13a activation, I compared the *trans*-cleavage activity of LwaCas13a induced by truncated microRNA-10b. microRNA-10b was truncated from its 5' end by 2, 4, and 6 nucleotides, resulting in 21, 19, and 17-nt targets. Another set of 23-nt targets adapted from microRNA-10b was also tested.

The 5’ ends of these targets were modified to contain 2 or 4 nt that did not match the crRNA, but the total length remained 23 nt.

The same crRNA (with the 23-nt spacer) was used for all the targets of different lengths. Pre-annealed crRNA and TCEP-treated Cas13a were first incubated in reaction buffer at 25 °C for 0.5 h and kept on ice. Then chilled microRNA or truncated RNA (IDT) and reporter were added. The final concentrations of the reagents were: 5 nM Cas13a, 0.5 nM crRNA, 30 nM reporter, 200 pM of targets for positive tests or 0 nM target for non-target controls (NTC), 40 mM Tris-HCl pH 7.5, 60 mM NaCl, 6 mM $MgCl_2$, and 0.005% Tween-20 in each 20 μL reaction. Fluorescence at 535 nm (excitation at 485 nm) was measured for 1 h at 10 °C or 25 °C using a StepOnePlus™ RT-PCR instrument (Applied Biosystems). The fluorescence intensity of the first measurement of each reaction was subtracted from all following fluorescence values.

3.2.3 Characterizing the effect of spacer length on the *trans*-cleavage activity of Cas13a

The *trans*-cleavage activity of LwaCas13a induced by four different targets was characterized. For each target, spacers of different lengths with truncations at the 3’ end were tested. (i) microRNA-10b: Pre-annealed crRNA with spacers of different lengths and TCEP-treated Cas13a were first incubated in reaction buffer at 25 °C for 0.5 h. Then miRNA (IDT) and reporters were added. The final concentration of each reagent was: 5 nM Cas13a, 0.5 nM crRNA, 30 nM reporter, 1 nM miRNA for positive tests or 0 nM target for non-target controls (NTC), 40 mM Tris-HCl pH 7.5, 60 mM NaCl, 6 mM $MgCl_2$, and 0.005% Tween-20, in each 20 μL reaction. Fluorescence at 535 nm (excitation at 485 nm) was measured for 1 h at 25˚C using a StepOnePlus™ RT-PCR instrument (Applied Biosystems). The fluorescence intensity

of the first measurement of each reaction was subtracted from all following fluorescence intensities. (ii) ssRNA1: Pre-annealed crRNA with spacers of different lengths and TCEP-treated Cas13a were first incubated in reaction buffer at 25 °C for 0.5 h. Then ssRNA1 (IDT) and reporter were added. The final concentration of each reagent was: 4 nM Cas13a, 0.4 nM crRNA, 24 nM reporter, 560 pM ssRNA1 or 0 pM target for non-target controls (NTC), 32 mM Tris-HCl pH 7.5, 48 mM NaCl, 4.8 mM $MgCl_2$, and 0.004% Tween-20, in each 25 μL reaction. Fluorescence at 535 nm (excitation at 485 nm) was measured for 1 h at 27 °C using a StepOnePlus™ RT-PCR instrument (Applied Biosystems). The fluorescence intensity of the first measurement of each reaction was subtracted from all following fluorescence intensities. (iii) ssRNA2: Pre-annealed crRNA with spacers of different lengths and TCEP-treated Cas13a were first incubated in reaction buffer at 25 °C for 10 min and kept on ice. Then chilled ssRNA2 (IDT) and reporters were added. The final concentration of each reagent was: 5 nM Cas13a, 0.5 nM crRNA, 30 nM reporter, 200 pM ssRNA2 or 0 pM target for non-target controls (NTC), 40 mM Tris-HCl pH 7.5, 60 mM NaCl, 6 mM $MgCl_2$, and 0.005% Tween-20, in each 20 μL reaction. Fluorescence at 535 nm (excitation at 485 nm) was measured for 1 h at 27 °C using a StepOnePlus™ RT-PCR instrument (Applied Biosystems). Due to the very fast initial cleavage rate, the fluorescence intensity from the first measurement was not subtracted from the following data points. (iv) ssRNA3: Pre-annealed crRNA with spacers of different lengths and TCEP-treated Cas13a were first incubated in reaction buffer at 25 °C for 10 min and kept on ice. Then chilled ssRNA3 (IDT) and reporters were added. The final concentration of each reagent was: 5 nM Cas13a, 0.5 nM crRNA, 30 nM reporter, 200 pM ssRNA3 or 0 nM target for non-target controls (NTC), 40 mM Tris-HCl pH 7.5, 60 mM NaCl, 6 mM $MgCl_2$, and 0.005% Tween-20. Fluorescence at 535 nm (excitation at 485

nm) was measured for 1 h at 27 °C using a StepOnePlus™ RT-PCR instrument (Applied Biosystems). The fluorescence intensity of the first measurement of each reaction was subtracted from all following fluorescence intensities.

3.3 Results and Discussion

3.3.1 The effect of short target RNA length on the *trans*-cleavage activity of LwaCas13a

One initial concern in the detection of short RNA was whether the protospacer flanking site (PFS) is necessary. A PFS is required for the detection of long RNA. PFS is the single nucleotide on the target next to the 3' end of the protospacer. It interacts with Cas13a and prevents the target RNA from further binding to the crRNA beyond the spacer region.[5] My successful detection of microRNA using crRNA with a 23-nt spacer suggests that the PFS is not necessary for the short targets to activate LwaCas13a (and LbuCas13a). I further confirmed this by comparing the activity of Cas13a triggered by microRNA-10b or end-extended microRNA-10b that contains a preferred non-G PFS (**Figure 3-1**). Removing the 3' overhang and the PFS did not affect Cas13a activity. Thus, the spacer can be designed to be complementary to the entire target strand when detecting short RNA.

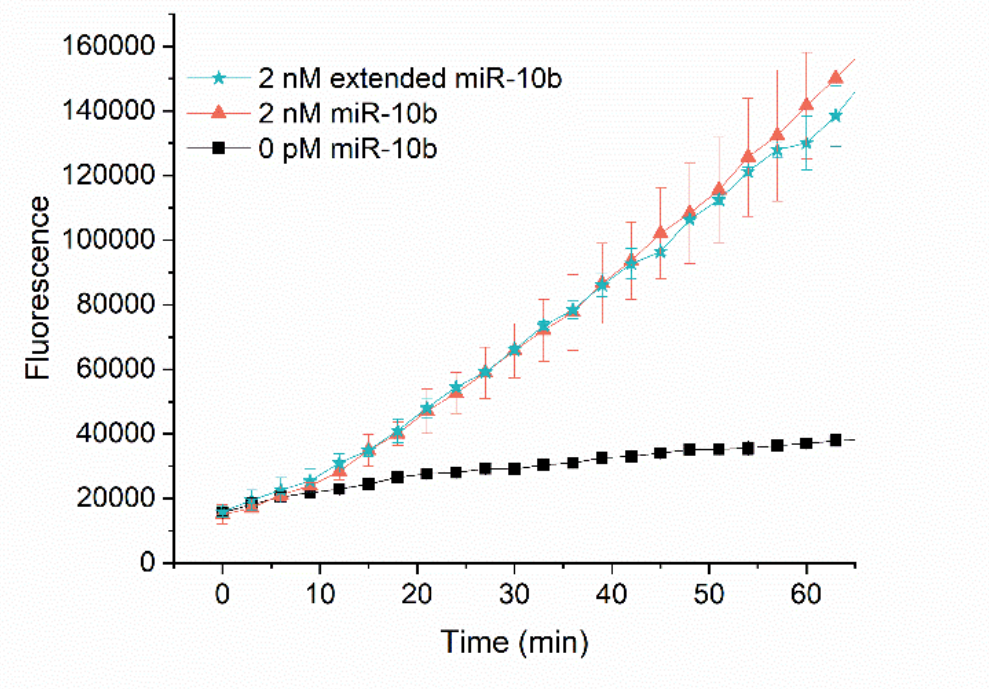

Figure 3-1. A comparison of the *trans*-cleavage activity of LwaCas13a in response to 23-nt microRNA-10b and an extended target. The longer target extends beyond both ends of the 23-nt spacer (microRNA-10b) and contains a preferred non-guanine protospacer flanking site (PFS). The reagents were 5 nM Cas13a, 0.5 nM crRNA, 30 nM reporter, *in vitro* transcribed miR-10b or its extended version, 40 mM Tris-HCl pH 7.5, 60 mM NaCl, 6 mM $MgCl_2$, and 0.005% Tween-20. The fluorescence generation was measured for 1 h at 25 °C using a microplate reader (Molecular Devices, FilterMax F5).

I demonstrated in Chapter 2 that LwaCas13a could be efficiently activated by targets as short as 23 nt, under optimal conditions. To further understand the limit of LwaCas13a on the length of targets, I studied the *trans*-cleavage activity when using shorter targets.

Using the optimized condition for microRNA detection, I tested the performance of LwaCas13a in response to further truncated targets. I truncated the 23-nt target RNA to test the minimum length of target RNA for the activation of LwaCas13a. I truncated only the 5' end because a previous structural study of LbuCas13a has shown that the 3' truncated target (protospacer) cannot activate Cas13a.[5] None of my truncated targets (17–21 nt) activated LwaCas13a (**Figure 3-2A and 3-2B**).

Although the 21-nt target failed to activate LwaCas13a, the addition of 2 unmatched nucleotides to the 5' end of the 21-nt target partially restored the activity of Cas13a (**Figure 3-3**). The two extra nucleotides contributed to Cas13a activation, even though they do not match with the 3' end of crRNA. I speculated that the 22nd and 23rd nucleotides at the 5' end of the target are important for the conformational change and the activation of Cas13a through the interaction between the sugar-phosphate backbone of RNA and Cas13a. The LwaCas13a-crRNA-target ternary structure is not available. Structural analysis of LbuCas13a showed that the 19th and 20th nucleotides of target RNA interact with the HEPN1 domain.[5] Meanwhile, removing these two nucleotides resulted in a significant reduction of Cas13a activity.[5] The role of the target nucleotides near the 3' end crRNA in the two Cas13a systems may be similar, except that the minimum target length and the location of the essential target nucleotides are slightly different. Shorter duplexes (19 nt or 17 nt) did not activate LwaCas13a. The "19 nt match" target sequence contains 4 nucleotides at its 5' end that do not match with crRNA. With 4 mismatches at the 5' end, the target-Cas13a interaction may be completely interrupted.

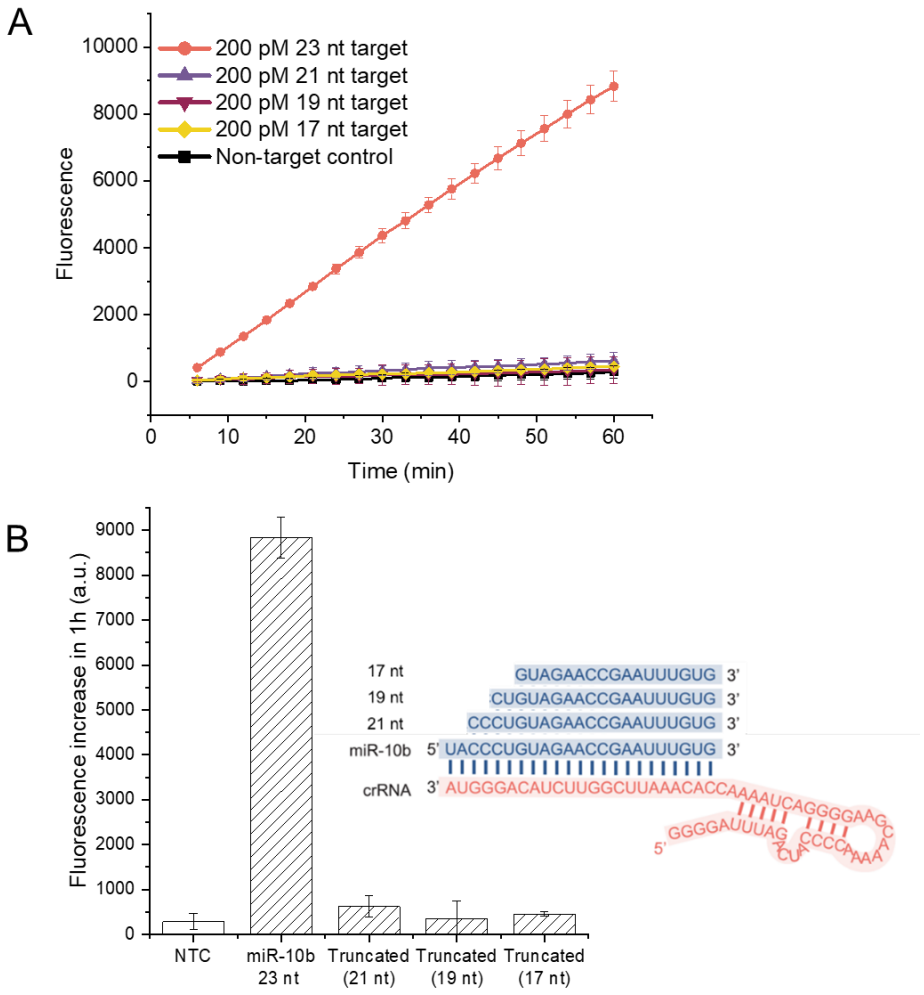

Figure 3-2. Insufficient activation of LwaCas13a by targets shorter than 23 nt. A. Real-time fluorescence monitoring of LwaCas13a activity in response to the target RNA with total lengths of 17 to 23 nt. **B.** Increase of fluorescence calculated from **Figure 3-2A**, and the sequences of truncated targets that aligned with microRNA-10b (miR-10b) from 3' end.

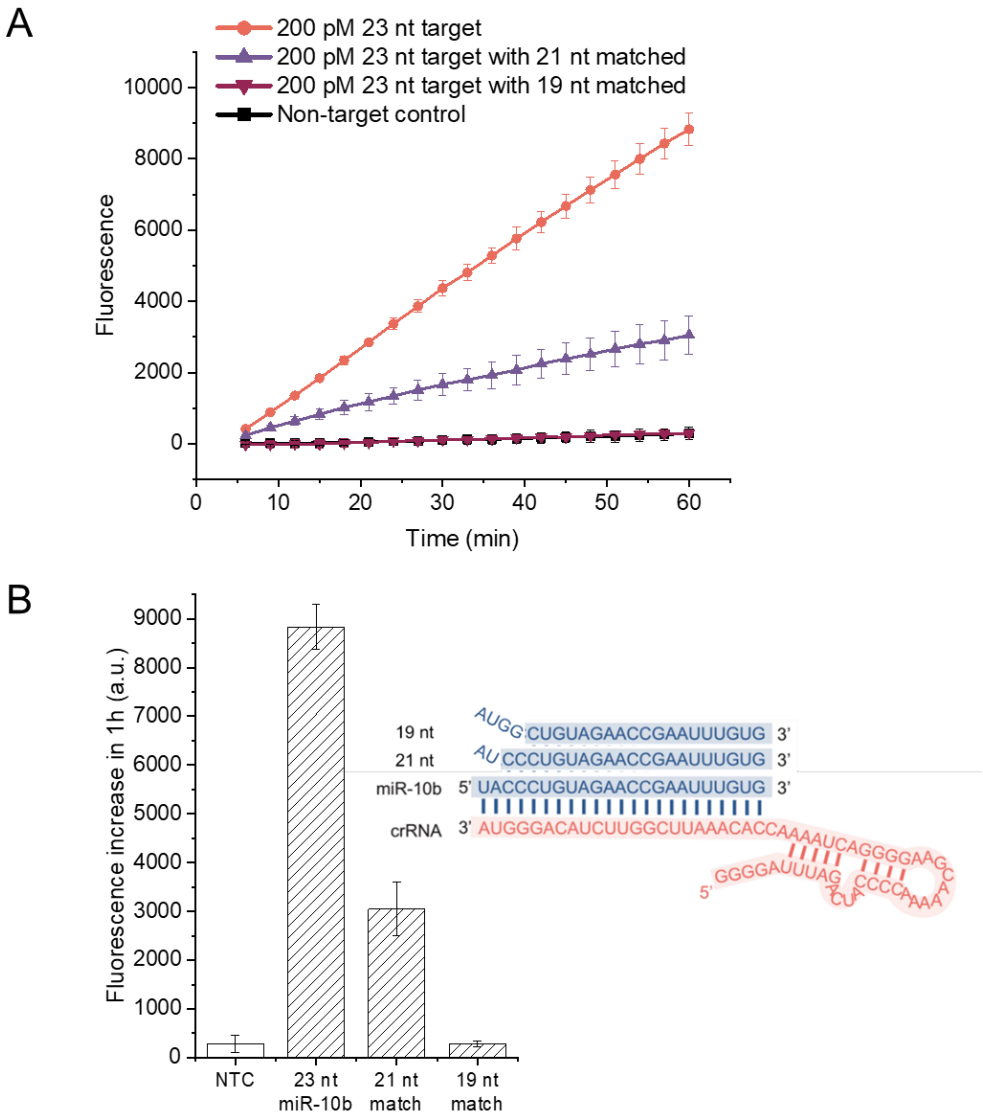

Figure 3-3. LwaCas13a activities in response to 23-nt target RNAs that form 19, 21, and 23-bp duplexes with crRNA. **A.** Real-time fluorescence monitoring of LwaCas13a activity in response to 23-nt target RNA with or without mismatch at its 5' end. **B.** Increase of fluorescence calculated from **Figure 3-3A**, and the sequences of targets that contain mismatches at 5' ends but align with microRNA-10b (miR-10b) at 3' end.

3.3.2 The effect of short spacer length on the *trans*-cleavage activity of LwaCas13a

Truncation of the spacer has been a strategy to improve the sequence specificity of CRISPR-Cas systems.[7] However, further truncating the spacer to be shorter than 23 nt also resulted in failed LwaCas13a activation, when I detected microRNA-10b (23 nt) (**Figure 3-4A**) and two other artificial short ssRNA without secondary structures, ssRNA2 (29 nt, **Figure 3-4C**) and ssRNA3 (**Figure 3-4D**). Even though a 22-nt spacer is not sufficient for LwaCas13a to be activated by short targets, it was enough if the target is long (for example, ssRNA1, **Figure 3-4B**), consistent with previous reports using different spacer lengths for the same target ssRNA1.[8]

The truncation of crRNA at its 3' end and the truncation at the 5' end of activators (target RNA) to 22 nt have both significantly impaired Cas13a activity. This suggests that the protein-RNA interaction is essential at the 3' end of crRNA, especially near the 22nd and 23rd nucleotides. Considering that the long target allowed the use of a shorter spacer (22 nt) (**Figure 3-4B**) and that the random extension of the target to 23 nt resulted in measurable Cas13a activity (**Figure 3-3**), I hypothesized that nucleotides near the 23rd position is essential for the interaction with Cas13a, but it is not important whether it is the spacer RNA or the target RNA.

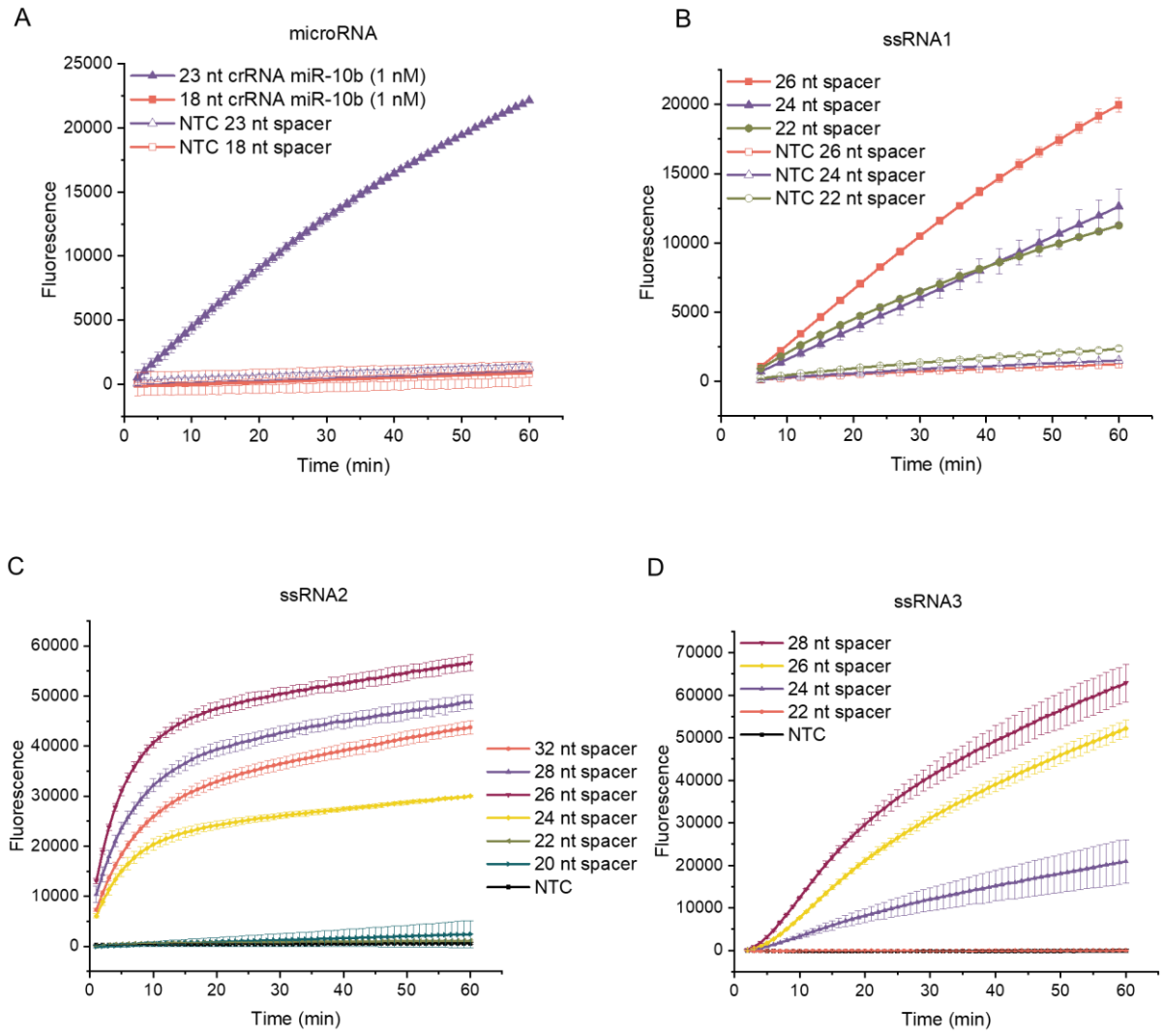

Figure 3-4. Effect of the spacer length on the *trans*-cleavage activity of LwaCas13a.

A. Unsuccessful detection of microRNA-10b with a truncated 18-nt spacer. Positive tests contained 1 nM miR-10b in each 20 µL reaction and non-target controls (NTC) contained 0 nM target. **B.** Effect of the spacer length on the *trans*-cleavage activity of LwaCas13a when using 161-nt target ssRNA1 as the activator. Positive tests contained 560 pM ssRNA1 in each 25 µL reaction and non-target controls (NTC) contained 0 nM target. **C.** Effect of the spacer length on the *trans*-cleavage activity of LwaCas13a when using 33-nt non-structural ssRNA2 as the activator. Positive tests contained 200 pM ssRNA2 in each 20 µL reaction and non-

target controls (NTC) contained 0 nM target. **D.** Effect of the spacer length on the *trans*-cleavage activity of LwaCas13a when using 37-nt non-structural ssRNA3 as the activator. Positive tests contained 200 pM ssRNA3 in each 20 μL reaction and non-target controls (NTC) contained 0 nM target.

3.3.3 LwaCas13a requires longer spacers and target RNA than LbuCas13a

Though LwaCas13a and LbuCas13a are both uracil-preferred Cas13a enzymes, their activation has different target and spacer length requirements. (**Table 3-2**) In summary, LwaCas13a requires longer RNA than LbuCas13a. (**Table 3-2**)

For target lengths, my experiment has shown that short targets (21-nt or less) failed to activate LwaCas13a. This is different from previous reports of LbuCas13a. Short targets (20-nt) activated LbuCas13a efficiently, and the 18-nt target triggered reduced *trans*-cleavage activity of LbuCas13a[5] (**Table 3-2**).

For spacer lengths, in my experiment, some short spacers (22-nt or shorter) failed to activate LwaCas13a. This is distinct from LbuCas13a. Shan et al.[9] have reported successful activation of LbuCas13a using spacers of 14–28 nt to recognize a 23-nt microRNA target. All the spacers allowed target-specific activation of LbuCas13a. Higher activity was achieved when using 20–28-nt spacers, and the activity reduced with the decrease of the spacer length from 20 nt to 14 nt[9] (**Table 3-2**).

For the length of the perfectly matched duplex, there is no data available for LbuCas13a. My data based on one target showed that a minimum of 21 matched nucleotides is required when the 3’ end of the spacer is not complementary to the target RNA.

Table 3-2. A comparison of the RNA length requirement of LwaCas13a and LbuCas13a

	LwaCas13a	LbuCas13a
The length of the natural spacer	29–30 nt [8]	20 nt [3]
The required spacer length	20–23 nt (varies among targets, my data)	14 nt [9] 18 nt [5]
The required target RNA (the activator) length when truncating from 5' end	22–23 nt (my data)	~ 18 nt [5]

3.3.4 Potential mechanism for the insufficient activation of LwaCas13a when using short RNA

The insufficient activation cannot be simply explained based on the RNA-RNA interaction behavior between two free RNA molecules. The reaction conditions I used for testing the truncated RNA are the conditions optimized for short RNA. I confirmed that the RNA-RNA binding of a 20-nt duplex is strong enough. First, analysis of melting temperatures of the crRNA-target duplex (10–23 bp) showed that RNA-RNA interaction is very favourable. The melting temperatures of 17 to 21 bp RNA (T_m ~55–70 °C) are much higher than the detection temperature of 25 °C (**Table 3-3**). Second, I tested the same short targets at 10 °C to minimize the effect of weak RNA-RNA binding. LwaCas13a still has 40% *trans*-cleavage activity at 10 °C (**Figure 2-9**), and in theory, the RNA-RNA interaction would be significantly enhanced at 10 °C. Still, none of the short targets (17 to 21 nt) activated LwaCas13a efficiently, but 23-nt targets did (**Figure 3-5**). Third, when activating LbuCas13a with RNA2, the same

activator I tested with LwaCas13a, 20 and 22-nt spacer successfully activated LbuCas13a, even though they both failed to active LwaCas13a (**Figure 3-6**).

Instead of a gradual reduction of Cas13a activity when truncating the crRNA or the target RNA, I observed an abrupt failure of LwaCas13a activation. I speculated that the truncation caused the loss of Cas13a activity through the disturbance of some key interactions near the 3' end of a 23-nt spacer or its complementary nucleotide on the 5' end of the target. These nucleotides may interact with Cas13a and contribute to the conformational change of LwaCas13a during activation. Such an interaction has been identified in the structural study of LbuCas13a. Near the 3' end of crRNA and the 5' end of target RNA, the crRNA and target nucleotides in the Cas13a central channel interact with Cas13a through the sugar-phosphate backbone.[5]

Table 3-3. The target-crRNA duplex melting temperatures (T_m) with different numbers of paired bases.

Number of paired bases (bp)	23	22	21	19	18	16	14	12	10
T_m of crRNA and target (°C)	70.3	69.5	67	60.1	58.5	52.6	46.2	39.7	22.2

T_m was estimated using IDT OligoAnalyzer. T_m was calculated based on the conditions of RNA target in 100 pM, with 60 mM Na^+ and 6 mM Mg^{2+}.

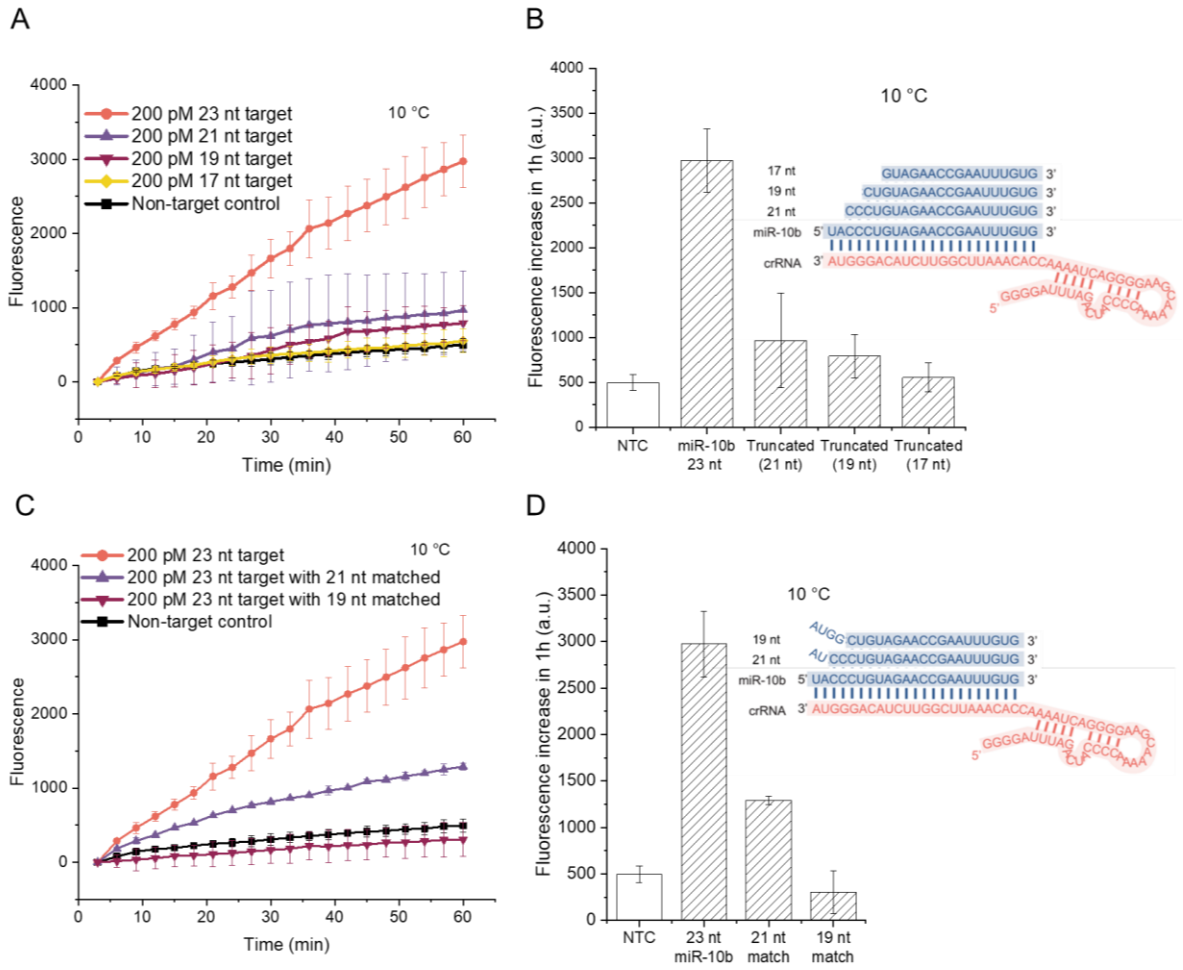

Figure 3-5. Insufficient activation of LwaCas13a by targets shorter than 23 nt, even if the temperature was reduced for better crRNA-target binding. A and B, LwaCas13a activity at 10 °C in response to the target RNA with total lengths of 17 to 23 nt. Short targets were aligned with miR-10b from the 3' end. **C and D**, LwaCas13a activity at 10 °C in response to the target RNA with a total length of 23 nt but only matching with crRNA by 19, 21, or 23 nt.

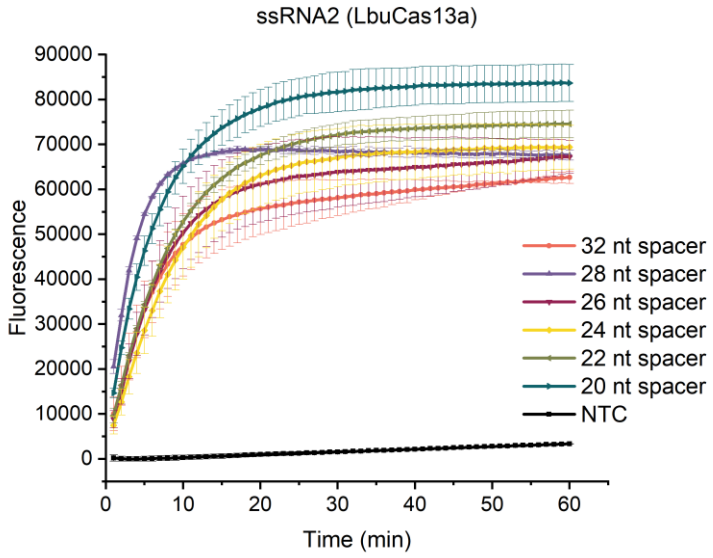

Figure 3-6. Effect of the spacer length on the *trans*-cleavage activity of LbuCas13a. The 33-nt non-structural ssRNA2 was used as the activator. Positive tests contained 200 pM ssRNA2 in each 20 μL reaction and non-target controls (NTC) contained 0 nM target.

3.4 Conclusion

Despite the high *trans*-cleavage activity of LwaCas13a in response to the 23-nt microRNA-10b, further truncation of the target led to insufficient activation of LwaCas13a. Meanwhile, using different target RNA (as an activator) and crRNA with different spacer lengths, I found that further reducing the length of the target or the crRNA to have only 20–22 nt spacer-target duplexes is not always sufficient for LwaCas13a activation. This was distinct from LbuCas13a which requires a shorter spacer-target duplex.[5, 9] For LbuCas13a, 20 nt spacer-target duplex allows very high *trans*-cleavage activity.

The loss of LwaCas13a activity when truncating the 3' end of spacers or the 5' end of the target is not caused simply by weak RNA-RNA hybridization. The reaction conditions were optimized for efficient short target binding and *trans*-cleavage activity of LwaCas13a. The RNA-RNA hybridization of a 21-nt duplex is very strong at 25 °C, as the melting temperature is 67 °C. I also reduced the temperature to 10 °C, to further enhance the RNA-RNA hybridization. Cas13a operated well at 10 °C with a 23-nt target, but not with truncated targets. In addition, crRNA with the same short spacer length (20 and 22 nt) successfully activated LbuCas13a but not LwaCas13a. Thus, the failed LwaCas13a activation may be because of the interruption of more complicated interactions.

I hypothesized that the truncation of crRNA and target disrupted key RNA-protein interactions. Though the 21-nt target RNA did not activate LwaCas13a, adding 2 extra non-matching nucleotides partially restored the activity. Thus, nucleotides at the 22nd and 23rd positions contributed to essential interactions other than base-pairing. Interactions between LbuCas13a and the backbone of crRNA and target RNA are related to the activity of LbuCas13a.[5] Nucleotides around position 22 may be important for the conformational change and activation of LwaCas13a. Chemical interactions between crRNA/target and Cas13a are through hydrogen bonds involving the 2'-OH, and PO_4^- on the phosphate-sugar backbone of RNA.[5] To further test my hypothesis, DNA or RNA nucleotides with chemical modifications of the 2'-OH and PO_4^- near position 23rd can be used to interrupt the RNA-protein interaction without affecting the RNA-RNA interaction and physical presence of nucleotide.

3.5 References

1. O'Connell, M. R., Molecular Mechanisms of RNA Targeting by Cas13-containing Type VI CRISPR–Cas Systems. *J Mol. Biol.* **2019,** *431* (1), 66-87.
2. Abudayyeh, O. O., Gootenberg, J. S., Konermann, S., Joung, J., Slaymaker, I. M., Cox, D. B. T., Shmakov, S., Makarova, K. S., Semenova, E., Minakhin, L., Severinov, K., Regev, A., Lander, E. S., Koonin, E. V. and Zhang, F., C2c2 is a single-component programmable RNA-guided RNA-targeting CRISPR effector. *Science* **2016,** *353* (6299), aaf5573.
3. East-Seletsky, A., O'Connell, M. R., Knight, S. C., Burstein, D., Cate, J. H. D., Tjian, R. and Doudna, J. A., Two distinct RNase activities of CRISPR-C2c2 enable guide-RNA processing and RNA detection. *Nature* **2016,** *538*, 270-273.
4. East-Seletsky, A., O'Connell, M. R., Burstein, D., Knott, G. J. and Doudna, J. A., RNA Targeting by Functionally Orthogonal Type VI-A CRISPR-Cas Enzymes. *Mol. Cell* **2017,** *66* (3), 373-383.
5. Liu, L., Li, X., Ma, J., Li, Z., You, L., Wang, J., Wang, M., Zhang, X. and Wang, Y., The Molecular Architecture for RNA-Guided RNA Cleavage by Cas13a. *Cell* **2017,** *170*, 714-726.
6. Tambe, A., East-Seletsky, A., Knott, G. J., Doudna, J. A. and O'Connell, M. R., RNA Binding and HEPN-Nuclease Activation Are Decoupled in CRISPR-Cas13a. *Cell Reports* **2018,** *24* (4), 1025-1036.
7. Fu, Y., Sander, J. D., Reyon, D., Cascio, V. M. and Joung, J. K., Improving CRISPR-Cas nuclease specificity using truncated guide RNAs. *Nat. Biotechnol.* **2014,** *32*, 279-284.
8. Gootenberg, J. S., Abudayyeh, O. O., Lee, J. W., Essletzbichler, P., Dy, A. J., Joung, J., Verdine, V., Donghia, N., Daringer, N. M., Freije, C. A., Myhrvold, C., Bhattacharyya, R.

P., Livny, J., Regev, A., Koonin, E. V., Hung, D. T., Sabeti, P. C., Collins, J. J. and Zhang, F., Nucleic acid detection with CRISPR-Cas13a/C2c2. *Science* **2017,** *356* (6336), 438-442.

9. Shan, Y., Zhou, X., Huang, R. and Xing, D., High-Fidelity and Rapid Quantification of miRNA Combining crRNA Programmability and CRISPR/Cas13a trans-Cleavage Activity. *Anal. Chem.* **2019,** *91* (8), 5278-5285.

Chapter 4. LwaCas13a and LbuCas13a have high *trans*-cleavage activity at ambient temperature upon activation

4.1 Introduction

CRISPR (Clustered Regularly Interspaced Short Palindrome Repeats) technology has greatly changed the field of genome editing and has been increasingly used for nucleic acid targeting and detection.[1] Among the Cas proteins, Cas13a is very useful for RNA targeting[2] and detection[3-4] due to its ability to directly recognize and cleave RNA and its *trans*-cleavage activity to non-specifically cleave any ssRNA.[5-6] Specifically, Cas13a operates with the guidance of a CRISPR RNA (crRNA). The crRNA contains a stem-loop region (usually 30–40 nt) for Cas13a binding and a single-stranded spacer region (usually 20–30 nt) for target recognition.[7] The crRNA-Cas13a complex or ribonucleoprotein (RNP) specifically targets RNA containing a protospacer, a sequence complementary to the spacer. Binding between Cas13a-RNP and its target RNA induces a conformational change of Cas13a and activates the RNase activity of Cas13a by bringing together two functional domains, the higher eukaryotes and prokaryotes nucleotide-binding (HEPN) domains. Activated Cas13a then cleaves the target RNA (*cis*-cleavage) and multiple single-stranded RNA (ssRNA) in close proximity regardless of the sequence (*trans*-cleavage).[6, 8-10] Such activity of Cas13a prevents viral proliferation in bacteria.[11]

The *trans*-cleavage activity of Cas13a facilitates the generation of amplified signals in response to the recognition of a specific target in molecular detection applications.[12-16] The kinetics of *trans*-cleavage determines the performance of RNA detection techniques, especially techniques that directly detect RNA without nucleic acid amplification.[5-6, 17] The

kinetics of the *trans*-cleavage activity can be affected by factors including target sequence, reaction temperature, subtypes/homologs of Cas, the sequence of crRNA, reporter type, and co-factor concentration.[16, 18] Further characterizations of the kinetics is required, and such understanding is important to further improve and define the limit of Cas13a-mediated RNA detection.[17]

Cas13a-mediated RNA recognition and signal generation have been conducted at different temperatures, mostly at 37 °C, but also at 25 °C.[6, 15-16, 19] Unfortunately, in the literature, the choice of reaction temperature was not based on systematic optimization or comparison of Cas13a activity at different temperatures. The optimal temperature for the *trans*-cleavage activity of Cas13a and the reduction of Cas13a activity at other temperatures are unclear. Some scattered information has shown a slightly higher *cis*-cleavage activity and *trans*-cleavage-based signal generation at 37 °C than 25 °C, supporting the use of 37 °C.[6, 15] The choice of 37 °C may also be affected by other considerations such as the temperature of isotheral amplification reactions into which Cas13a was integrated. Wu et al.[19] used Cas13a for room temperature detection, yet did not characterize the activity of Cas13a at different temperatures. The successful operation of Cas13a at room temperature indicates the potential for simplifying *in vitro* analytical techniques to address the need for point-of-care testing and broadening the application of Cas13a to ectotherm organisms or plants. Quantitative understanding of the thermal behavior of CRISPR-Cas13a systems is required to guide the development of novel techniques.

In addition, I have observed differences in the preferred temperature when detecting different targets using Cas13a. Evidence in the literature showed a preference for the *trans*-cleavage activity to operate at 37 °C. Thirty-seven degree Celsius is also consistent with the

temperature in the human oral cavity where *Leptotrichia wadei* (Lwa) and *Leptotrichia buccalis* (Lbu) bacteria, the origin of the two commonly used Cas13a, are present. However, I have seen faster kinetics at 25 °C than 37 °C in the detection of some targets (**Chapter 2**). This led me to ask whether the optimal temperature for *trans*-cleavage is affected by the sequence of target RNA. The target sequence and the spacer design affect the overall performance of Cas13a.[16] I anticipate that these RNA differences may affect the target RNA-crRNA interaction, and thus the target recognition and the stability of crRNA-Cas13a-target ternary complex. Once Cas13a is activated, would the *trans*-cleavage activity of activated Cas13a also be affected?

Here, I aim to understand how the *trans*-cleavage activity of activated Cas13a varies among different temperatures, and whether this is also affected by the sequence of target RNA and its corresponding crRNA. Naturally existing RNA molecules have distinct nucleotide composition and secondary structure. Meanwhile, for each target, the spacer can be designed to target different region to achieve the highest *trans*-cleavage activity or to have different lengths to meet the requirement of sequence specificity. Thus, I characterized the *trans*-cleavage of Cas13a upon activation by RNA that covers distinct characteristics in the above-mentioned aspects. Measurement of the *trans*-cleavage activity can be affected by other reactions, including the binding between crRNA and Cas13a, the binding between crRNA-Cas13a RNP, and the cleavage and release of the target. To assess these reactions separately and to look at the *trans*-cleavage activity independently, I carefully designed several sets of experiments. With different RNA and reaction conditions, I compared the *trans*-cleavage rate at different temperatures. I found that once the crRNA-Cas13a-target ternary complex is formed, *trans*-cleavage activity of LwaCas13a and LbuCas13a at ambient temperatures (23–

32 °C) can be higher than that at 37 °C. This is advantageous for point-of-care assay development and for potential application in ectotherm organisms and plants. Once the crRNA-Cas13a RNP bind to the target RNA properly, heating is not necessary.

4.2 Experimental Section

4.2.1 Cas13a expression and purification

Plasmids containing His-tagged LbuCas13a (Addgene, #83482) gene were first replicated in DH5α cells and extracted with QIAprep Spin Miniprep Kit (Qiagen, #27104). LbuCas13a plasmids were then transformed into Rosetta DE3 pLysS competent cells (Novagen, #70956-3). Rosetta cells containing His-tagged LwaCas13a (Addgene, #90097) or LbuCas13a were grown separately at 37 °C in 2xYT broth (Invitrogen, #22712-020) to reach an OD600 of 0.6. Then, protein expression was induced by supplementation with IPTG (Invitrogen, 15529-019) to a final concentration of 500 μM. Upon induction, cells were cooled to 18 °C and grown for 16 h.

Cas13a was purified by immobilized Ni affinity chromatography. Cell pellets were lysed by sonication, in lysis buffer (50 mM Tris-HCl pH 7.5, 500 mM NaCl, 0.5 mM PMSF, 5% glycerol, supplemented with EDTA-free protease inhibitor (Roche, #05892791001)). Then cell debris was removed by centrifuging at 10,000g for 20 min, at 4 °C. I optimized the imidazole concentration for Ni column loading and gradient elution. The lysis buffer was switched to 50 mM Tris-HCl pH 7.5, 500 mM NaCl, and 30 mM imidazole by 100K ultrafiltration (Millipore, #UFC810024/#UFC510096) and incubated with Ni-NTA agarose (Invitrogen, #R901-01) for 1 h at 4 °C. Before elution, the column was washed twice with buffer containing 50 mM of Tris-HCl and 500 mM of NaCl. Proteins were eluted with gradient

imidazole. One mL of imidazole in 50 mM Tris-HCl and 500 mM NaCl with increasing concentration (40 mM, 40 mM, 50 mM, 50 mM, 100 mM, 160 mM, and 250 mM) were added consecutively and the eluates were collected. Cas13a-containing eluate was concentrated by 100K ultrafiltration and stored in storage buffer (30 mM Tris-HCl pH 7.5, 300 mM NaCl, 1 mM TCEP, 0.3 mM PMSF, 35% of glycerol, supplemented with 0.33× EDTA-free protease inhibitor). SDS-PAGE gel analysis results of elution fractions are shown in **Figure 2-1**.

The total protein concentration of each eluate was measured by Bradford assay (Bio-Rad, #500-0006). The Cas13a purity was calculated by analyzing the photo intensity of each band in one elution fraction shown on the SDS-PAGE gel with Image J software. Purity = the photo intensity of Cas13a band / the total photo intensity of all bands in the same eluate. Unless otherwise specified, the Cas13a concentration refers to the total protein concentration.

4.2.2 Production of crRNA and target RNA

crRNAs and long RNA targets were produced by *in vitro* T7 transcription. The DNA templates for T7 transcription were produced by fill-in PCR. Two long primers with 20-nt overlaps at their 3' ends served as both primers and the template for fill-in PCR. The forward primer contained a T7 promoter region and the 5' region of the target or crRNA. The reverse primers were complementary to the produced RNA from the 3' end. PCR reactions were carried out using Q5® Hi-Fidelity DNA Polymerase (NEB, #M0491L). The PCR program was 95 ˚C for 30 s, then 35 cycles consisting of 95 °C 10s, 57 °C 10 s, and 72 °C 20 s, followed by 72 °C 20 s. PCR products were purified with a MinElute PCR Purification Kit (Qiagen, #28006) and used as the template for T7 transcription (HiScribe™ T7 High Yield RNA Synthesis Kit, NEB, #E2040S). crRNA was purified with TRIzol Reagent (ThermoFisher Scientific, #15596026) and quantified using a NanoVue Plus Spectrophotometer (GE

Healthcare). crRNA was subsequently aliquoted and stored at -80 °C. The crRNA and RNA target I tested are summarized in **Table 4-1**.

Table 4-1. crRNA and target sequences

Name of Sequence	Sequence
ssRNA1-161 nt	G GGG GCC AGU GAA UUC GAG CUC GGU ACC CGG GGA UCC UCU AGA AAU AUG GAU UAC UUG GTA GAA CAG CAA UCU A CUC GAC CUG CAG GCA UGC AAG CUU GGC GUA AUC AUG GUC AUA GCU GUU UCC UGU GUU UAU CCG CUC ACA AUU CCA CAC AAC AUA CGA
crRNA1-Lwa	GGG GAU UUA GAC UAC CCC AAA AAC GAA GGG GAC UAA AAC UAG AUU GCU GUU CUA CCA AGU AAU CCA U
ssRNA1-33 nt	GGA AAU AUG GAU UAC UUG GUA GAA CAG CAA UCU A
ssRNA-no-U	G GAA ACA CGG ACC ACA AGG AAG AAC AGC AAA CAA
crRNA-no-U-Lwa	GGG GAU UUA GAC UAC CCC AAA AAC GAA GGG GAC UAA AAC UUG UUU GCU GUU CUU CCU UGU GGU CCG U
ssRNA2	CAG UAG UAG UCG UCA GUC AGU UCA GUC AGG UAA GUA U
crRNA2-32nt-Lwa	GGG GAU UUA GAC UAC CCC AAA AAC GAA GGG GAC UAA AAC UA CUU ACC UGA CUG AAC UGA CUG ACG ACU ACU
crRNA2-28nt-Lwa	GGG GAU UUA GAC UAC CCC AAA AAC GAA GGG GAC UAA AAC UA CUU ACC UGA CUG AAC UGA CUG ACG AC
crRNA2-26nt-Lwa	GGG GAU UUA GAC UAC CCC AAA AAC GAA GGG GAC UAA AAC UA CUU ACC UGA CUG AAC UGA CUG ACG
crRNA2-24nt-Lwa	GGG GAU UUA GAC UAC CCC AAA AAC GAA GGG GAC UAA AAC UA CUU ACC UGA CUG AAC UGA CUG A
ssRNA3	AAU AGG AUG GAG UGA GAG AGG AGA AGA GU
crRNA3-28nt-Lwa	GGG GAU UUA GAC UAC CCC AAA AAC GAA GGG GAC UAA AAC ACU CUU CUC CUC UCU CAC UCC AUC CUA UU
crRNA3-26nt-Lwa	GGG GAU UUA GAC UAC CCC AAA AAC GAA GGG GAC UAA AAC ACU CUU CUC CUC UCU CAC UCC AUC CUA

Name of Sequence	Sequence
crRNA3-24nt-Lwa	GGG GAU UUA GAC UAC CCC AAA AAC GAA GGG GAC UAA AAC ACU CUU CUC CUC UCU CAC UCC AUC C
ssRNA-10b	UAC CCU GUA GAA CCG AAU UUG UG
cr10b-Lwa	GGG GAU UUA GAC UAC CCC AAA AAC GAA GGG GAC UAA AAC CAC AAA UUC GGU UCU ACA GGG UA
Lbu target 1	GGACCCCAAAAUCAGCGAAA
crRNA-t1-Lbu	GACCACCCCAAAAAUGAAGGGGACU AAAACUUUCGCUGAUUUUGGGGUCC
Lbu target 2	CGCAUUACGUUUGGUGGACC
crRNA-t2-Lbu	GACCACCCCAAAAAUGAAGGGGACU AAAACGGUCCACCAAACGUAAUGCG

4.2.3 Comparing *trans*-cleavage activities using different activators at different temperatures

Cas13a and annealed crRNA (80 °C for 5 min and cooled down) were first incubated at 25 °C for 10–30 min and cooled down on ice. Then chilled targets (activators) and reporters were added on ice. Cleavage reactions (20 μL) contained 5 nM Cas13a, 0.5 nM crRNA, 40 mM Tris-HCl pH 7.5, 60 mM NaCl, 6 mM $MgCl_2$, 0.005% Tween-20, 30 nM RNaseAlert reporter, plus 200 pM targets for positive tests or 0 pM target for non-target controls. Then fluorescence at 535 nm (excitation at 485 nm) was measured for 1 h at multiple temperatures using a StepOnePlus™ RT-PCR instrument (Applied Biosystems), by setting six individual heating blocks to 17, 22, 27, 32, 37, and 42 °C. To prevent lagging reaction initiation during the sample preparation period, I conducted two technical replicates for each reaction condition and mixed the reagents on ice. Fluorescence in the FAM channel was measured every minute. When plotting fluorescence *vs* time, the initial fluorescence intensity of each reaction using

LwaCas13a was subtracted from the following fluorescence intensities except for the reactions using ssRNA2 as the activator. The maximum cleavage rates were calculated by converting the average slopes within the fastest 5–10 min (unless otherwise stated) of real-time fluorescence curves to the rate of reporter cleaved (pM/min) based on a calibration curve of the fluorescence generated *vs* the concentrations of reporter fully cleaved (**Figure 4-1**), prepared using the same instrument. The reporter concentration for LbuCas13a was ~60 nM. Additional details were specified in the analysis of different targets under different conditions.

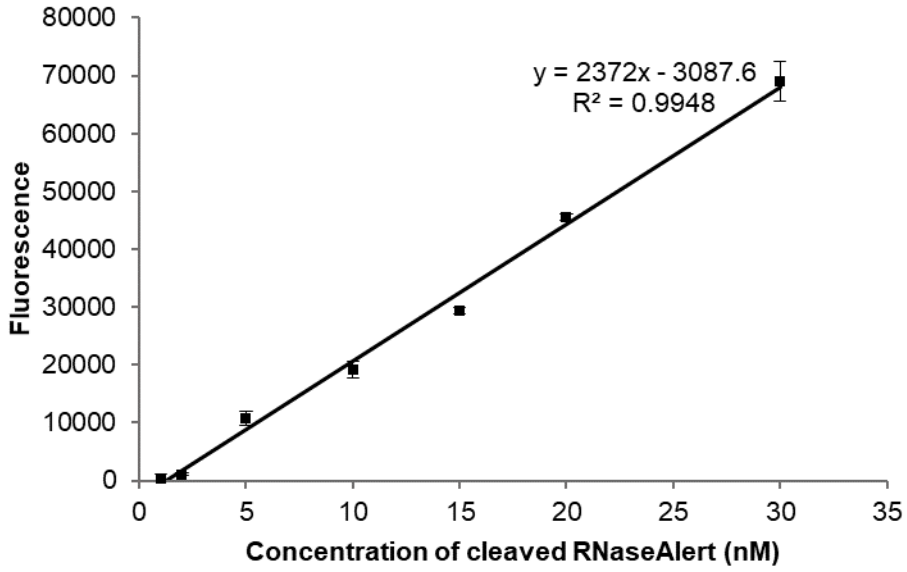

Figure 4-1. A calibration curve of the fluorescence generation in response to the cleavage of RNA reporter (RNaseAlert) measured by StepOnePlus™ RT-PCR instrument (Applied Biosystems). RNaseAlert at concentrations of 1, 2, 5, 10, 20, and 30 nM was completely cleaved by RNase A for 1 h. The volume of each reaction was 20 µL. (n = 3)

4.2.4 Comparing *trans*-cleavage activities with and without pre-annealing of crRNAs and targets

To ensure sufficient binding between crRNA and targets, I annealed crRNA and its target before mixing them with Cas13a or adding them to the cleavage reaction. 2 nM of the crRNA, with or without 0.8 nM of the corresponding target, in a buffer containing 40 mM Tris-HCl pH 7.5, 60 mM NaCl, 6 mM $MgCl_2$ and 0.005% Tween-20 were heated to 85 °C and slowly cooled down to 25 °C over 25 min to allow for annealing. Each cleavage reaction was 20 μL and contained: 4 nM of LwaCas13a (total protein concentration), 0.5 nM of crRNA, 0 or 200 pM of target RNA, 40 mM Tris-HCl pH 7.5, 60 mM NaCl, 6 mM $MgCl_2$, 0.005% Tween-20, 30 nM RNaseAlert reporter (Integrated DNA technology, #11-04-03-03), and 0.001× Rox dye (ThermoFisher, #12223-012). For reactions that did not use pre-annealed crRNA-target hybrids, Cas13a and crRNA were added to the reaction buffer first and incubated for 10 min before adding targets and reporters and the start of measurements. The *trans*-cleavage activity of Cas13a with and without pre-annealing at different temperatures was measured in the same run using a StepOnePlus™ RT-PCR instrument (Applied Biosystems) by setting individual heating block temperatures to 17, 22, 27, 32, 37, and 42 °C. The maximum cleavage rates were calculated by converting the slopes within the fastest 10 min of real-time fluorescence curves to the rate of reporter cleaved (pM/min) based on a calibration curve of the fluorescence generated *vs* the concentrations of reporter fully cleaved (**Figure 4-1**), prepared using the same instrument.

4.3 Results and Discussion

4.3.1 Design of experiments to study the *trans*-cleavage activity at different temperatures

I aimed to study the effect of temperature on the *trans*-cleavage activity of Cas13a upon activation (reaction d, highlighted in **Figure 4-2)**, and whether the temperature effect depends on RNA sequences. Considering the diversity of RNA molecules and the effect of the spacer design on the performance of Cas13a[16], I included activator RNA (target molecule) and crRNA with different characteristics in terms of nucleotide composition, secondary structure (length), and spacer length (**Table 4-2**), and studied individually whether these aspects affect the thermal behavior of the *trans*-cleavage of activated Cas13a. I measured the *trans*-cleavage activity by using fluorescence reporters as *trans*-cleavage substrates of the activated Cas13a (**Figure 4-2**).

The operation of Cas13a includes multiple reactions: (a) ribonucleoprotein formation, (b) RNP-target binding, (c) *cis*-cleavage of target RNA, (d) *trans*-cleavage of reporter RNA. To assess the behavior of Cas13a upon activation (reaction d), I minimized the effects of other reactions on our measurement of the *trans*-cleavage activity.

I ensured proper RNP formation (reaction a, **Figure 4-2**) before quantification of the *trans*-cleavage rate, especially for reactions at low temperatures, because the crRNA-Cas13a RNP formation (reaction a, **Figure 4-2**) was slow at temperatures lower than 23 °C (**Figure 4-3**). The formation of RNP was achieved by incubating crRNA with Cas13a beforehand. Also, in the assessment of *trans*-cleavage reaction rate, I avoided using the rate of the initial stage when the amount of RNP may be limited.

I anticipated that RNP-target binding (reaction b, **Figure 4-2**) could be affected by the activator RNA and the crRNA design, so to focus on the *trans*-cleavage activity once Cas13a

was activated: (i) I included shorter RNA activators that contained no secondary structures so that the binding between activator and crRNA-Cas13a was favorable; (ii) for complicated activator, I included a procedure of pre-annealing of crRNA and target in one set of experiments, to ensure that the reaction b was finished before the measurement of *trans*-cleavage activity; (iii) for situations in which the effects of the formation of RNP and the RNP-target binding on cleavage kinetics were unavoidable, I calculated and compared the maximum cleavage rate at each temperature within the time course of measurement.

Unlike Cas9 or Cas12, Cas13a does not cleave the protospacer at a specific location.[6] The distance between the HEPN catalytic site of LbuCas13a and the target RNA is long, so LbuCas13a may not be able to cleave the protospacer by the *cis*-cleavage activity (reaction c, **Figure 4-2**).[9] Therefore, there may not be a significant loss of LbuCas13a activity over time due to the *cis*-cleavage and the release of the cleaved target. Structural information for LwaCas13a is unavailable. Nevertheless, using the maximum *trans*-cleavage rate within the overall measurement period allowed me to minimize the effect of the deactivation of Cas13a caused by the *cis*-cleavage and potential subsequent activator release. Meanwhile, considering that LwaCas13a has a clear preference for uracil when cleaving RNA, I also included an ssRNA activator (ssRNA-no-U, **Table 4-2**) that contains no uracil to minimize the effect of *cis*-cleavage on the *trans*-cleavage rate.

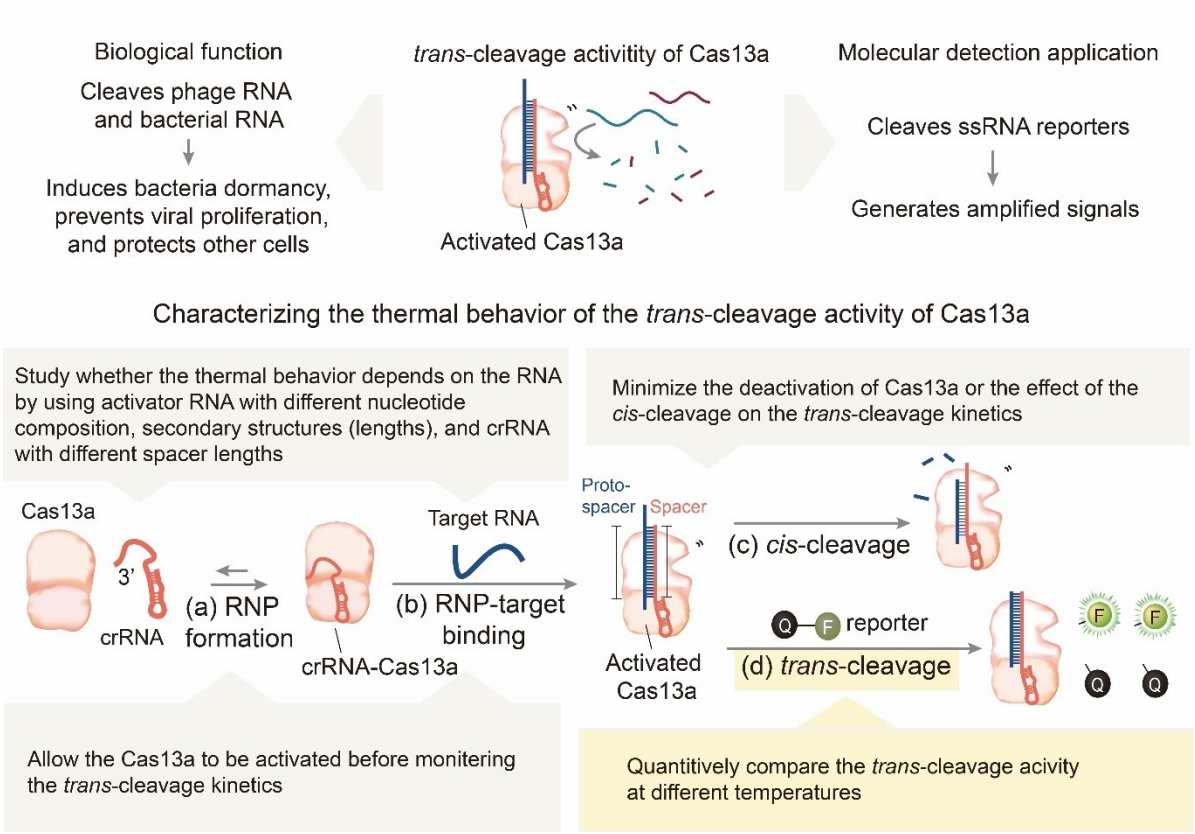

Figure 4-2. The *trans*-cleavage activity of Cas13a and the schematics of my study of its thermal behavior. The *trans*-cleavage activity of Cas13a naturally contributes to the bacterial adaptive immunity against phages and has been used to facilitate signal generation in molecular detection techniques. In both contexts, the operation of Cas13a contains multiple reactions. My research aims to characterize the thermal behavior of the *trans*-cleavage activity of Cas13a (reaction d). I minimized the effect of reactions of RNP (crRNA-Cas13 ribonucleoprotein) formation (reaction a), RNP-target binding (reaction b), and *cis*-cleavage (reaction c). Quantitively compared the *trans*-cleavage activity of activated Cas13a at different temperatures, and whether the thermal behavior depends on the activator and crRNA.

Table 4-2. Activator RNA sequences and secondary structures

Name of Sequence	Sequence and predicted secondary structures*
ssRNA3	AAUAGGAUGGAGUGAGAGAGGAGAAGAGU
ssRNA2	CAGUAGUAGUCGUCAGUCAGUUCAGUCAGGUAAGUAU
ssRNA-no-U	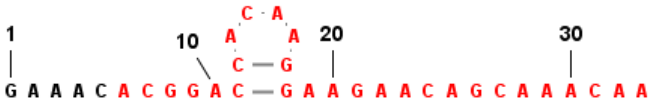
ssRNA1-161 nt	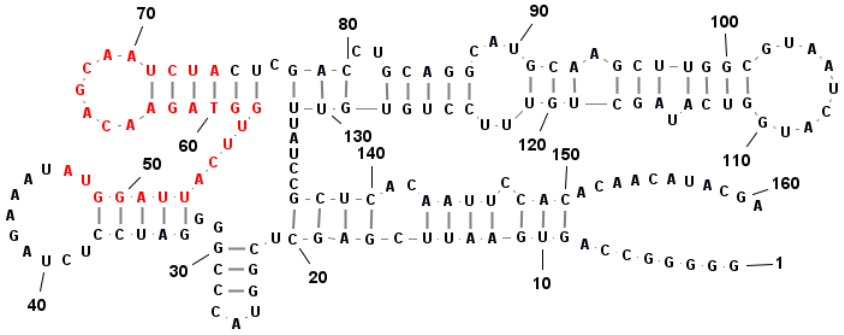
ssRNA1-33 nt	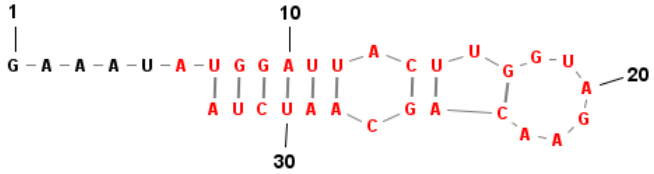
Lbu target 1	GGACCCCAAAAUCAGCGAAA
Lbu target 2	

* The secondary structures of activator RNA were predicted and drawn using RNAstructure V6.3 and StructureEditor. Nucleotides in red indicate protospacers where crRNA-Cas13a RNPs bind. Activator RNA sequences described with plain text are sequences with almost no secondary structure at testing temperatures.

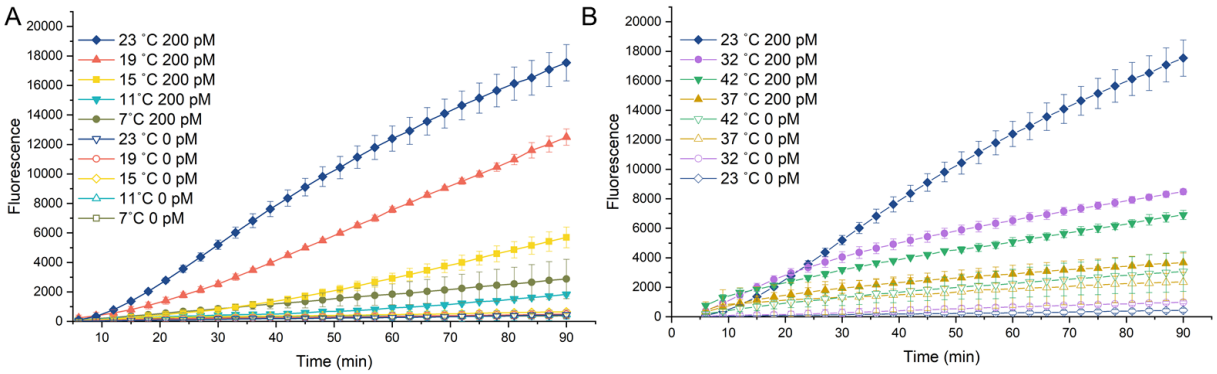

Figure 4-3. Delay in the initiation of *trans*-cleavage activity at low temperature suggests that low temperature (<23 °C) is not favorable for the formation of ribonucleoprotein. **A.** the kinetics of the overall reaction at 7–23 °C. **B.** Kinetics of the overall reaction at 23–42 °C. The fluorescence increase reflected the overall reaction kinetics of three steps: crRNA-Cas13a ribonucleoprotein (RNP) formation, RNP-target binding, and the cleavage of reporters by activated Cas13a. Each reaction contains: 5 nM Cas13a, 0.5 nM crRNA, 200 pM ssRNA-10b, 40 mM Tris-HCl pH 7.5, 60 mM NaCl, and 6 mM $MgCl_2$. 30 nM RNaseAlert. All reagents were mixed at the same time, and aliquots of the reaction were tested in two readings each by setting the heating blocks of StepOnePlus™ RT-PCR instrument (Applied Biosystems) to 5 temperatures (A) or 4 temperatures (B).

4.3.2 *Trans*-cleavage activity of activated LwaCas13a has an optimal temperature around 27–32 °C regardless of the protospacer sequence composition

I included RNA molecules with distinct nucleotide compositions and compared the *trans*-cleavage activity of activated LwaCas13a at different temperatures upon binding to these different activators. To simplify the measurement of the *trans*-cleavage activity at different temperatures, I tested two short RNA activators (ssRNA2 and ssRNA3) with

minimal secondary structure. Compared to complicated RNA, simple RNA is less self-protected and more accessible to the RNP at various temperatures, which minimizes the delay in the cleavage of reporters caused by the RNP-target binding.

ssRNA3 is a 29-nt RNA target, including a 28-nt protospacer, with no secondary structure (**Figure 4-4A**). I monitored the real-time fluorescence generated from the *trans*-cleavage of reporters at 6 temperatures in the same reading to minimize the batch-to-batch variation. The measurement started immediately after mixing RNP with all the other reagents. The kinetics were affected by the temperature. At lower temperatures, 17 to 22 °C, the increases in fluorescence were slow at the beginning, but very fast after the initial stage. (**Figure 4-4B**) This delay may be because of the slow formation of the ternary complex at low temperatures. At higher temperatures, 32 to 42 °C, the initial cleavage was higher than that at lower temperatures, but the reaction rate reduced significantly over time (**Figure 4-4B**). If the reporter had been completely cleaved, the fluorescence plateau would read ~70,000; thus, for most of the reactions at high temperatures, the reduction in cleavage rate is likely due to the deactivation of Cas13a rather than insufficient reporters as substrates.

The maximum cleavage rates represent the *trans*-cleavage rate better than either the initial cleavage rate or the fluorescence increase over 1 h (**Figure 4-4B and 4-4C**). The maximum cleavage rates were determined from the time at which the rates entered a relatively linear stage before they started to decline. Specifically, they were the average cleavage rate in the first 1–5 min for the aliquots tested at 32, 37 and 42 °C, while 10–14 min for 27 °C, 16–20 min for 22 °C, and 31–35 min for 17 °C. The highest *trans*-cleavage rate, ~1000 pM/min in response to 200 pM ssRNA3, was observed at 27 °C. (**Figure 4-4C**) This was twice as high as that of the second-best temperature of 22 °C. Because of the consistent cleavage rate since

the 20th min at 22 °C and the reduction of cleavage rate at 27 °C over time, the signals generated within 1 h at the two temperatures were comparable (**Figure 4-4B**).

Following the same procedure, I analyzed another short activator with different nucleotide composition, ssRNA-no-U (**Figure 4-4D**). As the RNA cleavage of Cas13a has a clear uracil preference, I included this target with no uracil to minimize the cleavage of the target. Consistent with the other activator (ssRNA3), the reaction entered the linear stage later at lower temperatures, and the activity reduced over time at higher temperatures. (**Figure 4-4E**) Meanwhile, the highest *trans*-cleavage was achieved at 27–32 °C after the crRNA-Cas13a-target ternary complexes were formed, similar to the optimal temperature of 27 °C for ssRNA2 (**Figure 4-4F**). The *trans*-cleavage activity varied when different activators were used. Others have also reported such observations, but there is still no conclusion on how the activator or the spacer sequence affects the *trans*-cleavage activity.[16, 18]

The preference for lower temperatures (27 °C) suggests that the targeting and detection of short and simple ssRNA do not require additional heating. Current *in vitro* RNA detection techniques commonly use 37 °C for incubation, but assays that operate at ambient temperature are more applicable in resource-limited settings or point-of-care analyses.

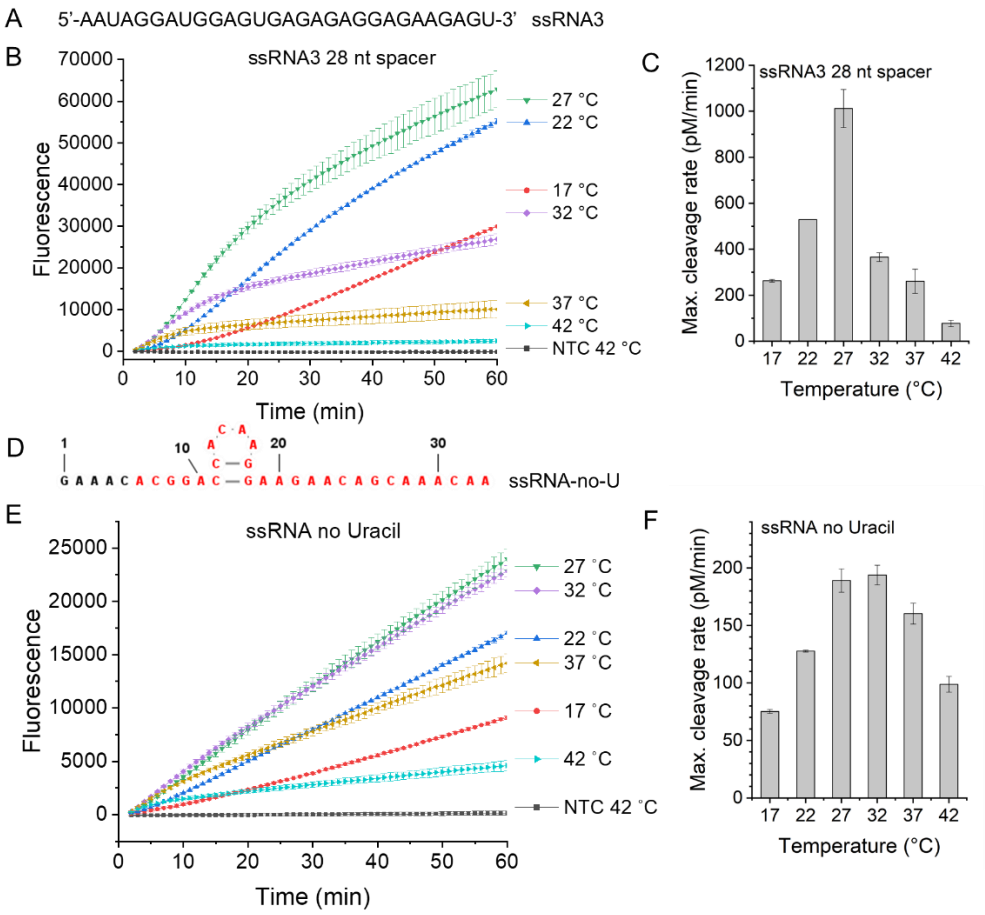

Figure 4-4. LwaCas13a shows higher *trans*-cleavage activity at 27 °C than 37 °C in response to 2 activators with different nucleotide composition. A. The sequence of ssRNA3, a 29-nt single-stranded RNA with no secondary structure. **B.** *Trans*-cleavage kinetics of Cas13a at 6 different temperatures when using ssRNA3 as the activator. **C.** The maximum cleavage rate at different temperatures calculated based on the part of each curve with the highest rate (slope) in **Figure 4-4B**. **D.** The sequence and structure of ssRNA-no-U, a 33-nt single-stranded RNA with no uracil. **E.** *Trans*-cleavage kinetics of Cas13a at 6 different temperatures when using ssRNA-no-U as the activator. **F.** The maximum cleavage rate at different temperatures calculated based on the part of each curve with the highest rate (slope) in **Figure 4-4E**.

4.3.3 The optimal temperature of the *trans*-cleavage activity of activated Cas13a is independent of the structure of RNA activators

RNA usually forms complicated secondary structures because of internal base-pairing or stacking. The protospacers in the RNA target for RNP recognition could be in such complicated regions, and the accessibility of the protospacer at different temperatures may also affect the kinetics. Therefore, in addition to the analysis of ssRNA with simple secondary structures and short lengths, I also analyzed two target RNAs with complicated secondary structures (predicted by Software RNA structure V6.3). (**Figure 4-5A** and **4-6A**)

I initially used the same procedure as that for the analysis of short RNA, i.e., allowing the RNP to form first and measuring the trans-cleavage kinetics after adding the activator and reporters. I observed a relatively slow initiation of the *trans*-cleavage (**Figure 4-5B**). Both the real-time fluorescence generation and the calculated maximum cleavage rate indicated an optimal temperature of 37 °C for the process of RNP-target binding and *trans*-cleavage when using ssRNA1-161nt as the activator (**Figure 4-5B** and **4-5C**). The maximum cleavage rate at 37 °C was 40% higher than that at 32 °C, and 150% higher than that at 27 ºC (**Figure 4-5C**). The 37 ºC optimum was consistent with the commonly used condition for *in vitro* RNA detection. However, this temperature was significantly higher when using shorter targets with simpler secondary structures as activators. I hypothesized that heating is required for the reaction of RNP-target binding rather than for the *trans*-cleavage reaction.

To differentiate the effect of temperature on the RNP-target binding from the *trans*-cleavage activity, I compared the *trans*-cleavage with and without pre-annealing of the crRNA with the complicated target. The pre-annealing of crRNA and target allowed crRNA-target binding to be completed before I started monitoring the *trans*-cleavage activity. Though

Cas13a is added to the reaction later together with the reporter instead of forming an RNP with crRNA in advance, it still bound to the crRNA-target hybrid efficiently, as there was no significant delay in the initiation of *trans*-cleavage reactions shown in **Figure 4-5D**.

With the pre-annealing of crRNA and target, the formation of the crRNA-Cas13a-target ternary complex was enhanced. I measured the *trans*-cleavage kinetics after mixing the crRNA-target duplex with Cas13a and reporters in parallel with reactions prepared without the crRNA-target annealing yet maintaining all reagents at the same concentration. Importantly, with the additional pre-annealing step, the fluorescence increase was higher than that from experiments without pre-annealing at corresponding temperatures, especially at temperatures of 17–37 ºC (**Figure 4-5B–D**). With pre-annealing, the maximum *trans*-cleavage activity at 37 ºC is not as high as that at 27 ºC or 32 ºC. The maximum *trans*-cleavage rate at 22–27 ºC increased by 4-fold because of the pre-annealing, while just 2-fold at 32 ºC and 70% folds at 37 ºC (**Figure 4-5D and 4-5E**).

To include different secondary structures, I truncated the ssRNA1 to 33 nt without changing the protospacer sequence of ssRNA1 (**Figure 4-6A,** in red). The 33-nt activator tended to form a different secondary structure, but the same crRNA can be used for both ssRNA1-161nt and ssRNA1-33nt. ssRNA1-33nt was able to activate Cas13a RNP as well. The optimal temperature was 37 ºC without annealing and shifted to a lower temperature when there was pre-annealing, which was consistent with the performance using the 161-nt RNA to activate Cas13a (**Figure 4-6**).

Even for complicated activators, once activated, the preferred temperature for *trans*-cleavage activity was relatively low, within the 27–32 ºC range. The temperature preference did not depend on RNA structures. Pre-annealing helped with the initiation of *trans*-cleavage

in the detection of long targets (**Figure 4-5B and 4-5D**). Thus, for the detection of human or pathogen RNA that is long and naturally has complicated structures, an alternative approach for RNA detection is to include a quick annealing step: heat up the sample-crRNA mix to a higher temperature for several minutes and then cool the reaction down for subsequent ambient temperature fluorescence detection.

The detection of complicated targets preferred higher temperatures (37 ºC), compared to short RNA or targets pre-annealed with crRNA. I speculated that high temperature is required for efficient RNP-target binding if the protospacer is hard to access. The extra heating might be used for opening the target RNA during the RNP-target binding process.

The *trans*-cleavage activity was different when using activators with the same protospacer but different structures and lengths, which may suggest that the sequence that extends beyond the protospacer region should be considered when predicting the *trans*-cleavage activity. Meanwhile, using a partial target RNA molecule to characterize assay performance may not be accurate.

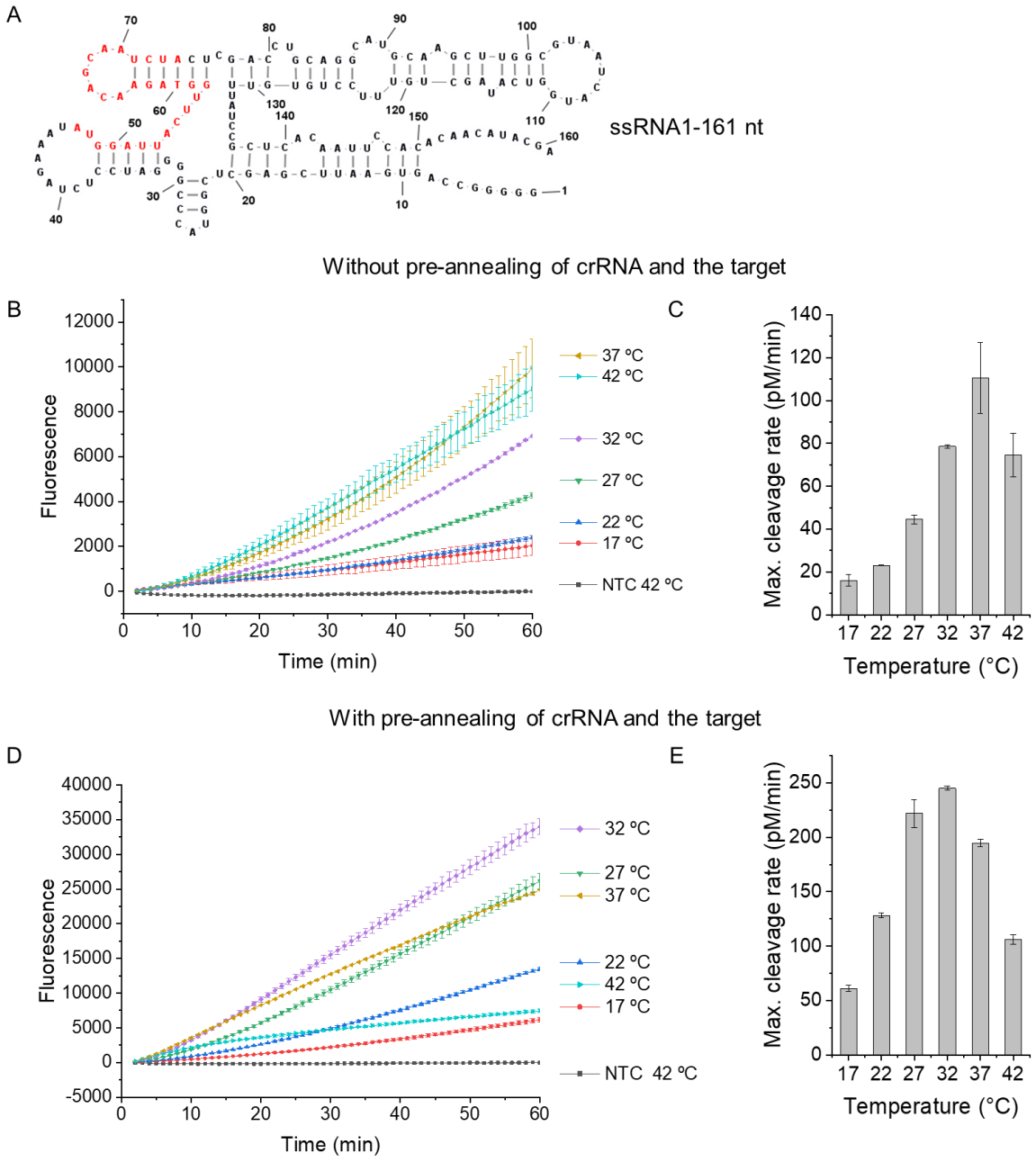

Figure 4-5. The effect of temperature on the *trans*-cleavage kinetics by LwaCas13a when using activator ssRNA1-161nt, and the reduction of the required temperature after the pre-annealing of crRNA and the target. A. ssRNA1-161nt, its predicted secondary structure, and the protospacer region (in red). **B.** T*rans*-cleavage kinetics by Cas13a at 6 different temperatures when using ssRNA1-161nt without pre-annealing with crRNA. **C.** The

maximum *trans*-cleavage rates at different temperatures after adding ssRNA1-161nt calculated based on the curves in **Figure 4-5B. D.** T*rans*-cleavage kinetics of Cas13a at 6 different temperatures when using pre-annealed ssRNA1-161nt with crRNA. **E.** The maximum *trans*-cleavage rates at different temperatures after mixing pre-annealed ssRNA1-161nt-crRNA duplex with other reagents. The rate was calculated based on the curves in **Figure 4-5D.**

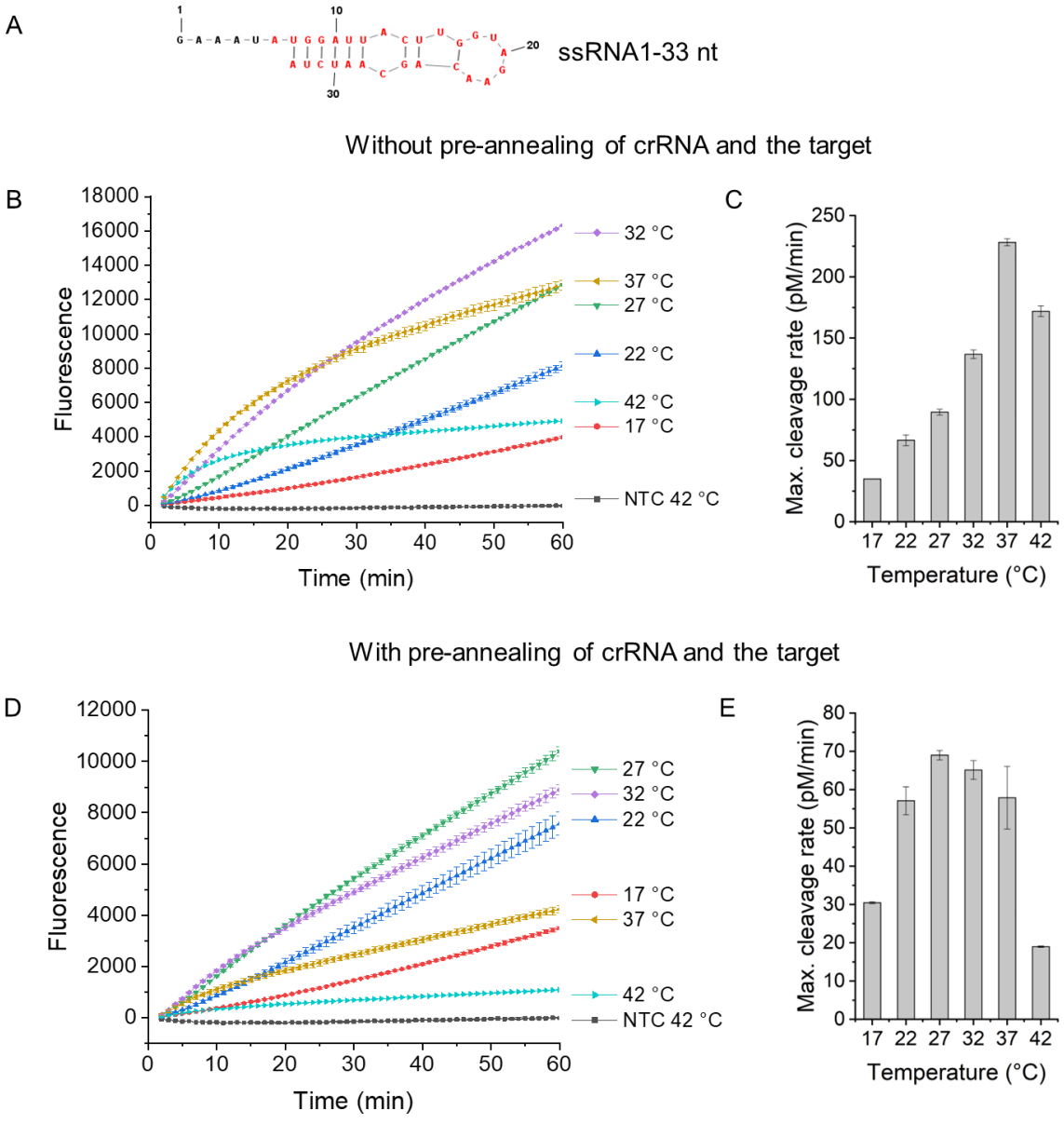

Figure 4-6. The effect of temperature on the *trans*-cleavage kinetics of LwaCas13a when using activator ssRNA1-33nt, with and without pre-annealing of crRNA and the target. **A.** Target ssRNA1-33nt, its predicted secondary structure, and the same protospacer region (in red) as in ssRNA1-161nt. **B.** *Trans*-cleavage kinetics of Cas13a at 6 different temperatures when using ssRNA1-33nt without pre-annealing with crRNA. **C.** The maximum *trans*-cleavage rates at different temperatures after the addition of ssRNA1-33nt calculated based on the curves in **Figure 4-6B. D.** *Trans*-cleavage kinetics of Cas13a at 6 different temperatures when using pre-annealed ssRNA1-33nt with crRNA. **E.** The maximum *trans*-cleavage rates at different temperatures after mixing pre-annealed ssRNA1-33nt-crRNA duplex with other reagents. The rate was calculated based on the curves in **Figure 4-6D.**

4.3.4 The optimal temperature of *trans*-cleavage activity is independent of the spacer length

To test whether our finding of the low optimal temperature is an intrinsic feature of LwaCas13a or is affected by protein-RNA and RNA-RNA interactions, I included additional targets and two sets of spacers of different lengths. (**Figure 4-7C and 4-8A**) The length and nucleotide composition of the spacer affects the strength of crRNA-target interaction as well as that of RNA-Cas13a interaction, and thus the sequence specificity and sensitivity of Cas13a-based techniques. I designed another 33-nt ssRNA (ssRNA2) that does not form stem-loop structures at temperatures above 20 ºC, so that no additional energy is required to open the stems in the target RNA during the RNP-target binding process (**Figure 4-8A**). For each of the ssRNA2 and ssRNA3, I designed a set of crRNA with spacers of different lengths by

truncating the 3' end of the crRNA (**Figure 4-7C** and **4-8A**). These spacers were sufficient for the activation of LwaCas13a (**Figure 4-7** and **Figure 4-8**).

The effects of temperature on the *trans*-cleavage kinetics when using 24- or 26-nt spacers for ssRNA3 were consistent with those when using the 28-nt spacer (**Figure 4-4B**, **4-7A** and **B**). The optimal temperature for *trans*-cleavage was also consistent among spacers, i.e. around 27 °C. (**Figure 4-4C, 4-7D and 4-7E**) For ssRNA2, the kinetics was distinct from other targets. Considering the fast initiation of the *trans*-cleavage and the quick deactivation of Cas13a (**Figure 4-8B, 4-8D, 4-8F, and 4-8H**), I calculated the maximum cleavage rate based on the cleavage within the first minute. The optimal temperatures were consistently around 27–32 °C when using spacers in lengths ranging from 24 to 32 nt. **(Figure 4-8C, 4-8E, 4-8G, and 4-8I)** Although the maximum cleavage rates at 32 °C were close to those at 27 °C, the number of reporters cleaved within 1 h was lower because of the reduction of Cas13a activity over time at 32 °C. Although when using different activators and crRNA the kinetics can be different, the optimal temperature for the *trans*-cleavage was consistently 27 °C.

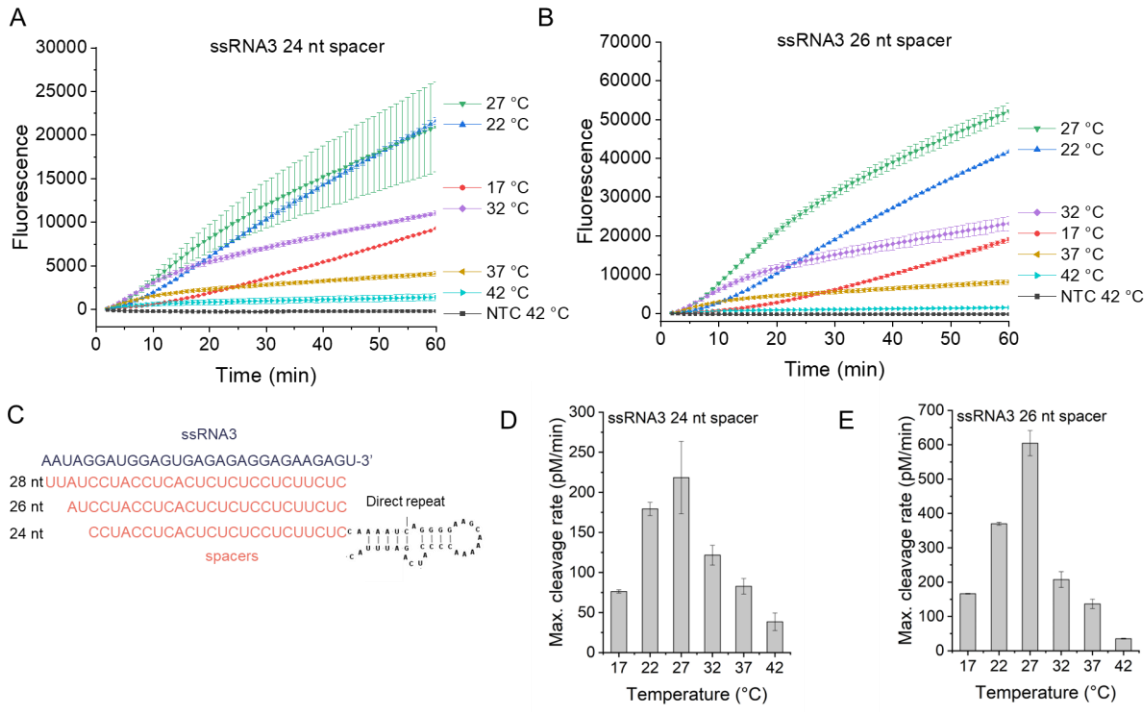

Figure 4-7. The consistent effect of temperature on the *trans*-cleavage kinetics of LwaCas13a when using activator ssRNA3 together with spacers of different lengths. A. *Trans*-cleavage kinetics of Cas13a at 6 different temperatures when using ssRNA3 with a 24-nt spacer. **B.** *Trans*-cleavage kinetics of Cas13a at 6 different temperatures when using ssRNA3 with a 26-nt spacer. **C.** ssRNA3 and corresponding crRNA with spacers of different lengths. **D.** The maximum *trans*-cleavage rates when using the 24-nt spacer at different temperatures calculated based on the part of each curve with the highest rate (slope) in **Figure 4-7A**. **E.** The maximum *trans*-cleavage rate when using the 26-nt spacer at different temperatures calculated based on the part of each curve with the highest rate (slope) in **Figure 4-7B**.

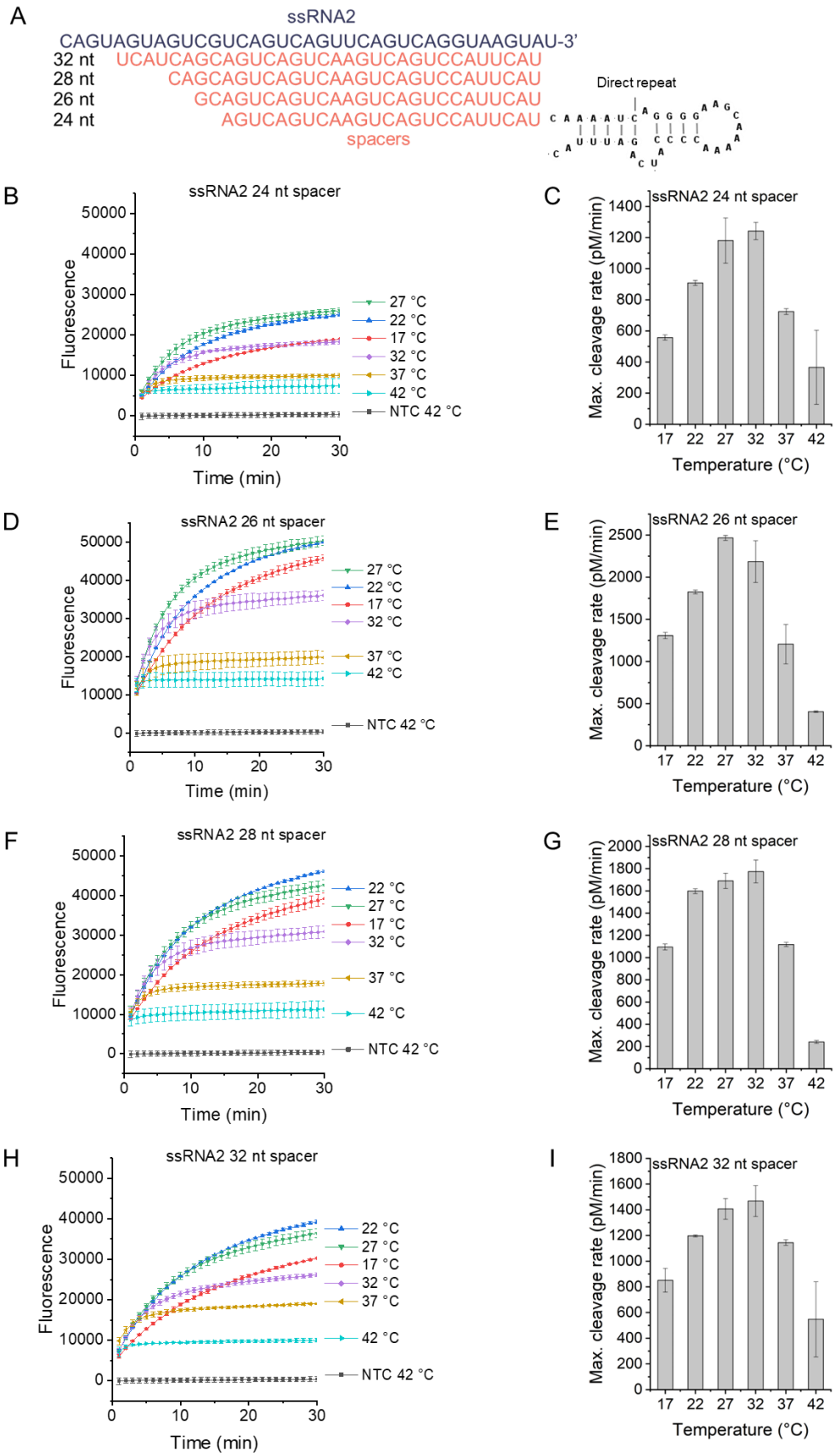
A
ssRNA2
CAGUAGUAGUCGUCAGUCAGUUCAGUCAGGUAAGUAU-3'
32 nt UCAUCAGCAGUCAGUCAAGUCAGUCCAUUCAU
28 nt CAGCAGUCAGUCAAGUCAGUCCAUUCAU
26 nt GCAGUCAGUCAAGUCAGUCCAUUCAU
24 nt AGUCAGUCAAGUCAGUCCAUUCAU
spacers
Direct repeat
B
ssRNA2 24 nt spacer
Fluorescence
Time (min)
27 °C
22 °C
17 °C
32 °C
37 °C
42 °C
NTC 42 °C
C
ssRNA2 24 nt spacer
Max. cleavage rate (pM/min)
Temperature (°C)
D
ssRNA2 26 nt spacer
Fluorescence
Time (min)
27 °C
22 °C
17 °C
32 °C
37 °C
42 °C
NTC 42 °C
E
ssRNA2 26 nt spacer
Max. cleavage rate (pM/min)
Temperature (°C)
F
ssRNA2 28 nt spacer
Fluorescence
Time (min)
22 °C
27 °C
17 °C
32 °C
37 °C
42 °C
NTC 42 °C
G
ssRNA2 28 nt spacer
Max. cleavage rate (pM/min)
Temperature (°C)
H
ssRNA2 32 nt spacer
Fluorescence
Time (min)
22 °C
27 °C
17 °C
32 °C
37 °C
42 °C
NTC 42 °C
I
ssRNA2 32 nt spacer
Max. cleavage rate (pM/min)
Temperature (°C)

Figure 4-8. The consistent effect of temperature on the *trans*-cleavage kinetics of LwaCas13a when using activator ssRNA2 together with spacers of different lengths. A. ssRNA2 and corresponding crRNA with spacers of different lengths ranging from 24 to 32 nt. **B. D. F. H.** *Trans*-cleavage kinetics of Cas13a at 6 different temperatures when using ssRNA2 with 24–32 nt spacers. **C. E. G. I.** The maximum *trans*-cleavage rates when using 24–32-nt spacer at different temperatures calculated based on the part of each curve with the highest rate (slope) in **Figure 4-8B, D, F, and H.**

4.3.5 The thermal behavior of the *trans*-cleavage activity of a second Cas13a, LbuCas13a

With the same consideration in mind, I studied the effect of temperature on the *trans*-cleavage activity of LbuCas13a activated by two targets. LbuCas13a target 1 contains minimal internal base-pairing and target 2 has moderate base-pairing. (**Figure 4-9**) For both targets, the *trans*-cleavage rate of LbuCas13a at different temperatures varied, but the shapes of the curves were consistent among temperatures. The initial cleavage rates correlated with the rates at later stages and the maximum cleavage rate within the 1 h period. There was no abrupt decrease in *trans*-cleavage activity over time, even at high temperatures (37 °C and 42 °C), suggesting the high stability of LbuCas13a RNP-target complexes. This agreed with the previous finding of no cleavage of the protospacer region by LbuCas13a[9]. If a protospacer is cleaved in the middle, the RNA-RNA binding stability will decrease, and Cas13a may be deactivated. The maximum cleavage rates were the cleavage rate in the first 1–6 min for the aliquots tested at 32, 37 and 42 °C, the first 1–10 min for 27 °C, 9–18 min for 22 °C, and 11–20 min for 17 °C. High *trans*-cleavage activities were observed between 27–37 °C, with optimal activity at 32 °C. (**Figure 4-9**)

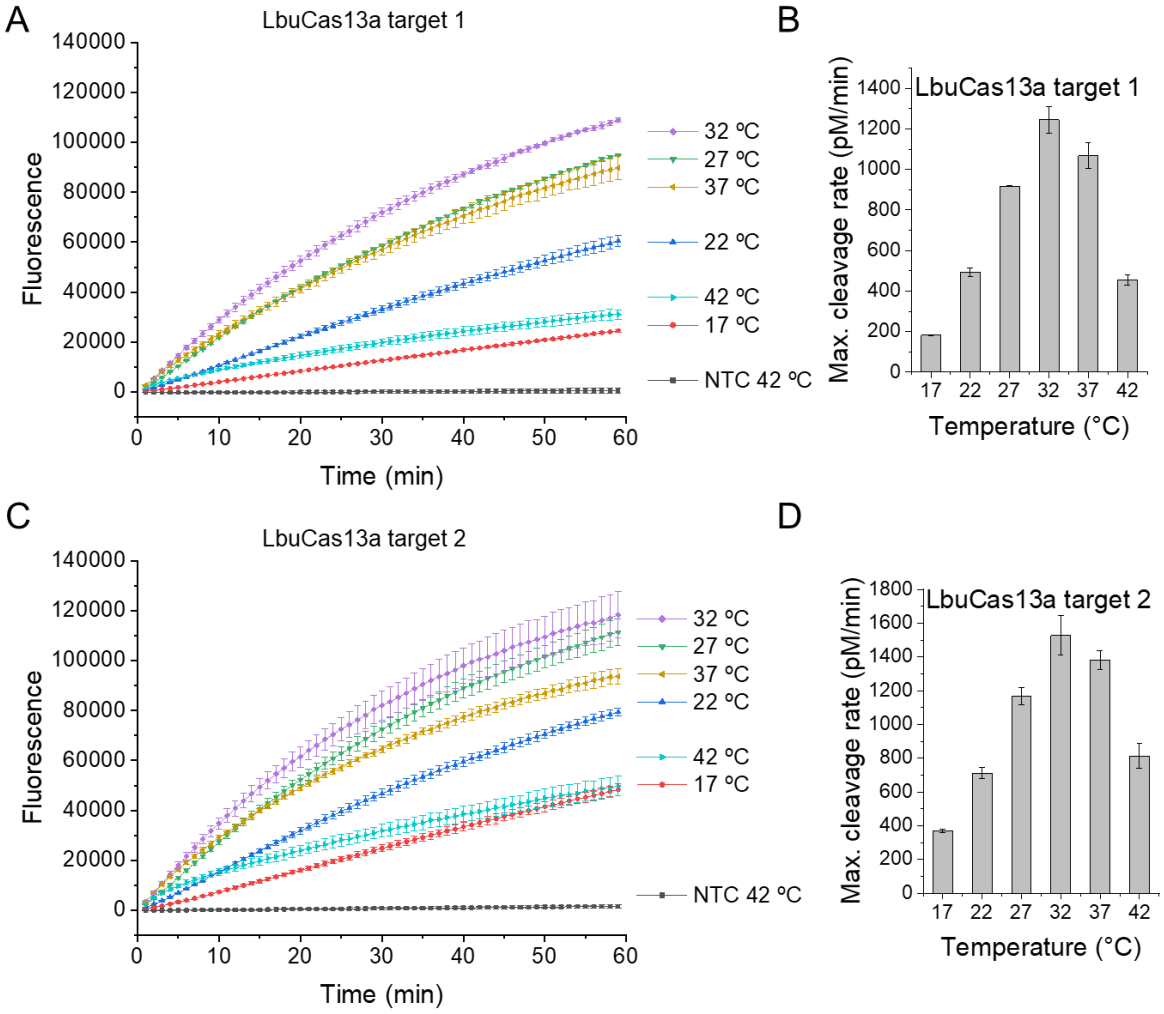

Figure 4-9. The *trans*-cleavage kinetics of LbuCas13a at 17–42 °C. A. *Trans*-cleavage kinetics of LbuCas13a at 6 different temperatures upon the addition of target 1. **B.** The maximum *trans*-cleavage rates at different temperatures calculated based on the curves in **Figure 4-9A. C.** *Trans*-cleavage kinetics of Cas13a at 6 different temperatures upon the addition of target 2. **D.** The maximum *trans*-cleavage rates at different temperatures calculated based on the curves in **Figure 4-9C.**

Similar to LwaCas13a, once activated, LbuCas13a showed a high *trans*-cleavage activity around 27 °C. Among Cas13a homologs, LbuCas13a and LwaCas13a are the two with the highest *trans*-cleavage activity and they can be activated by a low concentration of targets[20], so they have been widely used for RNA analysis. The high *trans*-cleavage at 27 °C is good for the development of simpler detection techniques. Once the RNP-target ternary complexes are properly formed, the *trans*-cleavage can proceed at 27 °C.

4.4 Conclusion

The thermal behavior of Cas13a is a substantial factor of Cas13a kinetics when applying Cas13a in different scenarios. Here, I studied the temperature effects for the *trans*-cleavage activity of LwaCas13a and LbuCas13a upon activation. The operation of Cas13a includes multiple interactions, from RNP formation, RNP-targeting binding, to *cis*-cleavage and *trans*-cleavage, and the reaction temperature affects each step differently. I eliminated, as much as possible, the effects of RNP formation and, RNP-target binding, and *cis*-cleavage, on the *trans*-cleavage kinetics measurement at different temperatures and analyzed the *trans*-cleavage of activated Cas13a. I rationally designed different target RNA and crRNA with different nucleotide compositions, secondary structures, and lengths to study whether the thermal behavior of activated Cas13a is target-dependent.

I quantitatively compared the kinetics of the *trans*-cleavage activity upon activation by different targets at temperatures between 17 and 42 °C. Once the RNP-target ternary complexes were formed, the highest *trans*-cleavage activity of LwaCas13a and LbuCas13a was achieved at 27–32 °C, instead of the often used 37 °C. This preferred 27 – 32 °C

temperature range for high *trans*-cleavage was consistent among targets with different nucleotide composition, secondary structure, or spacer length in crRNA.

The fast initiation and high *trans*-cleavage activity when using short RNA suggest that the detection of short and simple RNA can be performed at ambient temperature without compromising sensitivity. Meanwhile, the higher temperature (37 °C) required for the RNP-target binding when using long and complicated RNA suggests the importance of this target binding process on the sensitivity of the Cas13a-mediated RNA detection. In the detection of long RNA with complicated secondary structures, the assay can start with a short period of incubation at a higher temperature, yet the signal generation can be done at ambient temperature. Such a strategy may improve the performance of Cas13a-based detection, speed up the process, and reduce the dependence on instruments during RNA analysis. In addition, the optimal temperature is independent of spacer length, so a shorter spacer that usually provides higher sequence specificity can be used at ambient temperature.

The *trans*-cleavage kinetics of Cas13a can be easily affected by other factors such as cofactors and reporter substrates. These factors may also affect the overall kinetics of Cas13a at different temperatures. Additionally, further characterization of the kinetics of different reaction steps using different technology would provide more insights into the mechanism of Cas13a activity and preference.

4.5 References

1. Knott, G. J. and Doudna, J. A., CRISPR-Cas guides the future of genetic engineering. *Science* **2018,** *361* (6405), 866-869.
2. Abudayyeh, O. O., Gootenberg, J. S., Essletzbichler, P., Han, S., Joung, J., Belanto, J. J., Verdine, V., Cox, D. B. T., Kellner, M. J., Regev, A., Lander, E. S., Voytas, D. F., Ting, A. Y. and Zhang, F., RNA targeting with CRISPR-Cas13. *Nature* **2017,** *550*, 280-284.
3. Myhrvold, C., Freije, C. A., Gootenberg, J. S., Abudayyeh, O. O., Metsky, H. C., Durbin, A. F., Kellner, M. J., Tan, A. L., Paul, L. M., Parham, L. A., Garcia, K. F., Barnes, K. G., Chak, B., Mondini, A., Nogueira, M. L., Isern, S., Michael, S. F., Lorenzana, I., Yozwiak, N. L., MacInnis, B. L., Bosch, I., Gehrke, L., Zhang, F. and Sabeti, P. C., Field-deployable viral diagnostics using CRISPR-Cas13. *Science* **2018,** *360* (6387), 444-448.
4. Gootenberg, J. S., Abudayyeh, O. O., Kellner, M. J., Joung, J., Collins, J. J. and Zhang, F., Multiplexed and portable nucleic acid detection platform with Cas13, Cas12a, and Csm6. *Science* **2018,** *360* (6387), 439-444.
5. Abudayyeh, O. O., Gootenberg, J. S., Konermann, S., Joung, J., Slaymaker, I. M., Cox, D. B. T., Shmakov, S., Makarova, K. S., Semenova, E., Minakhin, L., Severinov, K., Regev, A., Lander, E. S., Koonin, E. V. and Zhang, F., C2c2 is a single-component programmable RNA-guided RNA-targeting CRISPR effector. *Science* **2016,** *353* (6299), aaf5573.
6. East-Seletsky, A., O'Connell, M. R., Knight, S. C., Burstein, D., Cate, J. H. D., Tjian, R. and Doudna, J. A., Two distinct RNase activities of CRISPR-C2c2 enable guide-RNA processing and RNA detection. *Nature* **2016,** *538*, 270-273.
7. O'Connell, M. R., Molecular Mechanisms of RNA Targeting by Cas13-containing Type VI CRISPR–Cas Systems. *J Mol. Biol.* **2019,** *431* (1), 66-87.

8. Knott, G. J., East-Seletsky, A., Cofsky, J. C., Holton, J. M., Charles, E., O'Connell, M. R. and Doudna, J. A., Guide-bound structures of an RNA-targeting A-cleaving CRISPR-Cas13a enzyme. *Nat. Struct. and Mol. Biol.* **2017,** (10), 825-833.
9. Liu, L., Li, X., Ma, J., Li, Z., You, L., Wang, J., Wang, M., Zhang, X. and Wang, Y., The Molecular Architecture for RNA-Guided RNA Cleavage by Cas13a. *Cell* **2017,** *170*, 714-726.
10. Liu, L., Li, X., Wang, J., Wang, M., Chen, P., Yin, M., Li, J., Sheng, G. and Wang, Y., Two Distant Catalytic Sites Are Responsible for C2c2 RNase Activities. *Cell* **2017,** *168* (1-2), 121-134.
11. Meeske, A. J., Nakandakari-Higa, S. and Marraffini, L. A., Cas13-induced cellular dormancy prevents the rise of CRISPR-resistant bacteriophage. *Nature* **2019**, *570*, 241-245.
12. Gootenberg, J. S., Abudayyeh, O. O., Lee, J. W., Essletzbichler, P., Dy, A. J., Joung, J., Verdine, V., Donghia, N., Daringer, N. M., Freije, C. A., Myhrvold, C., Bhattacharyya, R. P., Livny, J., Regev, A., Koonin, E. V., Hung, D. T., Sabeti, P. C., Collins, J. J. and Zhang, F., Nucleic acid detection with CRISPR-Cas13a/C2c2. *Science* **2017,** *356* (6336), 438-442.
13. Shan, Y., Zhou, X., Huang, R. and Xing, D., High-Fidelity and Rapid Quantification of miRNA Combining crRNA Programmability and CRISPR/Cas13a trans-Cleavage Activity. *Anal. Chem.* **2019,** *91* (8), 5278-5285.
14. Bruch, R., Baaske, J., Chatelle, C., Meirich, M., Madlener, S., Weber, W., Dincer, C. and Urban, G. A., CRISPR/Cas13a-Powered Electrochemical Microfluidic Biosensor for

Nucleic Acid Amplification-Free miRNA Diagnostics. *Adv. Mater.* **2019,** *31* (51), 1905311.

15. Chen, Y., Yang, S., Peng, S., Li, W., Wu, F., Yao, Q., Wang, F., Weng, X. and Zhou, X., N1-Methyladenosine detection with CRISPR-Cas13a/C2c2. *Chem. Sci.* **2019,** *10* (10), 2975-2979.
16. Fozouni, P., Son, S., Díaz de León Derby, M., Knott, G. J., Gray, C. N., D'Ambrosio, M. V., Zhao, C., Switz, N. A., Kumar, G. R., Stephens, S. I., Boehm, D., Tsou, C.-L., Shu, J., Bhuiya, A., Armstrong, M., Harris, A. R., Chen, P.-Y., Osterloh, J. M., Meyer-Franke, A., Joehnk, B., Walcott, K., Sil, A., Langelier, C., Pollard, K. S., Crawford, E. D., Puschnik, A. S., Phelps, M., Kistler, A., DeRisi, J. L., Doudna, J. A., Fletcher, D. A. and Ott, M., Amplification-free detection of SARS-CoV-2 with CRISPR-Cas13a and mobile phone microscopy. *Cell* **2021,** *184* (2), 323-333.e9.
17. Ramachandran, A. and Santiago, J. G., CRISPR Enzyme Kinetics for Molecular Diagnostics. *Anal. Chem.* **2021,** *93* (20), 7456-7464.
18. Nalefski, E. A., Patel, N., Leung, P. J. Y., Islam, Z., Kooistra, R. M., Parikh, I., Marion, E., Knott, G. J., Doudna, J. A., Le Ny, A.-L. M. and Madan, D., Kinetic analysis of Cas12a and Cas13a RNA-Guided nucleases for development of improved CRISPR-Based diagnostics. *iScience* **2021,** *24*, 102996.
19. Wu, Y., Liu, S.-X., Wang, F. and Zeng, M.-S., Room Temperature Detection of Plasma Epstein–Barr Virus DNA with CRISPR–Cas13. *Clin. Chem.* **2019,** *65* (4), 591-592.
20. East-Seletsky, A., O'Connell, M. R., Burstein, D., Knott, G. J. and Doudna, J. A., RNA Targeting by Functionally Orthogonal Type VI-A CRISPR-Cas Enzymes. *Mol. Cell* **2017,** *66* (3), 373-383.

Chapter 5. Integrating Reverse Transcription Recombinase Polymerase Amplification with CRISPR Technology for One-Tube Assay of RNA[†]

5.1 Introduction

CRISPR technology has significantly advanced genome editing as well as molecular detection.[1-5] CRISPR-associated (Cas) proteins can target different genes of interest with corresponding guide RNA designed to be complementary to the target nucleic acids.[6] This programmable RNA-guided site-specific recognition is simpler than the mechanisms of previous genome editing tools because CRISPR-Cas eliminates the need to engineer individual proteins for targeting each site.[7] In the CRISPR-Cas reaction cascade, target recognition activates Cas systems to either operate on the target nucleic acids for gene editing or function as a *trans*-cleavage nuclease to cleave collaterally nucleic acid reporters for molecular detection.[1, 4, 8-9] CRISPR-based diagnostics modularly combines nucleic acid amplification techniques with the target-specific detection capability of CRISPR-Cas systems. Combining isothermal amplification with CRISPR-Cas is especially advantageous for potential point-of-care applications. Isothermal amplification, such as loop-mediated isothermal amplification (LAMP)[10] and recombinase polymerase amplification (RPA),[11] can exponentially amplify DNA rapidly to improve analytical sensitivity, but is susceptible to nonspecific amplification, which weakens analytical specificity if the detection probes are not target-specific. Following isothermal exponential amplification, CRISPR-Cas systems

[†] Chapter 5 has been published: Feng, W. [Δ], Peng, H. [Δ], Xu, J., Liu, Y., Pabbaraju, K., Tipples, G., Joyce, M. A., Saffran, H. A., Tyrrell, D. L., Babiuk, S., Zhang, H. and Le, X. C., Integrating Reverse Transcription Recombinase Polymerase Amplification with CRISPR Technology for the One-Tube Assay of RNA. *Anal Chem* **2021,** *93* (37), 12808-12816.

specifically detect the amplicon of target molecules and thus improve analytical specificity.[5] Thus, methods of combining nucleic acid amplification with CRISPR-Cas have been successfully applied to the detection of pathogens, including SARS-CoV-2, the causative agent of coronavirus disease of 2019 (COVID-19).[12-14]

Limited by the incompatibility of the reaction temperature and reagents, most isothermal assays used the CRISPR technology for detection in a separate post-amplification step.[8, 13, 15] However, opening tubes after exponential amplification risks contaminating the working environment with the DNA amplicons and causing false positives.[16] Therefore, it is desirable to complete both the amplification and the detection in the same tube without opening the tube after the amplification step.

RPA typically operates at a moderate temperature (e.g., 40 °C),[11] matching the optimal reaction temperatures of most Cas enzymes, such as Cas13a and Cas12a.[17] Cas12a recognizes double-stranded DNA (dsDNA), and is suitable for direct detection of dsDNA amplicons. Cas13a recognizes RNA, and requires an extra step of T7 transcription of DNA amplicons for detection. Although RPA and CRISPR-Cas systems have been integrated into single-tube assays,[8, 18-26] most of these assays require the separate placement of RPA and CRISPR-Cas reagents to achieve sensitive detection (**Table A1**).[8, 18, 20-22] Ding et al. [23] recently developed a one-pot assay with the RT-RPA and CRISPR-Cas12a reactions taking place in the same solution. This assay used two crRNA-Cas12a ribonucleoproteins (RNPs), each activated by a displaced single-stranded region of the RPA amplicon, to generate fluorescence signals. However, the crRNA-Cas12a RNP is less specific for differentiating mismatches in ssDNA than in dsDNA.[8] Additionally, the use of the two RNPs requires the design of two crRNA sequences and increases the cost of the assay.

Previous studies also showed that the detection of RNA using RT-RPA and CRISPR-Cas is less sensitive than the detection of DNA,[13, 24] the reason for which has not been well elucidated. My research group hypothesized that rapid initiation of RPA was critical for the success of a single-tube assay and that dynamic formation of RNA-cDNA hybrids delays the initiation of RPA. I report here tests of the hypothesis, our understanding of the underlying problem, and an approach to overcome the problem. Using the detection of SARS-CoV-2 RNA as an example, I show the importance of generating single-stranded cDNA for rapid RPA initiation in an integrated RT-RPA-CRISPR-Cas12a technique and demonstrate a single-tube assay for rapid and semi-quantitative detection of a specific RNA target. For the high specificity of the assay, a crRNA was designed to recognize dsDNA of the RPA amplicons instead of ssDNA. An additional benefit of using the crRNA targeting dsRNA is that the *trans*-cleavage activity of Cas12a-crRNA RNPs is higher for dsDNA than for ssDNA. Thus, only one RNP is needed to generate readout signals for detection.

5.2 Experimental Section[‡]

5.2.1 SARS-CoV-2 viral RNA

[‡] Joyce, M. A. and Saffran, H. A. helped with the preparation of viral RNA. Pabbaraju, K. and Tipples, G. contributed to RT-qPCR analysis of clinical samples. Xu, J. and Liu, Y. contributed to RT-qPCR analysis of different genes. Peng, H. (H.P.) helped with the design and performance of experiments for the development of the DNA detection assay, optimization of reverse transcription enzymes, identification and characterization of the importance of RNase H for RT-RPA-Cas12a, stability of RNP, and the comparison of a two-step assay with our one-step RT-RPA-Cas12a assay. I conducted the rest of the experiments, including further study of the effect of RNase H and non-specific amplification, optimization of the RNA assay, characterization of the performance of our DNA and RNA assays, and applied the RNA assay to the analysis of clinical samples. I analyzed data and wrote the first draft of the manuscript and supplementary information and contributed to multiple rounds of editing.

The original SARS-CoV-2 virus strain (SARS-CoV-2/CANADA/VIDO 01/2020) was obtained from the University of Saskatchewan, Canada. SARS-CoV-2 was produced from the infection of Vero-E6 cells at a multiplicity of infection (MOI) of 0.01 for 48 h, followed by harvesting of the supernatant. The amount of SARS-CoV-2 RNA in the supernatant was measured by RT-quantitative PCR (RT-qPCR). RNA in 140 µL cell supernatants was isolated by using the QIAmp Viral RNA Mini kit (Qiagen) and reverse transcribed using Superscript IV Vilo Master Mix (Invitrogen). The S gene and RdRp gene were quantified using a lab-developed RT-qPCR assay. A 2 µL aliquot of RNA extracts was mixed with the RT-qPCR master mix which comprised 0.6 µL of 10µM each primer, 0.5 µL of 10µM probe, and 1× TaqPath™ 1-Step RT-qPCR Master Mix (ThermoFisher) to a final volume of 20 µL. The sequences of primers and probes and RT-PCR program are listed in **Table 5-1, 5-2, and 5-3**.

Table 5-1. Primers and probes for RT-PCR assay of the S gene and for *in vitro* RNA transcription.

Sequence name	Sequences (5'-3')
S-amplicon	GCCAATAGGTATTAACATCACTAGGTTTCAAACTTTACTTG CTTTACATAGAAGTTATTTGACTCCTGGTGATTCTTCTTCAG GTTGGACAGCTGGTGCTGCAGCTTATTATGTGGGTTATCTT CAACCTAGGACTTTTCTATTAAAATATAATG
RT-PCR-S-F	GGT TTC AAA CTT TAC TTG CTT TAC ATA GAA
RT-PCR-S-R	GGT TGA AGA TAA CCC ACA TAA TAA GCT
RT-PCR-S-probe	6-FAM/TT TGA CTC CTG GTG ATT CTT CTT CA/BHQ
PCR-T7-S-F	TCTAATACGACTCACTATAGAGGTTTCAAACTTTACTTGC
PCR-T7-S-R	TCCTAGGTTGAAGATAACCC

Table 5-2. Primers and probes for RT-PCR assays of the RdRP gene and for *in vitro* RNA transcription

Sequence name	Sequences (5'-3')
RdRP-amplicon	CGTGTTGTAGCTTGTCACACCGTTTCTATAGATTAGCTAAT GAGTGTGCTCAAGTATTGAGTGAAATGGTCATGTGTGGCG GTTCACTATATGTTAAACCAGGTGGAACCTCATCAGGAGA TGCCACAACTGCTTATGCTAATAGTGTTTTTAACATTTGTC AAGCTGTCACGGCCAATGTTAATGCACTTTTATCTACTGAT GGTAACAAAATTGCCGATAAGTATGTCCGCAATTTACAAC ACAGA
RT-PCR-RdRP-F	TCA TTG TTA ATG CCT ATA TTA ACC TTG AC
RT-PCR-RdRP-R	CAC TTA ATG TAA GGC TTT GTT AAG TCA
RT-PCR-RdRP-P	/6-FAM/TT AAC TGC AGA GTC ACA TGT T/BHQ_1/
PCR-T7-RdRP-F1	TCTAATACGACTCACTATAGCACCGTTTCTATAGATTAGC
PCR-T7-RdRP-R1	CATACTTATCGGCAATTTTG

Table 5-3. Thermal cycling program for RT-qPCR.

Steps	Temperature	Duration	Cycles
UNG activation	25 ℃	2 min	N/A
Reverse transcription	50 ℃	15 min	
Polymerase activation	95 ℃	2 min	
Denaturation	95 ℃	3 sec	50
Extension and detection	60 ℃	30 sec	

5.2.2 RT-RPA and Cas12a reactions in a single tube

LbCas12a RNP containing 0.5 μM LbCas12a (NEB) and 0.65 μM crRNA in 1× NEB Buffer 2.1 (10 mM Tris-HCl pH 7.9, 50 mM NaCl, 10 mM $MgCl_2$, 100 μg/ml BSA) was incubated at 37 °C for 0.5 h and kept on ice. Before each analysis, the RT mix for 8 reactions was prepared by mixing 1 μL 10× M-MuLV Buffer, 0.8 μL RPA primer mix (50 μM each), 2 μL 10 mM dNTP, 4 μL 200 U/μL M-MuLV Reverse Transcriptase (NEB, M0253L), and 2 μL 2 U/μL RNase H (ThermoFisher, 18021-014). The RPA mix was prepared by adding 52 μL of rehydration buffer, 0.8 μL RPA primer mix (50 μM each), and 10 μL 100 μM Cas12a reporter to 2 tubes of lyophilized RPA reagents (TwistAmp™ Basic Kit).

The single-tube assay was conducted in a MicroAmp™ Fast 8-Tube Strip (ThermoFisher, 4358293). To allow all reactions in the same batch to start at the same time with sufficient priming, 4 μL of sample and 1.1 μL of RT mix were added to the lid. Separate from this mixture, 1 μL MgOAc (280 mM) was added to another location of the lid. LbCas12a RNP (1 μL) was added to the bottom of the tube and RPA mix (7 μL) was added to the wall of the tube. Then the tubes were spun, and the reaction was mixed thoroughly (~10 inversions), followed by another spin before real-time fluorescence monitoring (StepOnePlus™ Applied Biosystems). The single-tube RPA-Cas12a assay for DNA followed the same protocol except for omitting the RT mix but adding a total of 1.6 μL RPA primer mix (50 μM each) into the RPA mix.

5.2.3 Analysis of clinical samples for the S gene of SARS-CoV-2 RNA

I analyzed RNA extracts from 46 clinical specimens of Alberta, Canada residents, comprising 21 SARS-CoV-2 positive specimens and 25 SARS-CoV-2 negative specimens

confirmed with a RT-qPCR assay.[27] RNA from each of the 46 respiratory nasopharyngeal swab specimens was extracted using one of three platforms: the easyMAG® (BioMerieux, Quebec, Canada), the KingFisher Flex automated extraction and purification systems (Thermo Fisher), or the Hamilton STARlet automated extractor (Hamilton, Reno, NV). The specimen input was 200 μL and the purified nucleic acid was extracted into 100 μL total volume of the RNA extract from each specimen. An aliquot of 1–4 μL of RNA extract was used as the sample input for the one-tube RT-RPA-Cas12a assay of the S gene of SARS-CoV-2.

5.3 Results and Discussion

5.3.1 Integration of reverse transcription (RT), recombinase polymerase amplification (RPA), and CRISPR-Cas12a detection in a single tube

The overall process of integrating reverse transcription (RT), recombinase polymerase amplification (RPA), and CRISPR-Cas12a-mediated signal generation, in order to detect specific RNA in a single tube under isothermal conditions (40 °C), is shown in **Figure 5-1**. I use the detection of viral RNA of SARS-CoV-2 as an example to illustrate the principles of our integrated RT-RPA-CRISPR-Cas12a assay, which includes the following reactions in one tube: reverse transcription of the RNA template producing a complementary DNA (cDNA); removal of RNA template from cDNA by RNase H; exponential amplification of the cDNA by RPA; CRISPR RNA (crRNA)-directed recognition of dsDNA amplicons by the crRNA-Cas12a ribonucleoprotein (RNP); and multiple cleavage of quencher-fluorophore ssDNA reporters by the activated RNP, resulting in detectable fluorescence.

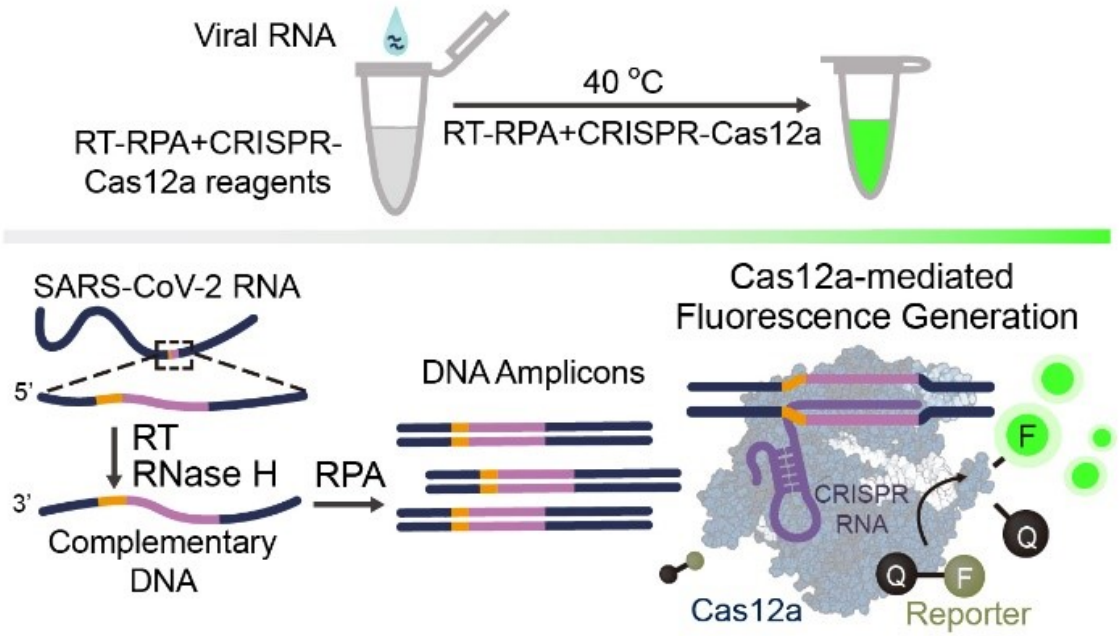

Figure 5-1. Schematics showing integration of reverse transcription (RT), recombinase polymerase amplification (RPA), and CRISPR-Cas12a-mediated fluorescence generation for isothermal (40 °C) single-tube detection of specific RNA. Once a sample is added to a reaction tube containing RT-RPA and CRISPR-Cas12a reagents, the tube is kept closed and maintained at 40 °C. RPA primers and reverse transcriptase interact with the target RNA to produce a complementary DNA (cDNA). RNase H cleaves the RNA template to make the cDNA free for exponential amplification by RPA. Directed by the CRISPR RNA (crRNA), the crRNA-Cas12a ribonucleoprotein (RNP) recognizes and binds to the specific sequence (shown in orange and purple) in dsDNA amplicons. Sequence-specific binding of the RNP/dsDNA complex activates the *trans*-cleavage activity of Cas12a, resulting in cleavage of short ssDNA reporters and thereby generating fluorescence.

5.3.2 Optimization of RPA-CRISPR-Cas12a in a single tube

To integrate RPA with CRISPR-Cas12a detection for high sensitivity and specificity, Dr. Peng first examined the detection of a specific DNA sequence which was reverse transcribed from a conserved region of SARS-CoV-2 RNA within the spike (S) protein. dsDNA was chosen as the target of CRISPR-Cas12a because CRISPR-Cas12a has a higher specificity for dsDNA than for ssDNA.[8] A crRNA was designed to target a specific sequence of dsDNA between the sequences recognized by the two RPA primers[15] **(Figure 5-2).** The CRISPR-targeting site contained a PAM domain of TTTV and a recognition domain of 20 nt (**Figure 5-2)**.

Dr. Peng optimized the reaction conditions for both RPA and CRISPR-Cas12a, with an emphasis on maximizing the amplification efficiency of RPA and thus the signal generation capability of CRISPR-Cas12a. A higher concentration of Mg^{2+} (21 mM) than that recommended for the RPA kit (14 mM) enhanced the hybridization between the primers and the DNA templates, thus improving amplification and detection (**Figure 5-3A**). The optimum crRNA-Cas12a RNP concentration of 30 nM provided the fastest kinetics of nuclease activity for the amplified fluorescence detection (**Figure 5-3B**). The design and use of a shorter ssDNA reporter than those used by others minimized the background fluorescence.

The integration of RPA and CRISPR-Cas12a reactions in one tube resulted in the successful detection of the specific DNA sequences corresponding to the S gene of SARS-CoV-2. The overall reaction took only 5-22 min to detect DNA ranging from 10^6 to 5 copies **(Figure 5-4)**. The intensity of the fluorescence signals increases with the concentration of the target DNA. I determined that the measured fluorescence intensity of 150,000 (arbitrary unit)

or higher corresponded to visible fluorescence easily recognizable by the naked eyes **(Figure 5-5)**. The time needed to reach this threshold fluorescence intensity was correlated inversely with the concentration of the target DNA **(Figure 5-4B)**. Detection of 5 copies of DNA took only 22 min to reach the threshold fluorescence intensity of 150,000.

A

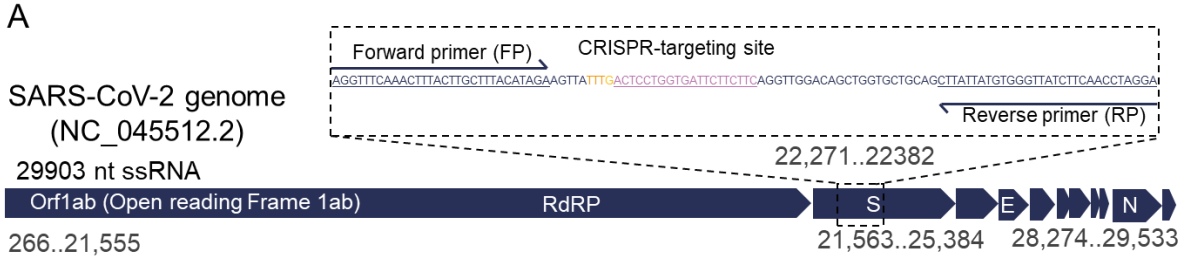

B

Sequence name	Sequences (5'-3')
S-amplicon	GCCAATAGGTATTAACATCACTAGGTTTCAAACTTTACTTGCTTTACATAGAAGTTATTTGACTCCTGGTGATTCTTCTTCAGGTTGGACAGCTGGTGCTGCAGCTTATTATGTGGGTTATCTTCAACCTAGGACTTTTCTATTAAAATATAATG
RPA-S-F (forward primer)	AGGTTTCAAACTTTACTTGCTTTACATAGA
RPA-S-R (reverse primer)	TCCTAGGTTGAAGATAACCCACATAATAAG
RPA-S-crRNA	UAAUUUCUACUAAGUGUAGAUACUCCUGGUGAUUCUUCUUC
S-dsDNA-activator	CATAGAAGTTATTTGACTCCTGGTGATTCTTCTTCAGGTTGGACAGCTGG

Figure 5-2. RPA primers, CRISPR RNA (crRNA), and their target region in the Spike gene (S gene) of the SARS-CoV-2 genome. The CRISPR-targeting site contained a PAM

domain of TTTV (orange color) and a recognition domain of 20 nt (light purple). The primers and primer-binding sequences are underlined.

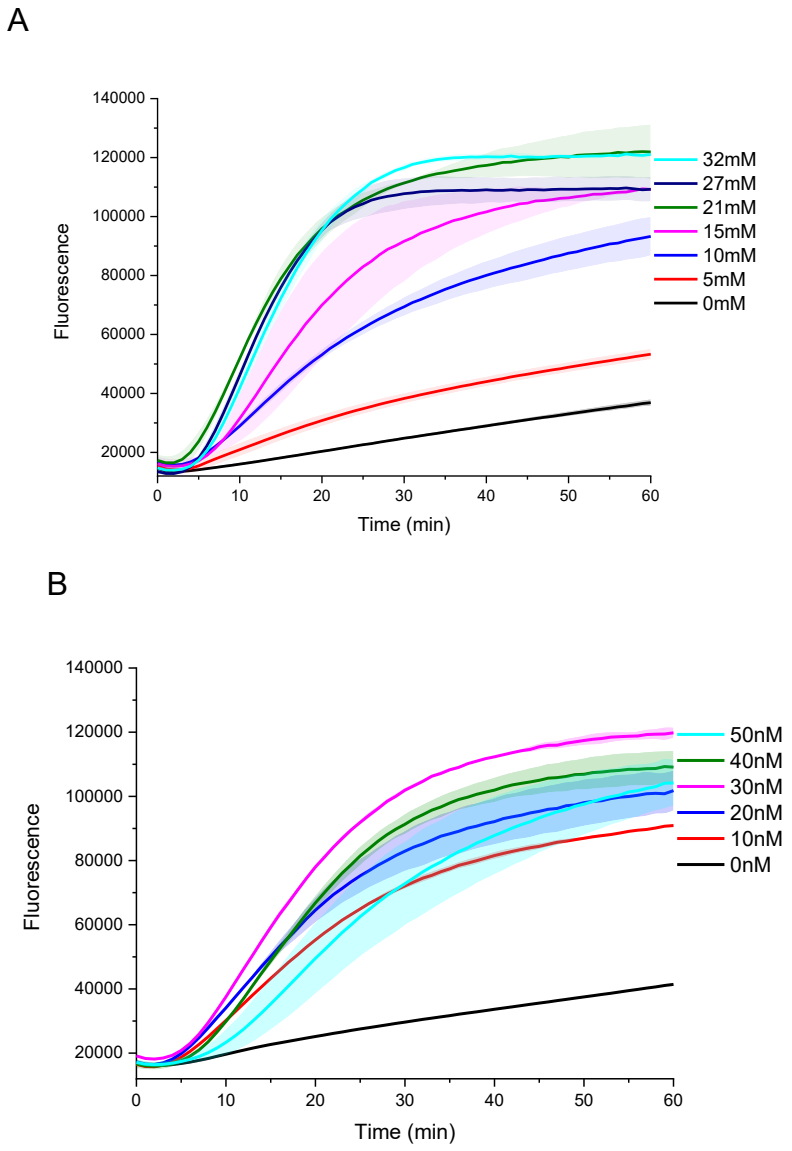

Figure 5-3. Optimization of the concentrations of MgOAc and crRNA-Cas12a ribonucleoprotein (RNP) for the single-tube RPA-Cas12a assay. Each reaction contained 20000 copies of the S gene DNA. The standard deviation from duplicate analyses under each condition is shown as a matching colored shadow around each curve. **A.** Effect of the MgOAc

concentration, from 0 to 32 mM, on the fluorescence intensity, measured continuously over the 60-min reaction time. **B.** Effect of the crRNA-Cas12a ribonucleoprotein (RNP) concentration, from 0 to 50 nM, on the fluorescence intensity, measured continuously over the 60-min reaction time.

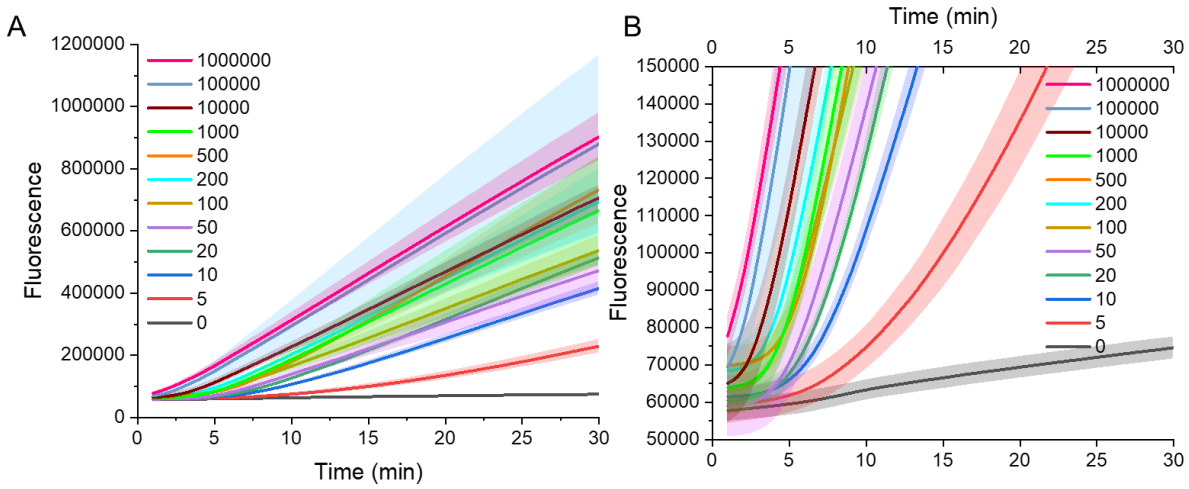

Figure 5-4. Fluorescence intensity, measured over time, from the single-tube RPA-Cas12a assay for the detection of DNA sequence of the SARS-CoV-2 S gene, ranging from 5 copies to 10^6 copies. The standard deviation from triplicate analyses of each DNA concentration is shown as a matching colored shadow band around each curve.

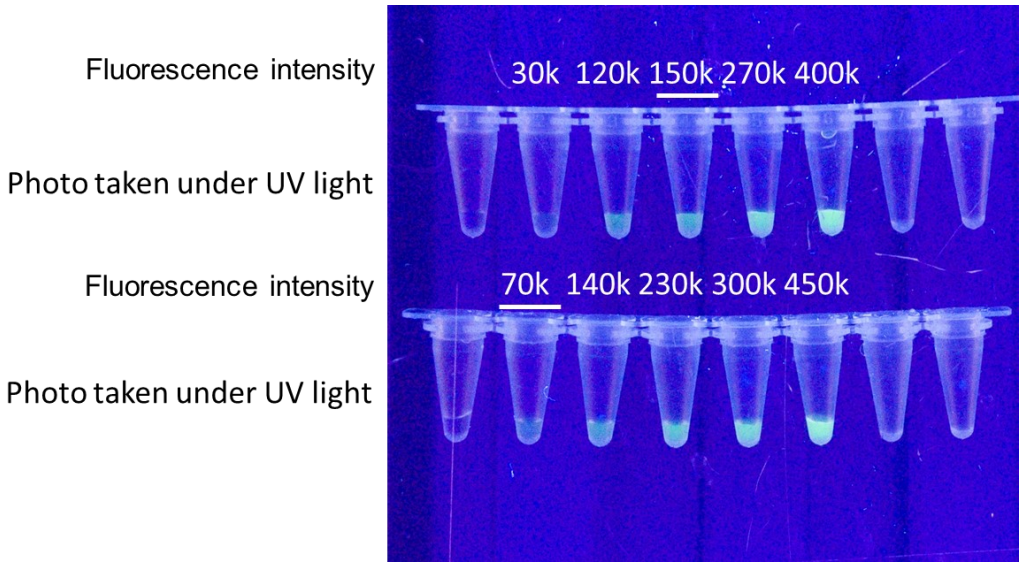

Figure 5-5. Detection of fluorescence intensity and visualization of fluorescence color captured on a smartphone camera. A StepOnePlus™ RT-PCR instrument (Applied Biosystems) was used to measure the fluorescence intensity (arbitrary unit) in the FAM channel (λ_{ex} ~470 nm and λ_{em} ~520 nm). A personal smartphone camera was used to take photos of the tubes under UV light (λ_{ex} 302 nm, GelVue UV Transilluminator, Syngene). The tubes with fluorescence intensity values of 150,000 or higher can be distinguished from the tube with fluorescence intensity of 70,000, a typical fluorescence intensity of non-target control, by the naked eyes.

5.3.3 Challenges and necessity for rapid initiation of the RPA reaction

Having succeeded in rapid and sensitive detection of DNA, the assay was extended to the detection of viral RNA from SARS-CoV-2. The assay was able to detect high concentrations of RNA. However, the detection of 10,000 copies of RNA required 35 min (**Figure 5-6**), whereas the detection of only 5 copies of the equivalent DNA sequence was

achieved in 22 min (**Figure 5-4B**). We investigated this dramatic decrease in sensitivity for the detection of RNA compared to the detection of DNA. We hypothesized that reverse transcription of RNA to cDNA delayed the initiation of the RPA reaction. The slow initiation of RPA could cause two problems in the one-tube assay: 1) nonspecific amplification reactions could consume the RPA reagents, and 2) the activity of the crRNA-Cas12 RNP decreased over time prior to its activation by the target dsDNA amplicons.

I first examined nonspecific amplification products using SYBR Green detection. In the absence of the target, SYBR Green fluorescence was detectable within 10 min of the one-tube reactions (**Figure 5-7**). Although the nonspecific amplicons were not detectable by CRISPR-Cas12a, the nonspecific reactions could deplete RPA reagents and impede the detection of low copy numbers of the target RNA.

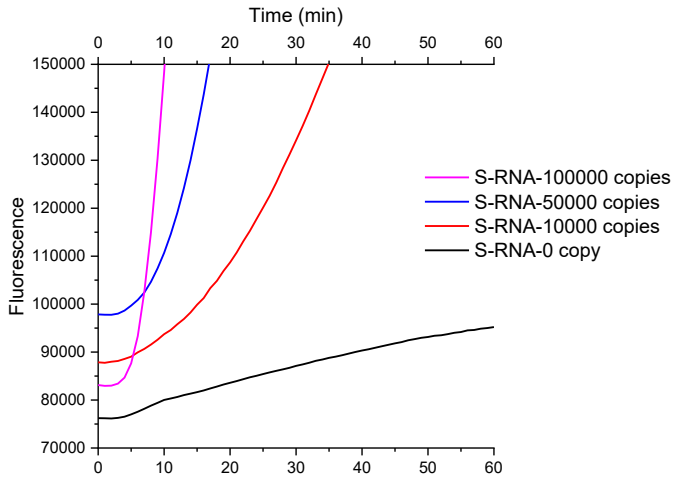

Figure 5-6. Detection of a specific S gene sequence of SARS-CoV-2 RNA using the one-tube RT-PRA-Cas12 assay. Each RT-RPA-Cas12a reaction contained 0.5 µL of 200 U/µL ProtoScript II reverse transcriptase. There was no addition of RNase H.

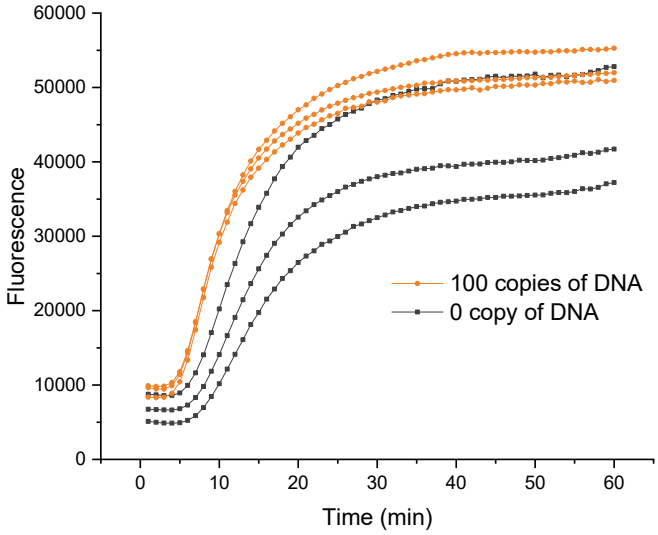

	Amplification of the target (100 copies of target)	Nonspecific amplification (0 copy of target)
Initial fluorescence	9303	6870
Plateau fluorescence	52740	42908
Fluorescence increase	43437	37037
Relative amount of dsDNA	100%	85%

Figure 5-7. SYBR Green detection of the RPA reaction mixtures containing either 100 copies of the target DNA or no target DNA. Previously optimized conditions for the integrated RPA-Cas12a reactions were used, except that the RNP and reporter were replaced with SYBR Green in order to detect all amplification products including nonspecific products. Specifically, an RPA mix for eight reactions was prepared by adding 52 µL of rehydration buffer, 1.6 µL of RPA primer mixture (50 µM each), and 10 µL of 10× SYBR Green to two tubes of lyophilized RPA reagents (TwistAmp^{TM} Basic Kit). For each reaction, 5 µL of DNA (or buffer as blank) and 1 µL of MgOAc (280 mM) were added onto the lid and then mixed with 7 µL of RPA reaction mixture. Triplicate analyses of 100 copies of the target DNA per

reaction and 0 copy of the target per reaction were performed in parallel. The relative amounts of dsDNA products from the target-specific amplification and nonspecific amplification were compared by measuring the increases in fluorescence over reaction time.

To understand the second problem, Dr. Peng and I tested the activity of the crRNA-Cas12a RNP in a scenario in which the DNA required to activate the RNP (DNA activator) was delayed. Normally, when the RNP was activated without delay (red curve in **Figure 5-8A and Figure 5-9A**), its catalytic activity remained over time (70 min) as indicated by the continuing increase of fluorescence due to the *trans*-cleavage of the reporters by the RNP. However, when the addition of the DNA activator was delayed by 20−50 min, the slower increase of fluorescence over time indicated lower activity of the RNP. If the activation of RNP was delayed by 20 min in the reaction mixture of RPA and CRISPR-Cas12a, the RNP lost 30% of its activity as indicated by the reduced initial cleavage rate (**Figure 5-8B**). A 40-min delay of the RNP activation resulted in more than 50% loss of the RNP activity in the reaction mixture. The decrease in the activity of non-activated Cas12a RNP was not caused by changes in the buffer pH or concentration of reagents. When fresh RNP and DNA activator were added to the RPA reaction mixture after a 60-min delay, a normal activity (and initial cleavage rate as shown in **Figure 5-8B and Figure 5-9B)** was observed. These results suggest that timely activation of the RNP by the DNA target is critical for the *trans*-cleavage activity of the RNP.

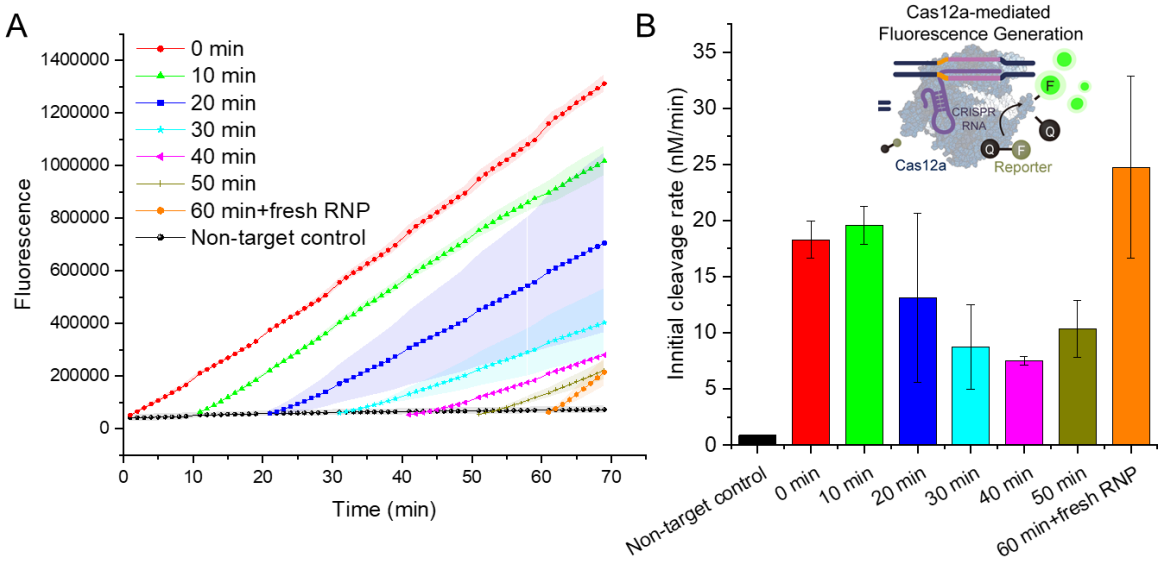

Figure 5-8. The stability of crRNA-Cas12a ribonucleoprotein (RNP) activity in RPA reaction solution, measured by fluorescence intensity of the reporter (A) and initial cleavage rate of the *trans*-cleavage activity of crRNA-Cas12a RNP (B). There was no amplification target in the mixture. Instead, a short dsDNA activator, containing only a CRISPR-targeting sequence but no primer binding sequence, was used to activate the RNP. The dsDNA activator (10 nM, 1.25 µL) and a quencher-fluorophore-labeled ssDNA reporter (100 µM, 1.25 µL) were added to separate tubes containing RPA reagents (11 µL) and RNP (0.5 µM, 1 µL) at different delay times (0−50 min). At a delay time of 60 min, fresh RNP (0.5 µM, 1 µL), along with the DNA activator and reporter, was added. The trans-cleavage of the quencher-fluorophore-labeled ssDNA reporter by the RNP generated fluorescence. The initial cleavage rate was calculated by converting the slopes of curves in **Figure 5-8A** to the concentration of reporters cleaved in 1 min based on a calibration curve of fluorescence intensity vs concentration of reporters cleaved (**Figure 5-9C).**

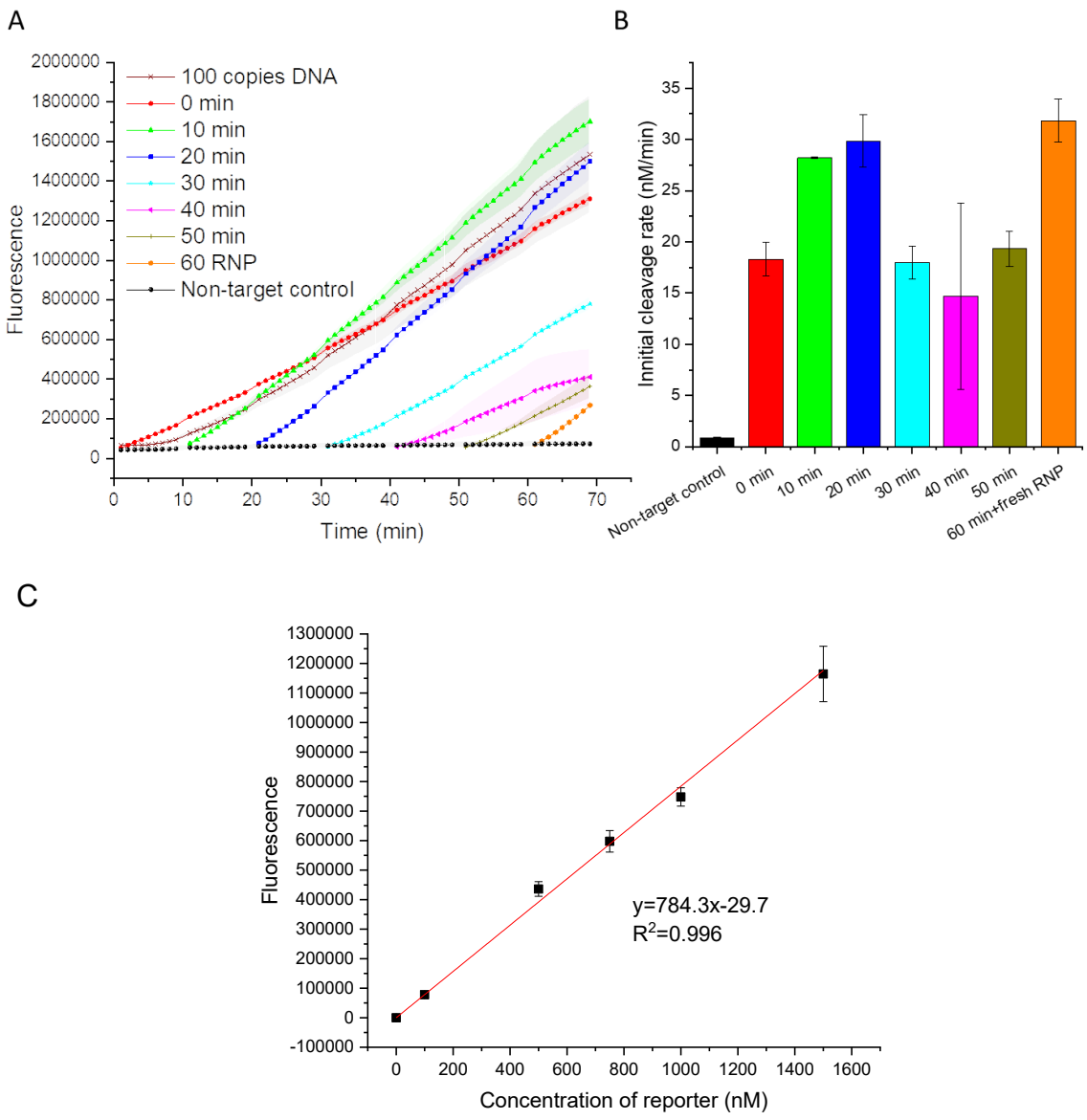

Figure 5-9. Activity of crRNA-Cas12a RNP in the RPA reaction solution supplemented with 100 copies of DNA target. The same experimental design as in **Figure 5-8** was used, except that 100 copies of DNA target containing both RPA primer regions and the CRISPR-targeting region were added to the RPA solution at the beginning. The DNA target (100 copies) and the ssDNA reporter were added to separate tubes containing RPA reagents and RNP at different delay times (0−50 min). At a delay time of 60 min, fresh RNP was added.

Fluorescence intensity of the cleaved reporter (**A**) and initial cleavage rate of the *trans*-cleavage activity of crRNA-Cas12a RNP (**B**) were measured. The initial cleavage rate was calculated by converting the slope of fluorescence curves (fluorescence intensity per unit time) shown in **(A)** to the amount of reporters cleaved (nM/min) using the calibration curve in **(C).** Each reaction contained 38 nM Cas12a RNP, 77 nM dsDNA, and 0–1500 nM reporter in 1× NEB 2.1 buffer. When all reporters were cleaved, the plateau fluorescence was plotted against the reporter concentration.

In the presence of all the reagents for RT, RPA, and CRISPR-Cas12a reactions in a single tube, both nonspecific amplification and loss of RNP activity occurred. Overcoming both problems requires rapid generation of DNA amplicons from trace amounts of the RNA target and rapid initiation of RPA.

5.3.4 Removal of the RNA template after reverse transcription significantly improves the performance of the single-tube RT-RPA-Cas12a assay

Reverse transcription of RNA and dissociation of the RNA-cDNA hybrid are two potential critical processes leading to rapid RPA initiation. Dr. Peng compared four different reverse transcriptases: Protoscript II,[28] AMV,[29] RevertAid,[30] and M-MuLV,[31] used in our assay for the detection of SARS-CoV-2 RNA **(Figure 5-10)**. With M-MuLV, the assay required only 15 min to produce fluorescence intensity of 150,000 (arbitrary unit), whereas 30 min was needed when the other three reverse transcriptases were used **(Figure 5-10A)**. M-MuLV is known to have a “functional RNase H domain”, whereas the other three reverse

transcriptases have either reduced or no RNase H activities.[28-31] The endoribonuclease activity of RNase H catalyzes the hydrolysis of phosphodiester bonds of RNA in RNA-DNA hybrids.[32] Removal of RNA from the RNA-cDNA hybrids leaves cDNA free to hybridize with RPA primers for amplification. We hypothesized that RNase H and its ability to remove RNA from the cDNA played an important role in fast RPA initiation.

To test the requirement for RNase H, Dr. Peng conducted assays with or without supplementing the single-tube mixtures of RT, RPA, and CRISPR-Cas12a reactions with RNase H (**Figure 5-10B**). One hundred copies of SARS-CoV-2 RNA were detectable in 44 min using the M-MuLV reverse transcriptase which has a functional RNase domain. Supplementing the reaction with additional RNase H resulted in a shorter time (35 min) to produce equivalent fluorescence for the detection of the same amount of RNA. When Protoscript II was used as the reverse transcriptase, the assay could not yield a positive detection of 100 copies of SARS-CoV-2 RNA after 60 min. With the addition of RNase H to the reaction mixture, detection of this low number of RNA molecules was achieved in 38 min (**Figure 5-10B**). These results demonstrate the importance of including RNase H to the single-tube reaction mixture. The addition of RNase H did not impair the *trans*-cleavage activity of Cas12a (**Figure 5-11**).

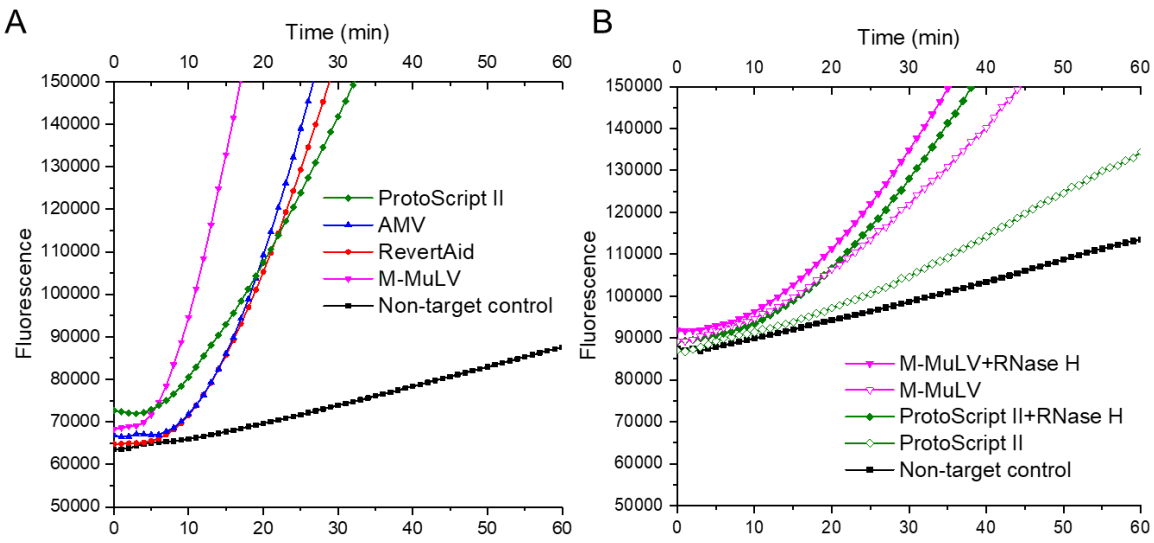

Figure 5-10. Comparison of reverse transcriptases and supplementation of RNase H in the detection of the S gene of SARS-CoV-2 RNA using the integrated RT-RPA-Cas12a assay. A. A comparison of four reverse transcriptases used in the detection of 1000 copies of SARS-CoV-2 RNA, namely ProtoScript II (200 U/µL, 0.5 µL/reaction), AMV (10 U/µL, 0.5 µL/reaction), RevertAid (200 U/µL, 0.5 µL/reaction), and M-MuLV (200 U/µL, 0.5 µL/reaction). **B**. Addition of RNase H to the RT-RPA-Cas12a reaction mixture for the detection of 100 copies of SARS-CoV-2 RNA.

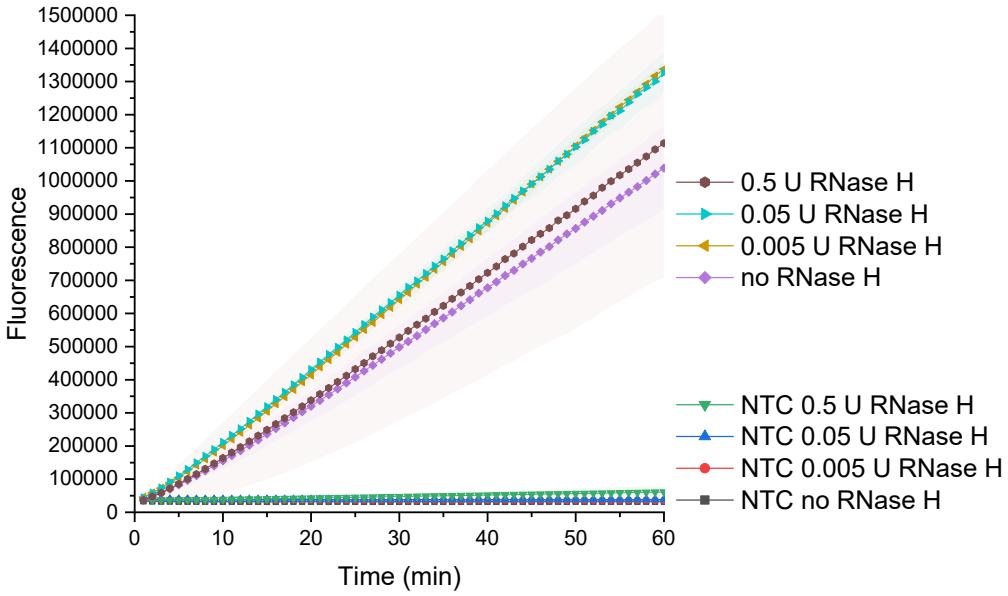

Figure 5-11. Fluorescence produced from the *trans*-cleavage of ssDNA reporter by Cas12a RNP in the presence or absence of RNase H. Concentrations of the reagents in the reaction solutions were consistent with those used for the single-tube RT-RPA-Cas12a assay. Each 14 µL reaction contained 1 µL of 5 µM Cas12a RNP, 1.25 µL of 100 µM ssDNA reporter, and 4 µL of 1 nM dsDNA activator. The non-target control (NTC) contained all reagents, except no dsDNA activator. RNase H (ThermoFisher, 18021-014) in the amount of 0.005 U, 0.05 U and 0.5 U was added to three Cas12a RNP reaction solutions. The results show that the addition of RNase H does not inhibit the *trans*-cleavage activity of Cas12a.

To further confirm that treatment of the RNA-cDNA hybrid with RNase H was important for detection of low copy numbers of SARS-CoV-2 RNA, I separated the reverse transcription of viral RNA from the subsequent RPA-Cas12a reaction and prepared RNA-cDNA hybrids using ProtoScript II. Since ProtoScript II reverse transcriptase has little RNase

H activity, and the reaction temperature is relatively low (37–40 °C), RNA-cDNA hybrids remain after reverse transcription. I then left one half aliquot untreated as RNA-cDNA hybrids, and added RNase H to the other aliquot to obtain free cDNA. Both aliquots were subsequently inactivated, diluted, and analyzed using the RPA-Cas12a assay. RNase H treatment shortened the time to positive detection of various amounts of RNA ranging from 50 to 500 copies per reaction (**Figure 5-12A**). The enhancement by the addition of RNase H was more significant at lower concentrations of the target RNA. I confirmed the finding of the RNase H treatment by extending the approach to the detection of low copy numbers of the RdRp gene of SARS-CoV-2 (**Figure 5-12B, Figure S8**). Fifty copies of the RdRp gene were detectable only after RNase H was added to the reaction (**Figure 5-12B**).

Our result demonstrated the necessity of RNase H in the single-tube assay of viral RNA involving RT, RPA, and CRISPR-12a reactions. The observed differences in the overall sensitivity between DNA detection and RNA detection may be explained by the requirement for rapid initiation of RPA and the function of the main proteins involved in RPA. For the detection of DNA by RPA, interaction of primers with the template is facilitated by a recombinase and a ssDNA-binding protein (SSB). The recombinase unwinds dsDNA and allows the primers to hybridize with the template strand for the subsequent polymerase extension. SSB binds to the displaced strand, preventing the primers from being displaced.[11] However, in RNA detection, the RNA-cDNA hybrid formed after reverse transcription of RNA has a lower binding affinity to SSB. Without SSB to bind and hold onto the displaced RNA strand, the ability of RPA to load the primers to the template is decreased. Therefore, additional RNase H activity is required to remove RNA from RNA-cDNA hybrids, making cDNA available for rapid initiation of RPA.

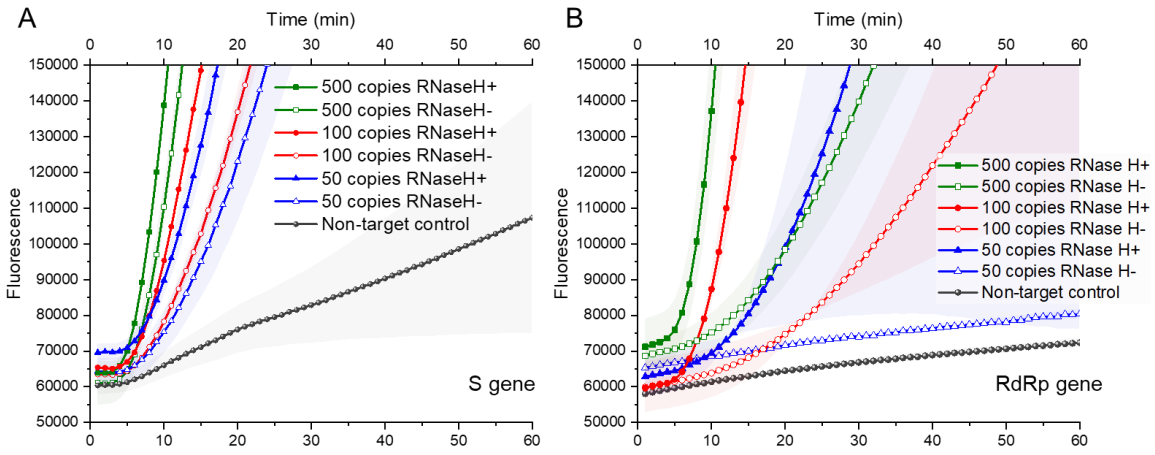

Figure 5-12. RNase H shortens the time for positive detection of the RNA targets in both the S gene and RdRp gene. A. The effect of RNase H treatment on the detection of the S gene cDNA at different concentrations. The RNA target (5×10^4 copies) was first reverse transcribed using ProtoScript II (NEB, M0368L) at 42 °C for 50 min in 1× ProtoScript II buffer with 1 μM of each RPA primer, 0.01 M DTT, and dNTP mix (1 mM each). Equal aliquots of the reverse transcription products were either treated with RNase H (1 U for 5 μL cDNA) at 42 °C for 10 min or an equivalent amount of water. The enzymes were then inactivated at 80 °C for 5 min. Serial dilutions corresponding to cDNA concentrations of 50, 100, and 500 copies/reaction, were made and analyzed using the RPA-Cas12a assay. **B.** The effect of RNase H treatment on the detection of the RdRp gene cDNA at different concentrations. Experimental procedures were the same as for the detection of the S gene, except RPA primers RdRP-F2-5 and Rd-R1, and CRISPR RNA RdRp-crRNA3 were used (sequences in **Figure 5-13**).

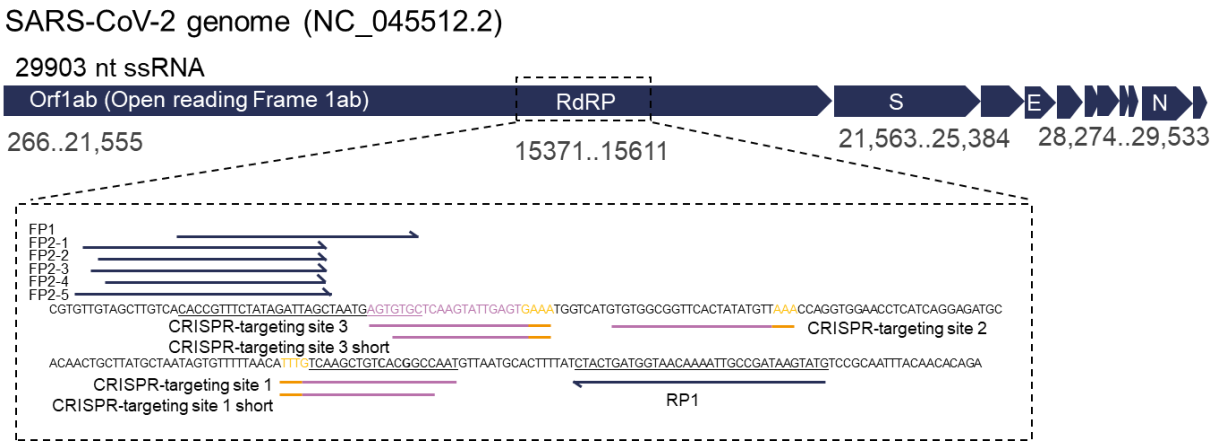

Sequence name	Sequences (5'-3')
RdRP-amplicon	CGTGTTGTAGCTTGTCACACCGTTTCTATAGATTAGCTAATGAG TGTGCTCAAGTATTGAGTGAAATGGTCATGTGTGGCGGTTCACT ATATGTTAAACCAGGTGGAACCTCATCAGGAGATGCCACAACT GCTTATGCTAATAGTGTTTTTAACATTTGTCAAGCTGTCACGGC CAATGTTAATGCACTTTTATCTACTGATGGTAACAAAATTGCCG ATAAGTATGTCCGCAATTTACAACACAGA
RPA-RdRP-F1	CACCGTTTCTATAGATTAGCTAATGAGTGTGC
RPA-RdRP-F2-1	TTGTAGCTTGTCACACCGTTTCTATAGATTAGC
RPA-RdRP-F2-2	GTAGCTTGTCACACCGTTTCTATAGATTAGC
RPA-RdRP-F2-3	TGTAGCTTGTCACACCGTTTCTATAGATTAGC
RPA-RdRP-F2-4	TAGCTTGTCACACCGTTTCTATAGATTAGC
RPA-RdRP-F2-5	GTTGTAGCTTGTCACACCGTTTCTATAGATTAGC
RPA-RdRP-R1	CATACTTATCGGCAATTTTGTTACCATCAGTAG
RPA-RdRP-crRNA1	UAAUUUCUACUAAGUGUAGAUUCAAGCUGUCACGGCCAAUG
RPA-RdRP-crRNA1s	UAAUUUCUACUAAGUGUAGAU UCAAGCUGUCACGGCCA
RPA-RdRP-crRNA2	UAAUUUCUACUAAGUGUAGAUACAUAUAGUGAACCGCCACA
RPA-RdRP-crRNA3	UAAUUUCUACUAAGUGUAGAUACUCAAUACUUGAGCACACU

Sequence name	Sequences (5'-3')
RPA-RdRP-crRNA3s	UAAUUUCUACUAAGUGUAGAU ACUCAAUACUUGAGCAC

Figure 5-13. RPA primers, CRISPR RNA (crRNA) sets, and their target regions in the RdRP gene of SARS-CoV-2.

5.3.5 Single-tube RT-RPA-CRISPR-Cas12a assay for detection of SARS-CoV-2 RNA

RT, RPA, and CRISPR-Cas12a were successfully integrated into a single tube for the detection of SARS-CoV-2 RNA. Compared with adding CRISPR-Cas12a at the end of RT-RPA reaction, real-time monitoring of the fluorescence signal in this single-tube assay also provided the relative SARS-CoV-2 RNA concentration (**Figure 5-14**). Viral RNA was extracted from SARS-CoV-2 infected Vero-E6 cell culture medium, and diluted to various concentrations, ranging from 10^5 copies/reaction to 1 copy/reaction. I was able to detect 120 copies of viral RNA in under 40 min **(Figure 5-15A)**. However, I observed an increasing variation among repeat tests of viral RNA samples with low copy numbers. In two of the three tests of 12 copies of viral RNA per reaction, the fluorescence signals were increasing and could be differentiated from background, but the fluorescence intensity did not reach the threshold value of 150,000 within 90 min. I therefore examined the reproducibility of our assay for the detection of low copy numbers of viral RNA. Viral RNA ranging from 50 to 400 copies was analyzed in nine replicate experiments. I consistently detected 9 positives in all 9 tests when 200 or more copies of viral RNA were present in each reaction (**Figure 5-16**). Detection of very low numbers of RNA was less consistent, resulting in 8 positives in 9 tests

of 100 copies of SARS-CoV-2 RNA/reaction and 7 positives in 9 tests of 50 copies/reaction. The limit of detection for RNA, 200 copies/reaction (or 50 copies/μL of RNA extract sample), meets the sensitivity requirement for a population SARS-CoV-2 screening test, which is estimated to be 100 copies/μL.[33] The S gene target of SARS-CoV-2 is sufficiently different from the corresponding regions in SARS-CoV and MERS-CoV (**Figure 5-17**) for the CRISPR-Cas12a RNP to differentiate them. Thus, the SARS-CoV and MERS-CoV gene (10^4 copies/reaction) did not generate any false positive result (**Figure 5-17**).

While other RPA-based assays have primarily been used for binary positive or negative screening tests, our RT-RPA-Cas12a assay provided semi-quantitative detection of SARS-CoV-2 RNA in a range of 100 to 100,000 copies/reaction (**Figure 5-15B**). The time to threshold correlated with the concentrations of SARS-CoV-2 RNA in the samples. Detection of SARS-CoV-2 RNA at concentrations over 10^5 copies (Ct = 18) was achieved in 7 min with the RT-RPA-Cas12a assay (**Figure 5-15B and S12**).

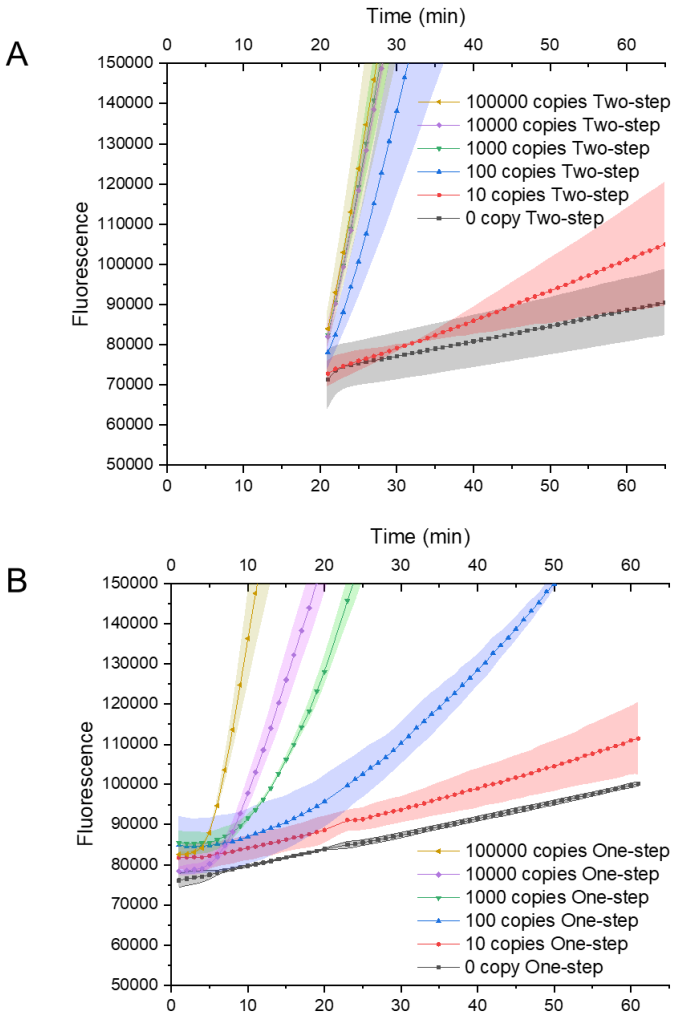

Figure 5-14. Comparison of a two-step (A) with a one-step (B) RT-RPA-Cas12a assay for the S gene of SARS-CoV-2 RNA. **(A)** For the two-step assay, the RT master mix for 8 reactions contained 4 µL of M-MuLV reverse transcriptase, 2 µL of 10× M-MuLV buffer, 0.4 µL of 100 µM RPA primer (each), 6.6 µL of dNTP, and 7 µL of H_2O. The RPA master mix for 8 reactions contained 60 µL of rehydration buffer, 10 µL of 100 µM reporter, 0.4 µL of 100 µM RPA primers (each), and 2 dehydrated RPA pellets. RT mix and RPA mix were then combined. For each reaction, 9 µL of the mixture were mixed with SARS-CoV-2 RNA and 1 µL MgOAc (280 mM). After RT-RPA reaction for 20 min, Cas12a RNP (1 µL, 50 µM) and

reporters (1.25 µL, 100 µM) were added to the tube. (**B)** For the one-step assay, the step of 20-min RT-RPA reaction was eliminated. The reagents for the RT-RPA and Cas12a reactions were included from the beginning. All other conditions were the same as in (**A**).

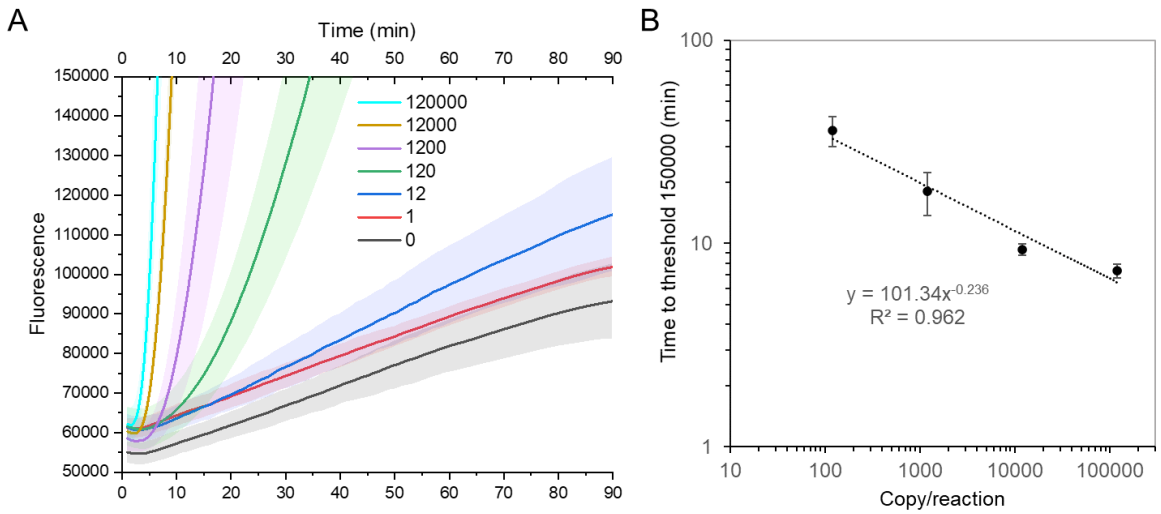

Figure 5-15. Detection of the S gene of SARS-CoV-2 RNA using the single-tube RT-RPA-Cas12a assay. A. Fluorescence generation over time in response to the SARS-CoV-2 RNA extracted from the Vero E6 cell culture medium. Standard deviation of triplicates in each SARS-CoV-2 RNA concentration is shown as a shadow around the curve in the same hue. **B.** A correlation of time to threshold and concentration of SARS-CoV-2 RNA.

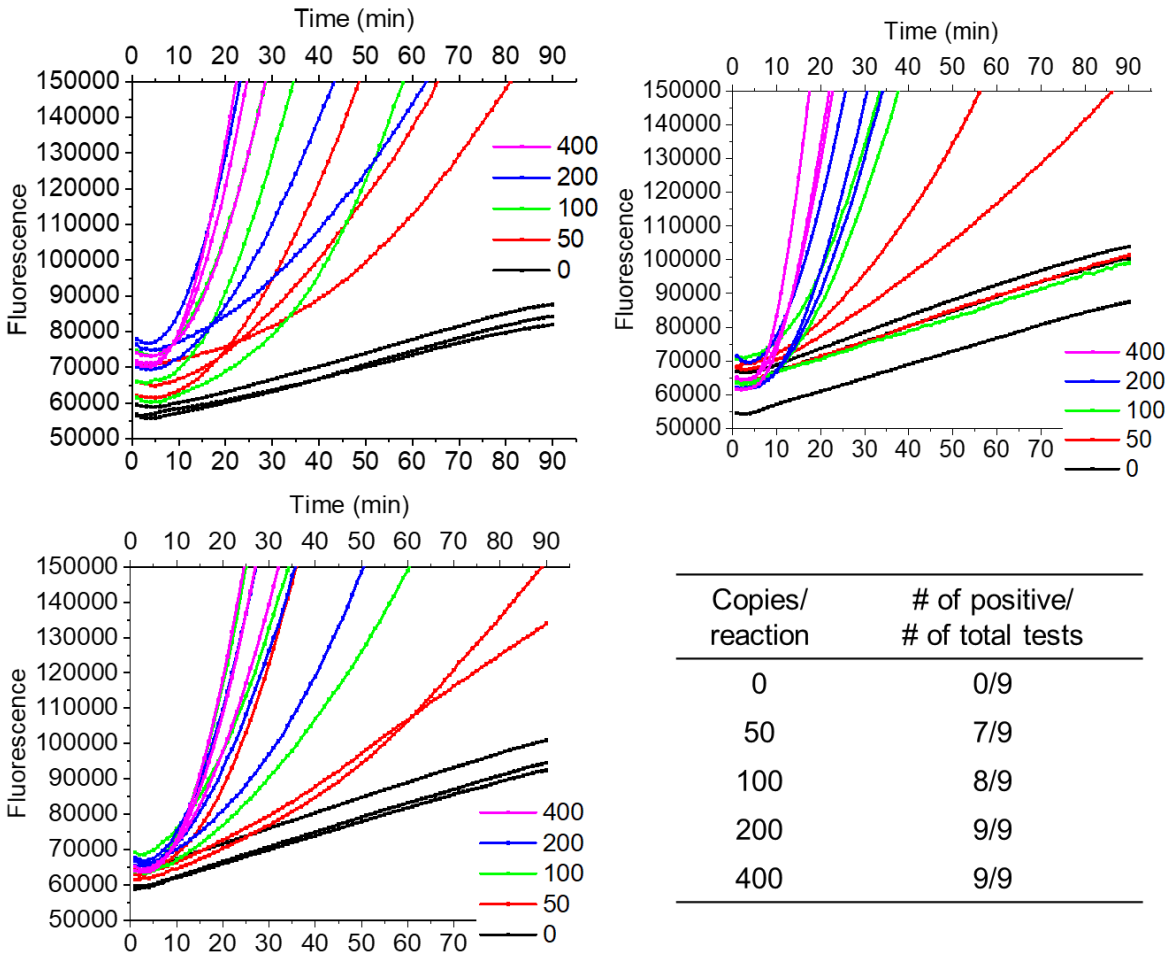

Copies/ reaction	# of positive/ # of total tests
0	0/9
50	7/9
100	8/9
200	9/9
400	9/9

Figure 5-16. Reproducibility of the single-tube RT-RPA-Cas12a assay for low levels of viral RNA. The S gene of SARS-CoV-2 RNA (50, 100, 200, or 400 copies) was analyzed in triplicate. Three curves of the same color in each graph were from triplicate analyses of the same concentration of viral RNA. Each set of experiments was repeated three times, resulting in nine tests of each concentration. A test was deemed positive if the fluorescence intensity reached the minimum value of 150,000 (arbitrary unit) within 90 min.

A

B

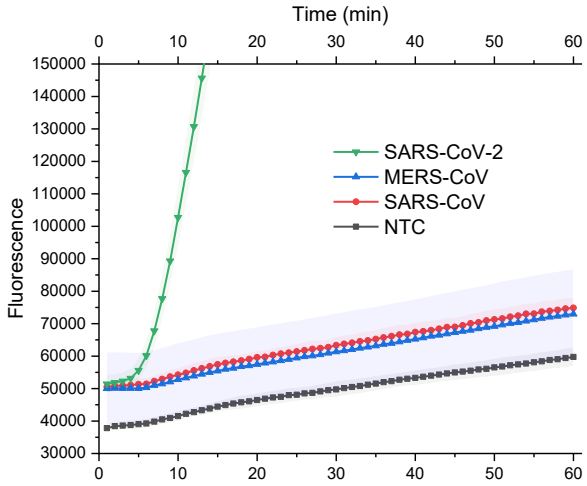

C

Sequence name	Sequences (5'-3')
SARS-CoV-2 S-amplicon	GCCAATAGGTATTAACATCACTAGGTTTCAAACTTTACTTGCTTTACATAGAAGTTATTTGACTCCTGGTGATTCTTCTTCAGGTTGGACAGCTGGTGCTGCAGCTTATTATGTGGGTTATCTTCAACCTAGGACTTTTCTATTAAAATATAATG
SARS-CoV S	TAA TAC GAC TCA CTA TAG GTA TTA ACA TTA CAA ATT TTA GAG CCA TTC TTA CAG CCT TTT CAC CTG CTC AAG ACA TTT GGG GCA CGT CAG CTG CAG CCT ATT TTG TTG GCT ATT TAA AGC CAA CTA CAT TTA TGC TCA
MERS-CoV S	TAA TAC GAC TCA CTA TAG GCC ACC TTG CCT GTT TAT GAT ACT ATT AAG TAT TAT TCT ATC ATT CCT CAC AGT ATT CGT TCT ATC CAA AGT GAT AGA AAA GCT TGG GCT GCC TTC TAC GTA TAT AAA CTT CAA CCG TTA A

Figure 5-17. Specificity of the single-tube RT-RPA-Cas12a assay for SARS-CoV-2 over SARS-CoV and MERS-CoV. **(A)** Sequences alignment of the S gene target site in the genome of SARS-CoV-2, SARS-CoV, and MERS-CoV. **(B)** Analysis of the S gene of SARS-CoV-2, SARS-CoV, and MERS-CoV using the single-tube RT-RPA-Cas12a assay, showing specificity for SARS-CoV-2 over SARS-CoV and MERS-CoV. In vitro transcribed RNA of SARS-CoV-2, SARS-CoV, and MERS-CoV were tested at 10000 copies/reaction, following the protocol of our single-tube RT-RPA-Cas12a assay for the S gene of SARS-CoV-2. The non-target control (NTC) contained all reaction reagents but no RNA sample. **(C)** Sequences of SARS-CoV-2, SARS-CoV, and MERS-CoV tested.

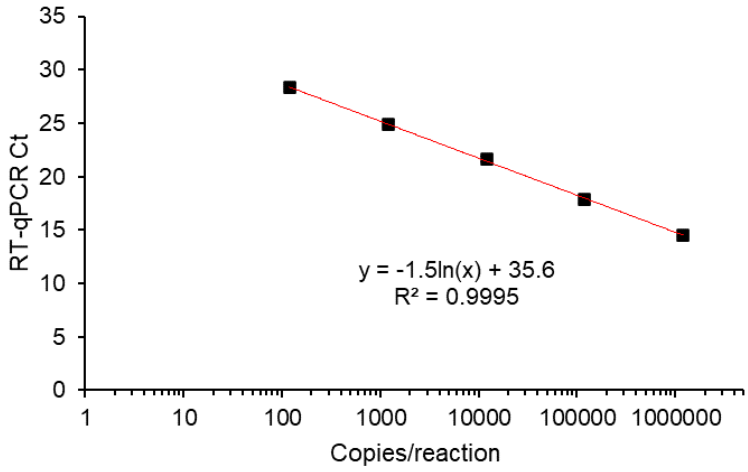

Copies/ reaction	RT-qPCR Ct	SD	RT-RPA-Cas12a time to threshold (Figure 5-15A)	SD
120	28.3	0.4	36	6.0
1200	24.9	0.1	18	4.2*
12000	21.6	0.2	9	0.6
120000	17.9	0.3	7	0.6
1200000	14.5	0.4	-	-

Figure 5-18. Results from the analysis of varying concentrations of SARS-CoV-2 S gene using RT-qPCR and the single-tube RT-RPA-Cas12a assay. (**A)** RT-qPCR calibration curve for the quantification of SARS-CoV-2 S gene. (**B)** Threshold cycles (Ct) from RT-qPCR analysis and time to reach threshold fluorescence intensity from the RT-RPA-Cas12a analysis of 120−1200000 copies of SARS-CoV-2 RNA. *Triplicate analyses were performed with the exception of duplicate analyses of this concentration.

5.3.6 Analysis of RNA extracted from respiratory swab clinical samples

I applied our single-tube assay to upper respiratory swab samples collected from 46 patients for COVID-19 diagnosis at Alberta Precision Laboratories (APL). APL analysed RNA extracts by RT-qPCR for the E gene or the N gene, and found that 25 samples were negative and 21 were positive with Ct values ranging from 19 to 34. I analyzed an aliquot (1−4 μL) of the sample extract using our single-tube RT-RPA-Cas12a assay. I successfully identified all the negative samples as negative **(Figure 5-19B, 5-20)** and 18 of the positive samples as positive **(Figure 5-19A, 5-20)**. Three samples (#4, #39, and #44) that required 33.9, 33.9, and 32.7 cycles (Ct) to achieve positive detection using RT-qPCR did not reach fluorescence intensity of 150,000 within 90 min using the RT-RPA-Cas12a assay. This was expected because the concentration of viral RNA was very low (<20 copies of S gene per reaction) in these three samples and the sample volume used for the RT-RPA-Cas12a assay (1−4 μL) was less than half for the RT-qPCR analysis (5−10 μL). Nonetheless, the results of the 18 positive samples from these two assays were consistent, with a Pearson correlation coefficient of 0.653 between the Ct values from RT-qPCR and the time to threshold from the RT-RPA-Cas12a analysis **(Figure 5-19A)**.

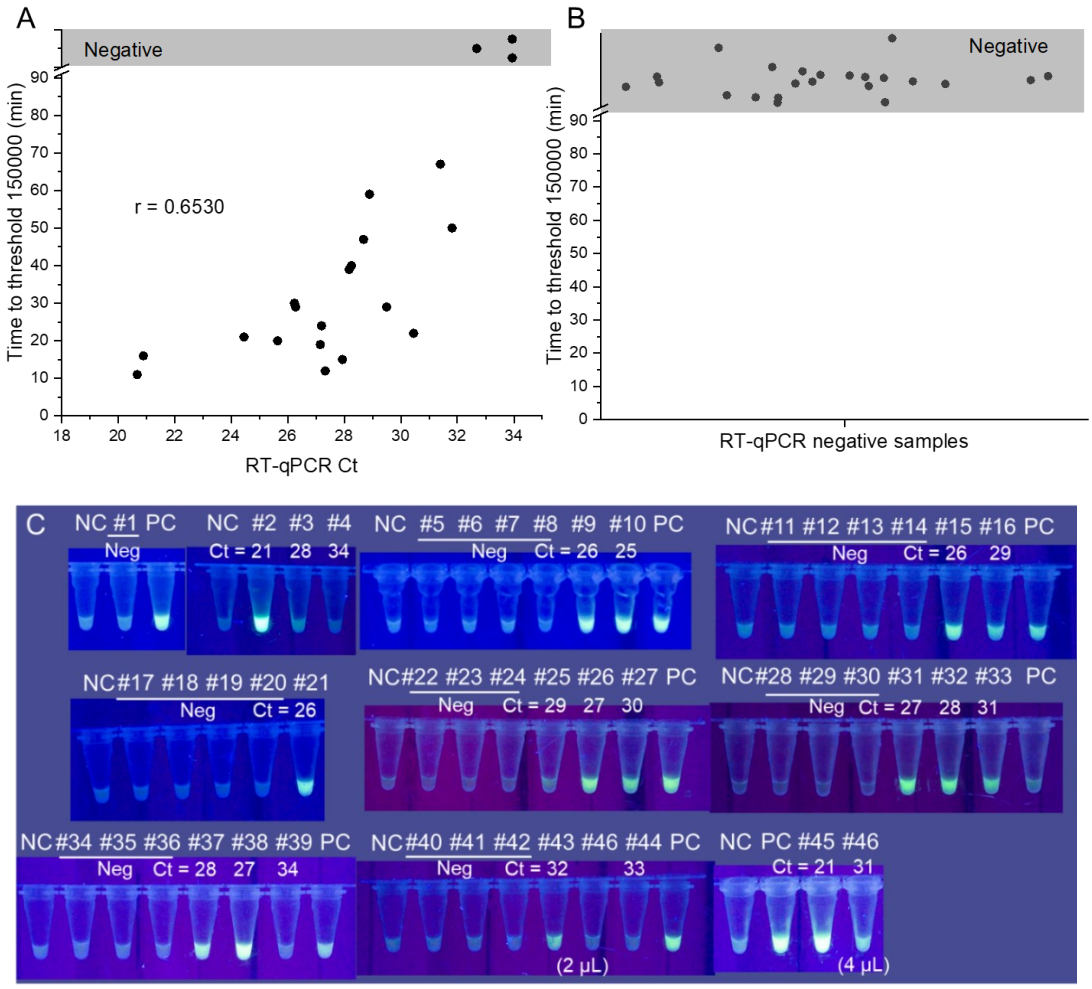

Figure 5-19. Results from the RT-RPA-Cas12a analysis of 46 clinical upper respiratory swab samples using real-time fluorescence detection (A and B) and end-point (90 min) visualization (C). **A**. Correlation between the results of RT-RPA-Cas12a analysis and RT-qPCR analysis of 21 positive samples. The time to reach the threshold fluorescence of 150,000 (arbitrary unit) was obtained from continued real-time monitoring of fluorescence at 1-min intervals. **B.** Results of RT-RPA-Cas12a analysis and RT-qPCR analysis of 25 negative samples. None of the negative samples reached threshold fluorescence after 90 min of reaction. **C**. End-point fluorescence visualization of 46 samples along with negative controls (NC) and positive controls (PC).

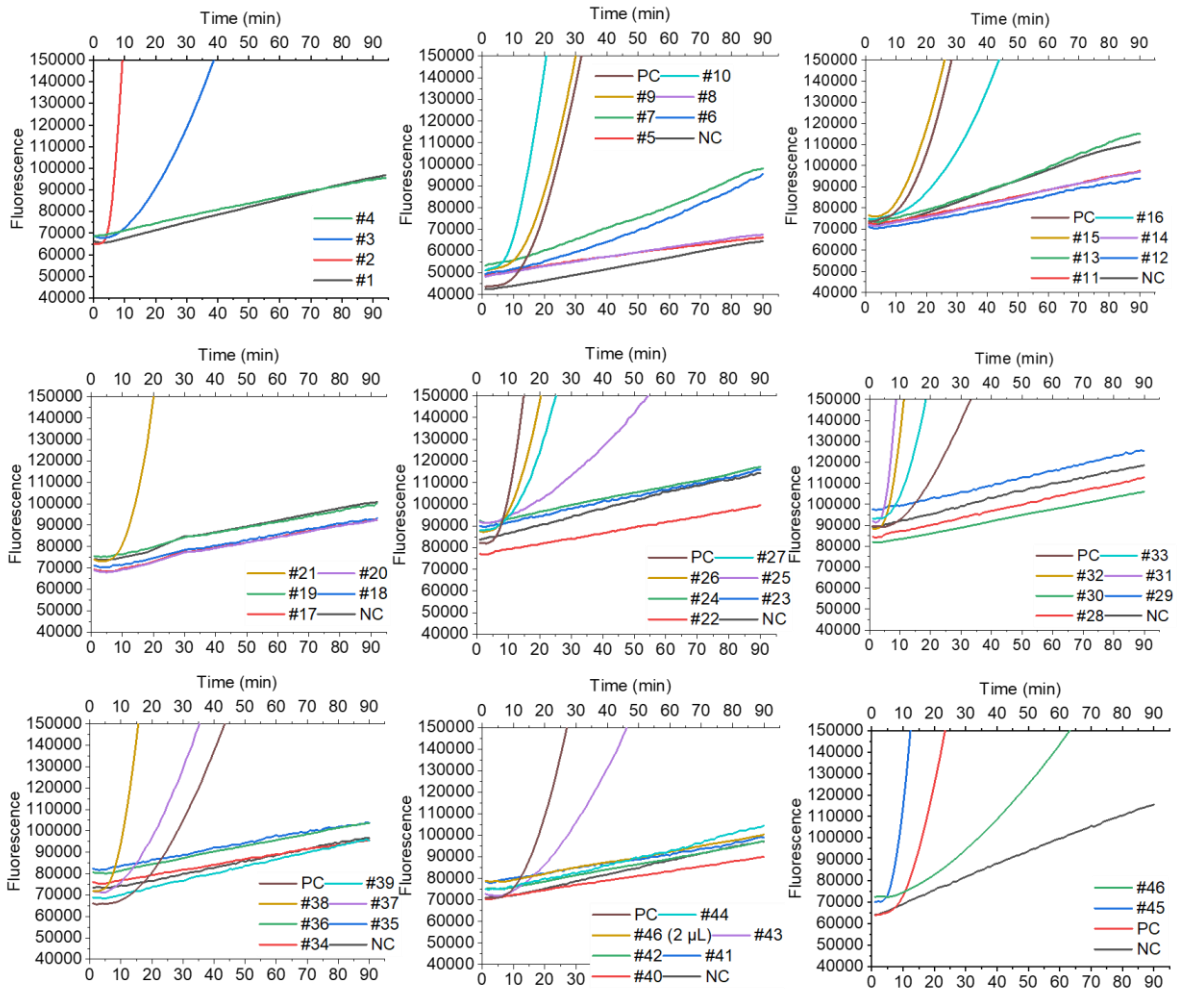

Figure 5-20. Fluorescence measurements from the analyses of 46 clinical samples (upper respiratory swabs samples) using the single-tube RT-RPA-Cas12a assay. Fluorescence was monitored in real-time at 1-min intervals for 90 min. For clarity of comparing positive and negative detections, fluorescence intensity up to 150,000 (arbitrary unit) was shown. Each set of sample analysis included a positive control (PC) and a negative control (NC). A test was deemed positive when the fluorescence intensity reached 150,000 (arbitrary unit).

I also visualized the end-point fluorescence of all 46 samples using our RT-RPA- Cas12a assay, thereby avoiding the use of an expensive RT-qPCR instrument. I was able to differentiate the positive samples with bright fluorescence from the negative samples with almost no fluorescence **(Figure 5-19C).** The results were consistent with our real-time fluorescence detection **(Figure 5-19A, 5-19B, Figure 5-20)**.

5.4 Conclusion

Reverse transcription (RT), recombinase polymerase amplification (RPA), and Cas12a-mediated detection were integrated in a single tube for rapid and sensitive RNA detection. The detection of a few copies of DNA was achieved in 20 min using the integrated RPA-Cas12a assay, but our initial attempt showed that the assay did not perform as well for RNA detection. Our study on the compatibility of RT, RPA, and Cas12a-mediated detection suggested the importance of rapid reverse transcription reaction and RPA initiation, because once all the reagents are mixed in a single tube, both nonspecific RPA amplification and loss of Cas12a RNP activity occur.

RNase H plays an important role in the overall reaction rate and sensitivity of the RT-RPA-Cas12a assay in a single tube for the detection of RNA. Free cDNA initiates the RPA-Cas12a reaction more efficiently than RNA-cDNA hybrids. When the RNA copy number is very low, there is little freely available cDNA. RNase H removed the RNA from RNA-cDNA hybrids and significantly enhanced the performance of the integrated RT-RPA-Cas12a assay. Research focusing on the development of RT-RPA techniques has also reported the importance of RNase H by quantifying the RPA products at the end of the reaction with

qPCR.[34] The real-time monitoring of our assay provides information on how the choice of reverse transcription and the addition of RNase H affect the reaction kinetics.

With RNase H and carefully optimized formulation of our one-tube RT-RPA-Cas12a assay, I am able to amplify and detect over 200 copies of S gene per reaction within 5–30 min incubation. Our results from the analysis of respiratory swab clinical samples using real-time fluorescence monitoring of our assay are correlated with the concentration of SARS-CoV-2 RNA quantified by RT-qPCR. The CRISPR-based detection improves the assay specificity. Our assay operates at one temperature (40 °C) in a single tube and uses different reagents from those of RT-PCR, and thus holds promise to complement current tests for COVID-19 screening. For point-of care testing, the test results can be directly visualized under UV light or detected by a portable fluorescence reader for semi-quantitative readings.

5.5 References

1. Jinek, M., Chylinski, K., Fonfara, I., Hauer, M., Doudna, J. A. and Charpentier, E., A Programmable Dual-RNA-Guided DNA Endonuclease in Adaptive Bacterial Immunity. *Science* **2012,** *337* (6096), 816-821.
2. Cong, L., Ran, F. A., Cox, D., Lin, S., Barretto, R., Habib, N., Hsu, P. D., Wu, X., Jiang, W. and Marraffini, L. A., Multiplex genome engineering using CRISPR/Cas systems. *Science* **2013,** *339* (6121), 819-823.
3. Mali, P., Yang, L. H., Esvelt, K. M., Aach, J., Guell, M., DiCarlo, J. E., Norville, J. E. and Church, G. M., RNA-Guided Human Genome Engineering via Cas9. *Science* **2013,** *339* (6121), 823-826.

4. East-Seletsky, A., O'Connell, M. R., Knight, S. C., Burstein, D., Cate, J. H. D., Tjian, R. and Doudna, J. A., Two distinct RNase activities of CRISPR-C2c2 enable guide-RNA processing and RNA detection. *Nature* **2016,** *538*, 270-273.
5. Gootenberg, J. S., Abudayyeh, O. O., Lee, J. W., Essletzbichler, P., Dy, A. J., Joung, J., Verdine, V., Donghia, N., Daringer, N. M., Freije, C. A., Myhrvold, C., Bhattacharyya, R. P., Livny, J., Regev, A., Koonin, E. V., Hung, D. T., Sabeti, P. C., Collins, J. J. and Zhang, F., Nucleic acid detection with CRISPR-Cas13a/C2c2. *Science* **2017,** *356* (6336), 438-442.
6. Knott, G. J. and Doudna, J. A., CRISPR-Cas guides the future of genetic engineering. *Science* **2018,** *361* (6405), 866-869.
7. Gaj, T., Gersbach, C. A. and Barbas, C. F., III, ZFN, TALEN, and CRISPR/Cas-based methods for genome engineering. *Trends Biotechnol.* **2013,** *31* (7), 397-405.
8. Chen, J. S., Ma, E. B., Harrington, L. B., Da Costa, M., Tian, X. R., Palefsky, J. M. and Doudna, J. A., CRISPR-Cas12a target binding unleashes indiscriminate single-stranded DNase activity. *Science* **2018,** *360* (6387), 436-439.
9. Harrington, L. B., Burstein, D., Chen, J. S., Paez-Espino, D., Ma, E., Witte, I. P., Cofsky, J. C., Kyrpides, N. C., Banfield, J. F. and Doudna, J. A., Programmed DNA destruction by miniature CRISPR-Cas14 enzymes. *Science* **2018,** *362* (6416), 839-842.
10. Notomi, T., Okayama, H., Masubuchi, H., Yonekawa, T., Watanabe, K., Amino, N. and Hase, T., Loop-mediated isothermal amplification of DNA. *Nucleic Acids Res.* **2000,** *28* (12), E63.
11. Piepenburg, O., Williams, C. H., Stemple, D. L. and Armes, N. A., DNA Detection Using Recombination Proteins. *PLOS Biol.* **2006,** *4* (7), e204.

12. Myhrvold, C., Freije, C. A., Gootenberg, J. S., Abudayyeh, O. O., Metsky, H. C., Durbin, A. F., Kellner, M. J., Tan, A. L., Paul, L. M., Parham, L. A., Garcia, K. F., Barnes, K. G., Chak, B., Mondini, A., Nogueira, M. L., Isern, S., Michael, S. F., Lorenzana, I., Yozwiak, N. L., MacInnis, B. L., Bosch, I., Gehrke, L., Zhang, F. and Sabeti, P. C., Field-deployable viral diagnostics using CRISPR-Cas13. *Science* **2018,** *360* (6387), 444-448.
13. Joung, J., Ladha, A., Saito, M., Kim, N.-G., Woolley, A. E., Segel, M., Barretto, R. P. J., Ranu, A., Macrae, R. K., Faure, G., Ioannidi, E. I., Krajeski, R. N., Bruneau, R., Huang, M.-L. W., Yu, X. G., Li, J. Z., Walker, B. D., Hung, D. T., Greninger, A. L., Jerome, K. R., Gootenberg, J. S., Abudayyeh, O. O. and Zhang, F., Detection of SARS-CoV-2 with SHERLOCK One-Pot Testing. *New Engl. J. Med.* **2020,** *383* (15), 1492-1494.
14. Broughton, J. P., Deng, X., Yu, G., Fasching, C. L., Servellita, V., Singh, J., Miao, X., Streithorst, J. A., Granados, A., Sotomayor-Gonzalez, A., Zorn, K., Gopez, A., Hsu, E., Gu, W., Miller, S., Pan, C.-Y., Guevara, H., Wadford, D. A., Chen, J. S. and Chiu, C. Y., CRISPR–Cas12-based detection of SARS-CoV-2. *Nat. Biotechnol.* **2020,** *38*, 870-874.
15. Zhang, F., Abudayyeh, O. O. and Gootenberg, J. S. A protocol for detection of COVID-19 using CRISPR diagnostics 2020. https://www.broadinstitute.org/files/publications/special/COVID-19%20detection%20(updated).pdf. (accessed May 11, 2020)
16. Wu, K.J. These Researchers Tested Positive. But the Virus Wasn't the Cause. Several scientists working with harmless genetic material have discovered that their research may have contaminated their coronavirus tests. *New York Times* November 12, 2020 https://www.nytimes.com/2020/11/12/health/coronavirus-testing-lab-contamination.html (accessed May 2, 2021).

17. New England BioLabs. EnGen® Lba Cas12a (Cpf1). https://www.neb.ca/detail.php?id=m0653 (accessed May 2, 2021).
18. Yin, K., Ding, X., Li, Z., Zhao, H., Cooper, K. and Liu, C., Dynamic Aqueous Multiphase Reaction System for One-Pot CRISPR-Cas12a-Based Ultrasensitive and Quantitative Molecular Diagnosis. *Anal. Chem.* **2020,** *92* (12), 8561-8568.
19. Kellner, M. J., Koob, J. G., Gootenberg, J. S., Abudayyeh, O. O. and Zhang, F., SHERLOCK: nucleic acid detection with CRISPR nucleases. *Nat. Protoc.* **2019,** *14*, 2986-3012.
20. Guo, L., Sun, X., Wang, X., Liang, C., Jiang, H., Gao, Q., Dai, M., Qu, B., Fang, S., Mao, Y., Chen, Y., Feng, G., Gu, Q., Wang, R. R., Zhou, Q. and Li, W., SARS-CoV-2 detection with CRISPR diagnostics. *Cell Discovery* **2020,** *6* (1), 34.
21. Sun, Y., Yu, L., Liu, C., Ye, S., Chen, W., Li, D. and Huang, W., One-tube SARS-CoV-2 detection platform based on RT-RPA and CRISPR/Cas12a. *J. Transl. Med.* **2021,** *19* (1), 74.
22. Wang, Y., Ke, Y., Liu, W., Sun, Y. and Ding, X., A One-Pot Toolbox Based on Cas12a/crRNA Enables Rapid Foodborne Pathogen Detection at Attomolar Level. *ACS Sens.* **2020,** *5* (5), 1427-1435.
23. Ding, X., Yin, K., Li, Z., Lalla, R. V., Ballesteros, E., Sfeir, M. M. and Liu, C., Ultrasensitive and visual detection of SARS-CoV-2 using all-in-one dual CRISPR-Cas12a assay. *Nat. Commun.* **2020,** *11* (1), 4711.
24. Arizti-Sanz, J., Freije, C. A., Stanton, A. C., Petros, B. A., Boehm, C. K., Siddiqui, S., Shaw, B. M., Adams, G., Kosoko-Thoroddsen, T.-S. F., Kemball, M. E., Uwanibe, J. N., Ajogbasile, F. V., Eromon, P. E., Gross, R., Wronka, L., Caviness, K., Hensley, L. E.,

Bergman, N. H., MacInnis, B. L., Happi, C. T., Lemieux, J. E., Sabeti, P. C. and Myhrvold, C., Streamlined inactivation, amplification, and Cas13-based detection of SARS-CoV-2. *Nat. Commun.* **2020,** *11*, 5921.

25. Ding, X., Yin, K., Li, Z. and Liu, C., All-in-One Dual CRISPR-Cas12a (AIOD-CRISPR) Assay: A Case for Rapid, Ultrasensitive and Visual Detection of Novel Coronavirus SARS-CoV-2 and HIV virus. *bioRxiv* **2020**, 2020.03.19.998724. https://doi.org/10.1101/2020.03.19.998724
26. de Puig, H., Lee, R. A., Najjar, D., Tan, X., Soekensen, L. R., Angenent-Mari, N. M., Donghia, N. M., Weckman, N. E., Ory, A., Ng, C. F., Nguyen, P. Q., Mao, A. S., Ferrante, T. C., Lansberry, G., Sallum, H., Niemi, J. and Collins, J. J., Minimally instrumented SHERLOCK (miSHERLOCK) for CRISPR-based point-of-care diagnosis of SARS-CoV-2 and emerging variants. *Sci. Adv.* **2021**, *7* (32), eabh2944.
27. Pabbaraju, K., Wong, A. A., Douesnard, M., Ma, R., Gill, K., Dieu, P., Fonseca, K., Zelyas, N. and Tipples, G. A., Development and validation of reverse transcriptase-PCR assays for the testing of SARS-CoV-2. *Off. J. Assoc. Med. Microbiol. Infect. Dis.* **2021,** 6(1), 16-22. DOI: 10.3138/jammi-2020-0026
28. New England BioLabs.ProtoScript® II Reverse Transcriptase. https://www.neb.ca/detail.php?id=m0368 (accessed May 2).
29. New England BioLabs. AMV Reverse Transcriptase. https://www.neb.ca/detail.php?id=m0277 (accessed May 2).
30. Thermofisher. RevertAid Reverse Transcriptase. https://www.thermofisher.com/order/catalog/product/EP0441#/EP0441 (accessed May 2).

31. New England Biolabs. M-MuLV Reverse Transcriptase. https://www.neb.ca/detail.php?id=m0368 (accessed May 2).

32. Our Cell Biology Correspondent, Enzymes: RNase H Activity. *Nature* **1973,** *241* (5390), 429-429.

33. Larremore, D. B., Wilder, B., Lester, E., Shehata, S., Burke, J. M., Hay, J. A., Tambe, M., Mina, M. J. and Parker, R., Test sensitivity is secondary to frequency and turnaround time for COVID-19 screening. *Sci. Adv.* **2021,** *7* (1), eabd5393.

34. Qian, J., Boswell, S. A., Chidley, C., Lu, Z.-x., Pettit, M. E., Gaudio, B. L., Fajnzylber, J. M., Ingram, R. T., Ward, R. H., Li, J. Z. and Springer, M., An enhanced isothermal amplification assay for viral detection. *Nat. Commun.* **2020,** *11* (1), 5920.

Chapter 6. Summarizing Discussion and Future Directions for Research

6.1 Summarizing Discussion

CRISPR technology continues to improve, and its application has been extended to diagnostics. Technological improvement relies on the discovery of CRISPR-Cas systems with specific features, the understanding of the mechanism and kinetics of CRISPR-Cas systems, engineering of proteins and RNA of the CRISPR-Cas systems, and understanding the compatibility of CRISPR-Cas systems with other pre-analytical and analytical techniques and biological matrices.

Quantification of RNA molecules for basic research and molecular diagnosis relies on RT-qPCR. The RNA is first extracted from samples, then reverse transcribed into complementary DNA, and amplified and detected through PCR, using primers, probes, polymerases, and thermocycling. CRISPR-based diagnostics have some features that make it useful to complement this standard technique for RNA detection. CRISPR-Cas13a recognizes RNA but not DNA, so detection is RNA-specific, and no reverse transcription is required. Meanwhile, the *trans*-cleavage activity of Cas13a is a multiple turnover process, so once activated by one target RNA, one Cas13a cleaves multiple reporters and generates multiple signals via its *trans*-cleavage activity.

To broaden the application of CRISPR technology to the detection of different types of RNA, in Chapter 2, I studied factors that affect the *trans*-cleavage activity of LwaCas13a and optimized them for the successful detection of microRNA. microRNA is relevant to the development of cancer and is usually found at a length of around 22 nt. Such short RNA is challenging to be amplified exponentially because the short length does not allow two or more

primers to bind. Special stem-loop-containing primers are used to detect microRNA using RT-qPCR. My assay for microRNA-10b using either LwaCas13a or LbuCas13a achieved a sensitivity of 5 pM. Such sensitivity makes the assay useful for the analysis of microRNA in cell lysates. The assay requires only one enzyme, and the reading only takes 20 min. One unique and advantageous feature of this assay over other established techniques is that it operates at ambient temperature.

In the development of the microRNA assay and the study of the activity of two Cas13a homologs, LwaCas13a and LbuCas13a, I realized that the activity of LwaCas13a was significantly reduced when short RNA targets were tested compared to long RNA targets. Thus, in Chapter 3, I studied the effect of short RNA length on the activity of LwaCas13a and LbuCas13a. Even under optimal conditions for the detection of the 23-nt short RNA target, LwaCas13a was not always activated by truncated target or crRNA, or if the spacer-target duplex was shorter than 23 nt. This suggests the length limit of RNA for LwaCas13a activation. This is different from the length of crRNA for LbuCas13a, as the latter requires only 20-nt spacers. The need for a longer crRNA-target duplex of LwaCas13a is consistent with the longer spacer LwaCas13a produces in the original organism than that of LbuCas13a. RNA-Cas13a interaction near the 22^{nd} and 23^{rd} positions at the 3' end of the crRNA may be important for the activation of LwaCas13a.

Another interesting observation from my research in Chapter 2 is that the optimal temperature for microRNA-10b detection is 23 °C rather than the commonly used 37 °C. In the literature, there is no systematic study of the thermal behavior of Cas13a. Scattered information has shown that for some targets, LwaCas13a and LbuCas13a perform better at 37 °C than 25 °C. The preferred operating temperatures of Cas13a determine the simplicity

of the assay and the temperature compatibility of the CRISPR component with other amplification techniques and pre-analytical techniques.

Therefore, in Chapter 4, I systematically studied the thermal behavior of Cas13a. The operation of Cas13a is a complicated process that includes steps of the activation of Cas13a ribonucleoprotein, Cas13a conformational change, and the cleavage of RNA through the *cis*-cleavage and *trans*-cleavage activities. I focused on the *trans*-cleavage activity of Cas13a upon target binding, and studied how the temperature affects the *trans*-cleavage activity once Cas13a is activated by the target RNA. I also studied whether the temperature preference depends on target sequences. I used a set of target RNA and crRNA with different characters in nucleotide composition, secondary structure (length), and spacer length. These are the key features of different types of RNA targets and the specificity of different crRNA. I quantitatively compared the *trans*-cleavage rate and found that LwaCas13a and LbuCas13a have high *trans*-cleavage activity at ambient temperature upon target binding. The *trans*-cleavage process itself operates the best at 27–32 °C for LwaCas13a and LbuCas13a. This is consistent among all the targets and crRNA I tested. The processes before the activation of Cas13a, the target binding step, prefer 37 °C if the target is in a complicated secondary structure. For the detection of short or simple targets, the detection can be performed at ambient temperature, and heating is not required. For the detection of complicated targets, the commonly used 37 °C improved the target binding. To simplify the detection, an alternative approach of quick annealing of target and crRNA followed by signal generation at ambient temperature is also efficient.

To detect pathogen RNA, using CRISPR-Cas13a alone is challenging to meet the sensitivity need. This is limited by the intrinsic enzyme recognition and cleavage kinetics

properties. Integrating CRISPR-Cas systems with nucleic acid amplification techniques ensures both analytical specificity and sensitivity. The operation temperature of reverse transcription, recombinant polymerase amplification (RT-RPA) is 37–42 °C, similar to that of LbCas12a (~37 °C). Using Cas13a would require an additional transcription of the DNA amplicon to RNA, which may increase the complicity of the assay, thus I chose LbCas12a for the integrated assay. RT-RPA isothermal amplification and CRISPR-Cas12a detection are considered compatible in principle. In practice, however, achieving reproducible detection of SARS-CoV-2 in a single tube is challenging. Previous studies indicated that the detection of RNA using RT-RPA and CRISPR-Cas is less sensitive than the detection of DNA, yet the reasons have not been well examined.

In Chapter 5, I elucidated the reason for the poor performance of RNA detection, and have successfully integrated reverse transcription (RT), recombinase polymerase amplification (RPA), and CRISPR-Cas12a nuclease reactions into a single tube under isothermal conditions (40 °C). Specific detection of a few copies of a viral DNA sequence was achieved in less than 20 min. However, the sensitivity was orders of magnitude lower for the detection of viral RNA due to the slow initiation of RPA from a cDNA/RNA template. During the delay in initiation of RPA, the crRNA-Cas12a ribonucleoprotein (RNP) gradually lost its activity in the RPA solution, and nonspecific amplification reactions consumed RPA reagents. In collaboration with Dr. Peng, I overcame these problems by using the endoribonuclease function of RNase H to remove RNA from the RNA-cDNA hybrids thus freeing the cDNA as the template for RPA reaction. As a consequence, we significantly enhanced the overall reaction rate of an integrated assay using RT-RPA and CRISPR-Cas12a for the detection of RNA. I can successfully detect 200 or more copies of the S gene sequence

of SARS-CoV-2 RNA between 5–30 min. I applied our one-tube assay to 46 upper respiratory swab samples, with 21 SARS-CoV-2 positive and 25 SARS-CoV-2 negative samples. The results from both real-time fluorescence intensity measurements and end-point visualization were consistent with those of RT-qPCR analysis. These strategies improved the sensitivity and speed of RT-RPA and CRISPR-Cas12a assays, making them useful for both semi-quantitative and point-of-care analyses of RNA molecules.

6.2 Future Directions for Research

6.2.1 Further understanding of the activation and operation mechanism of CRISPR-Cas systems for better performance of CRISPR-based diagnostics

In the field of CRISPR technology, basic research and practical application promote each other. The understanding of CRISPR-Cas9 systems promoted a revolution in genome editing technology. Prior to CRISPR-Cas technology, other nucleic acid binding proteins, such as zinc finger nucleases (ZFNs),[1] transcription activator-like effector nucleases (TALENs),[2] and meganucleases,[3] were engineered to bind to and operate on specific genomic loci.[4-5] Meganucleases, such as LAGLIDADG homing endonuclease, specifically recognize double-stranded DNA sequences of 14 to 40 base pairs and enable modification and deletion of DNA sequences.[3] ZFNs require multiple zinc-finger motifs to be linked tandemly, with each motif targeting one nucleotide triplet.[5] TALENs require a DNA-binding domain in which each amino acid binds specifically to one of the four types of nucleotides.[5] These systems require engineering different fusion proteins for different target sites, and therefore are not widely applicable. CRISPR-Cas technology overcomes this problem. Targeting a different gene sequence can be achieved by using a corresponding crRNA designed to recognize the

gene sequence. This programmable feature of the crRNA-mediated guidance of CRISPR is particularly advantageous.

The need to integrate CRISPR technology with the isothermal amplification reaction for simple diagnostic techniques promoted the discovery and characterization of different CRISPR-Cas systems. CRISPR-based diagnostics was established utilizing the *trans*-cleavage activity of Cas13a and has been continually improving to meet practical needs. Although there are a few successful example strategies of integrating isothermal amplification and CRISPR reagents into a single tube before the COVID-19 pandemic, the performance is not sufficient for SARS-CoV-2 RNA detection. Loop-mediated isothermal amplification (LAMP) is useful for such needs, yet the operation temperature is around 60 °C, and such a high temperature denatures most Cas proteins. Joung et al.[6] explored thermophilic Cas enzymes and chose AspCas12b from *Alicyclobacillus acidiphilus*. They also engineered a gRNA for AspCas12b. These allowed highly sensitive one-pot LAMP-CRISPR SARS-CoV-2 detection with a simple RNA extraction procedure in 1 h.

CRISPR-Cas technologies continue to be improved, and further understanding of the CRISPR-Cas systems is required. CRISPR-Cas systems have shown target preference, which affects the analytical sensitivity. The *trans*-cleavage kinetics and the sensitivity are significantly higher when using some spacer sequences than others.[7] Though there are prediction platforms trained with large-scale experimental data, such as ADAPT[8], to assist the choice of the targeting region and the design of crRNA, the molecular mechanism of the target preference is unclear. In addition, under optimized conditions, the *trans*-cleavage kinetics varies among targets (Chapter 4). For some targets, the quick activation and deactivation of the CRISPR-LwaCas13a may be related to the *cis*-cleavage and the release of some target

RNA. Meanwhile, the sequence-specific nucleic acid recognition of CRISPR-Cas systems ensured the specificity of human and pathogen nucleic acid detection. However, it is still challenging to completely discriminate single-nucleotide differences within the protospacer region, as the mutated target generates a reduced signal rather than no signal. This limits the performance of variant discrimination. For the variants of concern of SARS-CoV-2, key mutations are often single-nucleotide mutations. Tremendous advances made in modifications of Cas proteins and crRNA for the purpose of gene editing[9-13] could be harnessed and applied to developing and improving molecular diagnostics. The engineering is guided by understanding of the mechanism.

For clinical assays and point-of-care testing, practical aspects also need to be considered, such as robustness, simplicity, contamination, and possibility of automation. The simplicity has been improved by using lyophilized reagents, and the stability of reagents and the performance of using such strategies outside well-equipped labs require further optimization and validation. RNases, nucleases, and proteases that degrade CRISPR-Cas ribonucleoproteins and nucleic acids are abundant in biological samples. These interferences need to be further addressed when CRISPR-Cas technologies are used as diagnostic tools. These require the study of the compatibility of the CRISPR-Cas system with reagents and additives and the stability of crRNA-Cas ribonucleoproteins.

6.2.2 Utilizing the *trans*-cleavage activity for biosensing signal amplification in live cells

CRISPR-Cas systems have been used for DNA and RNA imaging in live cells,[14-16] but the target site is limited to repetitive sequences because of the low copy number of DNA or RNA in one cell and the lack of sufficient signal amplification.[17] CRISPR-Cas-integrated

amplification strategies allow for enhanced signal generation at a genomic locus in fixed cells and overcome the limitation of CRISPR-Cas probes that could only detect and image repetitive sequences.[18] Using *trans*-cleavages for signal amplification in live cells is challenging. The *trans*-cleavage activity in the cell environment is still unclear. Cas13 *cis*-activity clearly occurs in the modified human embryonic kidney cell line HEK293FT, while *trans*-activity is not observed.[19-20] However, it has been reported that *trans*-activity occurred within LN229 glioma cells.[21] The inconsistency may be attributed to the differences in cellular environments or methods of intracellular delivery from different studies.[21]

Factors that affect the *trans*-cleavage activity, such as the concentration of reporters and cofactors, may also affect the use of *trans*-cleavage in live cells, yet the effect is unclear. I observed a significant decrease in the *trans*-cleavage activity of LwaCas13a in physiological Mg^{2+} concentration at around 0.5–1 mM. (Figure 2-7) One successful example is the demonstration by Chen et al.[22] of the use of *trans*-cleavage activity Cas12a for sensing in live cells. They introduced high concentrations of transducer probes, crRNA-Cas12a ribonucleoprotein, and reporters into cells through lipofectamine transfection.[22] Transducer probes were first transfected through 3 h incubation, and then CRISPR reagents were transfected into cells through a 5 h incubation.

However, CRISPR-Cas-facilitated amplification strategies that do not depend on *trans*-activity may still work within live cells. The recently discovered Cas12f (Cas14) could be considered for use in live cells. Cas12f is only 400–700 amino acids long, which makes Cas12f easier to deliver into cells than other Cas effectors that are greater than 1000 amino acids in length. Due to the smaller size of Cas12f, both the Cas12f gene and sgRNA can be readily packaged[23] in the same adeno-associated virus (AVV) vector and delivered into live cells.

6.3 References

1. Urnov, F. D., Rebar, E. J., Holmes, M. C., Zhang, H. S. and Gregory, P. D., Genome editing with engineered zinc finger nucleases. *Nat. Rev. Genet.* **2010,** *11*, 636-646.
2. Joung, J. K. and Sander, J. D., TALENs: a widely applicable technology for targeted genome editing. *Nat. Rev. Mol. Cell Biol.* **2013,** *14* (1), 49-55.
3. Silva, G., Poirot, L., Galetto, R., Smith, J., Montoya, G., Duchateau, P. and Pâques, F., Meganucleases and other tools for targeted genome engineering: perspectives and challenges for gene therapy. *Curr. Gene Ther.* **2011,** *11* (1), 11-27.
4. Singh, A., Chakraborty, D. and Maiti, S., CRISPR/Cas9: a historical and chemical biology perspective of targeted genome engineering. *Chem. Soc. Rev.* **2016,** *45* (24), 6666-6684.
5. Gaj, T., Gersbach, C. A. and Barbas, C. F., III, ZFN, TALEN, and CRISPR/Cas-based methods for genome engineering. *Trends Biotechnol.* **2013,** *31* (7), 397-405.
6. Joung, J., Ladha, A., Saito, M., Kim, N.-G., Woolley, A. E., Segel, M., Barretto, R. P. J., Ranu, A., Macrae, R. K., Faure, G., Ioannidi, E. I., Krajeski, R. N., Bruneau, R., Huang, M.-L. W., Yu, X. G., Li, J. Z., Walker, B. D., Hung, D. T., Greninger, A. L., Jerome, K. R., Gootenberg, J. S., Abudayyeh, O. O. and Zhang, F., Detection of SARS-CoV-2 with SHERLOCK One-Pot Testing. *New Engl. J. Med.* **2020,** *383* (15), 1492-1494.
7. Fozouni, P., Son, S., Díaz de León Derby, M., Knott, G. J., Gray, C. N., D'Ambrosio, M. V., Zhao, C., Switz, N. A., Kumar, G. R., Stephens, S. I., Boehm, D., Tsou, C.-L., Shu, J., Bhuiya, A., Armstrong, M., Harris, A. R., Chen, P.-Y., Osterloh, J. M., Meyer-Franke, A., Joehnk, B., Walcott, K., Sil, A., Langelier, C., Pollard, K. S., Crawford, E. D., Puschnik, A. S., Phelps, M., Kistler, A., DeRisi, J. L., Doudna, J. A., Fletcher, D. A. and Ott, M.,

Amplification-free detection of SARS-CoV-2 with CRISPR-Cas13a and mobile phone microscopy. *Cell* **2021,** *184* (2), 323-333.e9.

8. Metsky, H. C., Welch, N. L., Pillai, P. P., Haradhvala, N. J., Rumker, L., Mantena, S., Zhang, Y. B., Yang, D. K., Ackerman, C. M., Weller, J., Blainey, P. C., Myhrvold, C., Mitzenmacher, M. and Sabeti, P. C., Designing sensitive viral diagnostics with machine learning. *Nat. Biotechol.* **2022**, https://doi.org/10.1038/s41587-022-01213-5
9. Rueda, F. O., Bista, M., Newton, M. D., Goeppert, A. U., Cuomo, M. E., Gordon, E., Kröner, F., Read, J. A., Wrigley, J. D. and Rueda, D. and Taylor, B. J. M., Mapping the sugar dependency for rational generation of a DNA-RNA hybrid-guided Cas9 endonuclease. *Nat. Commun.* **2017,** *8*, 1610.
10. Yin, H., Song, C.-Q., Suresh, S., Kwan, S.-Y., Wu, Q., Walsh, S., Ding, J., Bogorad, R. L., Zhu, L. J., Wolfe, S. A., Koteliansky, V., Xue, W., Langer, R. and Anderson, D. G., Partial DNA-guided Cas9 enables genome editing with reduced off-target activity. *Nat. Chem. Biol.* **2018,** *14* (3), 311-316.
11. Ryan, D. E., Taussig, D., Steinfeld, I., Phadnis, S. M., Lunstad, B. D., Singh, M., Vuong, X., Okochi, K. D., McCaffrey, R., Olesiak, M., Roy, S., Yung, C. W., Curry, B., Sampson, J. R., Bruhn, L. and Dellinger, D. J., Improving CRISPR–Cas specificity with chemical modifications in single-guide RNAs. *Nucleic Acids Res.* **2018,** *46* (2), 792-803.
12. Mir, A., Alterman, J. F., Hassler, M. R., Debacker, A. J., Hudgens, E., Echeverria, D., Brodsky, M. H., Khvorova, A., Watts, J. K. and Sontheimer, E. J., Heavily and fully modified RNAs guide efficient SpyCas9-mediated genome editing. *Nat. commun.* **2018,** *9*, 2641.

13. Kocak, D. D., Josephs, E. A., Bhandarkar, V., Adkar, S. S., Kwon, J. B. and Gersbach, C. A., Increasing the specificity of CRISPR systems with engineered RNA secondary structures. *Nat. Biotechnol.* **2019,** *37*, 657-666.

14. Chen, B., Gilbert, L. A., Cimini, B. A., Schnitzbauer, J., Zhang, W., Li, G.-W., Park, J., Blackburn, E. H., Weissman, J. S., Qi, L. S. and Huang, B., Dynamic imaging of genomic loci in living human cells by an optimized CRISPR/Cas system. *Cell* **2013,** *155* (7), 1479-1491.

15. Wu, X., Mao, S., Ying, Y., Krueger, C. J. and Chen, A. K., Progress and challenges for live-cell imaging of genomic loci using CRISPR-based platforms. *Genomics Proteomics Bioinformatics* **2019**, *17* (2), 119-128.

16. Wang, H., Nakamura, M., Abbott, T. R., Zhao, D., Luo, K., Yu, C., Nguyen, C. M., Lo, A., Daley, T. P., Russa, M. L., Liu, Y. and Qi, L. S., CRISPR-mediated live imaging of genome editing and transcription. *Science* **2019,** *365* (6459), 1301-1305.

17. Peng, H. Y., Newbigging, A. M., Reid, M. S., Uppal, J. S., Xu, J. Y., Zhang, H. Q. and Le, X. C., Signal Amplification in Living Cells: A Review of microRNA Detection and Imaging. *Anal. Chem.* **2020,** *92* (1), 292-308.

18. Zhang, K., Deng, R., Teng, X., Li, Y., Sun, Y., Ren, X. and Li, J., Direct visualization of single-nucleotide variation in mtDNA using a CRISPR/Cas9-mediated proximity ligation assay. *J. Am. Chem. Soc.* **2018,** *140* (36), 11293-11301.

19. Konermann, S., Lotfy, P., Brideau, N. J., Oki, J., Shokhirev, M. N. and Hsu, P. D., Transcriptome Engineering with RNA-Targeting Type VI-D CRISPR Effectors. *Cell* **2018,** *173* (3), 665-676.e14.

20. Abudayyeh, O. O., Gootenberg, J. S., Essletzbichler, P., Han, S., Joung, J., Belanto, J. J., Verdine, V., Cox, D. B. T., Kellner, M. J., Regev, A., Lander, E. S., Voytas, D. F., Ting, A. Y. and Zhang, F., RNA targeting with CRISPR-Cas13. *Nature* **2017,** *550*, 280-284.
21. Wang, Q., Liu, X., Zhou, J., Yang, C., Wang, G., Tan, Y., Wu, Y., Zhang, S., Yi, K. and Kang, C., The CRISPR-Cas13a Gene-Editing System Induces Collateral Cleavage of RNA in Glioma Cells. *Adv. Sci.* **2019,** *6* (20), 1901299.
22. Chen, S., Wang, R., Peng, S., Xie, S., Lei, C., Huang, Y. and Nie, Z., PAM-less conditional DNA substrates leverage trans-cleavage of CRISPR-Cas12a for versatile live-cell biosensing. *Chem. Sci.* **2022,** *13* (7), 2011-2020.
23. Wang, L., Zheng, W., Liu, S., Li, B. and Jiang, X., Delivery of CRISPR/Cas9 by novel strategies for gene therapy. *Chembiochem* **2019,** *20* (5), 634-643.

Bibliography

Abudayyeh, O. O., Gootenberg, J. S., Essletzbichler, P., Han, S., Joung, J., Belanto, J. J., Verdine, V., Cox, D. B. T., Kellner, M. J., Regev, A., Lander, E. S., Voytas, D. F., Ting, A. Y. and Zhang, F., RNA targeting with CRISPR-Cas13. *Nature* **2017,** *550*, 280-284.

Abudayyeh, O. O., Gootenberg, J. S., Konermann, S., Joung, J., Slaymaker, I. M., Cox, D. B. T., Shmakov, S., Makarova, K. S., Semenova, E., Minakhin, L., Severinov, K., Regev, A., Lander, E. S., Koonin, E. V. and Zhang, F., C2c2 is a single-component programmable RNA-guided RNA-targeting CRISPR effector. *Science* **2016,** *353* (6299), aaf5573.

Ackerman, C. M., Myhrvold, C., Thakku, S. G., Freije, C. A., Metsky, H. C., Yang, D. K., Ye, S. H., Boehm, C. K., Kosoko-Thoroddsen, T.-S. F., Kehe, J., Nguyen, T. G., Carter, A., Kulesa, A., Barnes, J. R., Dugan, V. G., Hung, D. T., Blainey, P. C. and Sabeti, P. C., Massively multiplexed nucleic acid detection using Cas13. *Nature* **2020,** *582*, 277-282.

Adli, M., The CRISPR tool kit for genome editing and beyond. *Nat. Commun.* **2018,** *9*, 1911.

Arizti-Sanz, J., Bradley, A. D., Zhang, Y. B., Boehm, C. K., Freije, C. A., Grunberg, M. E., Kosoko-Thoroddsen, T.-S. F., Welch, N. L., Pillai, P. P., Mantena, S., Kim, G., Uwanibe, J. N., John, O. G., Eromon, P. E., Kocher, G., Gross, R., Lee, J. S., Hensley, L. E., Happi, C. T., Johnson, J., Sabeti, P. C. and Myhrvold, C., Equipment-free detection of SARS-CoV-2 and Variants of Concern using Cas13. *medRxiv* **2021**, 2021.11.01.21265764. https://doi.org/10.1101/2021.11.01.21265764

Arizti-Sanz, J., Freije, C. A., Stanton, A. C., Petros, B. A., Boehm, C. K., Siddiqui, S., Shaw, B. M., Adams, G., Kosoko-Thoroddsen, T.-S. F., Kemball, M. E., Uwanibe, J. N., Ajogbasile, F. V., Eromon, P. E., Gross, R., Wronka, L., Caviness, K., Hensley, L. E., Bergman, N. H., MacInnis, B. L., Happi, C. T., Lemieux, J. E., Sabeti, P. C. and Myhrvold,

C., Streamlined inactivation, amplification, and Cas13-based detection of SARS-CoV-2. *Nat. Commun.* **2020,** *11*, 5921.

Broughton, J. P., Deng, X., Yu, G., Fasching, C. L., Servellita, V., Singh, J., Miao, X., Streithorst, J. A., Granados, A., Sotomayor-Gonzalez, A., Zorn, K., Gopez, A., Hsu, E., Gu, W., Miller, S., Pan, C.-Y., Guevara, H., Wadford, D. A., Chen, J. S. and Chiu, C. Y., CRISPR–Cas12-based detection of SARS-CoV-2. *Nat. Biotechnol.* **2020,** *38*, 870-874.

Bruch, R., Baaske, J., Chatelle, C., Meirich, M., Madlener, S., Weber, W., Dincer, C. and Urban, G. A., CRISPR/Cas13a-Powered Electrochemical Microfluidic Biosensor for Nucleic Acid Amplification-Free miRNA Diagnostics. *Adv. Mater.* **2019,** *31* (51), 1905311.

Bruch, R., Johnston, M., Kling, A., Mattmüller, T., Baaske, J., Partel, S., Madlener, S., Weber, W., Urban, G. A. and Dincer, C., CRISPR-powered electrochemical microfluidic multiplexed biosensor for target amplification-free miRNA diagnostics. *Biosens. Bioelectron.* **2021,** *177*, 112887.

Calin, G. A. and Croce, C. M., MicroRNA signatures in human cancers. *Nat. Rev. Cancer* **2006,** *6* (11), 857-866.

Carter, L. J., Garner, L. V., Smoot, J. W., Li, Y., Zhou, Q., Saveson, C. J., Sasso, J. M., Gregg, A. C., Soares, D. J., Beskid, T. R., Jervey, S. R. and Liu, C., Assay Techniques and Test Development for COVID-19 Diagnosis. *ACS Cent. Sci.* **2020,** *6* (5), 591-605.

Chan, J. F.-W., Yip, C. C.-Y., To, K. K.-W., Tang, T. H.-C., Wong, S. C.-Y., Leung, K.-H., Fung, A. Y.-F., Ng, A. C.-K., Zou, Z. and Tsoi, H.-W., Choi, G. K.-Y., Tam, A. R. Cheng, V. C.-C., Chan, K.-H., Tsang, O. T.-Y. and Yuen, K.-Y., Improved molecular diagnosis of COVID-19 by the novel, highly sensitive and specific COVID-19-RdRp/Hel real-time

reverse transcription-PCR assay validated *in vitro* and with clinical specimens. *J. Clin. Microbiol.* **2020,** *58* (5), e00310-20.

Chang, N. N., Sun, C. H., Gao, L., Zhu, D., Xu, X. F., Zhu, X. J., Xiong, J. W. and Xi, J. J., Genome editing with RNA-guided Cas9 nuclease in Zebrafish embryos. *Cell Res.* **2013,** *23* (4), 465-472.

Chen, B., Gilbert, L. A., Cimini, B. A., Schnitzbauer, J., Zhang, W., Li, G.-W., Park, J., Blackburn, E. H., Weissman, J. S., Qi, L. S. and Huang, B., Dynamic imaging of genomic loci in living human cells by an optimized CRISPR/Cas system. *Cell* **2013,** *155* (7), 1479-1491.

Chen, C. F., Ridzon, D. A., Broomer, A. J., Zhou, Z. H., Lee, D. H., Nguyen, J. T., Barbisin, M., Xu, N. L., Mahuvakar, V. R., Andersen, M. R., Lao, K. Q., Livak, K. J. and Guegler, K. J., Real-time quantification of microRNAs by stem-loop RT-PCR. *Nucleic Acids Res.* **2005,** *33* (20), e179.

Chen, J. S., Ma, E. B., Harrington, L. B., Da Costa, M., Tian, X. R., Palefsky, J. M. and Doudna, J. A., CRISPR-Cas12a target binding unleashes indiscriminate single-stranded DNase activity. *Science* **2018,** *360* (6387), 436-439.

Chen, N., Zhou, M., Dong, X., Qu, J., Gong, F., Han, Y., Qiu, Y., Wang, J., Liu, Y., Wei, Y., Xia, J. a., Yu, T., Zhang, X. and Zhang, L., Epidemiological and clinical characteristics of 99 cases of 2019 novel coronavirus pneumonia in Wuhan, China: a descriptive study. *Lancet* **2020,** *395* (10223), 507-513.

Chen, S., Wang, R., Peng, S., Xie, S., Lei, C., Huang, Y. and Nie, Z., PAM-less conditional DNA substrates leverage trans-cleavage of CRISPR-Cas12a for versatile live-cell biosensing. *Chem. Sci.* **2022,** *13* (7), 2011-2020.

Chen, Y., Yang, S., Peng, S., Li, W., Wu, F., Yao, Q., Wang, F., Weng, X. and Zhou, X., N1-Methyladenosine detection with CRISPR-Cas13a/C2c2. *Chem. Sci.* **2019,** *10* (10), 2975-2979.

Chu, D. K. W., Pan, Y., Cheng, S. M. S., Hui, K. P. Y., Krishnan, P., Liu, Y., Ng, D. Y. M., Wan, C. K. C., Yang, P., Wang, Q., Peiris, M. and Poon, L. L. M., Molecular diagnosis of a novel coronavirus (2019-nCoV) causing an outbreak of pneumonia. *Clin. Chem.* **2020,** *66* (4), 549-555.

Compton, J., Nucleic acid sequence-based amplification. *Nature* **1991,** *350*, 91-92.

Cong, L., Ran, F. A., Cox, D., Lin, S. L., Barretto, R., Habib, N., Hsu, P. D., Wu, X. B., Jiang, W. Y., Marraffini, L. A. and Zhang, F., Multiplex Genome Engineering Using CRISPR/Cas Systems. *Science* **2013,** *339* (6121), 819-823.

Corman, V. M., Landt, O., Kaiser, M., Molenkamp, R., Meijer, A., Chu, D. K. W., Bleicker, T., Brünink, S., Schneider, J., Schmidt, M. L., Mulders, D. G., Haagmans, B. L., van der Veer, B., van den Brink, S., Wijsman, L., Goderski, G., Romette, J.-L., Ellis, J., Zambon, M., Peiris, M., Goossens, H., Reusken, C., Koopmans, M. P. and Drosten, C., Detection of 2019 novel coronavirus (2019-nCoV) by real-time RT-PCR. *Euro Surveill.* **2020,** *25* (3), 2000045.

Dai, Y., Somoza, R. A., Wang, L., Welter, J. F., Li, Y., Caplan, A. I. and Liu, C. C., Exploring the Trans-Cleavage Activity of CRISPR-Cas12a (cpf1) for the Development of a Universal Electrochemical Biosensor. *Angew. Chem. Int. Ed.* **2019,** *58* (48), 17399-17405.

DiCarlo, J. E., Norville, J. E., Mali, P., Rios, X., Aach, J. and Church, G. M., Genome engineering in *Saccharomyces cerevisiae* using CRISPR-Cas systems. *Nucleic Acids Res.* **2013,** *41* (7), 4336-4343.

Ding, X., Yin, K., Li, Z., Lalla, R. V., Ballesteros, E., Sfeir, M. M. and Liu, C., Ultrasensitive and visual detection of SARS-CoV-2 using all-in-one dual CRISPR-Cas12a assay. *Nat. commun.* **2020,** *11* (1), 4711.

Ding, X., Yin, K., Li, Z. and Liu, C., All-in-One Dual CRISPR-Cas12a (AIOD-CRISPR) Assay: A Case for Rapid, Ultrasensitive and Visual Detection of Novel Coronavirus SARS-CoV-2 and HIV virus. *bioRxiv* **2020**, 2020.03.19.998724. https://doi.org/10.1101/2020.03.19.998724

East-Seletsky, A., O'Connell, M. R., Burstein, D., Knott, G. J. and Doudna, J. A., RNA Targeting by Functionally Orthogonal Type VI-A CRISPR-Cas Enzymes. *Mol. Cell* **2017,** *66* (3), 373-383.

East-Seletsky, A., O'Connell, M. R., Knight, S. C., Burstein, D., Cate, J. H. D., Tjian, R. and Doudna, J. A., Two distinct RNase activities of CRISPR-C2c2 enable guide-RNA processing and RNA detection. *Nature* **2016,** *538*, 270-273.

Erratum for the Report "CRISPR-Cas12a target binding unleashes indiscriminate single-stranded DNase activity" by J. S. Chen, E. Ma, L. B. Harrington, M. Da Costa, X. Tian, J. M. Palefsky, J. A. Doudna. *Science* **2021,** *371* (6531), eabh0317.

English, M. A., Soenksen, L. R., Gayet, R. V., de Puig, H., Angenent-Mari, N. M., Mao, A. S., Nguyen, P. Q. and Collins, J. J., Programmable CRISPR-responsive smart materials. *Science* **2019,** *365* (6455), 780-785.

Feng, W., Peng, H., Xu, J., Liu, Y., Pabbaraju, K., Tipples, G., Joyce, M. A., Saffran, H. A., Tyrrell, D. L., Babiuk, S., Zhang, H. and Le, X. C., Integrating Reverse Transcription Recombinase Polymerase Amplification with CRISPR Technology for the One-Tube Assay of RNA. *Anal. Chem.* **2021**, 93 (37), 12808-12816.

Feng, W., Newbigging, A. M., Le, C., Pang, B., Peng, H., Cao, Y., Wu, J., Abbas, G., Song, J., Wang, D.-B., Cui, M., Tao, J., Tyrrell, D. L., Zhang, X.-E., Zhang, H. and Le, X. C., Molecular Diagnosis of COVID-19: Challenges and Research Needs. *Anal. Chem.* **2020,** *92* (15), 10196-10209.

Feng, W., Newbigging, A. M., Tao, J., Cao, Y., Peng, H., Le, C., Wu, J., Pang, B., Li, J., Tyrrell, D. L., Zhang, H. and Le, X. C., CRISPR technology incorporating amplification strategies: molecular assays for nucleic acids, proteins, and small molecules. *Chem. Sci.* **2021,** *12* (13), 4683-4698.

Forster, P., Forster, L., Renfrew, C. and Forster, M., Phylogenetic network analysis of SARS-CoV-2 genomes. *Proc. Natl. Acad. Sci.* **2020,** *117* (17), 9241-9243.

Fozouni, P., Son, S., Díaz de León Derby, M., Knott, G. J., Gray, C. N., D'Ambrosio, M. V., Zhao, C., Switz, N. A., Kumar, G. R., Stephens, S. I., Boehm, D., Tsou, C.-L., Shu, J., Bhuiya, A., Armstrong, M., Harris, A. R., Chen, P.-Y., Osterloh, J. M., Meyer-Franke, A., Joehnk, B., Walcott, K., Sil, A., Langelier, C., Pollard, K. S., Crawford, E. D., Puschnik, A. S., Phelps, M., Kistler, A., DeRisi, J. L., Doudna, J. A., Fletcher, D. A. and Ott, M., Amplification-free detection of SARS-CoV-2 with CRISPR-Cas13a and mobile phone microscopy. *Cell* **2021,** *184* (2), 323-333.e9.

Fu, Y., Sander, J. D., Reyon, D., Cascio, V. M. and Joung, J. K., Improving CRISPR-Cas nuclease specificity using truncated guide RNAs. *Nat. Biotechnol.* **2014,** *32*, 279-284.

Fundation for Innovative New Diagnostics (FIND), SARS-CoV-2 Diagnostic Pipeline. https://www.finddx.org/covid-19/pipeline/?section=show-all#diag_tab (accessed May 6, 2020).

Gaj, T., Gersbach, C. A. and Barbas, C. F., III, ZFN, TALEN, and CRISPR/Cas-based methods for genome engineering. *Trends Biotechnol.* **2013,** *31* (7), 397-405.

Gasiunas, G., Barrangou, R., Horvath, P. and Siksnys, V., Cas9–crRNA ribonucleoprotein complex mediates specific DNA cleavage for adaptive immunity in bacteria. *Proc. Natl. Acad. Sci.* **2012,** *109* (39), E2579-E2586.

Gootenberg, J. S., Abudayyeh, O. O., Kellner, M. J., Joung, J., Collins, J. J. and Zhang, F., Multiplexed and portable nucleic acid detection platform with Cas13, Cas12a, and Csm6. *Science* **2018,** *360* (6387), 439-444.

Gootenberg, J. S., Abudayyeh, O. O., Lee, J. W., Essletzbichler, P., Dy, A. J., Joung, J., Verdine, V., Donghia, N., Daringer, N. M., Freije, C. A., Myhrvold, C., Bhattacharyya, R. P., Livny, J., Regev, A., Koonin, E. V., Hung, D. T., Sabeti, P. C., Collins, J. J. and Zhang, F., Nucleic acid detection with CRISPR-Cas13a/C2c2. *Science* **2017,** *356* (6336), 438-442.

Granados-Riveron, J. T. and Aquino-Jarquin, G., CRISPR/Cas13-Based Approaches for Ultrasensitive and Specific Detection of microRNAs. *Cells* **2021,** *10* (7), 1655.

Guo, L., Sun, X., Wang, X., Liang, C., Jiang, H., Gao, Q., Dai, M., Qu, B., Fang, S., Mao, Y., Chen, Y., Feng, G., Gu, Q., Wang, R. R., Zhou, Q. and Li, W., SARS-CoV-2 detection with CRISPR diagnostics. *Cell Discovery* **2020,** *6* (1), 34.

Harrington, L. B., Burstein, D., Chen, J. S., Paez-Espino, D., Ma, E., Witte, I. P., Cofsky, J. C., Kyrpides, N. C., Banfield, J. F. and Doudna, J. A., Programmed DNA destruction by miniature CRISPR-Cas14 enzymes. *Science* **2018,** *362* (6416), 839-842.

He, L. and Hannon, G. J., MicroRNAs: Small RNAs with a big role in gene regulation. *Nat. Rev. Genet.* **2004,** *5*, 522-531.

Hsu, P. D., Lander, E. S. and Zhang, F., Development and applications of CRISPR-Cas9 for genome engineering. *Cell* **2014,** *157* (6), 1262-1278.

Hsu, P. D., Scott, D. A., Weinstein, J. A., Ran, F. A., Konermann, S., Agarwala, V., Li, Y. Q., Fine, E. J., Wu, X. B., Shalem, O., Cradick, T. J., Marraffini, L. A., Bao, G. and Zhang, F., DNA targeting specificity of RNA-guided Cas9 nucleases. *Nat. Biotechnol.* **2013,** *31* (9), 827-832.

Huang, C., Wang, Y., Li, X., Ren, L., Zhao, J., Hu, Y., Zhang, L., Fan, G., Xu, J., Gu, X., Cheng, Z., Yu, T., Xia, J., Wei, Y., Wu, W., Xie, X., Yin, W., Li, H., Liu, M., Xiao, Y., Gao, H., Guo, L., Xie, J., Wang, G., Jiang, R., Gao, Z., Jin, Q., Wang, J. and Cao, B., Clinical features of patients infected with 2019 novel coronavirus in Wuhan, China. *Lancet* **2020,** *395* (10223), 497-506.

Jinek, M., Chylinski, K., Fonfara, I., Hauer, M., Doudna, J. A. and Charpentier, E., A Programmable Dual-RNA-Guided DNA Endonuclease in Adaptive Bacterial Immunity. *Science* **2012,** *337* (6096), 816-821.

Jinek, M., East, A., Cheng, A., Lin, S., Ma, E. B. and Doudna, J., RNA-programmed genome editing in human cells. *Elife* **2013,** *2*, e00471.

Joung, J., Ladha, A., Saito, M., Kim, N.-G., Woolley, A. E., Segel, M., Barretto, R. P. J., Ranu, A., Macrae, R. K., Faure, G., Ioannidi, E. I., Krajeski, R. N., Bruneau, R., Huang, M.-L. W., Yu, X. G., Li, J. Z., Walker, B. D., Hung, D. T., Greninger, A. L., Jerome, K. R., Gootenberg, J. S., Abudayyeh, O. O. and Zhang, F., Detection of SARS-CoV-2 with SHERLOCK One-Pot Testing. *New Engl. J. Med.* **2020,** *383* (15), 1492-1494.

Joung, J. K. and Sander, J. D., TALENs: a widely applicable technology for targeted genome editing. *Nat. Rev. Mol. Cell Biol.* **2013,** *14* (1), 49-55.

Karvelis, T., Bigelyte, G., Young, J. K., Hou, Z., Zedaveinyte, R., Budre, K., Paulraj, S., Djukanovic, V., Gasior, S., Silanskas, A., Venclovas, C. and Siksnys, V., PAM recognition by miniature CRISPR-Cas12f nucleases triggers programmable double-stranded DNA target cleavage. *Nucleic Acids Res.* **2020,** *48* (9), 5016-5023.

Kellner, M. J., Koob, J. G., Gootenberg, J. S., Abudayyeh, O. O. and Zhang, F., SHERLOCK: nucleic acid detection with CRISPR nucleases. *Nat. Protoc.* **2019,** *14*, 2986-3012.

Kleinstiver, B. P., Tsai, S. Q., Prew, M. S., Nguyen, N. T., Welch, M. M., Lopez, J. M., McCaw, Z. R., Aryee, M. J. and Joung, J. K., Genome-wide specificities of CRISPR-Cas Cpf1 nucleases in human cells. *Nat. Biotechnol.* **2016,** *34* (8), 869-874.

Knott, G. J. and Doudna, J. A., CRISPR-Cas guides the future of genetic engineering. *Science* **2018,** *361* (6405), 866-869.

Knott, G. J., East-Seletsky, A., Cofsky, J. C., Holton, J. M., Charles, E., O'Connell, M. R. and Doudna, J. A., Guide-bound structures of an RNA-targeting A-cleaving CRISPR-Cas13a enzyme. *Nat. Struct. and Mol. Biol.* **2017,** (10), 825-833.

Kocak, D. D., Josephs, E. A., Bhandarkar, V., Adkar, S. S., Kwon, J. B. and Gersbach, C. A., Increasing the specificity of CRISPR systems with engineered RNA secondary structures. *Nat. Biotechnol.* **2019,** *37*, 657-666.

Konermann, S., Lotfy, P., Brideau, N. J., Oki, J., Shokhirev, M. N. and Hsu, P. D., Transcriptome Engineering with RNA-Targeting Type VI-D CRISPR Effectors. *Cell* **2018,** *173* (3), 665-676.e14.

Larremore, D. B., Wilder, B., Lester, E., Shehata, S., Burke, J. M., Hay, J. A., Tambe, M., Mina, M. J. and Parker, R., Test sensitivity is secondary to frequency and turnaround time for COVID-19 screening. *Sci. Adv.* **2021,** *7* (1), eabd5393.

Li, L. X., Li, S. Y., Wu, N., Wu, J. C., Wang, G., Zhao, G. P. and Wang, J., HOLMESv2: A CRISPR-Cas12b-Assisted Platform for Nucleic Acid Detection and DNA Methylation Quantitation. *ACS synth. biol.* **2019,** *8* (10), 2228-2237.

Li, S.-Y., Cheng, Q.-X., Liu, J.-K., Nie, X.-Q., Zhao, G.-P. and Wang, J., CRISPR-Cas12a has both *cis*- and *trans*-cleavage activities on single-stranded DNA. *Cell Res.* **2018,** *28*, 491-493.

Li, S.-Y., Cheng, Q.-X., Wang, J.-M., Li, X.-Y., Zhang, Z.-L., Gao, S., Cao, R.-B., Zhao, G.-P. and Wang, J., CRISPR-Cas12a-assisted nucleic acid detection. *Cell Discovery* **2018,** *4*, 20.

Liu, L., Li, X., Ma, J., Li, Z., You, L., Wang, J., Wang, M., Zhang, X. and Wang, Y., The Molecular Architecture for RNA-Guided RNA Cleavage by Cas13a. *Cell* **2017,** *170*, 714-726.

Liu, L., Li, X., Wang, J., Wang, M., Chen, P., Yin, M., Li, J., Sheng, G. and Wang, Y., Two Distant Catalytic Sites Are Responsible for C2c2 RNase Activities. *Cell* **2017,** *168* (1-2), 121-134.

Lu, J., Getz, G., Miska, E. A., Alvarez-Saavedra, E., Lamb, J., Peck, D., Sweet-Cordero, A., Ebet, B. L., Mak, R. H., Ferrando, A. A., Downing, J. R., Jacks, T., Horvitz, H. R. and Golub, T. R., MicroRNA expression profiles classify human cancers. *Nature* **2005,** *435*, 834-838.

Lu, R., Zhao, X., Li, J., Niu, P., Yang, B., Wu, H., Wang, W., Song, H., Huang, B., Zhu, N., Bi, Y., Ma, X., Zhan, F., Wang, L., Hu, T., Zhou, H., Hu, Z., Zhou, W., Zhao, L., Chen, J., Meng, Y., Wang, J., Lin, Y., Yuan, J., Xie, Z., Ma, J., Liu, W. J., Wang, D., Xu, W., Holmes, E. C., Gao, G. F., Wu, G., Chen, W., Shi, W. and Tan, W., Genomic

characterisation and epidemiology of 2019 novel coronavirus: implications for virus origins and receptor binding. *Lancet* **2020,** *395* (10224), 565-574.

Ma, E., Harrington, L. B., O'Connell, M. R., Zhou, K. and Doudna, J. A., Single-stranded DNA cleavage by divergent CRISPR-Cas9 enzymes. *Mol Cell* **2015,** *60* (3), 398-407.

Ma, L., Teruya-Feldstein, J. and Weinberg, R. A., Tumour invasion and metastasis initiated by microRNA-10b in breast cancer. *Nature* **2007,** *449* (7163), 682-688.

Mahas, A., Marsic, T., Lopez-Portillo Masson, M., Wang, Q., Aman, R., Zheng, C., Ali, Z., Alsanea, M., Al-Qahtani, A., Ghanem, B., Alhamlan, F. and Mahfouz, M., Characterization of a thermostable Cas13 enzyme for one-pot detection of SARS-CoV-2. *Proc. Natl. Acad. Sci. U.S.A.* 2022, *119* (28), e2118260119.

Makarova, K. S., Wolf, Y. I., Iranzo, J., Shmakov, S. A., Alkhnbashi, O. S., Brouns, S. J. J., Charpentier, E., Cheng, D., Haft, D. H., Horvath, P., Moineau, S., Mojica, F. J. M., Scott, D., Shah, S. A., Siksnys, V., Terns, M. P., Venclovas, Č., White, M. F., Yakunin, A. F., Yan, W., Zhang, F., Garrett, R. A., Backofen, R., van der Oost, J., Barrangou, R. and Koonin, E. V., Evolutionary classification of CRISPR–Cas systems: a burst of class 2 and derived variants. *Nat. Rev. Microbiol.* **2020,** *18*, 67-83.

Mali, P., Yang, L. H., Esvelt, K. M., Aach, J., Guell, M., DiCarlo, J. E., Norville, J. E. and Church, G. M., RNA-Guided Human Genome Engineering via Cas9. *Science* **2013,** *339* (6121), 823-826.

Meeske, A. J., Nakandakari-Higa, S. and Marraffini, L. A., Cas13-induced cellular dormancy prevents the rise of CRISPR-resistant bacteriophage. *Nature* **2019**, *570*, 241-245.

Metsky, H. C., Welch, N. L., Pillai, P. P., Haradhvala, N. J., Rumker, L., Mantena, S., Zhang, Y. B., Yang, D. K., Ackerman, C. M., Weller, J., Blainey, P. C., Myhrvold, C.,

Mitzenmacher, M. and Sabeti, P. C., Designing sensitive viral diagnostics with machine learning. *Nat. Biotechol.* **2022**, https://doi.org/10.1038/s41587-022-01213-5

Mir, A., Alterman, J. F., Hassler, M. R., Debacker, A. J., Hudgens, E., Echeverria, D., Brodsky, M. H., Khvorova, A., Watts, J. K. and Sontheimer, E. J., Heavily and fully modified RNAs guide efficient SpyCas9-mediated genome editing. *Nat. commun.* **2018,** *9*, 2641.

Myhrvold, C., Freije, C. A., Gootenberg, J. S., Abudayyeh, O. O., Metsky, H. C., Durbin, A. F., Kellner, M. J., Tan, A. L., Paul, L. M., Parham, L. A., Garcia, K. F., Barnes, K. G., Chak, B., Mondini, A., Nogueira, M. L., Isern, S., Michael, S. F., Lorenzana, I., Yozwiak, N. L., MacInnis, B. L., Bosch, I., Gehrke, L., Zhang, F. and Sabeti, P. C., Field-deployable viral diagnostics using CRISPR-Cas13. *Science* **2018,** *360* (6387), 444-448.

Nalefski, E. A., Patel, N., Leung, P. J. Y., Islam, Z., Kooistra, R. M., Parikh, I., Marion, E., Knott, G. J., Doudna, J. A., Le Ny, A.-L. M. and Madan, D., Kinetic analysis of Cas12a and Cas13a RNA-Guided nucleases for development of improved CRISPR-Based diagnostics. *iScience* **2021,** *24*, 102996.

New England BioLabs. AMV Reverse Transcriptase. https://www.neb.ca/detail.php?id=m0277 (accessed May 2, 2021).

New England BioLabs. EnGen® Lba Cas12a (Cpf1). https://www.neb.ca/detail.php?id=m0653 (accessed May 2, 2021).

New England Biolabs. M-MuLV Reverse Transcriptase. https://www.neb.ca/detail.php?id=m0368 (accessed May 2, 2021).

New England BioLabs. ProtoScript® II Reverse Transcriptase. https://www.neb.ca/detail.php?id=m0368 (accessed May 2, 2021).

Nishimasu, H., Ran, F. A., Hsu, P. D., Konermann, S., Shehata, S. I., Dohmae, N., Ishitani, R., Zhang, F. and Nureki, O., Crystal structure of Cas9 in complex with guide RNA and target DNA. *Cell* **2014,** *156* (5), 935-949.

Notomi, T., Mori, Y., Tomita, N. and Kanda, H., Loop-mediated isothermal amplification (LAMP): principle, features, and future prospects. *J Microbiol.* **2015,** *53* (1), 1-5.

Notomi, T., Okayama, H., Masubuchi, H., Yonekawa, T., Watanabe, K., Amino, N. and Hase, T., Loop-mediated isothermal amplification of DNA. *Nucleic Acids Res.* **2000,** *28* (12), E63.

O'Connell, M. R., Molecular Mechanisms of RNA Targeting by Cas13-containing Type VI CRISPR–Cas Systems. *J Mol. Biol.* **2019,** *431* (1), 66-87.

O'Connell, M. R., Oakes, B. L., Sternberg, S. H., East-Seletsky, A., Kaplan, M. and Doudna, J. A., Programmable RNA recognition and cleavage by CRISPR/Cas9. *Nature* **2014,** *516*, 263-266.

Our Cell Biology Correspondent. Enzymes: RNase H Activity. *Nature* **1973,** *241*, 429-429.

Pabbaraju, K., Wong, A. A., Douesnard, M., Ma, R., Gill, K., Dieu, P., Fonseca, K., Zelyas, N. and Tipples, G. A., Development and validation of reverse transcriptase-PCR assays for the testing of SARS-CoV-2. *Off. J. Assoc. Med. Microbiol. Infect. Dis.* **2021,** *6* (1), 16-22. DOI: 10.3138/jammi-2020-0026

Pang, B., Xu, J., Liu, Y., Peng, H., Feng, W., Cao, Y., Wu, J., Xiao, H., Pabbaraju, K., Tipples, G., Joyce, M. A., Saffran, H. A., Tyrrell, D. L., Zhang, H. and Le, X. C., Isothermal Amplification and Ambient Visualization in a Single Tube for the Detection of SARS-CoV-2 Using Loop-Mediated Amplification and CRISPR Technology. *Anal. Chem.* **2020,** *92* (24), 16204-16212.

Pardee, K., Green, A. A., Takahashi, M. K., Braff, D., Lambert, G., Lee, J. W., Ferrante, T., Ma, D., Donghia, N., Fan, M., Daringer, N. M., Bosch, I., Dudley, D. M., O'Connor, D. H., Gehrke, L. and Collins. J. J., Rapid, low-cost detection of Zika virus using programmable biomolecular components. *Cell* **2016,** *165* (5), 1255-1266.

Pattanayak, V., Lin, S., Guilinger, J. P., Ma, E., Doudna, J. A. and Liu, D. R., High-throughput profiling of off-target DNA cleavage reveals RNA-programmed Cas9 nuclease specificity. *Nat. Biotechnol.* **2013,** *31*, 839-843.

Peng, H. Y., Newbigging, A. M., Reid, M. S., Uppal, J. S., Xu, J. Y., Zhang, H. Q. and Le, X. C., Signal Amplification in Living Cells: A Review of microRNA Detection and Imaging. *Anal. Chem.* **2020,** *92* (1), 292-308.

Piepenburg, O., Williams, C. H., Stemple, D. L. and Armes, N. A., DNA Detection Using Recombination Proteins. *PLOS Biol.* **2006,** *4* (7), e204.

de Puig, H., Lee, R. A., Najjar, D., Tan, X., Soenksen, L. R., Angenent-Mari, N. M., Donghia, N. M., Weckman, N. E., Ory, A., Ng, C. F., Nguyen, P. Q., Mao, A. S., Ferrante, T. C., Lansberry, G., Sallum, H., Niemi, J. and Collins, J. J., Minimally instrumented SHERLOCK (miSHERLOCK) for CRISPR-based point-of-care diagnosis of SARS-CoV-2 and emerging variants. *Sci. Adv.* **2021,** *7* (32), eabh2944.

Qi, L. S., Larson, M. H., Gilbert, L. A., Doudna, J. A., Weissman, J. S., Arkin, A. P. and Lim, W. A., Repurposing CRISPR as an RNA-guided platform for sequence-specific control of gene expression. *Cell* **2013,** *152* (5), 1173-1183.

Qian, J., Boswell, S. A., Chidley, C., Lu, Z.-x., Pettit, M. E., Gaudio, B. L., Fajnzylber, J. M., Ingram, R. T., Ward, R. H., Li, J. Z. and Springer, M., An enhanced isothermal amplification assay for viral detection. *Nat. Commun.* **2020,** *11* (1), 5920.

Qin, P., Park, M., Alfson, K. J., Tamhankar, M., Carrion, R., Patterson, J. L., Griffiths, A., He, Q., Yildiz, A., Mathies, R. and Du, K., Rapid and Fully Microfluidic Ebola Virus Detection with CRISPR-Cas13a. *ACS Sens.* **2019,** *4* (4), 1048-1054.

Ramachandran, A. and Santiago, J. G., CRISPR Enzyme Kinetics for Molecular Diagnostics. *Anal. Chem.* **2021,** *93* (20), 7456-7464.

Ran, F. A., Hsu, P. D., Lin, C.-Y., Gootenberg, J. S., Konermann, S., Trevino, A. E., Scott, D. A., Inoue, A., Matoba, S., Zhang, Y. and Zhang, F., Double nicking by RNA-guided CRISPR Cas9 for enhanced genome editing specificity. *Cell* **2013,** *154* (6), 1380-1389.

Rueda, F. O., Bista, M., Newton, M. D., Goeppert, A. U., Cuomo, M. E., Gordon, E., Kröner, F., Read, J. A., Wrigley, J. D. and Rueda, D. and Taylor, B. J. M., Mapping the sugar dependency for rational generation of a DNA-RNA hybrid-guided Cas9 endonuclease. *Nat. Commun.* **2017,** *8*, 1610.

Ryan, D. E., Taussig, D., Steinfeld, I., Phadnis, S. M., Lunstad, B. D., Singh, M., Vuong, X., Okochi, K. D., McCaffrey, R., Olesiak, M., Roy, S., Yung, C. W., Curry, B., Sampson, J. R., Bruhn, L. and Dellinger, D. J., Improving CRISPR–Cas specificity with chemical modifications in single-guide RNAs. *Nucleic Acids Res.* **2018,** *46* (2), 792-803.

Shan, Y., Zhou, X., Huang, R. and Xing, D., High-Fidelity and Rapid Quantification of miRNA Combining crRNA Programmability and CRISPR/Cas13a trans-Cleavage Activity. *Anal. Chem.* **2019,** *91* (8), 5278-5285.

Shao, N., Han, X., Song, Y., Zhang, P. and Qin, L., CRISPR-Cas12a Coupled with Platinum Nanoreporter for Visual Quantification of SNVs on a Volumetric Bar-Chart Chip. *Anal. Chem.* **2019,** *91* (19), 12384-12391.

Sheedy, P. and Medarova, Z., The fundamental role of miR-10b in metastatic cancer. *Am. J. Cancer Res.* **2018,** *8* (9), 1674-1688.

Shmakov, S., Abudayyeh, O. O., Makarova, K. S., Wolf, Y. I., Gootenberg, J. S., Semenova, E., Minakhin, L., Joung, J., Konermann, S., Severinov, K., Zhang, F. and Koonin, E. V., Discovery and Functional Characterization of Diverse Class 2 CRISPR-Cas Systems. *Mol. Cell* **2015,** *60* (3), 385-397.

Silva, G., Poirot, L., Galetto, R., Smith, J., Montoya, G., Duchateau, P. and Pâques, F., Meganucleases and other tools for targeted genome engineering: perspectives and challenges for gene therapy. *Curr. Gene Ther.* **2011,** *11* (1), 11-27.

Singh, A., Chakraborty, D. and Maiti, S., CRISPR/Cas9: a historical and chemical biology perspective of targeted genome engineering. *Chem. Soc. Rev.* **2016,** *45* (24), 6666-6684.

Slaymaker, I. M., Mesa, P., Kellner, M. J., Kannan, S., Brignole, E., Koob, J., Feliciano, P. R., Stella, S., Abudayyeh, O. O., Gootenberg, J. S., Strecker, J., Montoya, G. and Zhang, F., High-Resolution Structure of Cas13b and Biochemical Characterization of RNA Targeting and Cleavage. *Cell Rep.* **2019,** *26* (13), 3741-3751.e5.

Slaymaker, I. M., Mesa, P., Kellner, M. J., Kannan, S., Brignole, E., Koob, J., Feliciano, P. R., Stella, S., Abudayyeh, O. O., Gootenberg, J. S., Strecker, J., Montoya, G. and Zhang, F., High-resolution structure of cas13b and biochemical characterization of RNA targeting and cleavage. *Cell Rep.* **2021,** *34* (10), 108865.

Smargon, A. A., Cox, D. B., Pyzocha, N. K., Zheng, K., Slaymaker, I. M., Gootenberg, J. S., Abudayyeh, O. A., Essletzbichler, P., Shmakov, S., Makarova, K. S., Koonin, E. V. and Zhang, F., Cas13b is a type VI-B CRISPR-associated RNA-guided RNase differentially regulated by accessory proteins Csx27 and Csx28. *Mol. Cell* **2017,** *65* (4), 618-630.e7.

Stephenson, A. A., Raper, A. T. and Suo, Z., Bidirectional degradation of DNA cleavage products catalyzed by CRISPR/Cas9. *J. Am. Chem. Soc.* **2018,** *140* (10), 3743-3750.

Strutt, S. C., Torrez, R. M., Kaya, E., Negrete, O. A. and Doudna, J. A., RNA-dependent RNA targeting by CRISPR-Cas9. *elife* **2018,** *7*, e32724.

Swarts, D. C. and Jinek, M., Mechanistic Insights into the *cis*- and *trans*-Acting DNase Activities of Cas12a. *Mol. Cell* **2019,** *73* (3), 589-600.e4.

Sun, Y., Yu, L., Liu, C., Ye, S., Chen, W., Li, D. and Huang, W., One-tube SARS-CoV-2 detection platform based on RT-RPA and CRISPR/Cas12a. *J. Transl. Med.* **2021,** *19* (1), 74.

Tambe, A., East-Seletsky, A., Knott, G. J., Doudna, J. A. and O'Connell, M. R., RNA Binding and HEPN-Nuclease Activation Are Decoupled in CRISPR-Cas13a. *Cell Reports* **2018,** *24* (4), 1025-1036.

Tang, Y., Gao, L., Feng, W., Guo, C., Yang, Q., Li, F. and Le, X. C., The CRISPR–Cas toolbox for analytical and diagnostic assay development. *Chem. Soc. Rev.* **2021,** *50* (21), 11844-11869.

Thermofisher. RevertAid Reverse Transcriptase. https://www.thermofisher.com/order/catalog/product/EP0441#/EP0441 (accessed May 2).

Udugama, B., Kadhiresan, P., Kozlowski, H. N., Malekjahani, A., Osborne, M., Li, V. Y. C., Chen, H., Mubareka, S., Gubbay, J. B. and Chan, W. C. W., Diagnosing COVID-19: The Disease and Tools for Detection. *ACS Nano* **2020,** *14* (4), 3822-3835.

Uhler, C. and Shivashankar, G. V., Mechano-genomic regulation of coronaviruses and its interplay with ageing. *Nat. Rev. Mol. Cell Biol.* **2020,** *21*, 247-248.

The United States Food and Drug Administration (FDA), In Vitro Diagnostics EUAs - Molecular Diagnostic Tests for SARS-CoV-2. https://www.fda.gov/medical-devices/coronavirus-disease-2019-covid-19-emergency-use-authorizations-medical-devices/in-vitro-diagnostics-euas-molecular-diagnostic-tests-sars-cov-2 (accessed Febuary 24, 2022).

Urnov, F. D., Rebar, E. J., Holmes, M. C., Zhang, H. S. and Gregory, P. D., Genome editing with engineered zinc finger nucleases. *Nat. Rev. Genet.* **2010,** *11*, 636-646.

Wang, D., Hu, B., Hu, C., Zhu, F., Liu, X., Zhang, J., Wang, B., Xiang, H., Cheng, Z., Xiong, Y., Zhao, Y., Li, Y., Wang, X. and Peng, Z., Clinical characteristics of 138 hospitalized patients with 2019 novel coronavirus–infected pneumonia in Wuhan, China. *JAMA* **2020,** *323* (11), 1061-1069.

Wang, H., Nakamura, M., Abbott, T. R., Zhao, D., Luo, K., Yu, C., Nguyen, C. M., Lo, A., Daley, T. P., Russa, M. L., Liu, Y. and Qi, L. S., CRISPR-mediated live imaging of genome editing and transcription. *Science* **2019,** *365* (6459), 1301-1305.

Wang, L., Zheng, W., Liu, S., Li, B. and Jiang, X., Delivery of CRISPR/Cas9 by novel strategies for gene therapy. *Chembiochem* **2019,** *20* (5), 634-643.

Wang, Q., Liu, X., Zhou, J., Yang, C., Wang, G., Tan, Y., Wu, Y., Zhang, S., Yi, K. and Kang, C., The CRISPR-Cas13a Gene-Editing System Induces Collateral Cleavage of RNA in Glioma Cells. *Adv. Sci.* **2019,** *6* (20), 1901299.

Wang, Y., Ke, Y., Liu, W., Sun, Y. and Ding, X., A One-Pot Toolbox Based on Cas12a/crRNA Enables Rapid Foodborne Pathogen Detection at Attomolar Level. *ACS Sens.* **2020,** *5* (5), 1427-1435.

Wei, Y., Yang, Z., Zong, C., Wang, B., Ge, X., Tan, X., Liu, X., Tao, Z., Wang, P., Ma, C., Wan, Y. and Li, J., *trans* Single-Stranded DNA Cleavage *via* CRISPR/Cas14a1 Activated by Target RNA without Destruction. *Angew. Chem. Int. Ed.* **2021,** *60* (45), 24241-24247.

WHO, Molecular assays to diagnose COVID-19. https://www.who.int/who-documents-detail/molecular-assays-to-diagnose-covid-19-summary-table-of-available-protocols (accessed May 12, 2020).

WHO, Tracking SARS-CoV-2 variants https://www.who.int/en/activities/tracking-SARS-CoV-2-variants/ (accessed Febuary 24, 2022).

World Health Organization (WHO), Coronavirus disease (COVID-19) technical guidance: Laboratory testing for 2019-nCoV in humans. https://www.who.int/emergencies/diseases/novel-coronavirus-2019/technical-guidance/laboratory-guidance (accessed May 12, 2020).

Wu, F., Zhao, S., Yu, B., Chen, Y.-M., Wang, W., Song, Z.-G., Hu, Y., Tao, Z.-W., Tian, J.-H., Pei, Y.-Y., Yuan, M.-L., Zhang, Y.-L., Dai, F.-H., Liu, Y., Wang, Q.-M., Zheng, J.-J., Xu, L., Holmes, E. C. and Zhang, Y.-Z., A new coronavirus associated with human respiratory disease in China. *Nature* **2020,** *579*, 265-269.

Wu, K.J. These Researchers Tested Positive. But the Virus Wasn't the Cause. Several scientists working with harmless genetic material have discovered that their research may have contaminated their coronavirus tests. *New York Times* November 12, 2020 https://www.nytimes.com/2020/11/12/health/coronavirus-testing-lab-contamination.html (accessed May 2, 2021).

Wu, X., Mao, S., Ying, Y., Krueger, C. J. and Chen, A. K., Progress and challenges for live-cell imaging of genomic loci using CRISPR-based platforms. *Genomics Proteomics Bioinformatics* **2019**, *17* (2), 119-128.

Wu, Y., Liu, S.-X., Wang, F. and Zeng, M.-S., Room Temperature Detection of Plasma Epstein–Barr Virus DNA with CRISPR–Cas13. *Clin. Chem.* **2019,** *65* (4), 591-592.

Wu, Z. and McGoogan, J. M., Characteristics of and important lessons from the coronavirus disease 2019 (COVID-19) outbreak in China: summary of a report of 72 314 cases from the Chinese Center for Disease Control and Prevention. *JAMA* **2020,** *323* (13), 1239-1242.

Yin, H., Song, C.-Q., Suresh, S., Kwan, S.-Y., Wu, Q., Walsh, S., Ding, J., Bogorad, R. L., Zhu, L. J., Wolfe, S. A., Koteliansky, V., Xue, W., Langer, R. and Anderson, D. G., Partial DNA-guided Cas9 enables genome editing with reduced off-target activity. *Nat. Chem. Biol.* **2018,** *14* (3), 311-316.

Yin, K., Ding, X., Li, Z., Zhao, H., Cooper, K. and Liu, C., Dynamic Aqueous Multiphase Reaction System for One-Pot CRISPR-Cas12a-Based Ultrasensitive and Quantitative Molecular Diagnosis. *Anal. Chem.* **2020,** *92* (12), 8561-8568.

Zetsche, B., Gootenberg, J. S., Abudayyeh, O. O., Slaymaker, I. M., Makarova, K. S., Essletzbichler, P., Volz, S. E., Joung, J., van der Oost, J., Regev, A., Koonin, E. V. and Zhang, F., Cpf1 Is a Single RNA-Guided Endonuclease of a Class 2 CRISPR-Cas System. *Cell* **2015,** *163* (3), 759-771.

Zhang, B., Ye, Y., Ye, W., Perčulija, V., Jiang, H., Chen, Y., Li, Y., Chen, J., Lin, J., Wang, S., Chen, Q., Han, Y.-S. and Ouyang, S., Two HEPN domains dictate CRISPR RNA maturation and target cleavage in Cas13d. *Nat. Commun.* **2019**, 10, 2544.

Zhang, C., Konermann, S., Brideau, N. J., Lotfy, P., Wu, X., Novick, S. J., Strutzenberg, T., Griffin, P. R., Hsu, P. D. and Lyumkis, D., Structural basis for the RNA-guided ribonuclease activity of CRISPR-Cas13d. *Cell* **2018,** *175* (1), 212-223. e17.

Zhang, F., Abudayyeh, O. O. and Gootenberg, J. S. A protocol for detection of COVID-19 using CRISPR diagnostics 2020. https://www.broadinstitute.org/files/publications/special/COVID-19%20detection%20(updated).pdf. (accessed May 11, 2020)

Zhang, K., Deng, R., Teng, X., Li, Y., Sun, Y., Ren, X. and Li, J., Direct visualization of single-nucleotide variation in mtDNA using a CRISPR/Cas9-mediated proximity ligation assay. *J. Am. Chem. Soc.* **2018,** *140* (36), 11293-11301.

Zhou, F., Yu, T., Du, R., Fan, G., Liu, Y., Liu, Z., Xiang, J., Wang, Y., Song, B., Gu, X., Guan, L., Wei, Y., Li, H., Wu, X., Xu, J., Tu, S., Zhang, Y., Chen, H. and Cao, B., Clinical course and risk factors for mortality of adult inpatients with COVID-19 in Wuhan, China: a retrospective cohort study. *Lancet* **2020,** *395* (10229), 1054-1062.

Zhou, P., Yang, X.-L., Wang, X.-G., Hu, B., Zhang, L., Zhang, W., Si, H.-R., Zhu, Y., Li, B., Huang, C.-L., Chen, H.-D., Chen, J., Luo, Y., Guo, H., Jiang, R.-D., Liu, M.-Q., Chen, Y., Shen, X.-R., Wang, X., Zheng, X.-S., Zhao, K., Chen, Q.-J., Deng, F., Liu, L.-L., Yan, B., Zhan, F.-X., Wang, Y.-Y., Xiao, G.-F. and Shi, Z.-L., A pneumonia outbreak associated with a new coronavirus of probable bat origin. *Nature* **2020,** *579*, 270-273.

Zhu, N., Zhang, D., Wang, W., Li, X., Yang, B., Song, J., Zhao, X., Huang, B., Shi, W., Lu, R., Niu, P., Zhan, F., Ma, X., Wang, D., Xu, W., Wu, G., Gao, G. F. and Tan, W., A Novel Coronavirus from Patients with Pneumonia in China, 2019. *New Engl. J. Med.* **2020,** *382* (8), 727-733.

Appendix A. Additional information on techniques combining isothermal amplification and CRISPR-Cas systems for the detection of SARS-CoV-2[§]

Table A1. Techniques combining isothermal amplification and CRISPR-Cas systems with *trans*-cleavage activities for the detection of SARS-CoV-2 RNA

Tech-niques	Steps	Facilities	LOD	Linear range	Sequence specificity of Cas recognition	Clinical sensitivity *	Clinical Speci-ficity*	Assay time	Ref.
RT-RPA-Cas13a **SHERLOCK**	1. RT-RPA 2. T7 transcription and Cas13a detection 3. Strip readout	Water bath (37°C & 42°C), microcentrifuge & strips	10-100 copies/ µL of synthetic RNA sample (1 µL sample/reaction)	Binary positive or negative	Relies on Cas13a RNP	Not tested	Not tested	60 min (Step 1 requires 25 min incubation; step 2 requires 30 min incubation, plus step 3)	[1]

[§] Contents in Appendix A have been published in the supporting information of Feng, W. [Δ], Peng, H. [Δ], Xu, J., Liu, Y., Pabbaraju, K., Tipples, G., Joyce, M. A., Saffran, H. A., Tyrrell, D. L., Babiuk, S., Zhang, H. and Le, X. C., Integrating Reverse Transcription Recombinase Polymerase Amplification with CRISPR Technology for the One-Tube Assay of RNA. *Anal Chem* **2021,** *93* (37), 12808-12816.

Tech-niques	Steps	Facilities	LOD	Linear range	Sequence specificity of Cas recognition	Clinical sensitivity *	Clinical Speci-ficity*	Assay time	Ref.
RT-RAA-Cas12a	1. RT-RAA 2. Cas12a	Incubator (39°C & 37°C), 485 nm light for **naked eye readout** & smartphone	10 copies of Synthetic RNA (/reaction?) (2 µL sample/reaction)	Not quantitative	Relies on Cas12a RNP *E gene target is relatively consistent among beta coronaviruses, so single-nucleotide specificity is required*	100% (Ct not available)	100%	(Step 1 requires 30 min incubation; step 2 requires 15 min incubation, plus visualization)	[2]
RT-RPA-Cas12a	1. RT-RPA 2. Heat deactivation 3. Cas12a	Incubator (39°C & 75°C), **Lab developed fluorescence detector** & Smartphone	6.25 copies/µL of synthetic RNA sample (1 µL sample/reaction)	Not reported	Relies on Cas12a RNP	87% (95% for samples with Ct<33)	92%	70 min (Step 1 requires 30 min incubation; step requires 5 min incubation, step 3 requires 30 min incubation)	[3]
RT-RAA-Cas12b	1. RT-RAA 2. Cas12b **(lid)**	a. Incubator (42°C) & real-time PCR system b. Incubator, LED light & smartphone (*may require additional facilities to differentiate pos. and neg.*)	a. 10 copies/µLof Pseudovirus RNA sample (6 µL sample/reaction) b. Not specified	a. Not reported b. Not for quantification	Relies on Cas12a RNP	Not tested	Not tested	~60 min (Step 1 requires 30 min incubation; step 2 requires 30 min reading)	[4]
RT-RPA-Cas12a /Cas13a	1. RT-RPA 2. Cas12/13a **(lid)** (3. Strip)	Incubator (42°C), a. plate reader/b.strip	1-20 copy/µL sample (5 µL sample/reaction)	Not quantitative	Relies on Cas12a RNP	6/6 (Ct 24–39) (The assay using Cas12a)	8/8 (The assay using Cas12a)	~60 min (Step 1 requires 30 min incubation; step 2 requires 20 min incubation, plus step 3.)	[5]

Tech-niques	Steps	Facilities	LOD	Linear range	Sequence specificity of Cas recognition	Clinical sensitivity *	Clinical Speci-ficity*	Assay time	Ref.
RT-RPA-Cas12a	1. RT-RPA 2. Cas12a 3. a. Endpoint fluorescence detection b. fluorescence visualization or c. Lateral flow	heat block (80°C for lysis, 42°C for RT-RPA, 37°C for Cas12a) & a. Fluorescence detector/b. UV light imager/c. strip	1–10 copy/µL sample (1 µL sample/reaction) for all three different readouts	a. Not reported b and c. not for quantification	Relies on Cas12a RNP	100% (Ct 20–35) for all three different readouts	100% for all three different readouts	50 min (**5 min lysis,** step 1 requires 15-20 min incubation; step 2 requires 15-20 min incubation, step 3 requires 2-5 min)	[6]
RT-RPA-**Cas13a** (-lateral flow) **SHERLOCK**	**Single tube reaction**	a. Plate reader or b. strip	a. Synthetic RNA 10 copies/µL of sample b. 100 copies/µL of sample (1 µL sample in 20 µL reaction)	Not for quantification	Relies on Cas13a RNP	90% (Ct 13–27, extraction free)	100%	50 min **(including 10 min lysis, and 40 min detection**)	[7]
RT-RPA-Cas12a	**Single tube reaction**	a. Real-time PCR or b. incubator & UV light	IVT SARS-CoV-2 RNA 5 copies /reaction (1 µL sample/reaction) for both readouts	Not for quantification	May be less specific than normal Cas12a detection, as the recognition is PAM-free. Targets ssDNA rather than dsDNA.	8/8 (Ct not available)	100%	20 min	[8]

Tech-niques	Steps	Facilities	LOD	Linear range	Sequence specificity of Cas recognition	Clinical sensitivity *	Clinical Speci-ficity*	Assay time	Ref.
RT-RPA-Cas12a **(This assay)**	**Single tube reaction**	a. Real-time PCR or b. incubator & UV light	SARS-CoV-2 RNA from Vero E6 cells 50 copies/μL (4 μL/reaction) 12.5 copies/μL can also be detected with 78% chance	Semi-quantitative: 10^2–10^5 copies/reaction	Relies on Cas12a RNP	87% (Ct 20–34) 100% for samples Ct < 32)	100%	5–60 min incubation	My Chapter 5
RT-RPA-Cas12a	**Single tube reaction**	**Lab-developed detection POC platform for lay users to add saliva input, treat saliva, run detection, and get fluorescence readouts**	1.2 copies/μL (of reaction?) (~50 μL/reaction)	Not for quantification	Relies on Cas12a, optimized to differentiate variants	96% (Ct 14–38)	95%	55 min RT-RPA-Cas12a reaction plus 5 min sample treatment	[9]
RT-RPA-Cas12a-microfluidics	a. Two-step tube reaction: 1. RT-RPA 2. Cas12a b. reaction on chip: 1. RT-RPA-Cas12a	a. Incubator(42°C), plate reader b. Chip, Lab-developed fluorescence reader & smartphone	On-chip analysis: Inactivated SARS-CoV-2 "calculated LOD of 0.38 copy/μL" (5 μL lysate/reaction)	On-chip analysis: 1–10^5 copies/μL	Relies on Cas12a RNP	a. Tube reaction: 100% for swab and saliva b. On-chip: 100% for swab 98% for saliva (1–10^6 copies)	a. Tube reaction: 100% for swab 98.7% for saliva b. On-chip: 100% for swab and saliva	**5 min lysis of saliva,** then "room temperature", 10 min for RT-RPA-Cas12a reaction on chip	[10]

Tech-niques	**Steps**	**Facilities**	**LOD**	**Linear range**	**Sequence specificity of Cas recognition**	**Clinical sensitivity ***	**Clinical Speci-ficity***	**Assay time**	**Ref.**
RT-RPA-Cas12a-**lab-on-paper**	1. RT-RPA 2. Cas12a	Lab-developed reactor containing RPA reaction chamber and Cas12a detection chambers separated by sucrose valve & imaging system	100 copies/test	Not quantitative	Relies on Cas12a RNP	8/8 (Ct 18–29)	100%	~40 min (Step 1 requires 15 min incubation; valve opened; step 2 requires 25 min.)	[11]
RT-RPA-Cas12a	Single tube reaction	**Lab-developed fluorescence polarization device** & incubator	Determined to be 3 copies/μL (of reaction?) (2 μL sample/reaction) Reaction volume not specified	Dynamic range ~3–10^6 copies/μL	Relies on Cas12a RNP	100% (Ct not available)	100%	20 min	[12]
RT-RAA-Cas12a	1. RT-RAA 2. Cas12a 3. Beads separation 4. **glucose meter**	Incubator (42°C and 37°C), magnet & glucose meter	1 copies/μL of sample, SARS-CoV-2 RNA extracted from pseudovirus (2 μL sample/reaction)	10–10^4 copies/μL	Relies on Cas12a RNP	2/2 (Ct not available)	7/7	~60 min (Step 1 requires 20 min incubation; step 2 requires 30 min; plus step 3 and 4)	[13]
RT-RPA-Cas12a-AuNP	1. RT-RPA 2. Cas12a 3. **AuNP aggregation**	Incubator (37°C), UV-vis absorption & spectrum readout or naked eye	1 copies/reaction (13.2 μL sample/reaction)	With UV-vis absorption & spectrum 1 pM–100 nM	Relies on Cas12a RNP	Not reported	Not reported	60 min (Step 1 requires 20 min incubation; step 2 requires 10 min incubation; plus step 3)	[14]

Tech-niques	Steps	Facilities	LOD	Linear range	Sequence specificity of Cas recognition	Clinical sensitivity *	Clinical Speci-ficity*	Assay time	Ref.
RT-LAMP-Cas12a **DETECTR**	1. RT-LAMP 2. Cas12a 3. Strip	Incubator (62°C & 37°C) and strip	10 copies/µL of reaction (RT-LAMP reaction is 10 µL)	Binary positive or negative	Relies on Cas12a RNP	95% (Ct 13–38)	100%	~40 min (Step 1 requires 20–30 min incubation; step 2 requires 10 min incubation; step 3 requires 2 min)	[15]
RT-LAMP-Cas12a	1. RT-LAMP 2. Cas12a (lid)	Incubatior (62°C), UV light & smartphone	30-45 copies/µL of sample (5 µL sample/reaction)	Binary positive or negative	Relies on Cas12a RNP	94% (Ct 11–39)	100%	40 min (Step 1 requires 30 min incubation; step 2 requires 10 min incubation)	[16]
RT-LAMP-Cas12a-microfluidics& Isotachophoresis	1. RT-LAMP 2. ITP–CRISPR Detection	Chip, water bath (62°C), isotachophoresis (ITP) facilities	10 copies/µL reaction (RT-LAMP reaction is 10 µL)	Not reported	Relies on Cas12a RNP	93.8 % (Ct 16–36)	100%	~35 min (Including 2 min on chip RNA extraction, 20-30 min RT-LAMP reaction and 3 min ITP–CRISPR Detection)	[17]
RT-LAMP-Cas12a	1. RT-LAMP 2. Cas12a (same tube, separate by oil)	Thermo block (65°C &37°C) & bule light	5 copies (/reaction?) (1 µL IVT RNA or 20 µL sample in 40 µL of LAMP reaction)	Not reported	Relies on Cas12a RNP	100 % (Ct 25–38)	100%	45 min (Step 1 requires 40 min; step 2 requires 5 min incubation)	[18]
RT-LAMP-Cas12a	1. RT-LAMP 2. Cas12a (3. Strip)	Incubator (63°C) & strip	"3–300 copies/reaction"	Not quantitative	Improved Cas12a specificity (by engineering the crRNA)	Not tested	Not tested	40–60 min (Step 1 requires 20–30 min; step 2 requires 5–20 min incubation)	[19]

Tech-niques	Steps	Facilities	LOD	Linear range	Sequence specificity of Cas recognition	Clinical sensitivity *	Clinical Speci-ficity*	Assay time	Ref.
RT-LAMP-Cas12a	1. RT-LAMP 2. Cas12a (lid)	Incubator (65°C & 37°C), 3D-printed instrument & smartphone	20 copies/reaction	Not quantitative	Relies on Cas12a RNP	7/7	3/3	40 min (Step 1 requires 30-40 min; step 2 requires 5 min incubation)	[20]
RT-LAMP-Cas12b **SHERLOCK**	1. Single tube reaction at 60°C (2. Strip)	a. Real-time detection: magnet, incubator & UV light b. Strip detection: magnet, incubator, UV light & strip	100 copies/sample (0.033 copies/μL of sample before extraction)	Not reported	Relies on Cas12b RNP	93.1% (Ct 17–40)	98.5%	~15 min extraction+45 min incubation for real-time detection Or 80 min for strip detection	[21]
RT-LAMP-Cas12a-AuNP	1. RT-LAMP 2. Cas12a 3. **AuNP aggregation visual readout**	Incubator (62°C), spinner & smartphone	SARS-CoV-2 RNA from Vero E6 cells 225–300 copies/reaction (5 μL sample/reaction)	Binary positive or negative	Relies on Cas12a RNP	92.6% (Ct 20–37)	100%	45 min (Step 1 requires 30 min incubation; step 2 requires 10 min incubation; and step 3 requires 1 min incubation and 10 s spinning)	[22]

*Clinical sensitivity and specificity were reported as the number of samples having results in agreement with RT-PCR divided by the total number of samples if the sample number was below 10.

References for Appendix A

1. Zhang, F., Abudayyeh, O. O. and Gootenberg, J. S. A protocol for detection of COVID-19 using CRISPR diagnostics 2020. https://www.broadinstitute.org/files/publications/special/COVID-19%20detection%20(updated).pdf. (accessed May 11, 2020)
2. Wang, X., Zhong, M., Liu, Y., Ma, P., Dang, L., Meng, Q., Wan, W., Ma, X., Liu, J., Yang, G., Yang, Z., Huang, X. and Liu, M., Rapid and sensitive detection of COVID-19 using CRISPR/Cas12a-based detection with naked eye readout, CRISPR/Cas12a-NER. *Sci. Bull. (Beijing)* **2020,** *65* (17), 1436-1439.
3. Samacoits, A., Nimsamer, P., Mayuramart, O., Chantaravisoot, N., Sitthi-amorn, P., Nakhakes, C., Luangkamchorn, L., Tongcham, P., Zahm, U., Suphanpayak, S., Padungwattanachoke, N., Leelarthaphin, N., Huayhongthong, H., Pisitkun, T., Payungporn, S. and Hannanta-anan, P., Machine Learning-Driven and Smartphone-Based Fluorescence Detection for CRISPR Diagnostic of SARS-CoV-2. *ACS Omega* **2021,** *6* (4), 2727-2733.
4. Guo, L., Sun, X., Wang, X., Liang, C., Jiang, H., Gao, Q., Dai, M., Qu, B., Fang, S., Mao, Y., Chen, Y., Feng, G., Gu, Q., Wang, R. R., Zhou, Q. and Li, W., SARS-CoV-2 detection with CRISPR diagnostics. *Cell discovery* **2020,** *6* (1), 34.
5. Sun, Y., Yu, L., Liu, C., Ye, S., Chen, W., Li, D. and Huang, W., One-tube SARS-CoV-2 detection platform based on RT-RPA and CRISPR/Cas12a. *J. Transl. Med.* **2021,** *19* (1), 74.

6. Xiong, D., Dai, W., Gong, J., Li, G., Liu, N., Wu, W., Pan, J., Chen, C., Jiao, Y., Deng, H., Ye, J., Zhang, X., Huang, H., Li, Q., Xue, L., Zhang, X. and Tang, G., Rapid detection of SARS-CoV-2 with CRISPR-Cas12a. *PLOS Biol.* **2020,** *18* (12), e3000978.
7. Arizti-Sanz, J., Freije, C. A., Stanton, A. C., Petros, B. A., Boehm, C. K., Siddiqui, S., Shaw, B. M., Adams, G., Kosoko-Thoroddsen, T.-S. F., Kemball, M. E., Uwanibe, J. N., Ajogbasile, F. V., Eromon, P. E., Gross, R., Wronka, L., Caviness, K., Hensley, L. E., Bergman, N. H., MacInnis, B. L., Happi, C. T., Lemieux, J. E., Sabeti, P. C. and Myhrvold, C., Streamlined inactivation, amplification, and Cas13-based detection of SARS-CoV-2. *Nat. Commun.* **2020,** *11*, 5921.
8. Ding, X., Yin, K., Li, Z., Lalla, R. V., Ballesteros, E., Sfeir, M. M. and Liu, C., Ultrasensitive and visual detection of SARS-CoV-2 using all-in-one dual CRISPR-Cas12a assay. *Nat. commun.* **2020,** *11* (1), 4711.
9. de Puig, H., Lee, R. A., Najjar, D., Tan, X., Soekensen, L. R., Angenent-Mari, N. M., Donghia, N. M., Weckman, N. E., Ory, A., Ng, C. F., Nguyen, P. Q., Mao, A. S., Ferrante, T. C., Lansberry, G., Sallum, H., Niemi, J. and Collins, J. J., Minimally instrumented SHERLOCK (miSHERLOCK) for CRISPR-based point-of-care diagnosis of SARS-CoV-2 and emerging variants. *Sci. Adv.* **2021,** *7* (32), eabh2944.
10. Ning, B., Yu, T., Zhang, S., Huang, Z., Tian, D., Lin, Z., Niu, A., Golden, N., Hensley, K., Threeton, B., Lyon, C. J., Yin, X.-M., Roy, C. J., Saba, N. S., Rappaport, J., Wei, Q. and Hu, T. Y., A smartphone-read ultrasensitive and quantitative saliva test for COVID-19. *Sci. Adv.* **2021,** *7* (2), eabe3703.
11. Yin, K., Ding, X., Li, Z., Sfeir, M. M., Ballesteros, E. and Liu, C., Autonomous lab-on-paper for multiplexed, CRISPR-based diagnostics of SARS-CoV-2. *Lab on a chip* **2021**.

12. Lee, C. Y., Degani, I., Cheong, J., Lee, J.-H., Choi, H.-J., Cheon, J. and Lee, H., Fluorescence polarization system for rapid COVID-19 diagnosis. *Biosens. Bioelectron.* **2021,** *178*, 113049.
13. Huang, D., Shi, Z., Qian, J., Bi, K., Fang, M. and Xu, Z., A CRISPR-Cas12a-derived biosensor enabling portable personal glucose meter readout for quantitative detection of SARS-CoV-2. *Biotechnol. Bioeng.* **2021,** *118* (4), 1568-1577.
14. Zhang, W. S., Pan, J., Li, F., Zhu, M., Xu, M., Zhu, H., Yu, Y. and Su, G., Reverse Transcription Recombinase Polymerase Amplification Coupled with CRISPR-Cas12a for Facile and Highly Sensitive Colorimetric SARS-CoV-2 Detection. *Anal. Chem.* **2021,** *93* (8), 4126-4133.
15. Broughton, J. P., Deng, X., Yu, G., Fasching, C. L., Servellita, V., Singh, J., Miao, X., Streithorst, J. A., Granados, A., Sotomayor-Gonzalez, A., Zorn, K., Gopez, A., Hsu, E., Gu, W., Miller, S., Pan, C.-Y., Guevara, H., Wadford, D. A., Chen, J. S. and Chiu, C. Y., CRISPR–Cas12-based detection of SARS-CoV-2. *Nat. Biotechnol.* **2020,** *38* (7), 870-874.
16. Pang, B., Xu, J., Liu, Y., Peng, H., Feng, W., Cao, Y., Wu, J., Xiao, H., Pabbaraju, K., Tipples, G., Joyce, M. A., Saffran, H. A., Tyrrell, D. L., Zhang, H. and Le, X. C., Isothermal Amplification and Ambient Visualization in a Single Tube for the Detection of SARS-CoV-2 Using Loop-Mediated Amplification and CRISPR Technology. *Anal. Chem.* **2020,** *92* (24), 16204-16212.
17. Ramachandran, A., Huyke, D. A., Sharma, E., Sahoo, M. K., Huang, C., Banaei, N., Pinsky, B. A. and Santiago, J. G., Electric field-driven microfluidics for rapid CRISPR-

based diagnostics and its application to detection of SARS-CoV-2. *Proc. Natl. Acad. Sci.* **2020,** *117* (47), 29518-29525.

18. Wang, R., Qian, C., Pang, Y., Li, M., Yang, Y., Ma, H., Zhao, M., Qian, F., Yu, H., Liu, Z., Ni, T., Zheng, Y. and Wang, Y., opvCRISPR: One-pot visual RT-LAMP-CRISPR platform for SARS-cov-2 detection. *Biosens. Bioelectron.* **2021,** *172*, 112766.
19. Nguyen, L. T., Smith, B. M. and Jain, P. K., Enhancement of trans-cleavage activity of Cas12a with engineered crRNA enables amplified nucleic acid detection. *Nat. Commun.* **2020,** *11* (1), 4906.
20. Chen, Y., Shi, Y., Chen, Y., Yang, Z., Wu, H., Zhou, Z., Li, J., Ping, J., He, L., Shen, H., Chen, Z., Wu, J., Yu, Y., Zhang, Y. and Chen, H., Contamination-free visual detection of SARS-CoV-2 with CRISPR/Cas12a: A promising method in the point-of-care detection. *Biosens. Bioelectron.* **2020,** *169*, 112642.
21. Joung, J., Ladha, A., Saito, M., Kim, N.-G., Woolley, A. E., Segel, M., Barretto, R. P. J., Ranu, A., Macrae, R. K., Faure, G., Ioannidi, E. I., Krajeski, R. N., Bruneau, R., Huang, M.-L. W., Yu, X. G., Li, J. Z., Walker, B. D., Hung, D. T., Greninger, A. L., Jerome, K. R., Gootenberg, J. S., Abudayyeh, O. O. and Zhang, F., Detection of SARS-CoV-2 with SHERLOCK One-Pot Testing. *New Engl. J. Med.* **2020,** *383* (15), 1492-1494.
22. Cao, Y., Wu, J., Pang, B., Zhang, H. and Le, X. C., CRISPR/Cas12a-mediated gold nanoparticle aggregation for colorimetric detection of SARS-CoV-2. *Chem. Commun.* **2021,** *57*, 6871-6874.